

LONDON
SCHOOL of
HYGIENE
& TROPICAL
MEDICINE



LSHTM Research Online

Riezk, A; (2020) Insights into the application of chitosan as an anti-leishmanial compound. PhD thesis, London School of Hygiene & Tropical Medicine. DOI: <https://doi.org/10.17037/PUBS.04656180>

Downloaded from: <https://researchonline.lshtm.ac.uk/id/eprint/4656180/>

DOI: <https://doi.org/10.17037/PUBS.04656180>

Usage Guidelines:

Please refer to usage guidelines at <https://researchonline.lshtm.ac.uk/policies.html> or alternatively contact researchonline@lshtm.ac.uk.

Available under license. To note, 3rd party material is not necessarily covered under this license: <http://creativecommons.org/licenses/by-nc-nd/3.0/>

<https://researchonline.lshtm.ac.uk>

LONDON
SCHOOL of
HYGIENE
& TROPICAL
MEDICINE



UCL
SCHOOL OF PHARMACY

Insights into the application of chitosan as an anti-leishmanial compound.

Alaa Riezk

Thesis submitted in accordance with the requirements for the degree of
Doctor of Philosophy
of
the University of London

November 2019

Department of Infection Biology

Faculty of Infectious & Tropical Disease

London School of Hygiene & Tropical Medicine, University of London

Research supervisors: **Dr Vanessa Yardley**
Prof Simon L Croft
Dr Sudaxshina Murdan

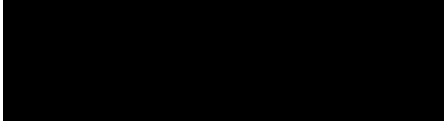
Funded by the London School of Hygiene & Tropical Medicine (Prof S L Croft) and
CARA (the Council for At-Risk Academics)

DECLARATION

I, Alaa Riezk, confirm that the work presented in this thesis is my own. Where information has been derived from other sources, I confirm that this has been indicated in the thesis.

Alaa Riezk

November-2019



Abstract

There is an urgent need for safe, efficacious, affordable and field-adapted drugs for the treatment of cutaneous leishmaniasis, a disease which affects around 1.5 million people worldwide every year. Chitosan, a biodegradable cationic polysaccharide, has previously been reported to have antimicrobial, anti-leishmanial and immunostimulatory activities. The work described here found that chitosan and its derivatives were approximately 7-20 times more active *in vitro* against *Leishmania* promastigotes and amastigotes at pH 6.5 than at pH 7.5, with high molecular weight chitosan being the most potent. Despite the *in vitro* activation of bone marrow macrophages by chitosan to produce nitric oxide and reactive oxygen species, this work showed that the anti-leishmanial activity of chitosan was not mediated by these metabolites. It was subsequently shown that rhodamine-labelled chitosan is taken up by pinocytosis and accumulates in the parasitophorous vacuole of *Leishmania*-infected macrophages. The application of chitosan in drug delivery systems was then studied by preparing two types of chitosan nanoparticles (positive (with tripolyphosphate sodium (TPP)) and negative (with dextran sulphate) surface charge with different sizes) and incorporation of amphotericin B within these nanoparticles. These amphotericin B-loaded nanoparticles demonstrated a good *in vitro* anti-leishmanial activity, similar to pure amphotericin B, and were also significantly less toxic than pure amphotericin B. The positive amphotericin B-loaded chitosan-TPP nanoparticles showed promising *in vivo* efficacy against cutaneous leishmaniasis caused by *L. major* in the BALB/c mouse model, via the intravenous route, and they were more active than AmBisome[®]. The impact of an *in vitro* media perfusion system on host cell phagocytosis and macropinocytosis was evaluated as well as the anti-leishmanial activity of chitosan solution and blank or amphotericin B-loaded chitosan-TPP nanoparticles. There was a significant difference between *in vitro* static and flow culture systems in the cell uptake and anti-leishmanial activity of the studied compounds.

Acknowledgements

I would like to express my sincere gratitude to my supervisors, Dr Vanessa Yardley and Prof Simon L Croft for the continuous support of my PhD study, for their enthusiasm, guidance, motivation, and immense knowledge. How can I ever thank you enough for all you have done? I 'm forever grateful. You helped shape my research and professional life and showed me how to transform my mistakes into skills. I really appreciate everything you have taught me!

Many thanks to my supervisor Dr Sudax Murdan (Department of Pharmaceutics, School of Pharmacy, UCL) for providing invaluable guidance, helping me improve my skills, and for all the advice, ideas, support and patience in guiding me through this project. My supervisors, three of you, have been role models over the last years and was a great pleasure to meet you and have you in my life.

Special thanks should also be given to my colleague Katrien Van Bocxlaer. Kat, your passion for the research is contagious, your ability to repair things keeps astonishing me. I am sure that, your thoughtfulness is a gift I will always treasure, a huge thanks.

And thanks to the rest of the Croft group for all the good times in and out of the lab: Alec O'Keeffe, Gert-Jan Wijnant and Markella Koniordou.

I wish to acknowledge Dr John Raynes for the technical support and guidance.

I acknowledge the facilities and the scientific and technical assistance of the LSHTM Wolfson Cell Biology Facility, with specific thanks to Dr Elizabeth McCarthy

Thanks to everyone at School of Pharmacy who helped me through my project, Dr S. Somavarapu, Dr Andrew Weston, Satinder Sembi.

Many thanks to CARA (Zeid, Laura, Riman, Lucia and all the team), LSHTM and Goodenough college, my PhD would not have been possible without their support.

I would also like to take this opportunity to thank Associate Prof Philippe M Loiseau and Dr Mohamed Alhnan- my viva examiners, for their very helpful comments and suggestions.

Thanks to all of my friends who have supported me throughout the process.

I would like to dedicate this PhD thesis to Simon L Croft, the symbol of love and giving. To my beloved wife Rana, never forget that I love you and this love will never fade for anything in the world, Rana I have faith in you. Carlos, you are one of the most amazing gifts I have ever received. Carlos, I thank Jesus for you every single day. You are a great blessing in my life, my always and forever.

Whatever I am today is because of my parents. It is their values and upbringing that have held me together despite all the struggles and adversities I have faced in such a hard time. Thanks to them, I have not crumbled under pressure, I have not stopped believing in myself and I am still fighting, Fadaa and Essam

Finally, my brothers and their families, despite the loneliness that comes with being so far from you, I hold on knowing that you truly love me, that our bond can't be broken, Nazier, Subee, Elie, Hala, Hala, Maram , Wisam, Tala, Lana, Rita, Essam, Jad, Ameer and Marcos with much love.

Contents

1. General introduction.....	1
1.1. Leishmaniasis and <i>Leishmania</i> species	1
1.2. Life cycle	6
1.3. Immune response in CL	7
1.4. Current treatment of cutaneous leishmaniasis	8
1.4.1. Systemic therapies.....	11
1.4.1.1. Pentavalent Antimony	11
1.4.1.2. Miltefosine	12
1.4.1.3. Amphotericin B (AmB).....	13
1.4.1.4. Pentamidine	15
1.4.1.5. Azoles	16
1.4.2. Local therapy	17
1.4.2.1. Paromomycin	17
1.4.2.2. Physical treatments.....	18
1.4.3. Immunomodulatory treatment	19
1.5. Challenges for CL treatment	20
1.6. Assays to test the anti-leishmanial activity of drugs	20
1.6.1. <i>In vitro</i> assays	21
1.6.2. <i>In vivo</i> assays	24
1.7. Drug development for CL: from pipeline to patients	25
1.8. New CL drugs	27
1.9. Drug delivery systems for leishmaniasis	29
1.10. Nanoparticles and their interaction with skin lesions	34
1.10.1. Mathematical models of skin permeability.....	38
1.11. Pharmacokinetics of ant-leishmanial drugs.....	40
1.12. Treatment challenges	45
1.13. Aims and objectives	46
2. Activity of chitosan and its derivatives against <i>Leishmania major</i> and <i>mexicana in vitro</i>.....	48
2.1. What is chitosan?.....	48
2.2. Chitosan solubility	48
2.3. Chitosan toxicity	49
2.4. Chitosan in wound healing	49
2.5. Chitosan derivatives.....	49
2.6. Antimicrobial activity of chitosan	50
2.7. Anti-leishmanial activity of chitosan	51
2.8. Materials and methods.....	55
2.8.1. Drugs and chemicals	55
2.8.2. Ethics statement.	57
2.8.3. Cell lines	57
2.8.4. Parasites	59
2.8.5. <i>In vitro</i> cytotoxicity assays.....	59
2.8.6. <i>In vitro</i> 72-hour activity of chitosan and its derivatives against extracellular <i>L. major</i> and <i>L. mexicana</i> promastigotes	59

2.8.7. <i>In vitro</i> 72- hour activity of chitosan and its derivatives against intracellular amastigotes of <i>L. major</i> and <i>L. mexicana</i>	60
2.8.8. Influence of the origin of the host cell on the <i>in vitro</i> activity of HMW chitosan against <i>L. major</i> amastigotes	61
2.8.9. Influence of incubation duration on chitosan activity against <i>L. major</i> amastigotes	61
2.8.10. The role of HMW chitosan on BMMs activation	61
2.8.10.1. Measurement of TNF- α	62
2.8.10.2. Measurement of ROS	62
2.8.10.3. Measurement of NO	62
2.8.11. Uptake of chitosan by macrophages	63
2.8.11.1. Activity of chitosan after inhibition of the endocytic pathway of BMMs	63
2.8.11.2. Microscopic imaging of the cellular uptake of rhodamine-labelled chitosan	64
2.8.12. Statistical analysis	65
2.9. Results	65
2.9.1. Cytotoxicity of chitosan and its derivatives against KB cells in RPMI (pH 7.5 and pH 6.5)	65
2.9.2. Analysis of anti-promastigotes activity	68
2.9.3. Analysis of anti-amastigotes activity in PEMs	70
2.9.4. Host cell dependence of antileishmanial activity of HMW chitosan and time to kill assay on amastigotes at pH 6.5	75
2.9.5. Effects of HMW chitosan on the production of TNF- α by uninfected or <i>L. major</i> infected macrophages at pH = 6.5	76
2.9.6. Effects of HMW chitosan on the production of ROS by macrophages at pH = 6.5	78
2.9.7. Effects of HMW chitosan on the production of NO by macrophages at pH = 6.5	82
2.9.8. Cellular uptake of HMW chitosan and inhibition of endocytosis	86
2.9.9. Fluorescence microscopy of the uptake of chitosan by macrophages	88
2.10. Discussion	90
3. Preparation and characterisation of amphotericin B loaded chitosan nanoparticles	95
3.1. Introduction	95
3.2. Material and methods	101
3.2.1. Preparation of blank chitosan nanoparticles	101
3.2.2. Preparation of AmB loaded chitosan nanoparticles	102
3.2.3. Physicochemical properties of the nanoparticles (size, charge and morphology)	104
3.2.4. Stability of nanoparticles regarding size and zeta potential	105
3.2.5. Determination of drug encapsulation efficiency and AmB loading and release	105
3.2.6. <i>In vitro</i> release of AmB	106
3.2.6.1. Quantification of AmB by HPLC	107
3.3. Results	108

3.3.1. Effects of the initial concentration of chitosan and sonication time on the quality of the nanoparticles	108
3.3.1.1. Conditions that resulted in poor quality nanoparticles	108
3.3.1.2. Conditions that resulted in good quality nanoparticles	111
3.3.2. Effects of pH of chitosan solution and the mass ratio on the size and charge of good quality nanoparticles	112
3.3.3. Effects of AmB loading and freeze-drying with and without cryoprotectants on physicochemical properties and the morphology of the nanoparticles.....	115
3.3.4. Stability of physicochemical properties of AmB loaded chitosan nanoparticles.....	119
3.3.5. Nanoparticles loading and encapsulation properties.....	123
3.3.6. <i>In vitro</i> release of AmB from the nanoparticles	124
3.4. Discussion.....	129
3.4.1. Conclusion	133
4. <i>In vitro</i> and <i>in vivo</i> activity of chitosan formulations in experimental cutaneous leishmaniasis	134
4.1. Introduction	134
4.2. Material and methods	140
4.2.1. Preparation of blank and AmB loaded chitosan nanoparticles	140
4.2.2. Red blood cells haemolysis.....	140
4.2.3. <i>In vitro</i> cytotoxicity assays.....	141
4.2.4. <i>In vitro</i> 72-hour activity of chitosan and its derivatives against extracellular <i>L. major</i> and <i>L. mexicana</i> promastigotes	142
4.2.5. <i>In vitro</i> 72- hour activity of chitosan and its derivatives against intracellular amastigotes of <i>L. major</i> and <i>L. mexicana</i>	142
4.2.6. Evaluation of the <i>in vivo</i> anti-leishmanial activity of chitosan formulations	143
4.2.6.1. <i>In vivo</i> <i>L. major</i> model of CL	143
4.2.6.2. Measurement of lesion size	146
4.2.6.3. Measurement of the bioluminescence signal	147
4.2.6.4. Quantification of AmB in skin samples	147
4.2.7. Skin permeation study by Franz diffusion cell (FDC) assay	148
4.2.7.1. Quantification of AmB by HPLC	149
4.2.7.2. Fluorescence microscopy of skin sections post formulation application.....	150
4.2.8. Statistical analysis.....	151
4.3. Results	152
4.3.1. Haemolysis activity of chitosan nanoparticles	152
4.3.2. Cytotoxicity of blank and AmB loaded chitosan nanoparticles against KB cells in RPMI (pH 7.5 and pH 6.5).....	154
4.3.3. Activity of blank and AmB loaded chitosan nanoparticles against <i>L. major</i> and <i>L. mexicana</i> promastigotes in RPMI (pH 7.5 and pH 6.5)	157
4.3.4. Activity of blank and AmB loaded chitosan nanoparticles against <i>L. major</i> and <i>L. mexicana</i> amastigotes infecting PEMs.....	160
4.3.5. Host cell dependence of the anti-leishmanial activity of chitosan nanoparticles at pH of 6.5	163

4.3.6. <i>In vivo</i> anti-leishmanial activity (intravenous route route).....	165
4.3.6.1. <i>In vivo</i> experiment 1	165
4.3.6.1.1. Evaluation of the lesion size progression	165
4.3.6.1.2. Evaluation of the parasite load (bioluminescent signal)	168
4.3.6.1.3. Intralesional amphotericin B levels.....	171
4.3.6.2. <i>In vivo</i> experiment 2 (dose-response effect)	172
4.3.6.2.1. Evaluation of the lesion size progression	172
4.3.6.2.2. Evaluation of the parasite load (bioluminescent signal)	175
4.3.6.2.3. Intralesional amphotericin B levels.....	178
4.3.6.2.4. Dose concentration-response of AmB loaded chitosan-TPP nanoparticles in <i>L. major</i> -infected mice.....	180
4.3.7. <i>Ex vivo</i> permeability of <i>Leishmania</i> -infected skin in Franz diffusion cells.....	182
4.4. Discussion.....	187
5. Comparison of <i>in vitro</i> static and dynamic culture systems to evaluate the macrophages functions and the anti-leishmanial efficacy of chitosan formulations **	196
5.1. Media perfusion system: an introduction.....	196
5.2. Material and methods	201
5.2.1. Preparation of chitosan solution and blank and AmB loaded chitosan nanoparticles.....	201
5.2.2. QV900 and media perfusion system	202
5.2.3. Macrophages	202
5.2.4. Infection of macrophages by <i>L. major</i> promastigotes.....	203
5.2.5. Measurement of macrophage functions.	203
5.2.5.1. Phagocytosis.....	203
5.2.5.2. Macropinocytosis	204
5.2.6. Evaluation of the anti-leishmanial activity of chitosan solutions, blank and AmB loaded chitosan TPP nanoparticles in the media perfusion system at pH 6.5	205
5.3. Results	206
5.3.1. Macrophage functions.....	206
5.3.1.1. Phagocytosis.....	206
5.3.1.2. Macropinocytosis	210
5.3.2. Effects of media perfusion system on the anti-leishmanial activity of chitosan formulations	216
5.4. Discussion.....	219
6. General discussion	224
6.1. Discussion and conclusion.....	224
6.2. Future work	229
7. References.....	231
8. Appendix.....	253
8.1. Appendix 1: Validation of HPLC methods	253
8.2. Appendix 2: Paper 1	255
8.3. Appendix 3: Paper 2	275

Abbreviations

3D	Three Dimensional
ADME	absorption, distribution, metabolism and excretion
AmB	Amphotericin B
AUC	Area under curve
BCG	Bacille Calmette-Guérin
BMMs	Murine bone-marrow macrophages
BMMs	Bone marrow-derived macrophages
C _{max}	Maximum concentration
CL	Cutaneous leishmaniasis
Cl _r	Clearance
CME	Clathrin-mediated endocytosis
C _{ss}	Steady-state concentration
C _{trough}	Trough plasma concentration 24 h after dose
DAPI	4',6-diamidino-2-phenylindole
DCFDA	2',7'-dichlorofluorescein diacetate
DCL	Diffuse cutaneous leishmaniasis
DCs	Dendritic cells
DDs	Drug delivery systems
DMSO	Dimethyl sulfoxide
DNDi	Drugs for Neglected Diseases initiative
DsCL	Disseminated cutaneous leishmaniasis
EC ₅₀	50% effective concentration
EC ₉₀	90% effective concentration
ED ₅₀	The required dose to achieve 50% of maximum effect
ED ₉₀	The required dose to achieve 90% of maximum effect
EE	Encapsulation efficiency
EM	Emission wavelength
EX	Excitation wavelength
FDA	Federal drug agency
FDC	Franz diffusion cell
GFP	Green fluorescent protein
GM-CSF	Granulocyte-macrophage colony stimulating factor
GRAS	Generally Recognized As Safe
HiFCS	Heat-inactivated fetal calf serum
HMW	High molecular weight
HPLC	High Performance Liquid Chromatography
HTS	High throughput screening
i.p.	Intraperitoneal
ISC	Indian subcontinent
i.v.	Intravenous
KB cells	Human squamous carcinoma cells
KDa	Kilodaltons
kp	Permeability coefficient
LD ₅₀	50% lethal dose
LMW	Low molecular weight

LPS	Lipopolysaccharides
LR	Leishmaniasis recidivans
MBCL	Methyl-benzethonium chloride
MCL	Mucocutaneous leishmaniasis
MES	2-N-morpholino ethanesulfonic acid
MF	Miltefosine
MIC	Minimum inhibitory concentration
MMW	Medium molecular weight
MW	Molecular weight
NAC	N-acetyl-L-cysteine
NaOH	Sodium hydroxide
NCEs	New chemical entities
nMDP	Normalized mean deviation product
NMMA	NG-methyl-L-arginine acetate salt
NO	Nitric oxide
NPs	Nanoparticles
NTD	Neglected tropical disease
PBMCs	peripheral blood mononuclear cells
PBS	Phosphate-buffered saline
PC1-CH	Phosphorylcholine substituted chitosan
PD	Pharmacodynamic
PDI	Polydispersity index
PDMS	Polydimethylsiloxane
PEMs	Murine peritoneal macrophages
PK	Pharmacokinetic
PLGA	Polylactic-co-glycolic acid
PM	Paromomycin
PMN	polymorphonuclear leukocytes
PV	Parasitophorous vacuole
QAD	Every other day
QD	Every day
QV	Quasi Vivo
R&D	Research and development
RBC ₅₀	50% haemolytic concentration
RBCs	Red blood cells
ROS	Reactive Oxygen Species
SbV	Pentavalent antimony
SC	Stratum corneum
SD	Standard deviation
SEM	Scanning electron microscopy
t _{1/2}	Half-life
TEM	Transmission electron microscopy
THP-1	Human leukemic monocyte-like derived cell line
t _{max}	Time-point corresponding with maximum concentration
TNF- α	Tumour necrosis factor alpha
TPP	Tripolyphosphate sodium

Trans-epidermal water loss	TEWL
VL	Visceral leishmaniasis
WHO	World Health Organization

List of figures

Figure 1.1. The distribution of cutaneous leishmaniasis WHO	3
Figure 1.2. <i>Leishmania</i> species and related clinical manifestations.	3
Figure 1.3. The life cycle of <i>Leishmania</i> parasites	7
Figure 1.4. Immune response against leishmaniasis. A: neutrophils play an important role during the early stage of infections. B: the essential role of monocytes in killing <i>Leishmania</i> and promoting the differentiation of Th-1, which leads to the elimination of parasites.....	8
Figure 1.5. Strategies for treatment of CL and the related limitations. Syst=systemic. Tx= treatment. ACL=asymptomatic CL	10
Figure 1.6. Proposed structural formula for 364 Da and 365 Da ions identified by ESI(-)-MS in aqueous solutions of meglumine antimoniate and stibogluconate, respectively, copied from	12
Figure 1.7. Chemical structure of miltefosine	13
Figure 1.8. Chemical structure of amphotericin B (A), Fungizone (B) and AmBisome® (C).....	15
Figure 1.9. Chemical structure of pentamidine.....	16
Figure 1.10. Chemical structure of some azoles	17
Figure 1.11. Chemical structure of paromomycin.....	18
Figure 1.12. The process of drug discovery and drug development. a) drug discovery stages b) drug development (107)	26
Figure 1.13. The Drug Development Pipeline - potential drugs for NTDs are frequently stuck in the early stage of development as a result of pipeline gaps	27
Figure 1.14. New treatment candidates for leishmaniasis.....	28
Figure 1.15. Route a drug must take to access intracellular <i>Leishmania</i> amastigotes within macrophages (A) and DDs to intracellular <i>Leishmania</i> amastigotes(B) (.....	29
Figure 1.16. Administration routes of DDs and anatomical barriers.	32
Figure 1.17. Factors to be considered in topical delivery	35
Figure 1.18. Pathways of skin nanoparticles penetration. 1) via hair follicles, 2) intracellularly through corneocytes and 3) intercellularly around corneocytes.....	36
Figure 1.19. Interaction of nanoparticles with lesions of CL.	38
Figure 1.20. The passive diffusion of drug through a membrane	39
Figure 2.1. Structure of chitin and chitosan and method of preparation chitosan from raw materials	48
Figure 2.2. Schematic illustration of chitosan's versatility	49
Figure 2.3. The structure of chitosan and its derivatives	57
Figure 2.4. Dose-response curves of the cytotoxicity of chitosan and its derivatives against KB cells at pH=7.5 (A) and 6.5 (B)	67
Figure 2.5. Dose-response curves of the activity of chitosan and its derivatives against <i>Leishmania</i> promastigotes at two pH values. A: <i>L. major</i> at pH=7.5; B: <i>L. mexicana</i> at pH = 7.5; C: <i>L. major</i> at pH = 6.5; D: <i>L.</i>	

<i>mexicana</i> at pH = 6.5. Promastigotes were cultured in the presence of different concentrations of chitosan and its derivatives.....	70
Figure 2.6. Dose-response curves of the activity of chitosan and its derivatives against <i>Leishmania</i> amastigotes at two pH values. A: <i>L. major</i> at pH=7.5; B: <i>L. mexicana</i> at pH = 7.5; C: <i>L. major</i> at pH = 6.5; D: <i>L. mexicana</i> at pH = 6.5.	73
Figure 2.7. Morphology of infected (PEMs) with <i>L. major</i> and <i>L. mexicana</i> after treatment with HMW chitosan	74
Figure 2.8. Influence of incubation duration on the chitosan and Fungizone activity against <i>L. major</i> intracellular amastigotes in BMMs.	76
Figure 2.9. TNF- α production in uninfected and <i>L. major</i> infected BMMs, PEMs and THP-1 macrophages* after 24 h of exposure to 1.64, 4.9,14.8, 44.4, 133.3 and 400 μ g/ml of chitosan at pH = 6.5	78
Figure 2.10. ROS production in uninfected and <i>L. major</i> infected BMMs, PEMs and THP-1 macrophages * after 4 h of exposure to 1.64, 4.9,14.8, 44.4, 133.3 and 400 μ g/ml of HMW chitosan at pH=6.5	80
Figure 2.11. Activity of HMW chitosan against <i>L. major</i> amastigotes in BMMs* after 4 h, with and without ROS scavenger at pH = 6.5.....	81
Figure 2.12. NO production in uninfected and <i>L. major</i> infected BMMs, PEMs and THP-1 macrophages * after 24 h of exposure to 1.64, 4.9,14.8, 44.4, 133.3 and 400 μ g/ml of chitosan at pH = 6.5.	84
Figure 2.13. Activity of HMW chitosan against <i>L. major</i> -infected BMMs* after 24 h in the presence or absence of an NO inhibitor at pH = 6.5.	85
Figure 2.14. Activity of HMW chitosan against <i>L. major</i> infected BMMs* after 4 h, pH=6.5 (A), 24 h, pH=6.5 (B) and at 24 h, pH=7.5 with or without phagocytosis inhibitor or pinocytosis (CME) inhibitor.....	87
Figure 2.15. Fluorescence microscopy images of the cellular uptake of rhodamine-labelled chitosan over 4 and 24 h at pH=6.5 by BMMs infected with <i>L. major</i> (XA) or with <i>L. mexicana</i> (XB).....	89
Figure 3.1. Preparation methods of chitosan nanoparticles	98
Figure 3.2. Chemical structure of TPP and dextran sulphate	100
Figure 3.3. Mechanisms of drug release from chitosan nanoparticles.	100
Figure 3.4. Schematic representation for Blank nanoparticles and AmB loaded chitosan nanoparticles with TPP or dextran sulphate.....	104
Figure 3.5. Poor quality nanoparticles at different conditions	110
Figure 3.6. Good quality chitosan-dextran sulphate nanoparticles with one peak (one population of nanoparticles at initial chitosan concentration 3 mg/ml and sonication for 15 mins	111
Figure 3.7. Good quality chitosan-TPP nanoparticles with one peak (one population of nanoparticles at initial chitosan concentration 3 mg/ml and sonication for 15 mins	112
Figure 3.8. Effectiveness of sucrose 5% and D-mannitol 5% as a cryoprotectant for freeze drying of blank and AmB loaded chitosan nanoparticles.....	117
Figure 3.9. TEM micrographs of unloaded and amphotericin B loaded chitosan nanoparticles	118

Figure 3.10. SEM micrographs of unloaded and amphotericin B loaded chitosan nanoparticles	119
Figure 3.11. Size of AmB loaded chitosan-TPP nanoparticle (A) and AmB loaded chitosan-dextran sulphate nanoparticle (B) in different media over time.....	120
Figure 3.12. Comparison of AmB encapsulation, loading and yield of the two types of nanoparticles	123
Figure 3.13. <i>In vitro</i> release profile of AmB loaded chitosan nanoparticles at 37 ° C.....	127
Figure 5.1. Microfluidic system (A) The integrated perfusion culture micro-chamber array chip. (B) Enlarged view of a micro-chamber array unit	199
Figure 5.2. Kirkstall LTD. Quasi Vivo 900 media perfusion system in use circulating RPMI 1640 media	199
Figure 5.3. Schematic overview of evaluation of the anti-leishmanial activity in static and flow culture systems.....	205
Figure 5.4. Phagocytosis of fluorescent latex beads (2 µm) by uninfected and infected PEMs (A), BMMs (B) and THP-1 (C) in static culture system.....	208
Figure 5.5. Phagocytosis of fluorescent latex beads (2 µm) by infected PEMs (A), BMMs (B) and THP-1 (C) in the three culture systems (static, slow flow rate 1.45×10^{-9} m/s and fast flow rate 1.23×10^{-7} m/s).....	210
Figure 5.6. Macropinocytosis of pHrodo Red dextran by uninfected and infected PEMs (A), BMMs (B) and THP-1 (C) in static culture system.....	213
Figure 5.7. Macropinocytosis of pHrodo Red dextran by infected PEMs (A), BMMs (B) and THP-1 (C) at the three culture systems (static, slow flow rate 1.45×10^{-9} m/s and fast flow rate 1.23×10^{-7} m/s)	216
Figure 5.8. Dose-response curve of the activity of chitosan solution (A), blank chitosan-TPP nanoparticles (B), AmB loaded chitosan-TPP nanoparticles (C) and AmB solution (pure) (D) against <i>L. major</i> amastigotes infecting PEMs in pH=6.5 under different flow conditions	218
Figure 5.9. Sedimentation under a) static conditions, b) homogeneous distribution of drugs under flow conditions	221
Figure 5.10. Accumulation of amphotericin B (left) and miltefosine (right) in peritoneal macrophages at three culture systems using the QV900 over time. Static and two flow rates (1.33×10^{-9} at the base of the chamber or 1.17×10^{-7} (m/s) on an insert)	222
Figure 5.11. A Hollow-Fibre model.....	222

List of tables

Table 1.1. Clinical and epidemiological characteristics of the main <i>Leishmania</i> species copied from (4)	4
Table 1.2. Clinical features of New World CL that might modify management copied from (23).....	9
Table 1.3. <i>In vitro</i> screening models with positive and negative drawbacks copied from (97).....	22
Table 1.4. <i>In vivo</i> models for leishmaniasis copied from (97)	24
Table 1.5. Experimental studies using nanosystems for CL treatment copied from (115).	30
Table 1.6. Chitosan-based drug delivery systems.....	34
Table 1.7. Basic PK parameters copied from (71)	41
Table 1.8. Pharmacokinetic profile of leishmaniasis drugs (70, 170).....	43
Table 2.1. The antimicrobial activities of chitosan and its derivatives (173, 185, 186, 187).....	51
Table 2.2. The anti-leishmanial activity of chitosan	53
Table 2.3. Details of chitosan and its derivatives used in the study	55
Table 2.4. <i>In vitro</i> cytotoxicity of chitosan and its derivatives against KB cells at two pH values after 72h of incubation	66
Table 2.5. <i>In vitro</i> activity of chitosan and its derivatives against promastigotes at two pH values after 72h of incubation.....	69
Table 2.6. <i>In vitro</i> activity of chitosan and its derivatives against amastigotes infecting PEMs after 72h of incubation.....	72
Table 2.7. <i>In vitro</i> activity of chitosans against promastigotes based on molarity	74
Table 2.8. <i>In vitro</i> activity of chitosans against amastigotes based on molarity	74
Table 2.9. HMW chitosan activity against <i>L. major</i> amastigotes in three different macrophage cultures after 72 h	75
Table 2.10. ROS production in uninfected and <i>L. major</i> infected BMMs after 8 h of exposure to different concentrations of HMW chitosan at pH=6.5	79
Table 2.11. ROS production in uninfected and <i>L. major</i> infected BMMs after exposure to chitosan in the presence of ROS scavenger	82
Table 2.12. NO production in uninfected and <i>L. major</i> -infected BMMs after 4h of exposure to different concentrations of HMW chitosan at pH=6.5	83
Table 2.13. NO production in uninfected and <i>L. major</i> infected BMMs after exposure to chitosan in the presence of NO inhibitor at pH=6.5	85
Table 2.14. Phagocytosis and pinocytosis by <i>L. major</i> infected BMMs in the presence of the uptake inhibitors	88
Table 3.1. HPLC parameters for AmB quantification	108
Table 3.2. Conditions which did not produce good quality nanoparticles ..	109
Table 3.3. Effect of pH and concentration of chitosan and mass ratio of the reactants on the physicochemical properties of blank chitosan-TPP nanoparticles.....	113

Table 3.4. Effect of pH and concentration of chitosan and mass ratio of the reactants on the physicochemical properties of blank chitosan-dextran sulphate nanoparticles	114
Table 3.5. Effect of cryoprotectants used during freeze drying on the physicochemical properties of unloaded and AmB loaded chitosan nanoparticles.....	116
Table 3.6. Variations of physicochemical properties of AmB loaded chitosan-TPP nanoparticles in different media upon storage at different temperatures	121
Table 3.7. Variations of physicochemical properties of AmB loaded-chitosan dextran sulphate nanoparticles in different media upon storage at different temperatures.....	122
Table 3.8. Percentage of AmB loading, encapsulation and yield.....	123
Table 3.9. <i>In vitro</i> cumulative release of AmB from the two formulations at different conditions.....	125
Table 4.1. Disadvantages of different DDs (67, 112, 279, 280, 281, 282, 283, 284).....	135
Table 4.2. Antimicrobial activity of chitosan nanoparticles (285)	137
Table 4.3. Anti-leishmanial activity of AmB loaded chitosan nanoparticles	138
Table 4.4. <i>In vitro</i> haemolytic activity of chitosan formulations after 1h of incubation	152
Table 4.5. <i>In vitro</i> cytotoxicity of chitosan formulations against KB cells at two pH values after 72h of incubation	154
Table 4.6. <i>In vitro</i> activity of chitosan formulations against promastigotes at two pH values	158
Table 4.7. <i>In vitro</i> activity of chitosan formulations against intracellular amastigotes at two pH values	161
Table 4.8. Activity of chitosan formulations against <i>L. major</i> amastigotes in three different macrophage cultures after 72 h at pH of 6.5	164
Table 4.9. Flux, lag time and the permeability coefficient (kp) for AmB loaded chitosan nanoparticles	184
Table 4.10. Disposition of topically applied AmB loaded chitosan nanoparticles on healthy and <i>L. major</i> infected BALB/ c mice skin using Franz diffusion cells	185
Table 5.1. Specifications of QV500 and QV900 media perfusion system(340, 341, 342).....	201
Table 5.2. Phagocytosis of fluorescent latex beads (2 µm) by uninfected and infected PEMs, BMMs and THP-1 in static culture system.	207
Table 5.3. Phagocytosis of fluorescent latex beads (2 µm) by infected PEMs, BMMs and THP-1 in the three culture systems (static, slow flow rate 1.45×10^{-9} m/s and fast flow rate 1.23×10^{-7} m/s).	209
Table 5.4. Macropinocytosis of pHrodo™ Red dextran by uninfected and infected PEMs, BMMs and THP-1 in static culture system.	212
Table 5.5. Macropinocytosis of pHrodo™ Red dextran by infected PEMs, BMMs and THP-1 at the three culture systems (static, slow flow rate 1.45×10^{-9} m/s and fast flow rate 1.23×10^{-7} m/s).	215

Table 5.6. <i>In vitro</i> activity of chitosan solution and nanoparticles against <i>L. major</i> amastigotes in RPMI medium (pH=6.5) at different flow rates	217
Table 8.1. HPLC validation parameters	253
Table 8.2. The precision of AmB HPLC assay	254

1. General introduction

1.1. Leishmaniasis and *Leishmania* species

Leishmaniasis is an infectious disease caused by parasites belonging to the genus *Leishmania* in the family Trypanosomatidae. *Leishmania* parasites are transmitted to mammals through the bite of sandflies that belong to the genus *Phlebotomus* (Old World) or *Lutzomyia* (New World). *Leishmania* species cause two main clinical forms, cutaneous leishmaniasis (CL) and visceral leishmaniasis (VL) (1). CL is the most common type of leishmaniasis and in addition to “simple” CL, there are other complex cutaneous leishmaniasis manifestations including mucocutaneous leishmaniasis (MCL), diffuse cutaneous leishmaniasis (DCL), disseminated cutaneous leishmaniasis (DsCL) and leishmaniasis recidivans (LR) (1, 2). CL is caused by *Leishmania* species that are classified into Old World species, for instance *Leishmania major* (*L. major*), *L. tropica*, and *L. aethiopica* and New World species, such as *L. amazonensis*, *L. mexicana*, *L. braziliensis* and *L. guyanensis* (Fig 1.1) (3, 4). CL occurs in 88 countries and 90% of the cases are reported in Afghanistan, Brazil, Iran, Peru, Saudi Arabia and Syria (Fig 1.2) (1). Recently, a recrudescence has been noticed in Syria as a result of the destruction of the public health system and the lack of sanitation caused by the current conflict (5). Because of the displacement of Syrian people and the millions forced to flee the country, with the majority of them residing in Lebanon, Jordan, Egypt and Iraq, reporting of CL has increased across the region (6).

The clinical features of leishmaniasis depend on the parasite, the host and the vectors – Fig 1.2 shows an overview of the taxonomy of *Leishmania* species and the related clinical manifestations (Fig 1.1 and Table 1.1) (7).

- VL, also known as kala-azar (black fever), a potentially fatal illness which is characterised by irregular fever lasting for 14 days, the enlargements of spleen and liver, pancytopenia and weight loss. The incubation time for VL is between 2 weeks and 8 months and without treatment, the disease is typically fatal. One of the big challenges for

VL is the co-infection with HIV. VL is caused mainly by *L. donovani*, *L. infantum* and rarely by *L. tropica* (8).

- LCL is associated with an erythemic papule at the bitten site (1 -10 mm diameter) and then can lead to rounded ulcers combined with nodal or thick edges. These ulcers or lesions can stay from 5 months to 20 years. Lesions caused by *L. mexicana* are typically self-healing within 3-9 months, 6-15 months in the case of *L. braziliensis*, *L. tropica* or *L. panamensis* and within 2-6 months for *L. major* infections (8).
- DCL is uncommon anergic dissemination form of CL caused by *L. aethiopica*, *L. amazonensis* or *L. mexicana*. It begins with erythematous nodules resembling lepromatous leprosy and infiltrative plaques and then might ulcerate. DCL starts firstly on the face and subsequently affects other parts of the body and could affect the complete skin surfaces in some cases (8).
- MCL is caused by *L. braziliensis*, *L. guyanensis*, or *L. panamensis*. MCL is identified by invasive and destructive lesions of the mucosal membrane of the face, mouth and throat cavities. MCL is more frequent in immunocompromised patients (4).
- DsCL is caused by *L. aethiopica*, *L. guyanensis* and *L. mexicana*, spotted in Latin America and characterised by ten or more lesions (mixed type) located in two or more parts of the body.
- LR is caused by *L. tropica* and *L. braziliensis* and usually identified as new lesions around the old scar that has been cured and infiltrated with lymphocytes.

Status of endemicity of cutaneous leishmaniasis worldwide, 2016

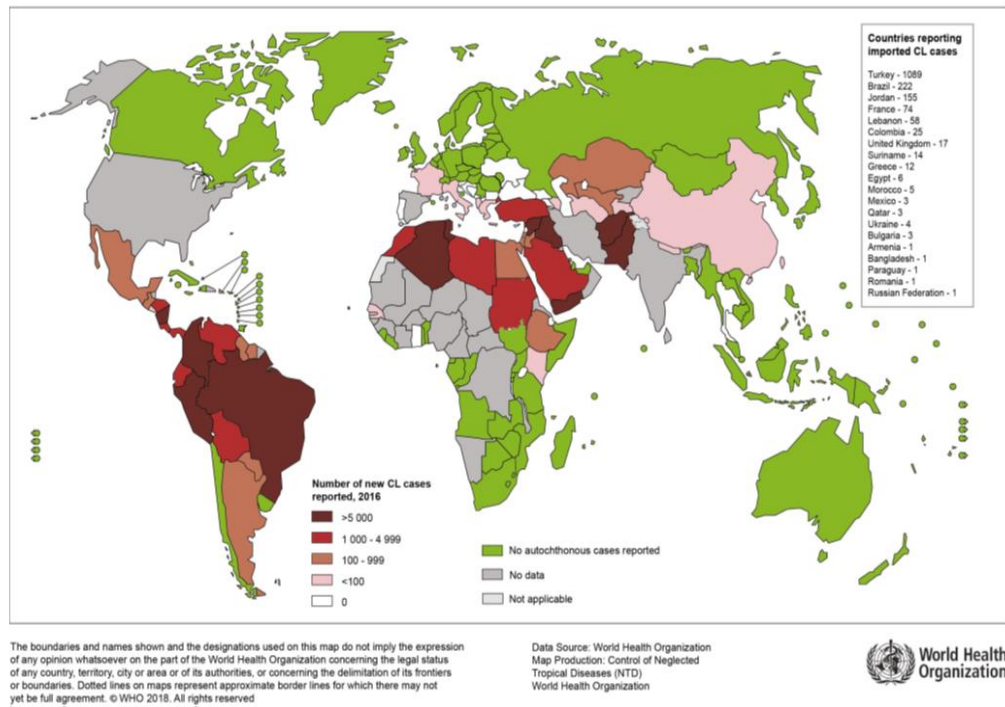


Figure 1.1. The distribution of cutaneous leishmaniasis WHO (9)

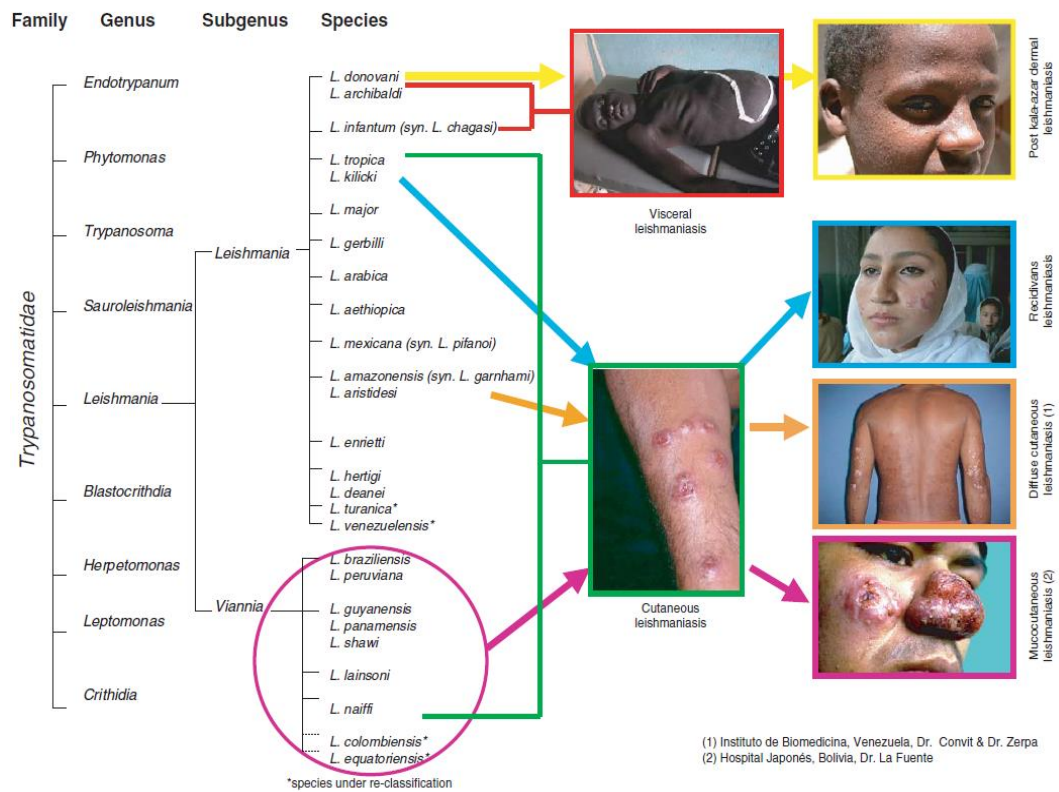


Figure 1.2. *Leishmania* species and related clinical manifestations (7).

Table 1.1. Clinical and epidemiological characteristics of the main *Leishmania* species copied from (4)

	Subgenus	Clinical form	Main clinical features	Natural progression	Risk groups	Main reservoir	High-burden countries or regions	Estimated annual worldwide incidence
<i>Leishmania donovani</i> *	<i>Leishmania</i>	VL and PKDL	Persistent fever, splenomegaly, weight loss, and anaemia in VL; multiple painless macular, papular, or nodular lesions in PKDL	VL is fatal within 2 years; PKDL lesions self-heal in up to 85% of cases in Africa but rarely in Asia	Predominantly adolescents and young adults for VL; young children in Sudan and no clearly established risk factors for PKDL	Humans	India, Bangladesh, Ethiopia, Sudan, and South Sudan	50 000–90 000 VL cases; unknown number of PKDL cases
<i>Leishmania tropica</i> *	<i>Leishmania</i>	CL, LR, and rarely VL	Ulcerating dry lesions, painless, and frequently multiple	CL lesions often self-heal within 1 year	No well defined risk groups	Humans but zoonotic foci exist	Eastern Mediterranean, the Middle East, and northeastern and southern Africa	200 000–400 000 CL
<i>Leishmania aethiopica</i> *	<i>Leishmania</i>	CL, DCL, DsCL, and oronasal CL	Localised cutaneous nodular lesions; occasionally oronasal; rarely ulcerates	Self-healing, except for DCL, within 2–5 years	Limited evidence; adolescents	Hyraxes	Ethiopia and Kenya	20 000–40 000 CL
<i>Leishmania major</i> *	<i>Leishmania</i>	CL	Rapid necrosis, multiple wet sores, and severe inflammation	Self-healing in >50% of cases within 2–8 months; multiple lesions slow to heal, and severe scarring	No well defined risk groups	Rodents	Iran, Saudi Arabia, north Africa, the Middle East, central Asia, and west Africa	230 000–430 000 CL
<i>Leishmania infantum</i> *	<i>Leishmania</i>	VL and CL	Persistent fever and splenomegaly in VL; typically single nodules and minimal inflammation in CL	VL is fatal within 2 years; CL lesions self-heal within 1 year and confers individual immunity	Children under 5 years and immunocompromised adults for VL; older children and young adults for CL	Dogs, hares, and humans	China, southern Europe, Brazil, and South America for VL and CL; Central America for CL	6200–12 000 cases of Old World VL and 4500–6800 cases of New World VL; unknown number of CL cases

	Subgenus	Clinical form	Main clinical features	Natural progression	Risk group	Main reservoir	High-burden countries or regions	Estimated annual worldwide incidence
<i>Leishmania mexicana</i> †	<i>Leishmania</i>	CL, DCL, and DsCL	Ulcerating lesions, single or multiple	Often self-healing within 3-4 months	No well defined risk groups	Rodents and marsupials	South America	Limited number of cases
<i>Leishmania amazonensis</i> †	<i>Leishmania</i>	CL, DCL, and DsCL	Ulcerating lesions, single or multiple	Not well described	No well defined risk groups	Possums and rodents	South America	Limited number of cases
<i>Leishmania braziliensis</i> †	<i>Viannia</i>	CL, MCL, DCL, and LR	Ulcerating lesions can progress to mucocutaneous form; local lymph nodes are palpable before and early on in the onset of the lesions	Might self-heal within 6 months; 2-5% of cases progress to MCL	No well defined risk groups	Dogs, humans, rodents, and horses	South America	Majority of the 187 200–300 000 total cases of New World CL‡
<i>Leishmania guyanensis</i> †	<i>Viannia</i>	CL, DsCL, and MCL	Ulcerating lesions, single or multiple that can progress to mucocutaneous form; palpable lymph nodes.	Might self-heal within 6 months`	No well defined risk groups	Possums, sloths, and anteaters	South America	Limited number of cases, included in the 187 200–300 000 total cases of New World CL‡

VL=visceral leishmaniasis. PKDL=post-kala-azar dermal leishmaniasis. CL=cutaneous leishmaniasis. LR=leishmaniasis recidivans. DCL=diffuse cutaneous leishmaniasis. DsCL=disseminated cutaneous leishmaniasis, MCL=mucocutaneous leishmaniasis. *Old World leishmaniasis. †=New World leishmaniasis. ‡Estimates are of all New World leishmaniases, with *Leishmania braziliensis* comprising the vast majority of these cases.

1.2. Life cycle

Many causative species for CL, have a zoonotic cycle¹ (*L. major*, *L. aethiopica*, and all the New World species), whilst few have an anthroponotic cycle² (*L. tropica*). Regarding the VL, humans are the main reservoir for *L. donovani* while dogs form the primary reservoir for *L. infantum*. The *Leishmania* life cycle starts when infected female sandflies (*Phlebotomus* species in the Old World, *Lutzomyia* species in the New World) bite their hosts and inject parasites (the infective metacyclic promastigote form) into the skin of a mammalian host (a sand fly injects 100-1000 promastigotes). Sandflies salivary chemoattractants enhance the flow of macrophages, dendritic cells (DCs) and neutrophils to the biting site. These promastigotes are then phagocytised by resident phagocytes. After which, promastigotes transform in these cells into amastigotes which replicate by simple division in the parasitophorous vacuole and infect other macrophages, either locally or in remote tissues (1, 4). Neutrophils play a critical role in leishmaniasis by acting as Trojan horses for *Leishmania* promastigotes before entering their target cells (macrophages). *Leishmania* survive in the neutrophils by inhibiting the phagosome acidification. *Leishmania* promastigotes directly infect DCs and reside within parasitophorous vacuoles. In macrophages, promastigotes are interlined into phagolysosome like compartment, named the *Leishmania* parasitophorous vacuole. The maturation of parasitophorous vacuole is regulated by *Leishmania* parasites to protect them from destruction by the macrophage microbicidal activity and to avoid the host immune defence responses (9, 10, 11)

Female sandflies become infected when they feed on an infected host and amastigotes transform into promastigotes in the midgut of the sandfly and then migrate to salivary glands and transform into infectious metacyclic promastigotes (Fig 1.3) (1, 12).

¹ In zoonotic cycles: animals are main reservoirs

² In anthroponotic cycles: humans are main reservoirs

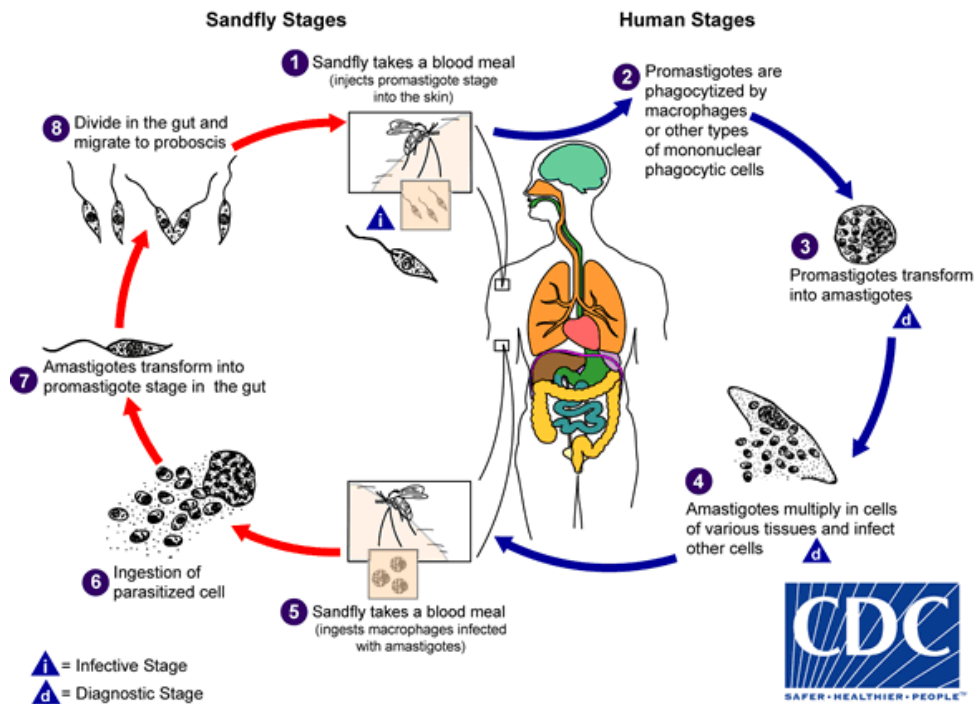


Figure 1.3. The life cycle of *Leishmania* parasites (13).

1.3. Immune response in CL

The cellular immune responses play a critical role in the control or progress of cutaneous leishmaniasis and have been widely studied in mouse models, often using *L. major*. Progressive lesions have been developed in susceptible mice (BALB/c mice) with a dominance of the Th2 response, leading to the production of anti-inflammatory cytokines, such as IL-4, IL-5, and IL-13, which suggests that Th2 cells are associated with develop progressive lesions. On the other hand, resistant mice (C57BL/6 and C3H/HeJ mice), infected by *L. major*, present small lesions with few parasites and a dominance of the Th1 response, with the production of IFN- γ , TNF- α and IL-12. These cytokines activate macrophages to produce reactive oxygen species (ROS) and nitric oxide (NO), which are responsible for killing intracellular parasites as seen in Fig 1.4 (14, 15, 16). In humans, resolution from cutaneous leishmaniasis is recognized by induction of specific IFN- γ releasing CD4⁺ T cells (17, 18). The response in individuals with moderate CL caused by *L. major* is a mixture of Th1 and Th2. There is an absence of a Th1 response in individuals with severe CL (17, 18).

To conclude, the control of CL is linked with *Leishmania*-specific T lymphocytes producing TNF- α and IFN- γ and this enhances macrophages in the skin to produce microbicidal materials (NO and ROS). It is obvious from Fig 1.5 that, the balance between pro- and anti-inflammatory factors controls the consequence of CL infection (19).

The functions of B cells are still a matter of debate. Several studies suggest that these cells enhance the *Leishmania* infection while some state that B cells have a protective function against *L. amazonensis* (20).

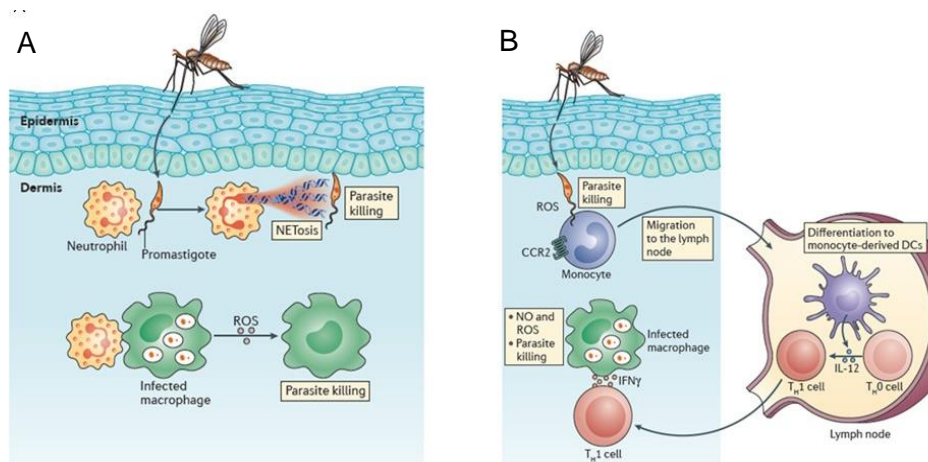


Figure 1.4. Immune response against leishmaniasis. A: neutrophils play an important role during the early stage of infections. B: the essential role of monocytes in killing *Leishmania* and promoting the differentiation of Th-1, which leads to the elimination of parasites (16)

1.4. Current treatment of cutaneous leishmaniasis

CL lesions can heal spontaneously in most cases within 2-18 months. Infection is not usually fatal but can cause considerable cosmetic morbidity, psychological disorders, social stigma leading to changes in individual self-esteem (4, 8). The important goal of making the decision to treat CL is to eradicate the *Leishmania* parasites and enhance the lesion healing process. This will reduce the risk of scarring and help to lower the risk of dissemination or progression other forms of more severe CL.

Other criteria to commence treatment includes the presence of many lesions (more than 5), large size (>4 cm), location over sensitive body areas such as the face, or lasting for more than 6 months and/or in Immunosuppressed patients (Table 1.2) (4, 21). The Infectious Diseases Society of America recently published comprehensive treatment guidelines for the management of CL according to the clinical characteristics, summarised in Table 1.2 (22).

Table 1.2. Clinical features of New World CL that might modify management copied from (23)

Simple CL	Complex CL
Caused by a <i>Leishmania</i> species unlikely to be associated with mucosal leishmaniasis	Caused by a <i>Leishmania</i> species that can be associated with increased risk for ML, particularly <i>Viannia</i> spp in the “mucosal belt” of Bolivia, Peru, and Brazil ^{a,b,c}
No mucosal involvement noted	Local subcutaneous nodules ^d
Absence of characteristics of complex CL	Large regional adenopathy ^d
Only a single or a few skin lesions	>4 skin lesions of substantial size (eg, >1 cm)
Small lesion size (diameter	Large individual skin lesion (diameter ≥5 cm)
Location of lesion feasible for local treatment	Size or location of lesion such that local treatment is not feasible
Nonexposed skin (ie, not cosmetically important)	Lesion on face, including ears, eyelids, or lips; fingers, toes, or other joints; or genitalia
Immunocompetent host	Immunocompromised host (especially with respect to cell-mediated immunity)
Lesion(s) resolving without prior therapy	Clinical failure of local therapy
	Unusual syndromes: leishmaniasis recidivans, diffuse CL, or disseminated CL
<p>Abbreviation: CL, cutaneous leishmaniasis.</p> <p>^a The highest risk areas for mucosal leishmaniasis (ML) are south of the Amazon basin in parts of Bolivia, Peru, and Brazil (defined here as the “mucosal belt”). Moderate-risk areas are south of Nicaragua to the Amazon basin. Low-risk areas for ML are in New World CL (<i>Viannia</i>)–endemic regions north of Costa Rica. Amazonian basin regions up to an altitude of approximately 2000 meters are referred to as increased ML-risk regions.</p> <p>^b <i>Leishmania</i> species with an increased risk of causing ML include <i>L. (V.) braziliensis</i> mainly, but also <i>L. (V.) guyanensis</i> and <i>L. (V.) panamensis</i>. There are other species that can be associated with ML less frequently. In this document, we refer to these 3 species as “increased ML-risk species.” Geographic regions in which there is an increased risk for ML are defined above.</p> <p>^c High therapeutic failure rates after treatment with pentavalent antimonial drugs have been observed in CL acquired in Amazonian Bolivia (eg, Madidi National</p>	

Park) and southeastern Peru (eg, Manu National Park and Puerto Maldonado). Poor efficacy after using miltefosine in the treatment of *L. (V.) braziliensis* was reported in Guatemala.

^d It is somewhat controversial whether the presence of small subcutaneous nodules is always associated with complex CL, but certainly complex CL applies if bubonic-like adenopathy is present in regional drainage area of lesions. These findings have been linked to complications or treatment failure when only local treatment is administered. Some experts would not consider systemic therapy needed for a few, small subcutaneous nodules in Old World CL

Treating CL can include (i) chemotherapy (anti-leishmanial drugs that kill the parasites directly) (ii) local physical methods (cryo- or thermotherapy), (iii) immunotherapy (by immune modulators for stimulating effective immune response against *Leishmania* parasites) (Fig 1.5) (24).

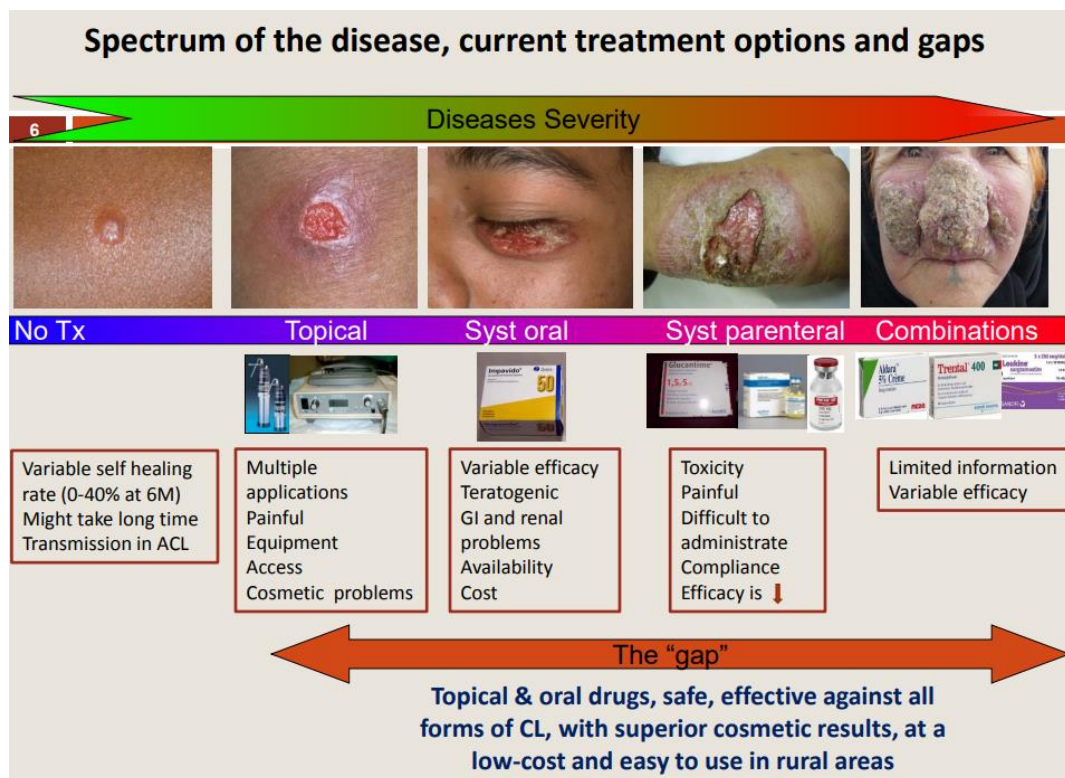


Figure 1.5. Strategies for treatment of CL and the related limitations. Syst=systemic. Tx= treatment. ACL=asymptomatic CL (25).

1.4.1. Systemic therapies

1.4.1.1. Pentavalent Antimony

Pentavalent antimony (SbV) compounds like sodium stibogluconate (SSG, Pentostam®, GSK, contains 100 mg/ml of SbV) and meglumine antimoniate (Fig 1.6) (MA, Glucantime®, Sanofi, contains 85 mg/ml) have been the standard therapy for CL since they were developed in the 1940s (26, 27). The severity of CL can determine the routes of administration (locally or systemically). In local treatment, SbV (1-5 ml) is administered by injection (1-5 times every 3-7 days for up to 5 sessions) in lesions edges with or without cryotherapy (application of liquid nitrogen after the injection) (28, 29). The parenteral route includes intravenous or intramuscular administration of 20 mg/kg/day of SbV, typically in the case of complex CL (28). Intralesional administration benefits include making a high enough concentration of the drug at the site of infection, reduced costs, limiting the systemic side effects and faster healing time (30). However, the problems with this route includes the difficulty of administration, pain of these injections, sensations of burning, itching and sometimes the appearance of inflammation in the location of the injections (31). On the other hand, parenteral injections can lead to adverse side effects (hepatotoxicity and cardiotoxicity) (32). There is a lack of placebo-controlled randomized clinical trials to compare the activity of SbV therapy against specific species of CL (31). Variability of the sensitivity of *Leishmania* (promastigotes and intracellular amastigotes) species to SbV has been confirmed *in vitro* (33, 34).

There is still no clear definition of the mechanism of the action of SbV, in spite of these drugs being used for several decades. One of the suggested mechanisms is that SbV is converted after administration to the trivalent form (SbIII) which is the active but more toxic form. This trivalent antimony (SbIII) intervenes with the trypanothione reductase system that protects the *Leishmania* amastigotes from the harm caused by the oxidation and toxicity of heavy metals (35, 36). Others suggested that SbIII can cause *Leishmania* apoptosis by fragmenting DNA of amastigotes (37, 38). A third mechanism has

suggested that SbV interacts with adenine ribonucleoside and produces a complex that causes a depletion of intracellular ATP and the prevention of macromolecule synthesis in amastigotes by inhibiting type I DNA topoisomerase (32, 39).

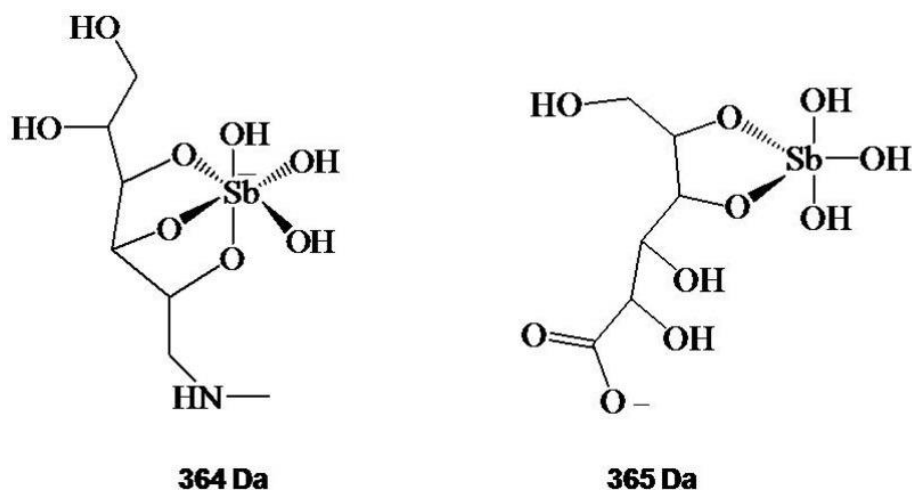


Figure 1.6. Proposed structural formula for 364 Da and 365 Da ions identified by ESI(-)-MS in aqueous solutions of meglumine antimoniate and stibogluconate, respectively, copied from (40)

1.4.1.2. Miltefosine

Miltefosine (MF), an alkylphospholipid, was developed as an antineoplastic agent (for cutaneous cancers). Croft *et al* in 1987 showed the anti-leishmanial activity of miltefosine and other phospholipid compounds (1). MF is recommended for VL and complex cases of CL and considered as the only effective drug that can be given orally for leishmaniasis treatment. The effective dose for CL is a daily oral dose 2.5 mg/kg for 28 days (1, 41).

However, different *Leishmania* species show significantly different sensitivity to MF (42). Randomized clinical trials have been conducted in different regions against different species with various clinical responses. For instance, in Colombia the cure rates against *L. panamensis* were 91% in comparison to 38% for placebo group (43). While the cure rates were just 53% in Guatemala

against *L. mexicana* and *L. braziliensis* compared to 32% in placebo treatment (43). *In vitro* studies confirmed the species variation in MF sensitivity (44). The two major concerns about this drug is that, (i) MF is a teratogenic agent and so cannot be given to women who are pregnant and (ii) the presence of resistance development *in vitro* (42). Some common side effects of MF treatment are gastrointestinal discomfort, renal disorders, headache and raised liver enzymes (45).

The mechanism of action of MF remains unclear. Different mechanisms have been suggested such as the inhibition of synthesis of phospholipids, interaction with the parasite membrane, dysfunction of mitochondria or stimulation of apoptosis-like cell death (46, 47, 48, 49).

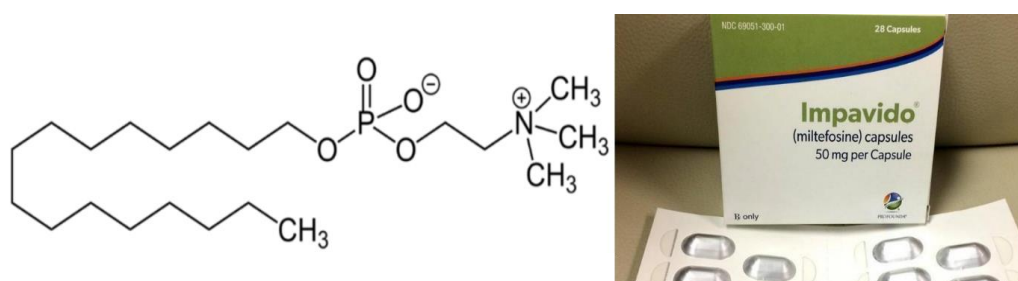


Figure 1.7. Chemical structure of miltefosine (50)

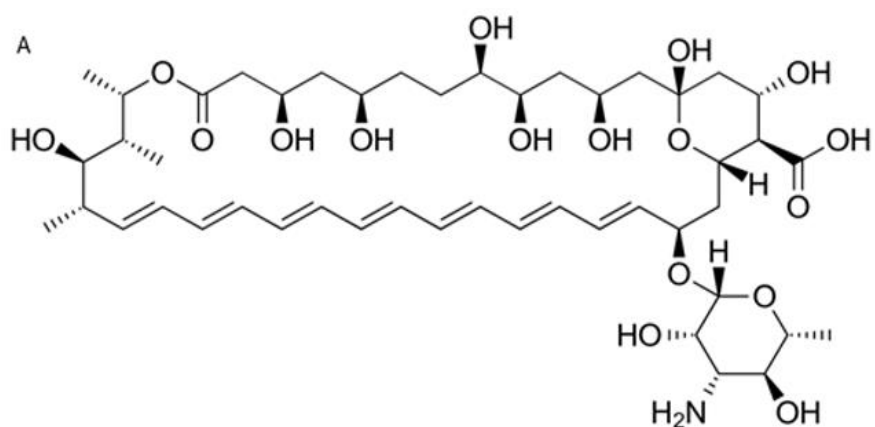
1.4.1.3. Amphotericin B (AmB)

The second most common treatment for leishmaniasis is amphotericin B, which is a polyene antibiotic (Fig 1.8), mainly used for VL and MCL (51). The therapeutic dose of AmB deoxycholate (Fungizone) is 0.7 mg/kg/day by slow intravenous infusion for 25-30 days or 2-3 mg/kg/day of liposomal formulations for 10-15 days (28). In 1950s, AmB was firstly noted and derived from *Streptomyces nodosus*. Sodium deoxycholate solution of AmB (DAmB, Fungizone) was brought to the market in 1959. Fungizone has been used intravenously as a standard treatment for invasive fungal infections for several decades. Fungizone has serious side effects such as nephrotoxicity and fever, anaemia, malaise and abdominal pain (52).

Several lipid formulations, including liposomal amphotericin B (AmBisome®), amphotericin B lipid complex (Abelcet®), and amphotericin B colloidal

dispersion (Amphocil™) have been developed and used in treatment of VL to reduce the previous toxicities since 1990s (53). AmBisome® (liposomal amphotericin B, LAmB; Gilead Sciences, Dimas, CA, USA) has been approved by the Food and Drug Administration (FDA) for treatment of VL in 1997 with 7 intravenously doses of 3 mg/kg/day over 21 days (54). Yardley and Croft (2000) found that AmBisome® (liposomal amphotericin B) was also successful in reducing the size of lesions in CL caused by *L. major* in BALB/c mouse model (55). The high cost of these formulations (up to 250 USD\$ per vial) prevents more widespread use (56, 57). Recently there is an agreement between WHO and Gilead Sciences for the donation through WHO of AmBisome® vials for VL treatment (58). Other problems related to AmBisome® were reported in a study with a low positive outcome of 63% among travellers infected with CL and MCL coming back from both Old- and New-World countries and 53% of these treated patients showed renal toxicity and infusion-related reactions (59) and higher rates of relapse were noticed in immunocompetent patients with VL treated with AmBisome® (60, 61).

Amphotericin B acts by forming a complex between its hydrophobic polyene region and the ergosterol in the plasma membrane of *Leishmania* or fungi which causes transmembrane channels, after which a death of the microbe is induced by the collapsing of ion gradient (62, 63). Recently, an alternative mode of action has been suggested, that AmB primarily exists as large, extra-membranous aggregates that results in the removal of ergosterol from the lipid bilayer leading to microbe death (64). Additionally, reports claim that AmB has immunomodulatory effects and stimulates oxidative stress in immune cells (52, 65, 66).



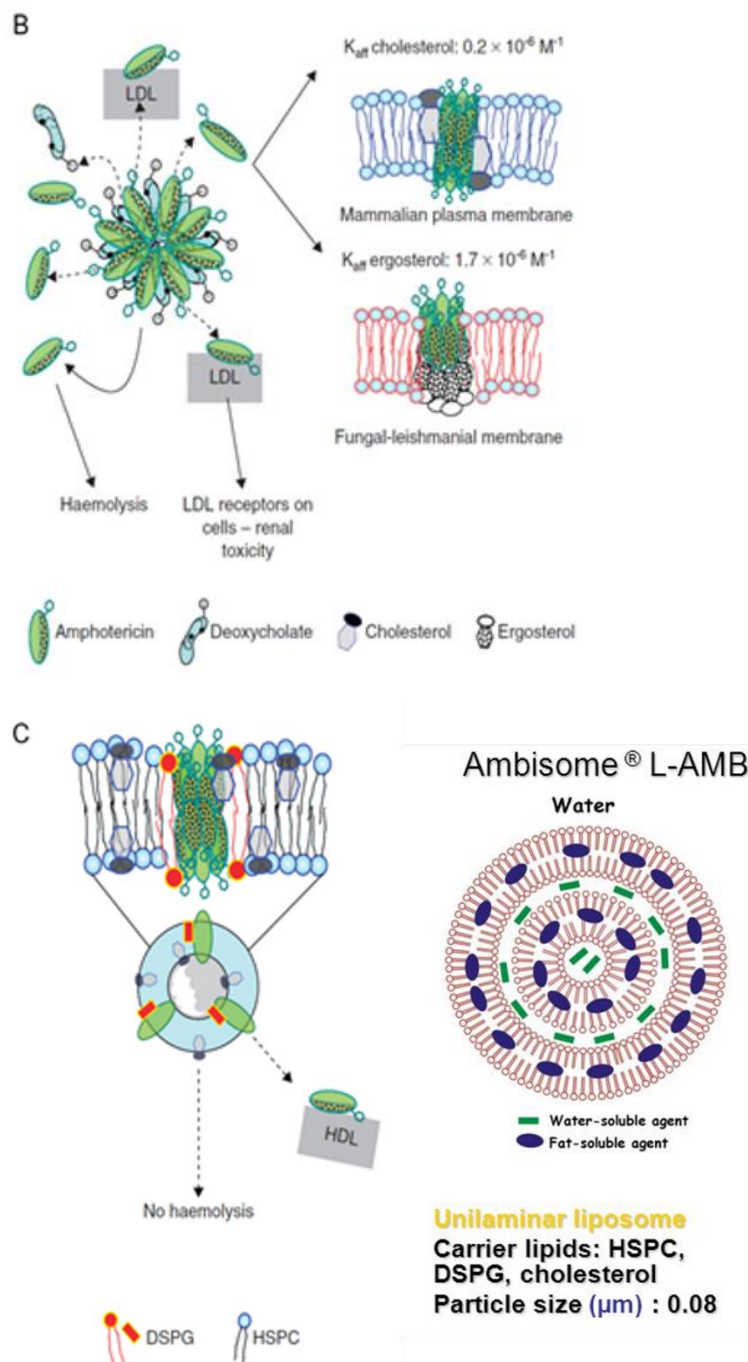


Figure 1.8. Chemical structure of amphotericin B (A), Fungizone (B) and AmBisome® (C) (67)

1.4.1.4. Pentamidine

Pentamidine is, an aromatic diamidine, as effective as antimonial drugs for healing CL caused by *L. panamensis* or *L. guyanensis* (30, 57). The cure rates of parenteral pentamidine with 7 doses of 2 mg/kg for 14 days vary from 35% to 95% (1). This drug offered significant advantages such as shorter duration

of the therapy and lower costs in comparison with other drugs for CL (68) but is rarely used due to low cure rates and significant side effects of diabetes, myocarditis and nephrotoxicity (69).

The mode of action is not completely clear but interference with *Leishmania* DNA and disruption of mitochondrial membrane have been suggested (70).

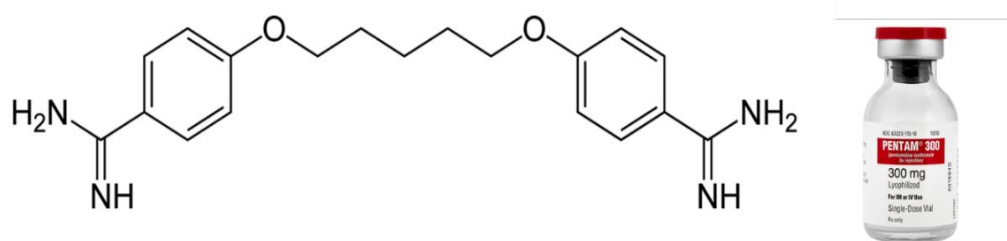


Figure 1.9. Chemical structure of pentamidine (71)

1.4.1.5. Azoles

Azoles are antifungal agents, which also have an anti-leishmanial activity because they inhibit the 14 α -demethylation of lanosterol and this inhibition leads to an accumulation of 14 α -methyl sterols and blocks ergosterol synthesis of *Leishmania* parasites (72). The most important azoles that are active against *Leishmania* parasites are fluconazole, ketoconazole and itraconazole which have been used orally with different results against CL. The effectivity of ketoconazole, with the oral dose 8 mg/kg/day for 4 to 6 weeks, was 76–90% in CL caused by *L. panamensis* and *L. mexicana* in Guatemala and Panama (28). However, in a clinical trial in Colombia, itraconazole (oral dose 200 mg twice daily for 28 days) was ineffective against CL caused by *L. panamensis* (73).

Fluconazole has important properties including a longer half-life and increased concentrations in cutaneous tissues. In *L. major* infections, there was a good evidence of the benefit for the use of 200 mg oral fluconazole for 6 weeks (31). A study in Saudi Arabia showed cure rates 79% in CL caused by *L. major* after 6-weeks of 200 mg daily of oral fluconazole (74). An important advantage of

azoles is the ease of administration via the oral route. However, these drugs have many side effects such as the low cure rates, hepatotoxicity and gastrointestinal symptoms (72).

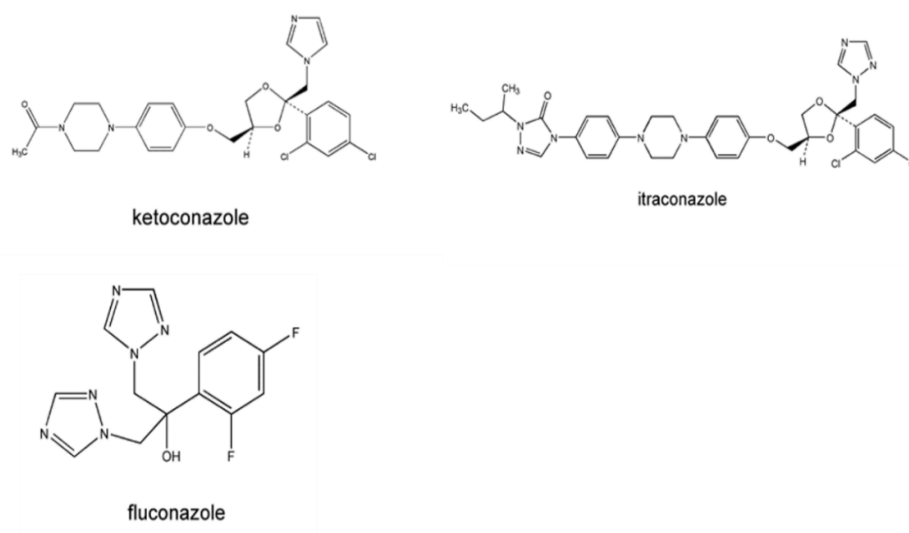


Figure 1.10. Chemical structure of some azoles(75)

1.4.2. Local therapy

1.4.2.1. Paromomycin

Paromomycin (PM) is an aminoglycoside antibiotic (Fig 1.11) and was identified as an anti-leishmanial drug in the 1960s. The sulphate salt of PM is given parenterally to treat VL, e.g. 11 mg/kg/day intramuscularly for 21 days. A topical formulation of paromomycin sulphate 15% plus 12% methylbenzethonium chloride (MBCL) ointment has been used for LCL by applying twice daily for 20 days (28, 76). Topical 15% PM + 12% MBCL was active in BALB/c mice infected with New World species (*L. mexicana*) but did not show activity against *L. panamensis* and *L. amazonensis* (77).

Different formulations with a lower skin irritancy including one containing 15% paromomycin with 0.5% gentamicin gave cure rates of 81-82% for CL caused by *L. major* and 80% in Panama for CL caused by *L. braziliensis* and *L.*

panamensis in phase 3 studies. However, these results compared with a placebo cure rate of 58%, and almost no difference between formulations combining paromomycin and gentamicin or paromomycin alone (4). Paromomycin has low cure rates against certain *Leishmania* species and in many cases, relapse can be found during the first year (30, 46).

The exact mechanism of PM against *Leishmania* parasites is not fully known, studies suggest PM inhibits protein synthesis by blocking the dissociation of ribosomal subunits (78) , others suggest that PM alters leishmanial lipid metabolism leading to the arresting of growth (79).

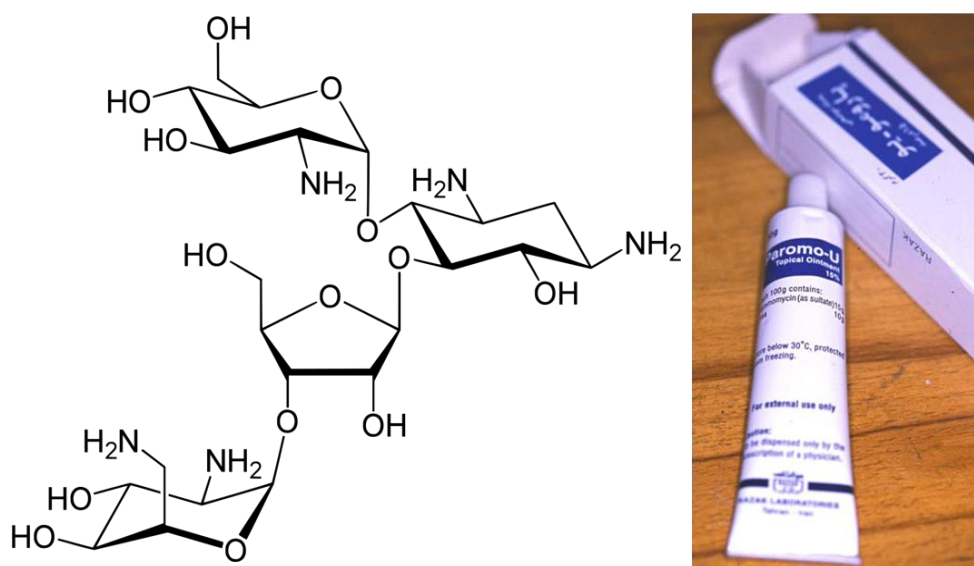


Figure 1.11. Chemical structure of paromomycin(71)

1.4.2.2. Physical treatments

Physical methods such as, localised heat or cryotherapy have been used in the treatment of CL. Localized heat is performed by using a device (e.g. Thermomed®) which provides a focused heat on the lesion (50°C for 30 seconds once per week for one month) and this method demonstrates about 69% overall efficacy against CL (1, 80). Cryotherapy is the use of liquid nitrogen to freeze lesions, repeated on three separate days. The efficacy of this procedure is about 57% against *L. major*. The benefits of localised heat or

cryotherapy methods are the ease of use and the safety. The problems with these methods include the low cure rates, the need for expensive equipment, and availability of electricity in rural areas (1). A comparison of the effects of three different therapies for CL was done in Iran: intralesional meglumine antimoniate or cryotherapy (liquid nitrogen (-195°C)) or a combination of these two methods. They found that combining both MA and cryotherapy gave a significant higher activity than the two monotherapies (81, 82).

1.4.3. Immunomodulatory treatment

The immune response plays an important role in the control of CL - cure depends upon the activation of macrophages to produce toxic nitrogen and oxygen metabolites to kill the intracellular amastigotes (83). Consequently, immunomodulators for CL and VL have been studied widely for many years either alone or in combination with other drugs (84). For example, 11532 Venezuelan patients with American cutaneous leishmaniasis were treated with a combination of an immunomodulator (heat killed *Leishmania* promastigotes and bacille Calmette-Guérin (BCG)) and chemotherapy (meglumine antimoniate). Cure rates of 91.2 to 98.7% were achieved (85).

Examples of other clinically used immunomodulators include:

- Imiquimod: an antiviral compound [1-(2-methylpropyl)-1H-imidazo (4, 5-c) quinolin-4-amine] used topically for the treatment of genital warts, caused by the human papillomavirus, via the stimulation of localised immune response. Macrophages are activated to produce cytokines and nitric oxide at the site of application (76). Many studies have shown that imiquimod has anti-leishmanial activity. A randomized, double-blind clinical trial in Peru showed that patients with CL treated with 5% Imiquimod cream in combination with meglumine antimonate therapy showed faster lesion cure in comparison with those received meglumine antimonate with placebo vehicle cream therapy
- Pentoxifylline: Pentoxifylline is a methylxanthine derivative that inhibits $\text{TNF-}\alpha$ and decreases tissue inflammation. A clinical study showed that patients with CL caused by *L. braziliensis* who received a combination of

pentoxifylline plus SbV had higher cure rates than in those receiving antimony plus placebo (86, 87).

- A topical immunomodulator which is cytokine granulocyte-macrophage colony stimulating factor (GM-CSF) was found to accelerate the lesion healing in CL patients (88).

1.5. Challenges for CL treatment

CL is classified as a neglected tropical disease (NTD). NTDs have been described by the WHO as a varied group of diseases that have an impact on more than one billion people and dominate in 149 countries in tropical and subtropical conditions. These diseases are commonly associated with poverty and cause a huge economic and health burden in low- and middle-income countries (89, 90).

Many factors form a challenge for CL treatments. CL happens in tropical areas with high temperatures, humidity and without cold chains and these conditions affect the stability of drug formulations for CL and even for other diseases (91). For example, AmBisome® requires a cold chain to protect its activity and a consistent supply of electricity is often difficult in rural regions. Moreover, some patients live in remote areas and are unable to access treatment easily. Availability of medicine(s) is also a challenge (92). Besides that, WHO estimated the cost of CL treatment to be between 12-40 USD\$ per patient (28), this cost is prohibitive for many as the monthly income in many CL-endemic areas is only 7-17 USD\$ /per person (28). Additionally, a delay between recognition of CL and starting the treatment increases the possibility of lesion progression to an ulcer with subsequent treatment complications and scarring (93, 94).

1.6. Assays to test the anti-leishmanial activity of drugs

The existing predictive models to study the anti-leishmanial activity of compounds are classified into *in vitro* and *in vivo* assays.

1.6.1. *In vitro* assays

These models are classified as either promastigote, axenic (extracellular) amastigote or intracellular amastigote assays.

The advantages of using promastigote and axenic (extracellular) amastigotes are higher-throughput, cheaper, quicker and more straightforward screening. However, the drawbacks encompass that promastigotes are significantly different from intracellular amastigotes (target form in mammals resides within the macrophages of the dermal skin layer) in terms of metabolism and ecology. Moreover, these promastigotes grow at 26°C and this could affect the anti-leishmanial action of drugs while *in vivo* temperature of 37 °C (34 °C skin temperature) (95, 96). The axenic amastigotes test is semi – predictive as it does not examine the penetration of the compound into the host cell and does not reflect the activity of the compound in the host environment and accordingly, is prone to false positive and negative results (95, 97).

On the other hand, the intracellular amastigote test (infected macrophages) is the gold standard model. In this model, macrophages can be derived from a range of sources, for example murine peritoneal macrophages (PEMs) or murine bone-marrow macrophages (BMMs), or chemically differentiated from human cancer cell lines (THP-1) (71).

The activity of tested drugs is evaluated by exposing infected macrophages to particular concentrations of the drug for a specific period (such as 2, 3 or 5 days), and then stained with Giemsa after fixation with methanol. Activity is measured by either microscopical counting of number of amastigotes per macrophage or the percentage of infected macrophages (containing at least one parasite) (% infection). The selections of new compounds as anti-leishmanial depend on the 50 % and 90 % effective concentrations (EC₅₀, EC₉₀) after comparison with an untreated control and a positive control drug (95, 97).

In addition, there are more *in vitro* methods used to test the anti-leishmanial activity of drugs are summarised in Table 1.3 with positive and negative points for each assay.

Table 1.3. *In vitro* screening models with positive and negative drawbacks copied from (97).

<i>In vitro</i> models	Merits	Demerits
Promastigote	Rapid method and very little amount of test compounds are required for screening.	Not relevant life cycle stage for mammalian leishmanial infection. Data correlation with amastigote screening is unreliable.
Axenic amastigotes	Test is direct on relevant stage of the parasite.	The assay is semi – predictive.
	This stage is as easy to manipulate as the promastigotes.	It neither tests for penetration of compound into host cell nor for activity in peculiar environment of the macrophage phagolysosome
	Quantification of drug activity is simple and often inexpensive.	Different metabolic processes than intracellular amastigotes. Screening of axenic amastigotes from clinical isolates is not possible as they require time to get adapted in the cultures.
Intracellular amastigotes	Effective screening method.	Labour intensive and subjective.
	Mimic the environment encountered by the target cell.	Provide an approximation of the macrophages that are counted. Rendered difficult the screening of several drugs at a time and incompatible with HTS.
	Shows the effect of drug mediated toxicity on host cell.	
Reporter gene assays: (GFP) Green fluorescent protein	Simple	Fluorescence intensity in parasites decreased with time in the absence of geneticin sulphate (antibiotic G 418), thereby necessitating its regular addition.

	Easier kinetic monitoring.	Application for drug-drug screening is limited to promastigotes.
	Low cost and enhanced biosafety.	
β -galactosidase	Colorimetric detection can be performed	Large size (the monomer is 116 kDa). Low sensibility. Endogenous expression of β -galactosidase by some mammalian cell types including macrophages.
β -lactamase	Simple colorimetric β -lactamase assay for quantifying <i>Leishmania</i> amastigotes grown in micotiter plates. High-level stable expression of the enzyme	Not very sensitive.
Luciferase	The method is rapid. Very sensitive. Highly reproducible. Does not require any very specialized instrument or training. Detection of only live, metabolically active cells by biophotonic imaging. Absence of background activity in the host cell. Compatible with HTS.	Luminescent read out transient. Mixing of the samples and reagents needs to be timed with entering samples into the luminometer.
HTS, high throughput screening		

These *in vitro* screening models have a major drawback related to their lack of biological relevance - they involve traditional cell culture methods (static and two-dimensional culture systems). Static cell culture systems that use the micro well plates are widely used. However, cells in human and animal tissues are sensitive to their microenvironment and face different mechanical stimulants due to interstitial flow and nutrient diffusion. Static cell culture systems are unable to provide these mechanical and physical factors arguably significantly limiting the cellular response *in vitro* (98, 99). Dynamic culture systems have the potential to overcome these limitations and better mimic the *in vivo* situation for drug discovery process (100) .

1.6.2. *In vivo* assays

Different animal models (summarized in Table 1.4) are used to evaluate the effectiveness of drugs against leishmaniasis. These models imitate some of the pathological features and immunological responses shown in humans when exposed to *Leishmania* infections. *In vivo* assays allow the determination of drug activity in association with drug administration, excretion, and distribution. They can identify adverse events (toxic side effects) resulting from a particular treatment (101, 102). Murine models are widely used to evaluate the effectiveness of new drugs against leishmaniasis and to study the pathogenesis of this disease. *L. major*-BALB/c is the most used, with high reproducibility, and relatively fast progress of skin lesions (within 3 weeks). In this model, only potent drugs show anti-leishmanial efficacy as self-healing of CL is rare due to the immunological incapability of BALB/c mice (97, 101, 102).

The anti-leishmanial activity of compounds in the animal model is typically determined by a reduction of lesion size compared to untreated controls. However, inflammation plays a key role in lesion size. Therefore, size alone does not accurately reflect the anti-leishmanial activity. An additional indicator of therapeutic effect, e.g. determination of parasite burden should be considered. This can be achieved by different assays such as quantitative polymerase chain reaction (qPCR) or *in vivo* imaging (semi-quantitative) of bioluminescent parasites (97, 101, 102). A Therapeutic Index (TI) is often used to express the window between the required effective dose and the toxic/lethal doses of the drug (ED₅₀/LD₅₀) (95, 97).

Table 1.4. *In vivo* models for leishmaniasis copied from (97)

Animal Species	Examples	Main strength
Mice	BALB/c	Immunology, Vaccines, Chemotherapy
	C57BL/6	Negative model-Immunology, Vaccines, Chemotherapy
	Transgenic mice	Immunology
Hamster	Syrian golden hamster	Pathology, Chemotherapy

Dogs	Different breeds	Pathology, Vaccines, Chemotherapy
Non-human primates	Langurs, Monkeys - vervet, rhesus, owl, mandrills, baboon, marmoset, squirrel	Vaccine, Pathogenesis, Chemotherapy, Pathology

1.7. Drug development for CL: from pipeline to patients

The currently available drugs for CL have some drawbacks such as, low cure rates, toxicity, and high costs. These limitations clearly highlight the need for short, safe, efficacious, affordable and field-adapted treatments against *Leishmania* parasites (84). The process of developing and discovering new drugs is long, slow, expensive and challenging (Fig 1.12). For example, screening 100,000 compounds can lead to just one compound from a research and development (R&D) pipeline to a marketed drug and may take more than 10 years with an estimated expenditure around 2.6 billion USD\$ (87). NTDs are generally considered commercially unattractive for Pharma research and development (R&D) (103) (81). In the last 40 years, only few new drugs have been developed for NTDs despite the great knowledge in the field of NTDs (88). NTDs usually involve populations with low purchasing power in low income countries - not a monetary incentive for the private sector to develop new therapies. Publication is typically the end of the line for NTD R&D or at other stages in the drug development pipeline (Fig 1.13) (88).

Nonetheless, there has been a considerable moving forward in VL treatment and in the developing of new drugs of this disease. In contrast, no great attentions have been paid for CL drugs development (more details later) (90).

One of the strategies to overcome the high cost and long time lines of developing a new drug or chemical entity is “drug repurposing” (90). In this strategy, a known drug for a specific target is tested against different diseases. The drug has already been tested for toxicity, and other pharmacokinetic and pharmacodynamic studies have already been carried out, all in relation to its original indication. This can save time and money. As a result, getting a drug

to market can take less time. For instance, three drugs have been repurposed and used clinically for leishmaniasis; AmB was originally developed for fungal infections, paromomycin was primarily used for amoeba infections as an oral drug, and miltefosine was developed as an anti-cancer treatment (104, 105). Many researchers, worldwide, have identified a large number of compounds that show anti-leishmanial activity, either via re-purposing (tamoxifen, nelfinavir, imipramine, delamanid, fexinidazole) or isolating new chemical entities (NCEs) from natural sources (quinones, pyrimidines) (90). Another strategy is optimising the drug by reformulation of the active ingredient in the current drug or by using drug delivery systems for currently active drugs (more details later) (104, 105, 106).

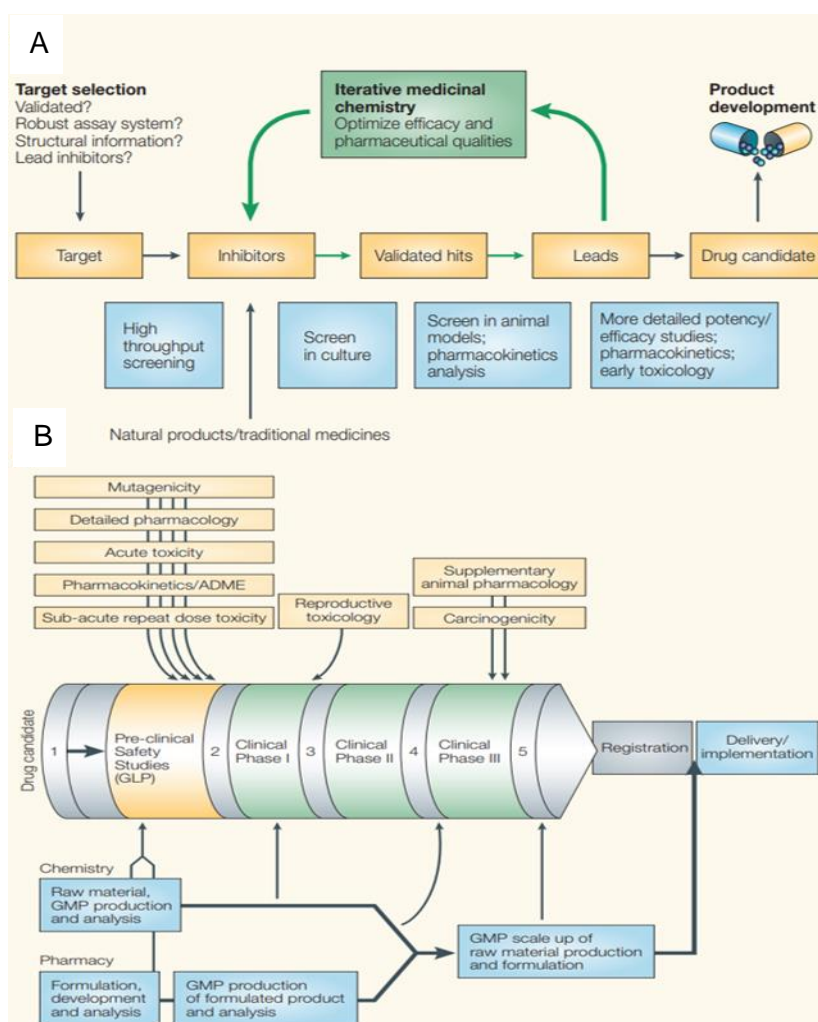


Figure 1.12. The process of drug discovery and drug development. a) drug discovery stages b) drug development (107)

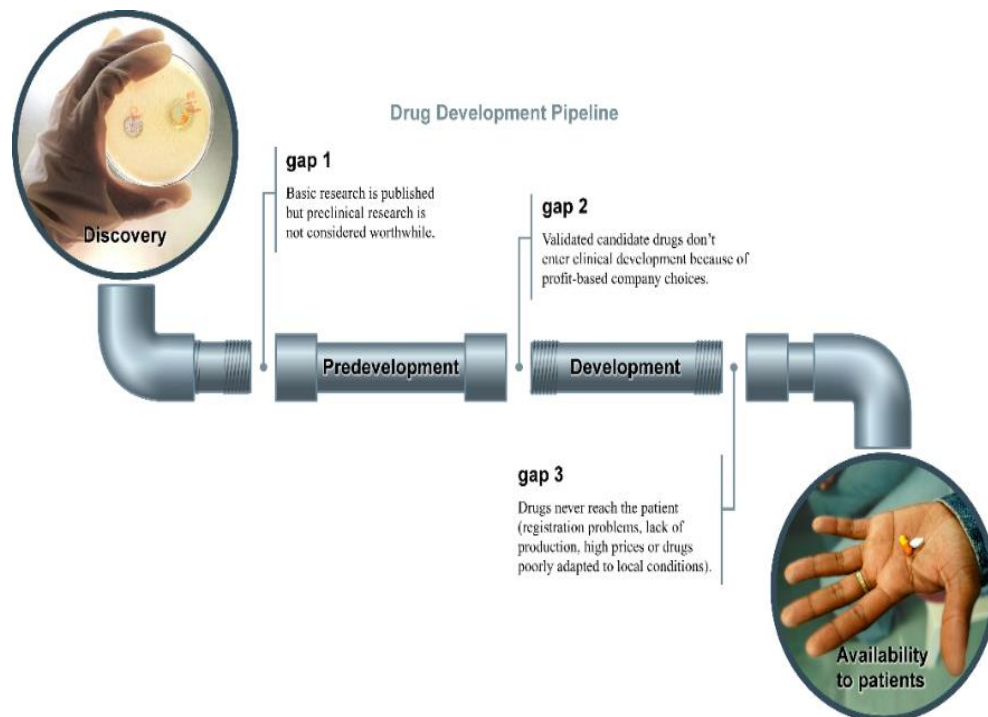


Figure 1.13. The Drug Development Pipeline - potential drugs for NTDs are frequently stuck in the early stage of development as a result of pipeline gaps (108)

1.8. New CL drugs

Despite limited resources, there have been recent developments in the NTD drug development arena. Some non-profit organisations such as TDR³, have been involved in the development of 12 new drugs for NTDs. Another collaborative, patients' needs-driven, non-profit drug R&D organisation developing new treatments for neglected diseases, is the Drugs for Neglected Diseases initiative (DNDi). The partners and collaborators, which include academic institutions, Pharma and other non-governmental organizations (NGOs) work together, using their knowledge of NTDs, clinical trials and the capability of manufacturing drugs. DNDi facilitate these complex partnerships to enable rapid development and deployment to patients (80, 108, 109).

Drug discovery for CL is especially complex as CL is not a single disease with a single etiological agent, by contrast it is caused by more than 15 different *Leishmania* species with known variability in susceptibility to drugs. Identifying

³ the Special Programme for Research and Training in Tropical Diseases, supported by the WHO, the United Nations Children's Fund (UNICEF) and the United Nations Development Programme (UNDP).

a drug that shows activity against all forms and species of CL is a tall order (109, 110).

Some potential new treatment candidates in the DNDi pipeline for NTDs are shown in Fig 1.14. Those for CL are:

- CPG-D35 oligonucleotides - synthetic DNA molecules working as an immunomodulator (by activating skin immune cells) for use as a monotherapy or in combination (111).
- DNDi-6148 and DNDi-0690 from oxaborole and nitroimidazole classes respectively, are undergoing Phase I clinical studies after completing the pre-clinical development as drugs for VL and CL.
- A combination of miltefosine (orally for three weeks) with thermotherapy (50°C for 30 seconds once during the treatment course) is in Phase II clinical trial (111).

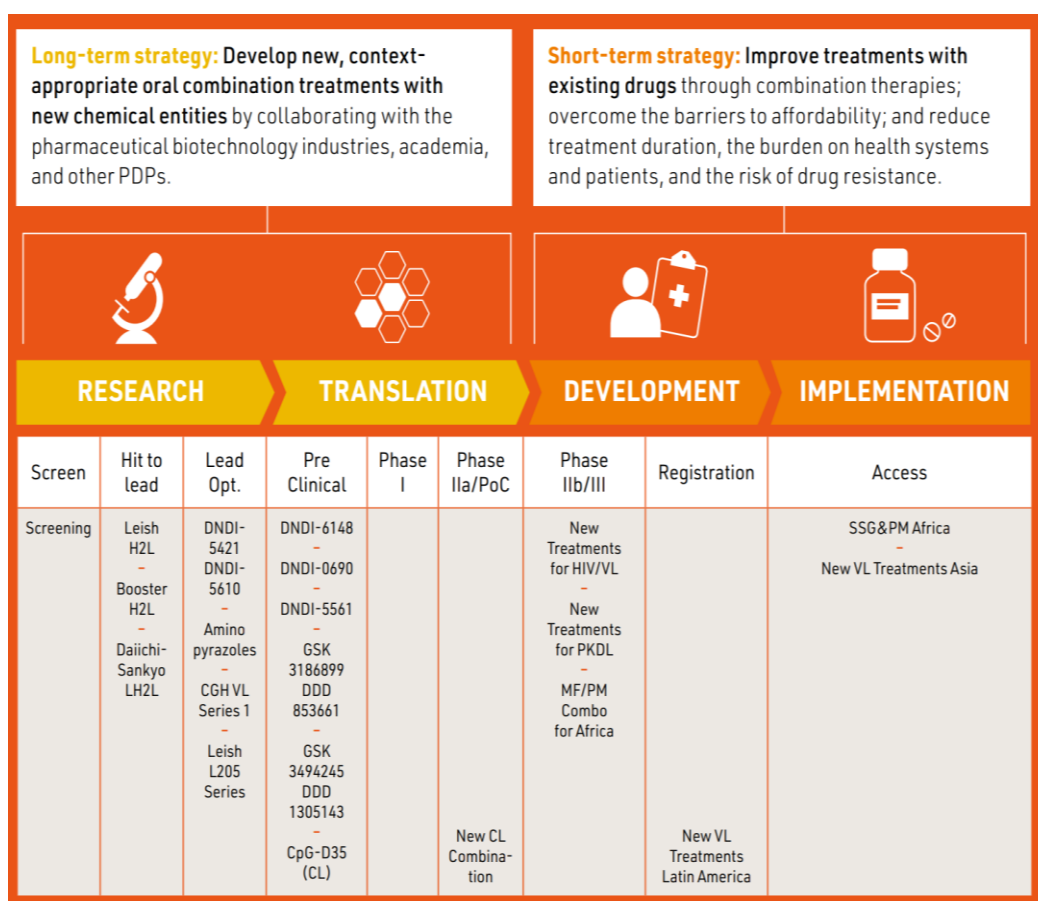


Figure 1.14. New treatment candidates for leishmaniasis (111)

1.9. Drug delivery systems for leishmaniasis

Great attention has been paid in the field of drug development to drug delivery systems (DDs). These systems are used to increase efficacy and decrease toxicity of already active drugs by controlling their pharmacokinetic properties, such as absorption, distribution, metabolism, and excretion and also by enabling drug targeting to infected tissues/cells (112, 113).

The accomplishment of CL treatment depends on the physical accessibility of the drug delivery systems to the infected macrophages in the dermis. The DDs should be able to penetrate the infected macrophages and by the time, the drug reaching the infection site of CL; the drug must cross the infected macrophage membrane, then permeate through the membrane of the PV and at the end crossing the plasma membrane of the *Leishmania* parasite, releasing the drug inside the PVs, leading to a local high concentration of the drug (Fig 1.15) (67, 113).

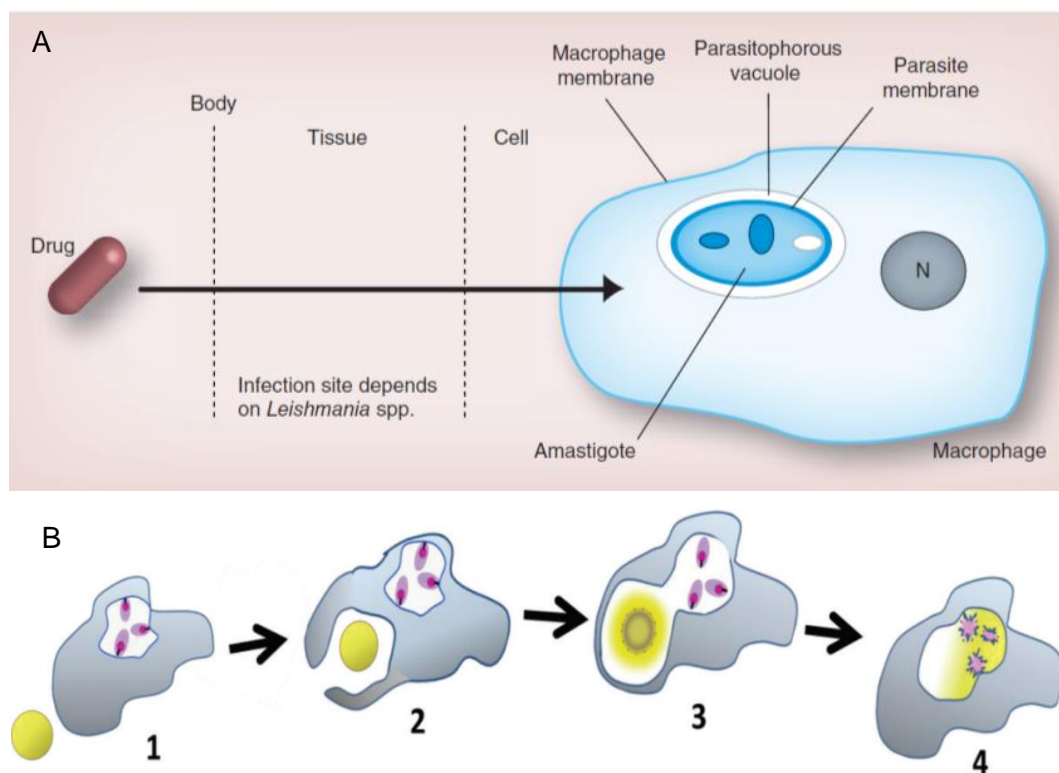


Figure 1.15. Route a drug must take to access intracellular *Leishmania* amastigotes within macrophages (A) (114) and DDs to intracellular *Leishmania* amastigotes (B) (115). A drug-loaded lipid or polymeric nanoparticle (yellow) is reaching the infected macrophage (1). This DDs is successfully phagocytosed by this infected macrophage (2). The DDs-including endolysosome (or phagolysosome) fuses with the amastigote-including parasitophorous vacuole (3). Drug is released from phagocytized DDs to kill *Leishmania* amastigotes (4).

Another promising approach for leishmaniasis treatment is related to the use of anti-leishmanial drugs with nanocarriers (DDs). There are different classes of nanocarriers e.g. particles, liposomes, emulsions etc, and many drug delivery systems have been evaluated in CL treatment (summarised in Table 1.5), some with promising results. Liposomal nanocarriers are the most studied over the past 30 years (67, 112, 113).

Using these nanocarriers DDs for CL therapies may facilitate drug solubility, reduce the toxicity, improve efficacy, modulate drug pharmacokinetics, permit sustainable drug release at the site of infection and protect the drug from degradation (113). An additional potential benefit is reducing the number of doses and the total dose, which would be significant for a drug like amphotericin B. The physicochemical properties (size, charge, morphology) and the rate of drug release from these DDs will significantly affect drug release into surrounding tissues, both before and after reaching cells at the uptake site (114). Generally, the efficacy of these DDs against CL depends on the administration route (Fig 1.16), for example in 1997, the intravenous administration once a day on six alternate days of AmBisome® (liposomal AmB) in a BALB/c *L. major* model of CL produced a dose-response effect, while the treatment was ineffective by the subcutaneous route (51). Liposomal SbV by the intravenous route is effective (116).

Table 1.5. Experimental studies using nanosystems for CL treatment copied from (115).

Routes	Drug	Nanosystem	Parasite	Efficacy
Parenteral	Amphotericin B	Chitosan and chondroitin sulphate nanoparticles	<i>L. amazonensis</i>	Yes
	Amphotericin B	Poloxamer 407-micelles	<i>L. amazonensis</i>	Yes
	Amphotericin B	PLGA-DMSA nanoparticles	<i>L. amazonensis</i>	Yes
	Amphotericin B	Liposome	<i>L. tropica</i>	No
	Amphotericin B	Liposome (AmBisome®)	<i>L. major</i>	Yes
	Amphotericin B	DSHemsPC-liposome	<i>L. major</i>	Yes

	Amphotericin B	Nanodisks	<i>L. major</i>	Yes
	Amphotericin B	PADRE-derivatized dendrimer complexed with liposome	<i>L. major</i>	Yes
	Chalcone DMC	PLA Nanoparticles	<i>L. amazonensis</i>	Yes
	Nanoselenium	Inorganic nanoparticle	<i>L. major</i>	Yes
	Paromomycin	Solid lipid nanoparticle	<i>L. major</i>	Yes
	Paromomycin	Solid lipid nanoparticle	<i>L. tropica</i>	Yes
	Pentamidine	Methacrylate nanoparticles	<i>L. major</i>	Yes
	Pentavalent antimonial	Nanohybrid hydrosols	<i>L. amazonensis</i>	Yes
	Sodium stibogluconate	Liposome	<i>L. mexicana</i> / <i>L. major</i>	Yes
Oral	Quercetin	Lipid-core nanocapsules	<i>L. amazonensis</i>	Yes
	Meglumine antimoniate	Beta-cyclodextrin	<i>L. amazonensis</i>	Yes
	Meglumine antimoniate	Polarity-sensitive nanocarrier	<i>L. amazonensis</i>	Yes
Topical	Amphotericin B	Liposome	<i>L. mexicana</i>	NO
	Amphotericin B	Gamma-cyclodextrin	<i>L. amazonensis</i>	Yes
	Chalcone CH8	Liposome	<i>L. amazonensis</i>	Yes
	Paromomycin	Liposome	<i>L. major</i>	Yes
	Paromomycin	Liposome	<i>L. major</i>	Yes
	Meglumine antimoniate	Liposome	<i>L. major</i>	Yes
	Nano silver	Inorganic nanoparticles	<i>L. major</i>	No
	Nano silver	Inorganic nanoparticles	<i>L. major</i>	No
Intralesional	Amphotericin B	Liposome (AmBisome®)	<i>L. major</i>	No
	Chalcone CH8	PLGA microparticles	<i>L. amazonensis</i>	Yes
	Nano silver	Inorganic nanoparticles	<i>L. amazonensis</i>	Yes
	Meglumine antimoniate	Liposome	<i>L. major</i>	No
	Miltefosine	Liposome	<i>L. major</i>	Yes
	Paromomycin	Liposome	<i>L. major</i>	No
	Paromomycin	Solid lipid nanoparticle	<i>L. tropica</i>	Yes

	Sodium stibogluconate	Liposome	<i>L. mexicana</i> / <i>L. major</i>	Yes
--	-----------------------	----------	---	-----

Note: Chalcone DMC – 2',6'-dihydroxy-4'-methoxychalcone; Chalcone CH8 – 3-nitro-2'-hydro-4',6'-dimethoxychalcone; DMSA – dimercaptosuccinic acid; DSHemsPC – 1,2-distigmasterylhemi-succinoyl-sn-glycero-3-phosphocholine; PADRE – pan DR-binding epitope; PLA – poly(D,L-lactide); PLGA – poly(lactic-co-glycolic acid); UVB – ultraviolet B radiation.

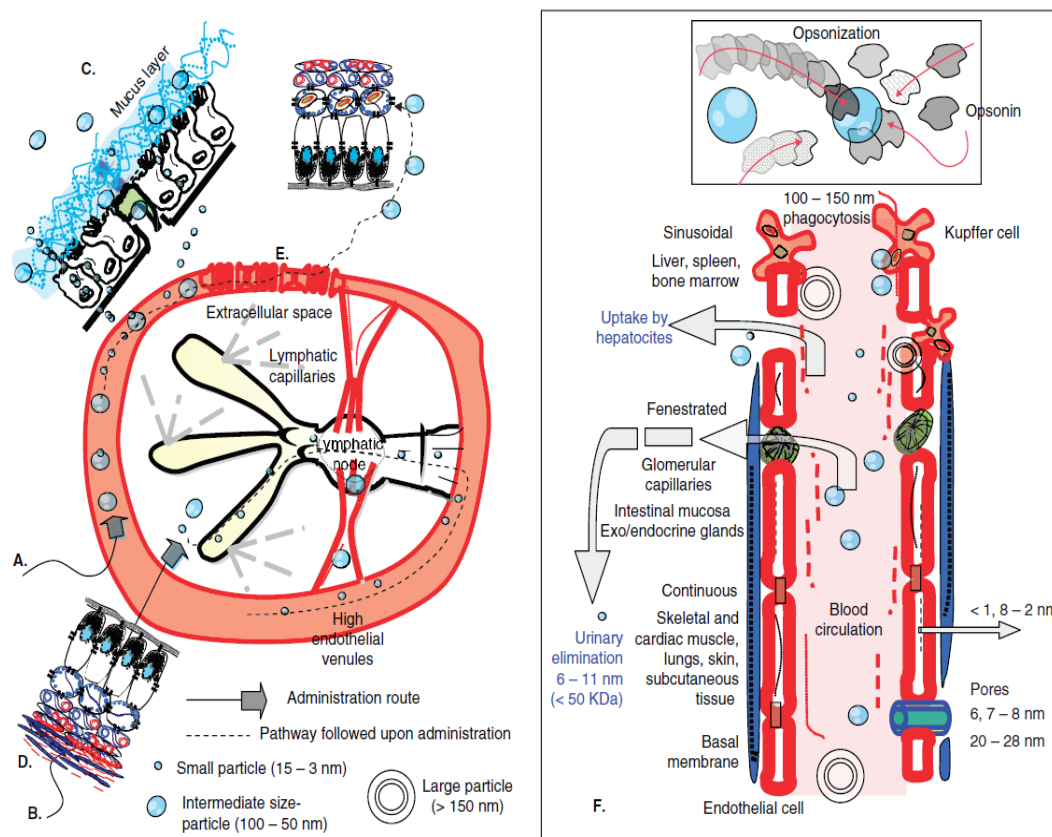


Figure 1.16. Administration routes of DDs and anatomical barriers. A. Intravenous route. B. Subcutaneous, intramuscular and intraperitoneal route. C. Oral route. D. Topical route. E. CL causes regional inflammation is associated with leaky vasculature. In this situation, particles in blood circulation can permeate barrier to become close to the infected cells. F. Particles in blood circulation (67).

Despite the promising effectivity against leishmaniasis and the safety profile of liposomal formulations, their high cost decreases their use in the leishmaniasis field. Subsequently, more attention has been paid recently to polymeric nanoparticles, Carvalho *et al* found that a nanoparticle delivery system (consisting of free deoxycholate AmB encapsulated in polylactic-co-glycolic acid (PLGA)) was more active in the treatment of experimental cutaneous leishmaniasis (*L. amazonensis*) in C57BL/6 mice than free drug (117). Kumar *et al* demonstrated that PLGA-PEG (poly(D,L-lactide-co-

glycolide)–block–poly(ethylene glycol)) encapsulated amphotericin B nanoparticles were significantly more effective than free amphotericin B against *L. donovani* strain MHOM/IN/83/AG83 in both *in vitro* and *in vivo* (Female hamsters) studies (117). Similarly, Ahmed *et al* found that a noncovalent complex of amphotericin B (AmB) and poly (α -glutamic acid) (PGA) with a size of ~100 nm, to be significantly less toxic against KB-cells in comparison with free amphotericin B and amphotericin B deoxycholate (Fungizone™) whilst keeping the same anti-leishmanial activity against *L. major* (MHOM/SA/85/JISH118) or *L. donovani* (MHOM/ET/67/HU3) intracellular amastigotes (118). Unfortunately, most of these delivery systems required organic solvents or heat for preparation - using these solvents or temperatures is not ideal as they can influence the integrity of the polyenic substances used and besides increase the toxicity of the DDs (119). In contrast, ionotropic gelation is a widely used method for preparing polymer nanoparticles and this method does not require the use of organic solvents or heat (120). In this method, nanoparticles are prepared by the interaction between two oppositely charged groups (120). Some benefits of this method are the ease of preparation, aqueous environment, low toxicity and protection of the chemical structure of the encapsulated drug (120).

Recently, a nanoparticle delivery system for AmB has been developed using the ionotropic gelation method with chitosan as a positive molecule and chondroitin sulphate (glycosaminoglycans in the extracellular matrix of cartilage) as a negative one. These loaded nanoparticles were 10 times less toxic than unincorporated AmB against murine macrophages and showed *in vitro* anti-leishmanial activity against *L. infantum* and *L. amazonensis* promastigotes and amastigotes. The efficacy of these AmB-loaded nanoparticles against *L. amazonensis*-infected BALB/c mice have been evaluated and showed a significant reduction in parasite load at 1 mg/kg/day/intravenously for 10 days. These nanoparticles induced significantly higher levels of IFN- γ and IL-12 in the mice (121, 122).

Chitosan is a widely used compound in drug delivery systems because of its interesting structure - chitosan has a cationic feature, is soluble in acidic media and has mucoadhesive properties (123). Chitosan is reported to have

immune-stimulatory effects which include inducing NO and ROS production (124, 125, 126) and antimicrobial and anti-leishmanial activity (127, 128, 129). Chitosan can be used in various formulations in the drug delivery systems and these forms are summarised in Table 1.6 with some example of associated loaded drugs (130, 131, 132) and molecules (133, 134). Chitosan nanoparticles are biocompatible and biodegradable, important properties for drug safety and controlled release, and are increasingly being considered for a variety of biomedical applications, e.g. wound healing (130, 135). Chitosan nanoparticles can be prepared in different sizes and different charges, and are suitable for different routes of administrations (123) (more details later).

Table 1.6. Chitosan-based drug delivery systems.

DDs	Method of preparation	Drug	References
Tablets	Matrix	theophylline, mesalamine, glipizide and diclofenac sodium	(120, 136, 137, 138, 139)
Capsules	Capsule shell	insulin	(140)
Microspheres/ Microparticles	Emulsion cross-linking, Coacervation/precipitation, Spray-drying	clarithromycin, propranolol HCl, gentamicin sulphate, famotidine and cimetidine	(141, 142, 143, 144, 145)
Nanoparticles	Emulsion-droplet coalescence, Ionotropic gelation, Reverse micellar method, Coacervation/precipitation	doxorubicin, cyclosporin A, gadopentetic acid, levofloxacin, amphotericin B and miltefosine	(120, 146, 147, 148, 149, 150)
Beads	Coacervation/ precipitation	insulin	(151)
Films	Solution casting	ofloxacin and paclitaxel	(152, 153)
Gel	Cross-linking	5-Fluorouracil	(154)

1.10. Nanoparticles and their interaction with skin lesions

The ease of administration and reduced systemic side effects of topical formulations prioritise them over systemic therapy for uncomplicated CL (30). Topical formulations for CL encounter different barriers in the skin and some

are shown in Fig 1.17. Nanoparticle carriers have been widely used in topical formulations to treat skin disease such as fungal infections, psoriasis and, for cosmetic purposes (155). The penetration of nanoparticles through the skin can occur by one of these three routes: intercellularly in between corneocytes, intracellularly through corneocytes or via dermal structures like the hair follicles (Fig 1.18) (155).

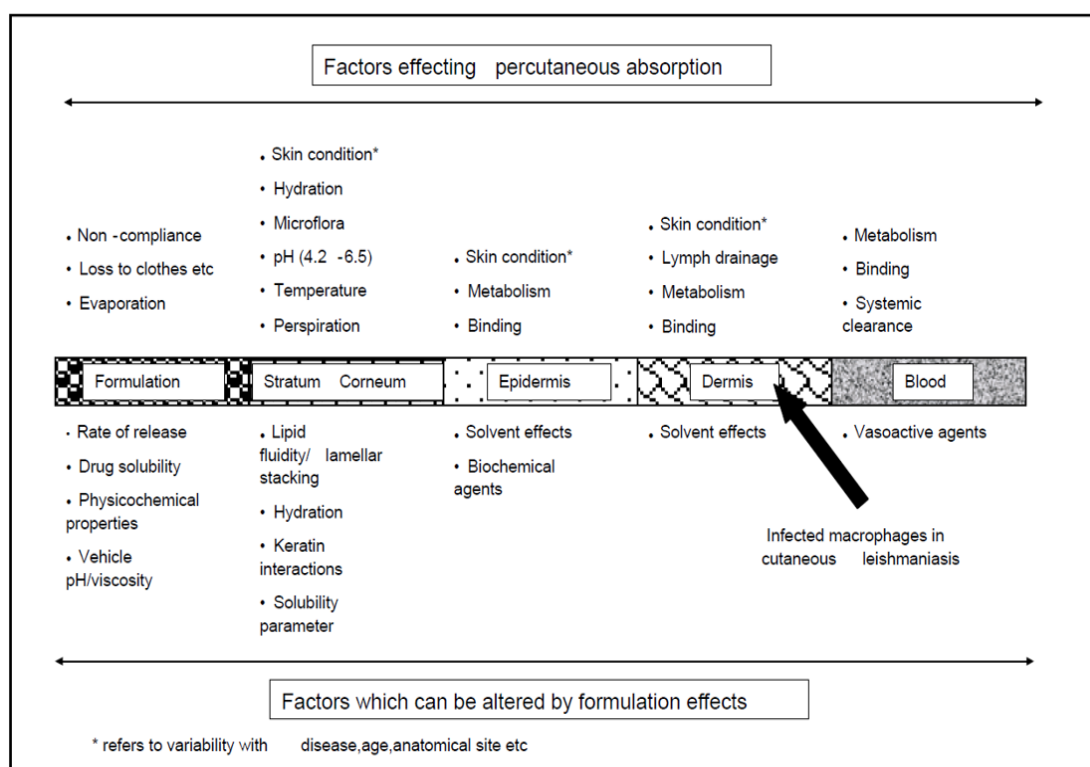


Figure 1.17. Factors to be considered in topical delivery (30).

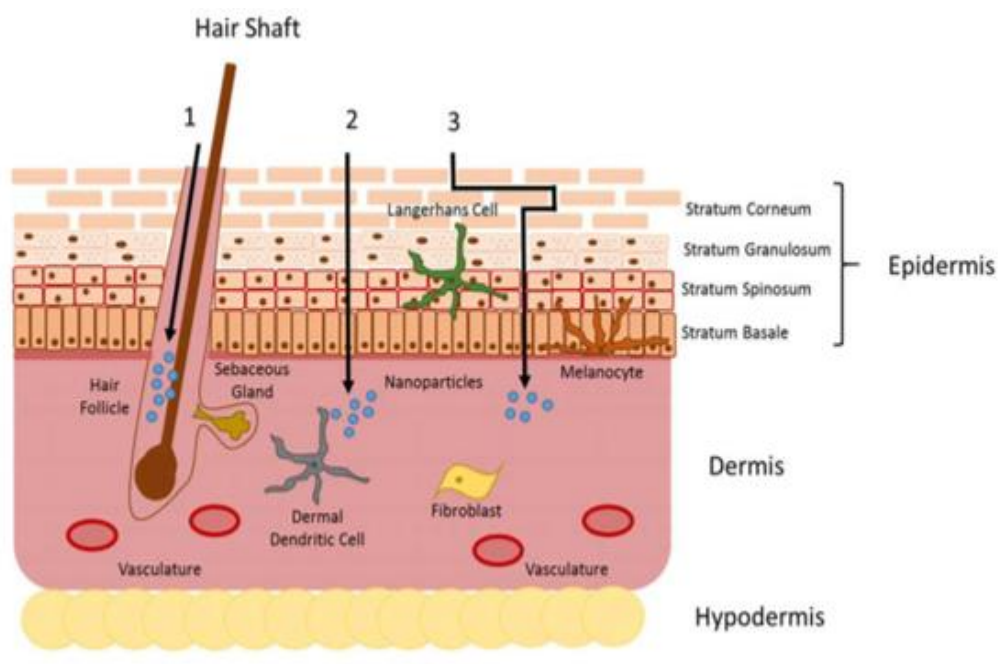


Figure 1.18. Pathways of skin nanoparticles penetration. 1) via hair follicles, 2) intracellularly through corneocytes and 3) intercellularly around corneocytes (155) .

The biological effects (toxicity, immune interactions), depth and mechanism of skin penetration of the nanoparticles are based on their structure and properties such as size, zeta potential, aggregation, solubility in the skin, skin lipid composition and drug release from these nanoparticles. The condition of the skin, healthy or otherwise, influences nanoparticle permeation. Current dogma avers that biodegradable polymeric nanoparticles accumulate in the hair follicle and on the surface (*stratum corneum*) of healthy skin (156). In CL, drug permeation may be influenced by the morphology of ulcers, such as necrotic centres and high borders to the lesion. CL causes an inflammation response involving higher permeability and vasodilatation of blood vessels of the dermis at the infection site, and moreover several types of immune cells, including macrophages, are infiltrated to the infection site and this could promote the permeation of the topical drug through the damaged epidermis (157), see Fig 1.19.

Despite this ease of drug permeation caused by the local inflammation in CL, the location of *Leishmania* parasites in the dermis, instead of the superficial portions of the epidermis where most fungi typically reside, forms a major impediment to the permeation of topical drugs (157).

The most favourable drug formulation for topical treatment of CL is the one in which the drug has a high anti-leishmanial activity and can permeate through the skin to reach *Leishmania* parasites located in the dermis, in high enough concentrations to act (115).

Chitosan nanoparticles have been reported to (i) improve the drug permeation into skin in comparison to other vehicles and, (ii) provide a sustain drug release from these nanoparticles. Moreover, chitosan has wound healing effects, mucosal adhesion properties and antimicrobial activity (158). Many clinical studies demonstrated the positive effects of using chitosan as wound dressing in accelerating the rapid wound re-epithelialisation and the regeneration of the granular layer, haemostasis in patients undergoing plastic surgery (159), skin grafting (160, 161) and endoscopic sinus surgery (162). Chitosan nanoparticles have been repeatedly administered for topical skin delivery; retinol encapsulated in chitosan-TPP nanoparticles showed less toxicity than unloaded retinol and potential activity for acne and anti-wrinkle treatment (163). Acyclovir (an antiviral medication) loaded chitosan-TPP nanoparticles caused an increase in the drug stability and stimulated drug penetration through porcine skin (164). Chitosan–dextran sulphate nanoparticles also showed mucoadhesive properties and potent activity in the treatment of ocular surface infections (165). Therefore, these encouraging properties make chitosan a suitable candidate for further studies in terms of topical treatment of CL.

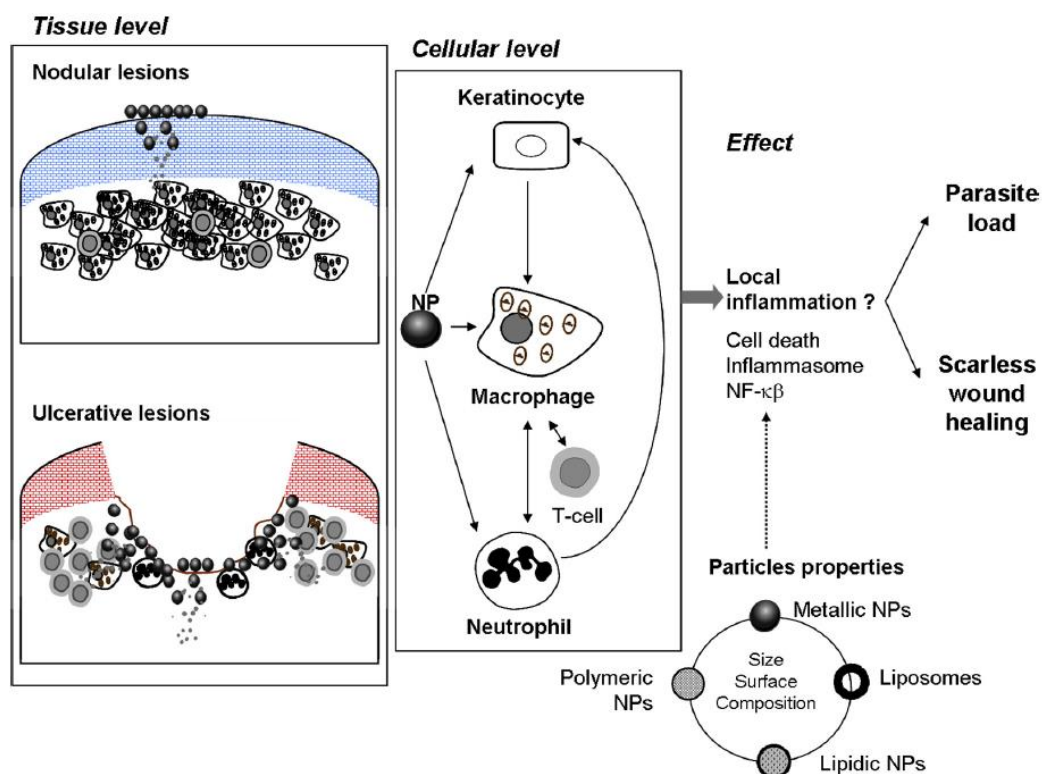


Figure 1.19. Interaction of nanoparticles with lesions of CL (156). A high parasitic load, low lymphocytes infiltrate and small tissue necrosis is observed in nodular lesions. On the contrast, the parasite load is low with higher lymphocytes infiltrate and tissue injury. While in the necrotic tissue the neutrophils are gathered, infected macrophages and lymphocytes are situated in the border of the ulcers. In nodular lesions, nanoparticles are applied to the epidermis. Based on their physicochemical properties they either (i) stay on the surface, (ii) penetrate the epidermis (small, deformable NPs), and/or(iii) fuse with the epidermis. After which a drug release will occur and diffuse to the dermis to meet the infected macrophage and then this drug being eliminated by lymphatic and blood clearance. The time of retention in the dermis is crucial for the treatment efficacy. However, these drug carriers encounter fibrotic and necrotic dermal tissue with infiltration of neutrophils in the centre of the ulcer. The chance to reach infected macrophages is higher in ulcerative lesions. Nanoparticles can promote stress and proinflammatory signalling that enable the elimination of parasites and accelerate the wound healing and according to the nanoparticles physicochemical properties this can be happened by either direct influence on macrophages or indirectly by their effects in keratinocytes and neutrophils. The design of these nanoparticles should take into consideration the maximal eradication of parasites and lowering the tissue injury.

1.10.1. Mathematical models of skin permeability

Small uncharged drug molecules mainly permeate through skin by passive diffusion in which, move from an area of higher concentration to an area of lower concentration (Fig 1.20) (166).

Infinite dose permeation experiment is usually used to examine the permeation behaviour of a compound or to determine the influences of penetration enhancer on percutaneous permeation. Infinite dose is applied to

keep a steady rate of absorption of the compound through the skin, that is called the steady state flux and will produce a cumulative permeation amount of compound permeated through a unit area of membrane over time (166, 167).

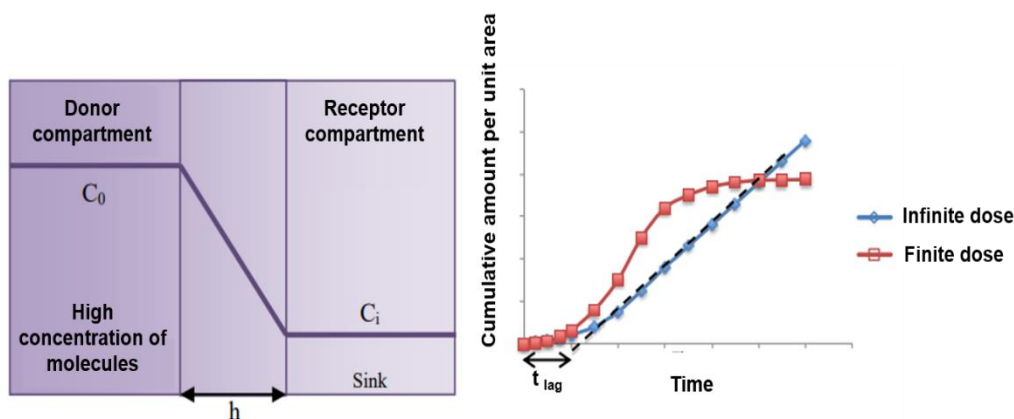


Figure 1.20. The passive diffusion of drug through a membrane (168)

Fick's first law can give the main equation (Equation 1) to identify the skin permeation after exposing the skin membrane to the diffusing molecules on one side of the skin when steady state conditions have been reached. This equation states the amount of molecule (Q) permeating the skin membrane of area (A) over a period of time (T) with the steady concentration gradient across the skin membrane, ΔC_s (in mol/cm³) and it relates the diffusion coefficient in the skin membrane, D (diffusion coefficient) (in cm²/s), and the path length, h (in cm) (166, 169).

Equation (1) $Q = \frac{DAT \Delta C_s}{h}$, $\Delta C_s = C_0 - C_i$ (C_0 represents the concentration of compound applied to the skin surface and C_i stands for the concentration of compound inside the skin)

This equation assumes that the skin barrier (stratum corneum (SC)) is acting as a pseudo homogenous membrane and no changes happen in SC properties with time and position.

Fick's first law, applied when steady state conditions have been reached, states that the rate of transfer of the diffusing molecules per unit area is proportional to the concentration gradient measured across the membrane (Equation 2). Therefore, equation 2 is indicated as the flux of the permeant per unit area (in mol/(cm²·s)) (166, 169),

Equation (2) $J = \frac{Q}{AT} = \frac{K.D.\Delta C_s}{h}$, J is the flux of the permeant per unit area (in mol/(cm²·s))

As in most practical situations $C_0 \gg C_i$ therefore equation 2 becomes:

Equation (3) $J = \frac{Q}{AT} = \frac{K.D.C_0}{h}$

Additionally, the permeability coefficient (kp) is described as the flux of the permeant per unit area normalised by the concentration gradient and by characterising the skin as a single pseudo-homogenous membrane therefore kp (in cm/s) is identified as

Equation (4) $kp = \frac{K.D}{h}$, K is the *stratum corneum*-formulation partition coefficient

Accordingly, from both equations 3 and 4, the flux of the permeant per unit area (in mol/(cm²·s)) is:

Equation (5) $J = Kp.C_0$ (166, 169)

Several assumptions should be taken into consideration before applying these equations to skin permeation into the experimental design including:

- 1- The stratum corneum forms the rate-limiting barrier
- 2- The stratum corneum is considered isotropic and its nature is not altered by the application of the vehicle of the drug formulation
- 3- The drug diffusion is not based on time, concentration or distance
- 4- The diffusing compound dissolves in the stratum corneum

However, in the clinical situations, patients mostly apply finite dose of the formulation. The amount of permeated compound through stratum corneum will accomplish a peak and stay constant (equation 6) and the diffusion is determined as below:

Equation (6) $\frac{\partial C}{\partial T} = D \frac{\partial^2 C}{\partial x^2}$, c is the concentration of the permeating molecule at time t at depth x within the skin. This equation is applied just by presuming a unidirectional diffusion through an isotropic membrane (166, 167, 169).

1.11. Pharmacokinetics of ant-leishmanial drugs

Pharmacodynamic (PD) refers to the link between drug concentration and the influences on the biological system and illustrates how the drug influences the

parasite and can be determined in regards with effectivity (EC_{50} , EC_{90}), potency (maximal effect) and the kill rate (time-dependence of the effect) (70, 71). While pharmacokinetic (PK) refers to the study of time course of the drug absorption, distribution, metabolism and excretion (ADME). The basic PK parameters are summarised in Table 1.7. Some concepts that affect importantly PK of CL drugs encompass: i) the target site of CL drug as *Leishmania* parasites survive and multiply in the macrophages of the dermis of the skin lesion and ii) the route of drug administration, for example, a topical drug should have the ability to penetrate through the stratum corneum of the epidermis and to retain in the dermis of the lesion. Moreover, iii) the metabolism of the parasite or the host (in macrophages, skin and liver) can activate or inactivate the drug. Drugs are divided into three groups according to PK/PD profile: 1- concentration-dependent antimicrobial effect -, 2- time-dependent antimicrobial effect or 3- dependent on both time and concentration (70, 71).

Table 1.7. Basic PK parameters copied from (71)

Parameter	Symbol	Description	Unit (example)	Formula
Dose	D	the dose of drug administered	Mg	Design parameter
Dose interval	T	once per day (QD) twice per day (BD) trice per day (TID)	Per hour, per day	Design parameter
C_{max}	C _{max}	the maximal concentration in a specific matrix (usually in plasma, but can be in any part of the body) after drug administration	µg/ml	Direct measurement
t_{max}	t _{max}	the time corresponding to C _{max}	Hours	Direct measurement
Volume of distribution	Vd	the apparent volume in which a drug is distributed. Relates drug concentration to the amount of drug in the body and can give information about tissue distribution	Litre	$=D/C_0$
Elimination rate constant	K _e	the rate at which a drug is removed from the system	Per hour	$= Cl/V_D$ $= \ln(2)/T_{1/2}$

Clearance	CL_r	the volume of body fluid cleared per time unit quantifies drug elimination from the system by kidney, liver and other organs	litre/hour	$= V_d \cdot K_e$ $= D/AUC$
Half-life	$t_{1/2}$	the time needed for the concentration to fall to half of its previous value	Hours	$= \ln(2)/K_e$
AUC	AUC	the area under the curve, an expression of total exposure	mg/liter.ho ur	$= [\int_0^\infty C. dt]$
Bioavailability	F	oral bioavailability, the fraction of the administered dose that reaches the systemic circulation.	N/A (fraction)	$= AUC_{(po)} / AUC_{(i.v.)}$ $\times \text{Dose}(i.v.) / \text{Dose}(po)$

Regarding the pharmacokinetic of leishmaniasis drugs, pentavalent antimony has a long terminal half-life because of the intracellular conversion of SbV to SbIII which forms with the quick renal excretion the main characterisations of this drug pharmacokinetics. Miltefosine pharmacokinetics are characterised mainly by the accumulation in peripheral blood mononuclear cells (PBMCs) and long terminal half-life (70). However, paromomycin is characterised by the fastest excretion by the kidneys from the body in comparison with other leishmaniasis drugs. On the other hand, AmB pharmacokinetics have not been evaluated widely in leishmaniasis. It has been reported that the renal and faecal excretion of liposomal AmB (AmBisome®) is much slower than AmB deoxycholate (Fungizone) excretion which leads to higher exposure (70, 71). Wijnant *et al* reported that liposomal AmB (AmBisome®) caused a higher plasma peak and systemic exposure compared with AmB deoxycholate (Fungizone, after a single dose of 1 mg/Kg/ i.v. in *L. major*-infected mice) (170) and Table 1.8 summarizes the PK of leishmaniasis drugs including pentavalent antimonial, paromomycin, miltefosine, Fungizone and AmBisome® in clinical and mouse model studies. The application of PK and PD comprehension and understanding the relation between PK and PD produce a fundamental base for detecting the optimal dosage and effective therapeutic management of drugs for CL treatment and will be helpful in antileishmanial drugs combination to increase in an attempt to improve drug efficacy and decrease the duration of treatment (70, 170)

Table 1.8. Pharmacokinetic profile of leishmaniasis drugs (70, 170)

Patients		Weight (kg)	Daily dose	Sampling day	C_{max} ($\mu\text{g} / \text{ml}$)	C_{trough} ($\mu\text{g} / \text{ml}$)	t_{max} (h)	k_a (h^{-1})	V_d/F (L)	CL_r/F (L/h)	AUC (mg.h/L)	$t_{1/2}$ (h)
SbV	(CL) Humans Adults:	62 (56–120)	20 mg/kg/days, 20 days (IM)	Day 19	38.8 ± 2.1	0.198 ± 0.023	1.0 (1.0–2.0)	NA	0.30 ± 0.01 ^{b,c}	0.106 ± 0.006 ^b	AUC ₂₄ : 190 ± 10	$t_{1/2,\beta}$: 1.99 ± 0.08 $t_{1/2,24-48\text{ h}}$: 20.6 ± 1.8
	(CL) Humans Children:	15 (13–18)	20 mg/kg/day, 20 days (IM)	Day 19	32.7 ± 0.9	0.113 ± 0.015	0.875 (0.5–1.5)	NA	0.39 ± 0.03 ^{b,c}	0.185 ± 0.013 ^b	AUC ₂₄ : 111 ± 7	$t_{1/2,\beta}$: 1.48 ± 0.02
Paromomycin	(VL) Humans	35.5±11.8 ^a	15 mg/kg (11 mg/kg base), 21 days (IM)	Day 1	20.5 ± 7.01	4.53 ± 6.71	NA	2.11 (7.68%) ^e	15.3 (2.27%) ^e	4.06 (3.05%) ^e	NA	2.62
				Day 21	18.3 ± 8.86	1.31 ± 4.16						
Data given as either mean ± standard deviation or median (range), unless indicated otherwise AUC area under the concentration–time curve, AUC ₂₄ AUC from time zero to 24 h, , CL _r clearance, C _{max} peak plasma concentration, C _{trough} trough plasma concentration 24 h after dose, F bioavailability, k _a absorption rate constant, NA not available, t _{1/2} plasma elimination half-life, t _{1/2, β} elimination half-life, t _{1/2,24–48 h} apparent half-life between 24 and 48 h (an approximation of the c-elimination half-life), t _{max} time to C _{max} , V _d volume of distribution. ^b Per kg, ^c V ^β apparent volume of distribution during the b-elimination phase and ^e Mean (% standard error)												
Patients		Weight (kg)	Daily dose	C _{ss} ^a ($\mu\text{g}/\text{ml}$)	k _a (day ¹)	t _{max} (h)	V _{central} /F (L)	CL _r /F (L/day)	V _{peripheral} /F (L)	Q (L/day)	AUC ^b ($\mu\text{g}.\text{day}/\text{ml}$)	t _{1/2} (days)

Miltefosine	(CL) Humans Adults:	70.84 ± 11.73	2.11 ± 0.16 mg/kg/day, 28 days (Orally)	31.9 (17.2–42.4)	NA	NA	NA	NA	NA	NA	628 (213–861)	34.4 (9.5–46.15)
	(CL) Humans Children:	26.22 ± 7.62	2.27 ± 0.16 mg/kg/day, 28 days (Orally)	22.7 (17.0–29.3)	NA	NA	NA	NA	NA	NA	448 (304–583)	37.1 (7.4–47.0)
Patients		Weight (g)	Daily dose	C_{max} (µg/ml)	AUC (h · µg/ml)	Clearance (ml/h/kg)	$t_{1/2}$ (h)	V (ml/kg)				
Fungizone	<i>L. major</i> -infected mice	20	a single i.v. 1-mg/kg dose	1	30.2	18.9	39.7	1075				
AmBisome®	<i>L. major</i> -infected mice	20	a single i.v. 1-mg/kg dose	8.2	71	13.5	8.5	143				
<p>AUC area under the concentration–time curve, CLr clearance, C_{ss} steady-state concentration, F bioavailability, k_a absorption rate constant, NA not available, Q intercompartmental clearance, t_{max} time to C_{max} within one dosing interval, V volume of distribution, t plasma elimination half-life, V central volume of distribution of the central compartment, $V_{peripheral}$ volume of distribution of the peripheral compartment. ^a Miltefosine accumulates during treatment and reaches C_{ss} during the last week of treatment</p> <p>^b AUCD28 (AUC from start to end of treatment) unless indicated otherwise</p> <p>^c Unclear whether this is the mean C_{ss} or the maximum C_{ss}</p> <p>^d AUC from start of treatment to infinity (AUC[∞])</p>												

1.12. Treatment challenges

As described in this chapter, current treatments for CL have drawbacks, for instance high toxicity (nephrotoxicity, cardiotoxicity, hepatotoxicity etc), the high cost (such as liposomal amphotericin B), instability, or sometimes low cure rates etc and this draws the attention to the need for new safe, effective, economically feasible new treatments for CL. Drug discovering and developing is a long, slow and very expensive process (71).

Drug delivery system is considered one of the effective strategies to overcome the cost and long process of developing new drugs in which DDs of already known active drugs can be used to increase the activity of loaded drugs and to reduce their toxicity.

Chitosan has shown promising features in therapeutic delivery systems because of its biocompatibility, biodegradability, cationic structure, mucoadhesive properties, wound healing effects and the antimicrobial activity (130, 135). Therefore, chitosan has been chosen in this study as a carrier for AmB and the potential to treat CL. AmB is a highly active drug against CL but its use has been decreased because of the toxicity and we aimed to improve the therapeutic window of AmB by using chitosan as a nanocarrier (171).

There are different methods for chitosan nanoparticles preparation and the ionotropic gelation method was chosen in this study as this method is a simple and quick method and can be used to synthesize spherical nanoparticles with different sizes and charges. Moreover, this method has been reported to produce very stable chitosan nanoparticles with sustainable drug release (171).

In literatures, chitosan nanoparticles showed encouraging properties as DDs for the treatment of leishmaniasis. However, there is just a study that used the ionotropic gelation method and used chitosan nanoparticles with positive surface charge and with size of 136 ± 11 nm and these studies need more detailed and controlled studies (83, 122).

Topical treatments have many advantages over systemic treatment for instance, (i) increasing the compliance with patients, (ii) affording a high local concentration of the drug at the lesion site and (iii) reduce the toxic effects of systemic drugs (158). Therefore, the possibility of using AmB loaded chitosan nanoparticles in this route could be of interest to benefit from the small size of the nanoparticles, mucoadhesive and wound healing effects of chitosan.

1.13. Aims and objectives

The overall aim of this project was to optimise an effective, safe and economically feasible nanoparticle delivery system of amphotericin B with the potential to treat cutaneous leishmaniasis.

- Hence, the aim of the first experimental chapter (chapter 2) was to:
 - I. Determine the *in vitro* anti-leishmanial activity of chitosan and its derivatives against *L. major* and *L. mexicana* promastigotes and intracellular amastigotes at two different pH values of the culture medium (the medium pH 7.5 and at lower pH 6.5)
 - II. To evaluate the *in vitro* role of chitosan in the activation of macrophage and M1 proinflammatory phenotype, via the measurement of NO, ROS and TNF- α production by host cells and by measuring parasite survival
 - III. Investigate chitosan uptake by macrophages to explain activity against intracellular amastigotes.

- The purpose of the second experimental chapter (chapter 3) was to:
 - I. Prepare two types of chitosan nanoparticles by using the inotropic gelation method; one with a positive surface charge using tripolyphosphate sodium (TPP) and the other with a negative surface charge, using dextran sulphate.
 - II. Evaluate the characterisations of blank and amphotericin B loaded chitosan TPP or dextran sulphate nanoparticles by studying their physicochemical properties (size, morphology, zeta-potential and stability). The optimal conditions for nanoparticle preparation were chosen with regard to the smallest sizes and different charges.
 - III. Determine amphotericin B loading and drug release from the amphotericin B loaded chitosan TPP or dextran sulphate nanoparticle

- The third experimental chapter aimed to (chapter 4):
 - I. Evaluate the *in vitro* effectiveness of blank and amphotericin B loaded chitosan TPP or dextran sulphate nanoparticles against *L. major* and *L. mexicana* promastigotes and amastigotes after evaluating their haemolytic activity and cytotoxicity against KB-cells.

- II. Evaluate the intravenous activities of blank and amphotericin B loaded chitosan TPP or dextran sulphate nanoparticle *in vivo* in BALB/c mice infected with *L. major*.
- III. Measure the permeation of blank and amphotericin B loaded chitosan TPP or dextran sulphate nanoparticle through uninfected and *L. major* infected mouse BALB/c skin by *In vitro* Franz diffusion cell permeation studies.

- The fourth experimental chapter (chapter 5) aimed to:

- I. Study the effects of media perfusion on the *in vitro* host cell phagocytosis and macropinocytosis.
- II. Study the effects of the flow on the *in vitro* anti-leishmanial activity of chitosan solution and blank and amphotericin B loaded chitosan TPP or dextran sulphate nanoparticles

2. Activity of chitosan and its derivatives against *Leishmania major* and *mexicana* in vitro.

2.1. What is chitosan?

Chitosan is produced by the deacetylation of chitin (Fig 2.1). Chitin is the second most abundant natural polysaccharide and originates from the shells of crustaceans and the cell walls of fungi (172). Chitosan is a biodegradable, biocompatible and positively charged nontoxic mucoadhesive biopolymer (172, 173).

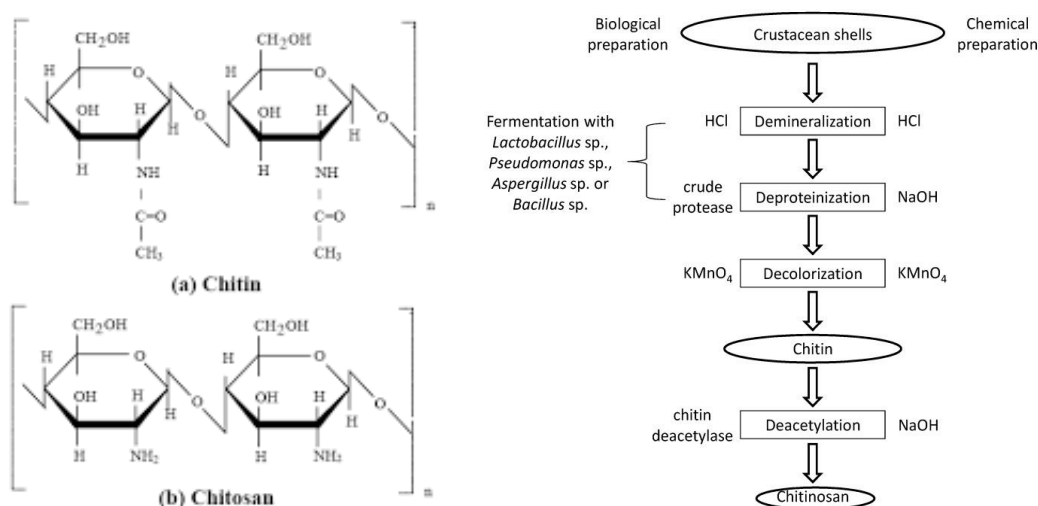


Figure 2.1. Structure of chitin and chitosan and method of preparation chitosan from raw materials (172, 174).

2.2. Chitosan solubility

Chitosan is insoluble at alkaline pH but is soluble in dilute acidic solvents like glacial acetic acid and acid solvents to form a cationic polymer ($-NH_3^+$ groups) (Fig 2.2). Chitosan in acidic media has a positive charge and the ability to form gels at low pH values because it is hydrophilic and can retain water in its structure (175). Chitosan pKa is approximately 6.3 and therefore, the approximate ionisation degree of chitosan is a 61% and 6% at pH 6.5 and 7.5 respectively.

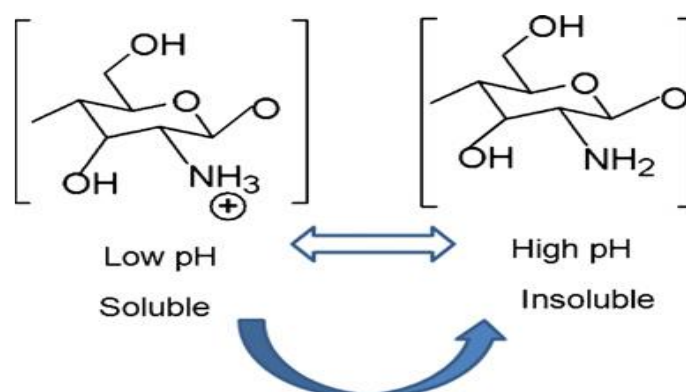


Figure 2.2. Schematic illustration of chitosan's versatility (135).

2.3. Chitosan toxicity

Chitosan is widely considered as a non-toxic, biological polymer and has been approved by the FDA for use in wound dressings. Chitosan has been recognized by FDA as GRAS (Generally Recognized As Safe, GRAS Notice No. GRN 000073, EU 2011) (176) and approved for use in dietary applications in Italy and France (173). The lethal dose, 50% (LD_{50}) of chitosan for mice and rats are orally 16000 and 1500 mg/kg respectively (177).

2.4. Chitosan in wound healing

Chitosan has a similar chemical structure to hyaluronic acid and additionally enhances the functions of inflammatory cells such as polymorphonuclear leukocytes (PMN) (phagocytosis, production of osteopontin and leukotriene B₄), macrophages (phagocytosis, production of interleukin (IL-1), transforming growth factor and platelet-derived growth factor) and fibroblasts (production of IL-8) (135, 175). Because of these properties, chitosan promotes skin wounds granulation with improving collagen production, angiogenesis and re-epithelialization of skin tissue. As a result, chitosan induces wound healing and produces less scarring. Also using chitosan hydrogel will provide a painless, antimicrobial and ideal dressing for wounds (135, 175).

2.5. Chitosan derivatives

The poor solubility of chitosan and the loss of the cationic nature charge at neutral and alkaline pH are two of the major obstacles to the usefulness consideration of chitosan as a useful antimicrobial material. Recently, the

chemical modification of chitosan to produce various derivatives to improve its solubility and widen its application, has gained a great attention. The presence of certain functional -NH_2 and -OH groups on chitosan structure provides the basis for many methods of structural modification. The most used method is graft copolymerization (an attractive technique to conjugate bioactive molecules on the surface). Derivation of chitosan can be used to improve its antimicrobial activity, solubility and the mucoadhesive properties (178, 179).

2.6. Antimicrobial activity of chitosan

Many reports mention that chitosan has a potential activity against microbes (detailed in Table 2.1) but the actual mechanism has not yet been fully elucidated [35]. Three mechanisms have been suggested to explain this activity. The first one is the interaction between the protonated NH_3^+ groups of chitosan and the negative cell membrane of microbes. This interaction leads to change the permeability of the microbes' membrane wall, causes osmotic imbalances, and as a result prevents the growth of the microbes (174, 180). Another mechanism is that chitosan binds to microbial DNA and inhibits DNA transcription and mRNA synthesis (180, 181). The third mechanism is the chelation of metals and binding the basic nutrients for microbes. These three mechanisms lead to killing of the microbes (124). A fourth indirect mechanism of action may be related to the known pro-inflammatory activity effect of chitosan on macrophages. This involves stimulation of tumour necrosis factor ($\text{TNF-}\alpha$), interleukin 6 (IL-6), nitric oxide (NO), reactive oxygen species (ROS) and interferon gamma ($\text{IFN-}\gamma$) which play critical roles in the proinflammatory response against intracellular microbes (by enhancing the production of microbicidal reactive nitrogen species) (125, 126, 182, 183, 184).

Table 2.1. The antimicrobial activities of chitosan and its derivatives (173, 185, 186, 187)

Microbe	MIC of chitosan or derivative
<i>Escherichia coli</i>	Chitosan 8 µg/ml; chitosan nanoparticles 0.0625 µg/ml; Cu loaded chitosan nanoparticles 0.0313 µg/ml
<i>Pseudomonas aeruginosa</i>	Chitosan 0.0125%(w/v); chitosan-Zn complex 0.00625%(w/v); N, N-diethyl-N-methyl-chitosan 32 µg/ml
<i>Proteus mirabilis</i>	Chitosan 0.025%(w/v); chitosan-Zn complex 0.00625%(w/v)
<i>Salmonella enteritidis</i>	Chitosan 0.05%(w/v); chitosan-Zn complex 0.00625%(w/v)
<i>Enterococcus faecalis</i>	Chitosan 8 µg/ml; chitosan-Zn complex 0.125; N, N-diethyl-N-methyl-chitosan 16 µg/ml
<i>Staphylococcus aureus</i>	Chitosan 0.025%(w/v); chitosan-Zn complex 0.0125%(w/v); N-methyl-chitosan 16 µg/ml
<i>Candida albicans</i>	Chitosan 5 µg/ml; chitosan-Zn complex 0.1%(w/v)

2.7. Anti-leishmanial activity of chitosan

A few researchers have evaluated the activity of chitosan against *Leishmania* parasites under different conditions and the results are summarised in Table 2.2. It was observed that chitosan presented an anti-leishmanial activity with EC₅₀ (50% effective concentration) values ranging from around 50 to 240 µg/ml against different strains of *Leishmania* promastigotes and amastigotes. In these studies, there are inconsistent values of the activity of chitosan against *Leishmania* parasites. Accordingly, a lot of clarification and detailed controlled studies are needed to determine whether chitosan is a suitable candidate to find new chemotherapeutic alternatives for the treatment of leishmaniasis. The aim of this chapter was to: (i) determine the *in vitro* anti-leishmanial activity of chitosan and its derivatives against *L. major* and *L. mexicana* promastigotes and intracellular amastigotes at two different pH values (the culture medium pH of 7.5 and a lower pH of 6.5, which are both suitable for macrophage and parasite growth (188, 189, 190), (ii) to evaluate

the *in vitro* role of chitosan in the activation of macrophage and M1 proinflammatory phenotype, via the measurement of NO ,ROS and TNF- α production by host cells and by measuring parasite survival and (iii) investigate chitosan uptake by macrophages to explain its activity against intracellular amastigotes.

Table 2.2. The anti-leishmanial activity of chitosan

Strain	Drug	Type of study	Results
<i>L. infantum</i>	Chitosan solution in acetic acid	<i>In vitro</i> , against promastigotes and amastigotes	- EC ₅₀ =112.64-µg/ml promastigotes - EC ₅₀ = 100.81 µg/ml amastigotes (127)
<i>L. amazonensis</i>	Chitosan solution in acetic acid	<i>In vitro</i> , against promastigotes and amastigotes	- EC ₅₀ = 73.00 µg/ml promastigotes. -100 µg/ml: Percentage of infected macrophages after treatment 66% (122)
<i>L. amazonensis</i>	Chitosan nanoparticles	<i>In vitro</i> , against promastigotes and amastigotes	- EC ₅₀ = 52 µg/ml promastigotes. -100 µg/ml: Percentage of infected macrophages after treatment 39% (122)
<i>L. chagasi</i>	Chitosan solution in acetic acid	<i>In vitro</i> , against promastigotes	EC ₅₀ = 67 µg/ml promastigotes (122).
<i>L. chagasi</i>	Chitosan nanoparticles	<i>In vitro</i> , against promastigotes	EC ₅₀ = 46 µg/ml promastigotes (122).
<i>L. infantum</i>	Chitosan solution	<i>In vitro</i> , against promastigotes	EC ₅₀ = 240 µg/ml (128)
<i>L. major</i>	nanochitosan film	<i>In vivo</i> study, female BALB/c mice were treated with nano-chitosan film four times/day	There was no significant difference between nanochitosan and Glucantime in reduction of lesion size of <i>L. major</i> infected mice (191)
<i>L. major</i>	Chitosan microparticles	<i>In vivo</i> , (100 µg/100 µl) were subcutaneously injected in the infected BALB/c mice) with two-day intervals until two weeks	Lesions of <i>L. major</i> infected mice were significantly smaller in chitosan treated groups (1.2 ± 0.8 mm) than in the control group (6.2 ± 1.7 mm) (129)
<i>L. major</i>	Chitosan solution in acetic acid	<i>In vivo</i> (BALB/c mice), chitosan 200 and 400 µg/ml were applied topically for 28 continuous days	Lesion size <i>L. major</i> infected mice was 8.47 mm for untreated group and 2.07 and 1.05 mm in groups treated with the 200 and 400 µg/ml of chitosan, respectively (192).

A pilot clinical study for 10 patients with CL (patients did not respond to traditional treatment)	poly (vinyl alcohol)/chitosan/clay nanocomposite film	Chitosan films were applied on the lesion for 7 days. This dressing was repeated every week until the complete healing.	Lesions were completely cured after 16 weeks with no side effects or recurrences (193).
--	---	---	---

2.8. Materials and methods

2.8.1. Drugs and chemicals

Stocks of amphotericin B deoxycholate (5.2 mM [aq]) (Fungizone; Gibco, UK) were prepared, aliquoted, and kept at -20°C until use. Chitosan with three different molecular weights and its derivatives were used and are summarised in Table 1. Solutions of chitosan and derivatives were prepared by dissolving 1 g in 100 ml of 1% (v/v) acetic acid solution at room temperature with continuous stirring for 24 hours until a clear solution was obtained. The pH of the solution was adjusted to approximately 6 by adding sodium hydroxide 2N (NaOH, Sigma, UK) solution with a pH meter (Orion Model 420A). The chitosan solutions were autoclaved (121 °C; 15 mins). Phosphorylcholine substituted chitosan was kindly provided by Prof F Winnik (Montreal University, Canada) generated through reductive amination of PC-glyceraldehyde with primary amines of deacetylated chitosan (57 KDa). Percentage of substitution was controlled and determined by NMR (194). In our study, two pH values have been used: 7.5 is the medium culture pH and a lower pH 6.5. pH 6.5 is a suitable and safe pH for both macrophages and parasites, while pH<6.5 affects the growth of both macrophages and intracellular amastigotes.

Chitosan pKa is approximately 6.3 and therefore, the approximate ionisation degree of chitosan is a 61% and 6% at pH 6.5 and 7.5 respectively.

Table 2.3. Details of chitosan and its derivatives used in the study

Compounds	Properties	Supplier
HMW (source: crustacean shells)	MW=310-375 KDa	Sigma, UK
MMW (source: crustacean shells)	MW=190-310 KDa	Sigma, UK
LMW (source: crustacean shells)	MW=50-190 KDa	Sigma, UK
Fungal chitosan (white mushroom)	MW=110-150 KDa	Dr Somavarapu

Chitosan oligosaccharide(synthetic)	MW= \leq 5KDa	Dr Somavarapu
Chitosan oligosaccharide lactate (synthetic)	MW=average Mn 5, oligosaccharide 60%	Dr Somavarapu
Chitosan- HCl (synthetic)	MW= 47 - 65 KDa	Dr Somavarapu
Carboxymethyl chitosan (synthetic)	MW=543.519 Da, level of substitution is 95%	Dr Somavarapu
PC1-CH (Phosphorylcholine substituted chitosan) (synthetic)	MW=33 KDa, PC(mol%)= 30	Prof Winnik (194)
PC2-CH (synthetic)	MW=108 KDa, PC(mol%)= 20	Prof Winnik (194)
PC3-CH (synthetic)	MW=109 KDa, PC(mol%)= 30	Prof Winnik (194)

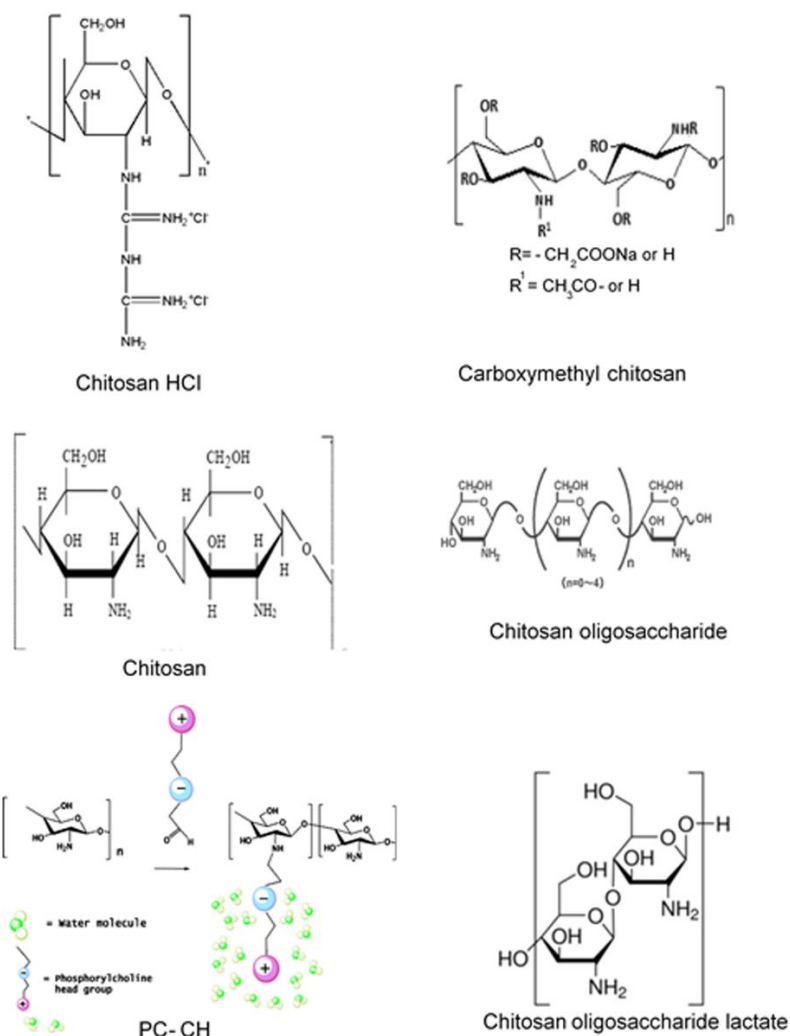


Figure 2.3. The structure of chitosan and its derivatives (194, 195, 196, 197)

2.8.2. Ethics statement.

All animal work is carried out under a UK Home Office project licence according to the Animal (Scientific Procedures) Act 1986 and the new European Directive 2010/63/EU. The Project Licence (70/8427) has been reviewed by LSHTM Animal Welfare & Ethical Review Board prior to submission and consequent approval by the UK Home Office.

2.8.3. Cell lines

Preparation of macrophages

- Peritoneal mouse macrophages (PEMs) were obtained from 8-12-week-old female CD1-mice (Charles River Ltd, UK). Two ml of a 2% (w/v) starch solution in phosphate-buffered saline (PBS, Sigma, UK) was injected intraperitoneally (i.p.). After 24 h, the animal was sacrificed and the PEMs were harvested by peritoneal lavage with cold RPMI 1640 medium (Sigma, UK) containing 200 units penicillin and 0.2 mg streptomycin/ml (PenStrep; Sigma, UK). Subsequently, PEMs were centrifuged at 450 g at 4°C for 15 min and then the pellet was resuspended in RPMI 1640 with 10% (v/v) heat-inactivated fetal calf serum (HiFCS; Gibco, UK).
- Bone marrow-derived macrophages (BMMs) were obtained from femurs of 8-12-week-old female BALB/c mice (Charles River Ltd). Briefly, the bone marrow cells were carefully flushed from the bone with Dulbecco's Modified Eagle's Medium (DMEM; Thermofisher, UK) with 10% (v/v) HiFCS, 100 U/ml penicillin and 100 mg/ml streptomycin (Sigma, UK). Cells were pelleted by centrifugation (450 g, 10 min) and re-suspended in 10ml DMEM with 10% (v/v) HiFCS and human macrophage colony stimulating factor 50ng/ml (HM-CSF; Thermofisher, UK). After plating out in T175 flasks (Greiner Bio-One, Stonehouse, UK), BMMs were kept at 37°C, 5% CO₂ for 7-10 days after which they were harvested, counted and used.
- THP-1 cell is a human leukemic monocyte-like derived cell line. THP-1 cells were cultured in RPMI 1640 medium supplemented with L-glutamine and 10% HiFCS. THP-1 cells were incubated in RPMI 1640 plus 10% (v/v) HiFCS and 20 ng/ml phorbol 12-myristate 13-acetate (PMA; Sigma, UK) at 37°C and 5% CO₂ for 72 h to induce maturation transformation of these monocytes into adherent macrophages (198).

Human squamous carcinoma (KB) cells are adherent cells derived from epidermal carcinoma from the mouth. KB cells were cultured in RPMI 1640 medium 10% HiFCS (199).

The number of cells and macrophages was estimated by counting with a Neubauer haemocytometer by light microscopy (x 400 total magnification).

2.8.4. Parasites

Four *Leishmania* species; two GFP labelled species (*L. major* (MHOM/SU/73/5ASKH) and *L. mexicana* (MNYC/BZ/62/M379), kindly donated by Dr G Getti (University of Greenwich, UK) were used for the fluorescence microscope study. They were cultured in Schneider's insect medium (Sigma, UK) with 23% (v/v) HiFCS, 1× penicillin-streptomycin-glutamine (Gibco-Invitrogen) and supplemented with 700 µg/ml G418 (an aminoglycoside antibiotic, Sigma, UK). *L. major* (MHOM/SA/85/JISH118) and *L. mexicana* (MNYC/BZ/62/M379) were used for other experiments as described, minus the G418. Promastigotes were incubated at 26°C, maximum passage number used = 7.

2.8.5. *In vitro* cytotoxicity assays

Re-suspended KB cells (4×10^4 /100 µl) were allowed to adhere to the bottom of 96-well plate overnight and then exposed to specific concentrations of the compounds for 72 h at 37°C and 5% CO₂ incubator. Podophyllotoxin (Sigma, UK) was included as a positive control at a starting concentration of 0.05 µM. Cytotoxicity was evaluated by a cell viability assay using the resazurin sodium salt solution (AlamarBlue, Sigma, UK) which was prepared according to the manufacturer's instructions. 20µL of the resazurin solution was added to each well of the plates and fluorescence (cell viability(200)) was measured over a period of 1 to 24 h using a Spectramax M3 plate reader (EX/EM 530 / 580 nm and 550 nm cut off). Results were expressed as percentage inhibition = $(100 - x)\%$ viability (means \pm standard deviation σ). Cytotoxicity was evaluated in RPMI 1640 at two pH values (at normal pH of RPMI 7.5 and at a lower pH 6.5). The pH of RPMI 1640 was reduced from 7.5 to 6.5 by adding 0.05M acidic buffer, 2-N-morpholino ethanesulfonic acid (MES, Sigma, UK). RPMI 1640 plus MES (0.05M) at pH=6.5 did not show any toxicity to KB-cells.

2.8.6. *In vitro* 72-hour activity of chitosan and its derivatives against extracellular *L. major* and *L. mexicana* promastigotes

Promastigotes in RPMI 1640 medium were tested while in the exponential growth phase. The promastigotes were diluted to a density of 5×10^6

promastigotes/ml and then exposed to different concentrations of (HMW, MMW, and LMW) chitosan, chitosan derivatives and Fungizone (positive control) in 96 well plates for 72 h at 26°C. The activity of the compounds against promastigotes was evaluated using the Alamar Blue™ assay as previously described. pH plays a critical role in the solubility and protonation of chitosan, so the activity against promastigotes was evaluated at two different pH values (pH=7.5 and a lower pH of 6.5 by adding MES). In addition to the colorimetric method of measuring parasite viability, promastigotes were manually counted microscopically in a Neubauer haemocytometer. Results were expressed as percentage inhibition= 100% - x% viability (means ± SD).

2.8.7. *In vitro* 72- hour activity of chitosan and its derivatives against intracellular amastigotes of *L. major* and *L. mexicana*

One hundred microliters of PEMs culture at 4×10^5 cells/ml, dispensed into each well of a 16-well LabTek tissue culture slide (Thermo Fisher, UK) at pH 7.5 or pH 6.5 and incubated for 24 h at 37 °C in 5 % CO₂. After 24 h, the wells were washed with fresh culture medium to remove non-adherent cells. Stationary phase, low-passage-number *Leishmania* promastigotes were then added at a ratio of 5 :1 PEM. This infection ratio was previously found to give sufficiently high and reproducible infection levels. Slides were incubated for another 24h at 34 °C to mimic dermal temperatures in 5 % CO₂ (201). Any free, extracellular parasites were removed by washing the wells with cold culture medium. One slide was fixed with 100 % methanol for >30sec and stained with 10 % Giemsa for 5 minutes. The number of PEMs infected with *Leishmania* amastigotes per 100 macrophages was microscopically counted. All the experiments were conducted at macrophages infection levels above 80% prior to addition of chitosan. Chitosan, its derivatives and Fungizone® (a micellar suspension) at a range of concentrations (in quadruplicate) were added to the wells (100µl) and the slides were incubated for 72 h at 34 °C in 5 % CO₂. After 72 hours, the slides were fixed with 100% methanol for >30sec and stained with 10% Giemsa for 5 min. The slides were examined and the % of macrophages which were infected was counted. The anti-leishmanial activity of compounds was expressed as percentage reduction in infected

macrophages compared to untreated control wells (202). RPMI 1640 plus MES (0.05M) with pH=6.5 had no activity against *Leishmania* amastigotes

2.8.8. Influence of the origin of the host cell on the *in vitro* activity of HMW chitosan against *L. major* amastigotes

A further two host cell types, THP-1 and BMMs were infected with *L. major* and the activity of HMW chitosan was assessed. THP-1 cells (were cultured in RPMI 1640 with 10% HiFCS) and BMMs (were cultured in DMEM with 10% HiFCS) were used to assess the host cell dependence of the anti-leishmanial activity of HMW chitosan (198). The experiment was conducted as described in section (vii) at pH 6.5.

2.8.9. Influence of incubation duration on chitosan activity against *L. major* amastigotes

The experiment was conducted using *L. major* amastigotes in BMMs host cell at pH 6.5 as described in section 2.8.7 after 4, 24, 48 and 72h of incubation with HMW chitosan and Fungizone as a positive control.

2.8.10. The role of HMW chitosan on BMMs activation

One hundred microliters of BMMs, PEMs and THP-1 macrophages (4×10^5 /ml) in DMEM (BMMs) or RPMI (PEMs and THP-1) at pH=6.5 were plated in each well of 96 well plates (standard clear plates for nitric oxide assay and black wall/clear bottom plates for ROS and TNF- α assay) and incubated for 24 hours at 37 °C in 5 % CO₂. Plates were washed with DMEM (BMMs) or RPMI (PEMs and THP-1) to remove non-adherent macrophages. *L. major* at 1:5 ratio (5 parasites per host cell) was then added to the wells and the plates were incubated for 24h at 34 °C in 5 % CO₂ to allow infection of the adherent macrophages. After 24h incubation with macrophages infection rate more than 80%, the immune stimulatory effects of HMW chitosan was determined by quantifying the release of TNF- α , ROS and NO by the macrophages, as described below at pH 6.5. Then We have chosen BMMs to evaluate if the immunostimulatory effects of HMW chitosan have any important role in its anti-amastigotes activity as these macrophages are more homogenous than

PEMs and THP-1 cells (203). Both PEMs and BMMs have been reported to have a similar acidic pH \approx 5.5 of parasitophorous vacuoles of *L. amazonensis* infected PEMs and BMMs (204, 205, 206).

2.8.10.1. Measurement of TNF- α

HMW chitosan at a range of concentrations (1.64, 4.9, 14.8, 44.4, 133.3 and 400 μ g/ml) was added to infected and uninfected macrophages and the plates were incubated for 4 and 24 h at 34°C in 5% CO₂. Lipopolysaccharides from *Escherichia coli* O26:B6 (LPS, 100ng/ml; Sigma, UK) was used as a positive control and inducer. TNF- α release by the macrophages was measured using a mouse TNF- α ELISA kit (ab208348, abcam, UK) according to the manufacturer's instructions using a Spectramax M3 microplate reader (wavelength 450 nm) to determine if HMW chitosan stimulates T helper 1 or T helper 2 cells.

2.8.10.2. Measurement of ROS

ROS was measured using a 2',7'-dichlorofluorescein diacetate (DCFDA, cellular reactive oxygen species detection assay kit, abcam, UK). Uninfected and infected macrophages were treated with 25 μ M DCFDA in phosphate-buffered saline (PBS) buffer for 45 min at 37°C and then washed once in buffer. The cells were cultured at 34°C in 5% CO₂ for 0.5, 1, 2, 4, 8 and 24 h, with a range of concentrations (1.64, 4.9, 14.8, 44.4, 133.3 and 400 μ g/ml) of HMW chitosan or in the presence of H₂O₂ (25mM) (Thermofisher, UK) as a positive control in DMEM (BMMs) or RPMI (PEMs and THP-1) + 10% HiFCS (pH=6.5) in quadruplicate wells. In some experiments, cells were pre-treated with a selective inhibitor of ROS, N-acetyl-L-cysteine (NAC, 5mM; Sigma, UK), for 2 hours before the addition of the inducer or chitosan. At 0.5, 1, 2, 4, 8 and 24 h the plates were read, using a Spectramax M3 microplate reader (Ex=485nm, Em=535nm).

2.8.10.3. Measurement of NO

NO was measured by the Griess reagent (Thermofisher, UK). HMW chitosan at a range of concentrations (1.64, 4.9, 14.8, 44.4, 133.3 and 400 μ g/ml) was

added to infected and uninfected macrophages and the plates were incubated at 4 and 24 h at 34°C in 5% CO₂. LPS (100ng/ml) was used as a positive control. In some experiments, cells were pre-treated with a selective inhibitor of nitric oxide with NG-methyl-L-arginine acetate salt (0.4 mM, L-NMMA; Sigma, UK) for 2 hours before the addition of LPS. NO was quantified according to the kit protocol, Briefly, 150 µl of the cell culture supernatants (particulates were removed by centrifugation) was mixed gently with 150µl of the Griess reagent in a 96 well plates and the mixture was incubated for 30 mins at room temperature. The absorbance was measured using a Spectramax M3 plate reader (wavelength 548 nm). Sodium nitrite (Sigma, UK) at different concentrations was used to create a standard curve(207).

2.8.11. Uptake of chitosan by macrophages

The uptake of HMW chitosan was evaluated using two methods. The first method used two endocytosis inhibitors: cytochalasin D (1µg/ml , Sigma, UK) which is a phagocytosis inhibitor and dynasore (30 µg/ml, Sigma, UK) which inhibits pinocytosis (clathrin-mediated endocytosis (CME) by blocking GTPase activity of dynamin) (208, 209, 210) . The second method used dynasore and rhodamine-labelled chitosan (MW 200 kDa, Creative PEGWorks, USA) to track cellular uptake of chitosan over time by fluorescence microscopy. We chose BMMs to evaluate the uptake of chitosan by macrophages as these macrophages are more homogenous than PEMs (203).

2.8.11.1. Activity of chitosan after inhibition of the endocytic pathway of BMMs

One hundred microliters of BMMs culture (4×10^5 /ml) in DMEM at pH 6.5 or pH=7.5 were dispensed into each well of 16-well LabTek™ culture slides and were infected with stationary phase *L. major* promastigotes. Some of the infected BMMs were pretreated with dynasore (30 µg/ml) or cytochalasin D (1µg/ml) for two hours. Subsequently, HMW chitosan was added to each well at concentrations of 1.64, 4.9, 14.8, 44.4, 133.3 or 400 µg/ml and macrophages were incubated for 4 or 24 h at 34 °C in 5 % CO₂. After each point, the slides were examined as described in section (vii). The inhibition activity of the uptake

(phagocytosis or pinocytosis) of the two inhibitor was evaluated by using a fluorescence plate reader, by using fluorescent latex beads and pHrodo™ Red dextran (211). We showed that cytochalasin caused 94% and 84% phagocytosis inhibition of fluorescent latex beads (Sigma-Aldrich, UK) after 4 h and 24 h respectively and dynasore caused 95% and 90% pinocytosis inhibition of pHrodo™ Red dextran (Mw= 10,000 MW, Thermo Fisher, UK) after 4h and 24h respectively.

2.8.11.2. Microscopic imaging of the cellular uptake of rhodamine-labelled chitosan

The qualitative characterisation of chitosan uptake of cells was carried out by wide-field microscopy (Nikon Ti-E inverted microscope). Briefly, after deriving BMMs, 500µl of the BMMs (in DMEM plus 10% HiFCS at pH 6.5, 4×10^4 macrophages per ml) was seeded on each well of a 4-well LabTek tissue culture slide (Thermo Fisher, UK) and incubated for 24h at 37°C in 5% CO₂. Subsequently, 5 µg/ml of Hoechst 33342 stain (Ex/Em = 350/461 nm, Thermofisher, UK) as a nuclear dye was added and the slides were incubated for 30 min at 37°C in 5% CO₂. The macrophages were washed with PBS, *L. major*-GFP of *L. mexicana*-GFP was then added, at a ratio of 10:1 and further incubated for 24h at 34°C in 5% CO₂ (We used 10:1 ratio not 5:1 as previously as at this experiment different species of *L. major*-GFP and *L. mexicana*-GFP were used and the ratio 10:1 was sufficient to obtain a high infection rate). Macrophages were then washed with PBS and 500 µl of LysoTracker® far Red (50 nM, Ex/Em;647/668nm; Thermo Fisher, UK) was added to each well. The labelled, infected macrophages were then exposed to 30 µg/ml rhodamine-labelled chitosan (MW 200kDa, Creative PEGWorks, USA) in 500 µl of fresh DMEM plus 10% HiFCS pH 6.5 and incubated for 4 h and 24h at 37°C with live imaging at each time point. In some experiments, infected BMMs were pre-incubated with dynasore 30 µg/ml for 2 h before adding rhodamine-labelled chitosan. All the images were collected using a Nikon Ti-E inverted microscope equipped with (63x objective) using Nikon Elements software. Three images for each experiment were then analysed using ImageJ software (v 1.52, National Institutes of Health, USA). The degree of correlation

between pixels in the red and green channels was assessed by the Colocalization Colormap plugin in the ImageJ software. This plugin enables quantitative visualisation of colocalization by calculating the normalized mean deviation product (nMDP) in a colour nMDP scale (from -1 to 1): negative refers (cold colours) to no co-localization while indexes more than 0 display co-localization and the higher number refers to more colocalization (212, 213).

2.8.12. Statistical analysis.

Dose-response curves and EC₅₀ values were calculated by using GraphPad Prism version 7.02 software and the corresponding sigmoidal dose-response curves were established by using a nonlinear fit with variable slope models. Results represent means \pm SD. EC₅₀ values were compared by using extra-sum-of-squares F tests. ANOVA and t-test were used to compare differences between two groups means or more. *p* values of 0.05 were considered statistically significant.

2.9. Results

2.9.1. Cytotoxicity of chitosan and its derivatives against KB cells in RPMI (pH 7.5 and pH 6.5)

The cytotoxicity of chitosan and its derivatives against KB cells was clearly observed in a dose-dependent manner at two pH values (6.5 and 7.5) as shown in Fig 2.4. Chitosan and its derivatives had a low toxicity toward KB cells at both pH values and there was no significant difference in the cytotoxicity at these two pH values ($p < 0.05$ by an extra sum-of-squares F test) (Table 2.4). No significant difference in the cytotoxicity was observed between

the chitosans and the derivatives with $LD_{50} \approx 800 \mu\text{g/ml}$, except carboxymethyl chitosan with $LD_{50} \approx 1100 \mu\text{g/ml}$ was significantly lower toxic ($p < 0.05$ by an extra sum-of-squares F test).

Table 2.4. *In vitro* cytotoxicity of chitosan and its derivatives against KB cells at two pH values after 72h of incubation

Compound	pH=7.5*, **		pH=6.5*, **	
	$LD_{50} \mu\text{g/ml}$	$LD_{90} \mu\text{g/ml}$	$LD_{50} \mu\text{g/ml}$	$LD_{90} \mu\text{g/ml}$
Podophyllotoxin	0.8 ± 0.03	2 ± 0.3	0.8 ± 0.04	2 ± 0.4
Fungizone	61 ± 8	228 ± 9	58 ± 8	190 ± 9
HMW chitosan	751 ± 88	3146 ± 377	752 ± 90	3022 ± 366
MMW chitosan	752 ± 87	3033 ± 410	758 ± 89	3019 ± 400
LMW chitosan	811 ± 93	3095 ± 425	803 ± 90	3088 ± 420
Fungal chitosan	734 ± 95	3046 ± 377	759 ± 91	3134 ± 380
Chitosan Oligosaccharide	727 ± 97	3115 ± 402	765 ± 93	3232 ± 400
Chitosan Oligosaccharide-lactate	777 ± 98	3134 ± 388	754 ± 92	3058 ± 390
Chitosan HCL	748 ± 90	3340 ± 409	781 ± 92	3589 ± 405
PC1-CH	757 ± 91	3398 ± 388	756 ± 93	3364 ± 398
PC2-CH	794 ± 90	3613 ± 400	800 ± 92	3709 ± 410
PC3-CH	777 ± 90	3484 ± 357	786 ± 93	3719 ± 378
Carboxymethyl chitosan	1183 ± 89	3800 ± 488	1184 ± 99	3999 ± 500

Experiments were conducted in triplicate cultures, data expressed as mean \pm SD (experiment was reproduced further two times with confirmed similar data and data not shown). Chitosan and its derivatives had a low toxicity at both pH values (6.5 and 7.5) toward KB-cells and there was no significant difference in the cytotoxicity at these two pH values ($p < 0.05$ by t-test). ** No statistically significant difference was found in LD_{50} (50% lethal dose) values between three types of chitosan and other derivatives against KB-cells (except carboxymethyl chitosan which is the least toxic) ($p > 0.05$ by an extra sum-of-squares F test).

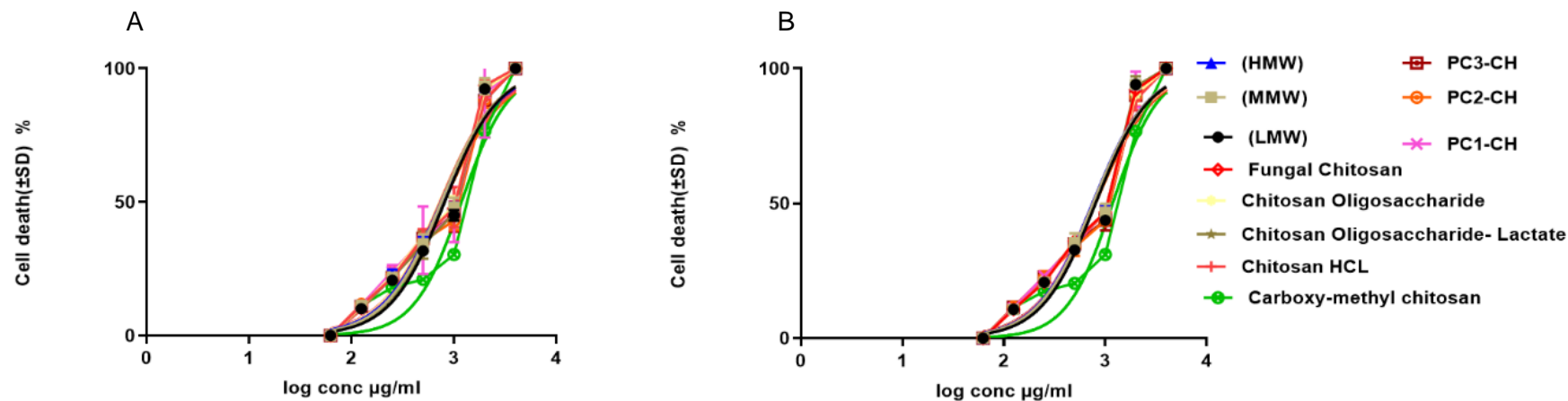


Figure 2.4. Dose-response curves of the cytotoxicity of chitosan and its derivatives against KB cells at pH=7.5 (A) and 6.5 (B). KB cells were cultured in the presence of different concentrations of chitosan and its derivatives. The toxicity of drugs was measured after 72 hours by measuring the inhibition of metabolic activity. Values are expressed as % inhibition of KB cells relative to untreated controls. No statistically significant difference was observed in LD50 values of chitosan and its derivatives against KB cells between pH=6.5 and pH=7.5 ($p>0.05$ by an extra sum-of-squares F test).

2.9.2. Analysis of anti-promastigotes activity

Anti-leishmanial activity (against promastigotes) of high, medium and low molecular weight (HMW, MMW and LMW respectively) chitosan and its derivatives (a total of 11) was tested. Dose-dependent activity (Fig 2.5) against *Leishmania* promastigotes was observed for chitosan and its' derivatives except for carboxymethyl chitosan which showed no activity against parasites within the experimental parameters tested (pH 7.5 or 6.5 and concentrations up to 400 µg/ml). Chitosan and its derivatives showed a higher anti-leishmanial activity (with around 7-20 times) at low pH compared with higher pH. Furthermore, (HMW, MMW and LMW) chitosan from crustacean source and fungal chitosan at pH= 6.5 showed a remarkable activity against *L. major* and *L. mexicana* promastigotes and were more active than other derivatives ($p < 0.05$ by an extra sum-of-squares F test) as shown in Table 2.5.

Table 2.5. *In vitro* activity of chitosan and its derivatives against promastigotes at two pH values after 72h of incubation

Compound	pH=7.5 * <i>L. major</i>		pH=7.5* <i>L. mexicana</i>		pH=6.5*,** <i>L. major</i>		pH=6.5*,** <i>L. mexicana</i>	
	EC ₅₀ µg/ml	EC ₉₀ µg/ml	EC ₅₀ µg/ml	EC ₉₀ µg/ml	EC ₅₀ µg/ml	EC ₉₀ µg/ml	EC ₅₀ µg/ml	EC ₉₀ µg/ml
Fungizone	0.05 ± 0.01	0.2 ± 0.02	0.14 ± 0.01	0.3 ± 0.03	0.07 ± 0.02	0.3 ± 0.1	0.13 ± 0.07	0.3 ± 0.02
HMW chitosan	105 ± 12	1549 ± 525	140 ± 12	2187 ± 928	5.9 ± 0.5	37 ± 9	10.4 ± 1.6	98 ± 33
MMW chitosan	113 ± 9	1277 ± 580	150 ± 12	2223 ± 681	6.2 ± 0.3	43 ± 8	10.9 ± 1.4	96 ± 27
LMW chitosan	118 ± 11	1238 ± 582	157 ± 13	2225 ± 723	6.7 ± 0.3	40 ± 8	10.2 ± 1.5	84 ± 28
Fungal chitosan	118 ± 11	1228 ± 560	150 ± 13	1991 ± 580	6.2 ± 0.3	42 ± 6	10.5 ± 1.3	61 ± 17
Chitosan Oligosaccharide	153 ± 15	1680 ± 506	190 ± 20	2366 ± 461	62.5 ± 4	446 ± 92	77 ± 2.7	452 ± 36
Chitosan Oligosaccharide-lactate	98 ± 9	1226 ± 130	125 ± 14	765 ± 83	14 ± 0.1	135 ± 2	23 ± 1.4	311 ± 25
Chitosan HCL	96 ± 7	1189 ± 211	110 ± 24	746 ± 169	13.2 ± 1	118 ± 34	20.8 ± 2.4	264 ± 61
PC1-CH	111 ± 20	1875 ± 230	176 ± 14	2832 ± 412	19.9 ± 2.8	187 ± 90	32 ± 2.2	328 ± 48
PC2-CH	104 ± 6	1485 ± 259	170 ± 8	2744 ± 377	16.5 ± 2.7	138 ± 49	28 ± 2.4	296 ± 53
PC3-CH	119 ± 19	1860 ± 365	187 ± 16	3175 ± 580	23.3 ± 2.5	218 ± 44	37 ± 2.5	442 ± 65
Carboxymethyl chitosan	No activity up to 400 µg/ml							
Experiments were conducted in triplicate cultures, data expressed as mean +/- SD (experiment was reproduced further two times with confirmed similar data and data not shown). *Statistically significant differences were found for the EC ₅₀ values of chitosan and its derivatives at pH=6.5 and pH=7.5 (<i>p</i> <0.05 by using t-test). ** <i>L. major</i> promastigotes were significantly more susceptible to chitosan and derivatives than <i>L. mexicana</i> ((<i>p</i> <0.05 by an extra sum-of-squares F test)). Amphotericin B deoxycholate (Fungizone) was used as a positive control. Both pH of 6.5 and chitosan solvent did not show any activity against promastigotes. Both RPMI alone pH 6.5 and chitosan solvent did not show any activity against promastigotes.								

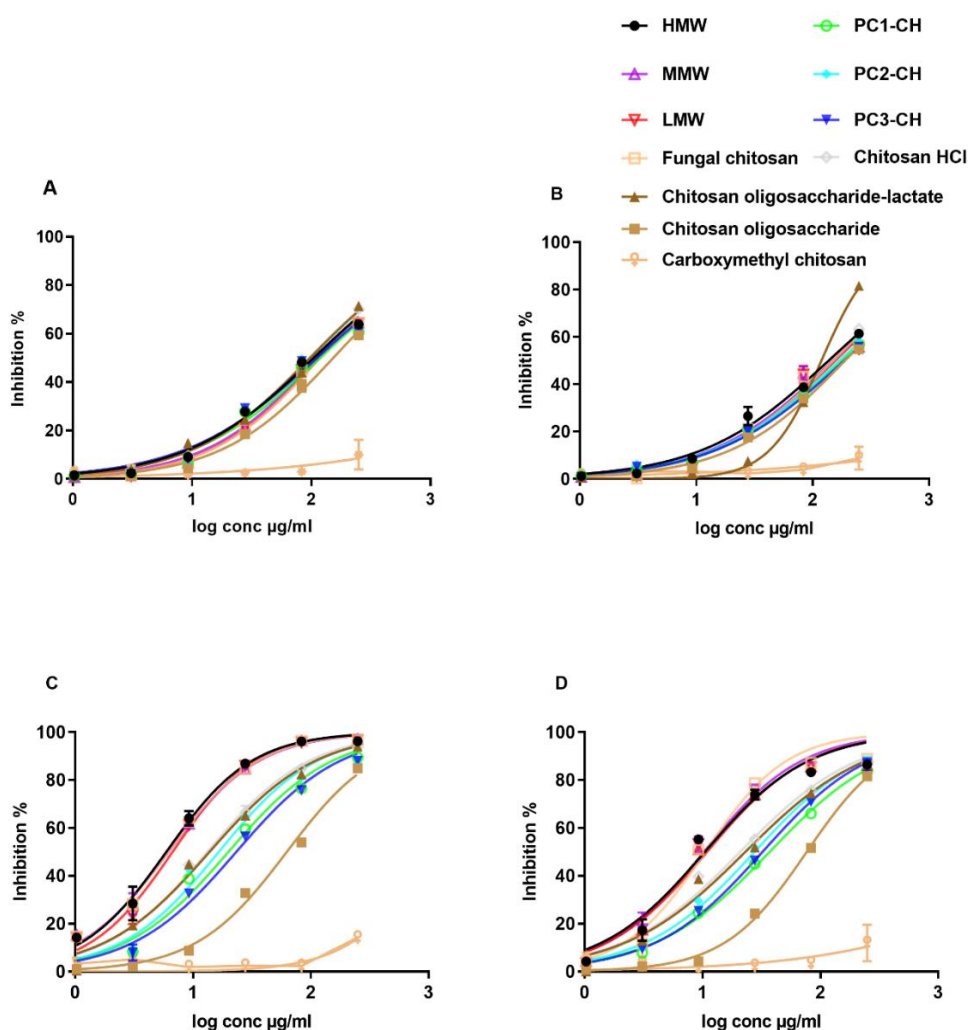


Figure 2.5. Dose-response curves of the activity of chitosan and its derivatives against *Leishmania* promastigotes at two pH values. A: *L. major* at pH=7.5; B: *L. mexicana* at pH = 7.5; C: *L. major* at pH = 6.5; D: *L. mexicana* at pH = 6.5. Promastigotes were cultured in the presence of different concentrations of chitosan and its derivatives. The activity of drugs was measured after 72h by measuring the inhibition of metabolic activity. Values are expressed as % inhibition of promastigotes relative to untreated controls. Statistically significant difference was observed in EC_{50} values of chitosan and its derivatives against *L. mexicana* and *L. major* promastigotes between pH=6.5 and pH=7.5 ($p<0.05$ by t-test). Both RPMI alone pH 6.5 and chitosan solvent did not show any activity against promastigotes.

2.9.3. Analysis of anti-amastigotes activity in PEMs

Anti-leishmanial activity (against amastigotes) of high, medium and low molecular weight (HMW, MMW and LMW respectively) chitosan and its derivatives (a total of 11) was tested. Dose-dependent activity (Fig 2.6) against *Leishmania* amastigotes was observed for chitosan and its' derivatives except for carboxymethyl chitosan which showed no activity against amastigotes

within the experimental parameters tested (pH 7.5 or 6.5 and concentrations up to 400 µg/ml). In the 72 hour assays, chitosan and its derivatives were significantly more active (with around 7-20 times) against intracellular *L. major* and *L. mexicana* amastigotes at pH 6.5 than pH 7.5 ($p < 0.05$ by a paired t-test) as shown in Fig 2.6. (HMW, MMW and LMW) chitosan from crustacean source and fungal chitosan exhibited a significantly higher activity against *L. major* and *L. mexicana* intracellular amastigotes ($EC_{50} \approx 12$ µg/ml against *L. major* and 16 µg/ml against *L. mexicana*) than other derivatives at pH= 6.5 ($p < 0.05$ by an extra sum-of-squares *F* test) as shown in Table 2.6.

Table 2.6. *In vitro* activity of chitosan and its derivatives against amastigotes infecting PEMs after 72h of incubation

Compound	pH 7.5*		pH 7.5*		pH 6.5*		pH 6.5*	
	<i>L. major</i>		<i>L. mexicana</i>		<i>L. major</i>		<i>L. mexicana</i>	
	EC ₅₀ µg/ml	EC ₉₀ µg/ml	EC ₅₀ µg/ml	EC ₉₀ µg/ml	EC ₅₀ µg/ml	EC ₉₀ µg/ml	EC ₅₀ µg/ml	EC ₉₀ µg/ml
Fungizone	0.07 ± 0.01	0.13 ± 0.05	0.19 ± 0.05	1.5 ± 0.2	0.06 ± 0.01	0.11 ± 0.06	0.18 ± 0.06	1.7 ± 0.3
HMW chitosan	98 ± 6	1635 ± 245	119 ± 9	1804 ± 304	11.4 ± 1	69 ± 18	15.4 ± 2	103 ± 28
MMW chitosan	103 ± 8	1652 ± 287	125 ± 10	1793 ± 323	12.9 ± 1	81 ± 18	16.3 ± 2	122 ± 34
LMW chitosan	102 ± 7	1651 ± 282	125 ± 10	1795 ± 320	12.1 ± 1	74 ± 14	16.1 ± 2	116.6 ± 33
Fungal chitosan	102 ± 7	1650± 276	124 ± 9	1796 ± 316	12.6 ± 3	92 ± 27	16.9 ± 2	144 ± 44
Chitosan Oligosaccharide	145 ± 12	2473 ± 500	175 ± 14	2543 ± 505	73 ± 4	260 ± 32	86.2 ± 6	288 ± 39
Chitosan Oligosaccharide- lactate	93 ± 7	1957 ± 174	120 ± 9	2365 ± 239	39 ± 1	201 ± 16	47 ± 2	245 ± 23
chitosan HCl	97 ± 11	2080 ± 516	121 ± 15	2402 ± 667	40 ± 2	210 ± 23	47.9 ± 3	243 ± 33
PC1-CH	144 ± 10	1292 ± 217	169 ± 12	1365 ± 212	68 ± 3	246 ± 26	81.7 ± 6	274 ± 38
PC2-CH	133 ± 6	1005 ± 194	159 ± 6	1705 ± 170	60 ± 3	202 ± 22	71.9 ± 5	237 ± 36
PC3-CH	163 ± 11	1052 ± 144	187 ± 10	1107 ± 142	71 ± 4	251 ± 30	83.5 ± 6	286 ± 41
Carboxymethyl chitosan	No activity up to 400 µg/ml							
Experiments were conducted in quadruplicate cultures, data expressed as mean +/- SD (experiment was reproduced further two times with confirmed similar data and data not shown). *Statistically significant differences were found between the EC ₅₀ values of chitosan and its derivatives at pH=6.5 and pH=7.5 (<i>p</i> <0.05 by using t-test). Both pH of 6.5 and chitosan solvent did not show any activity against amastigotes. Both RPMI alone pH 6.5 and chitosan solvent did not show any activity against amastigotes.								

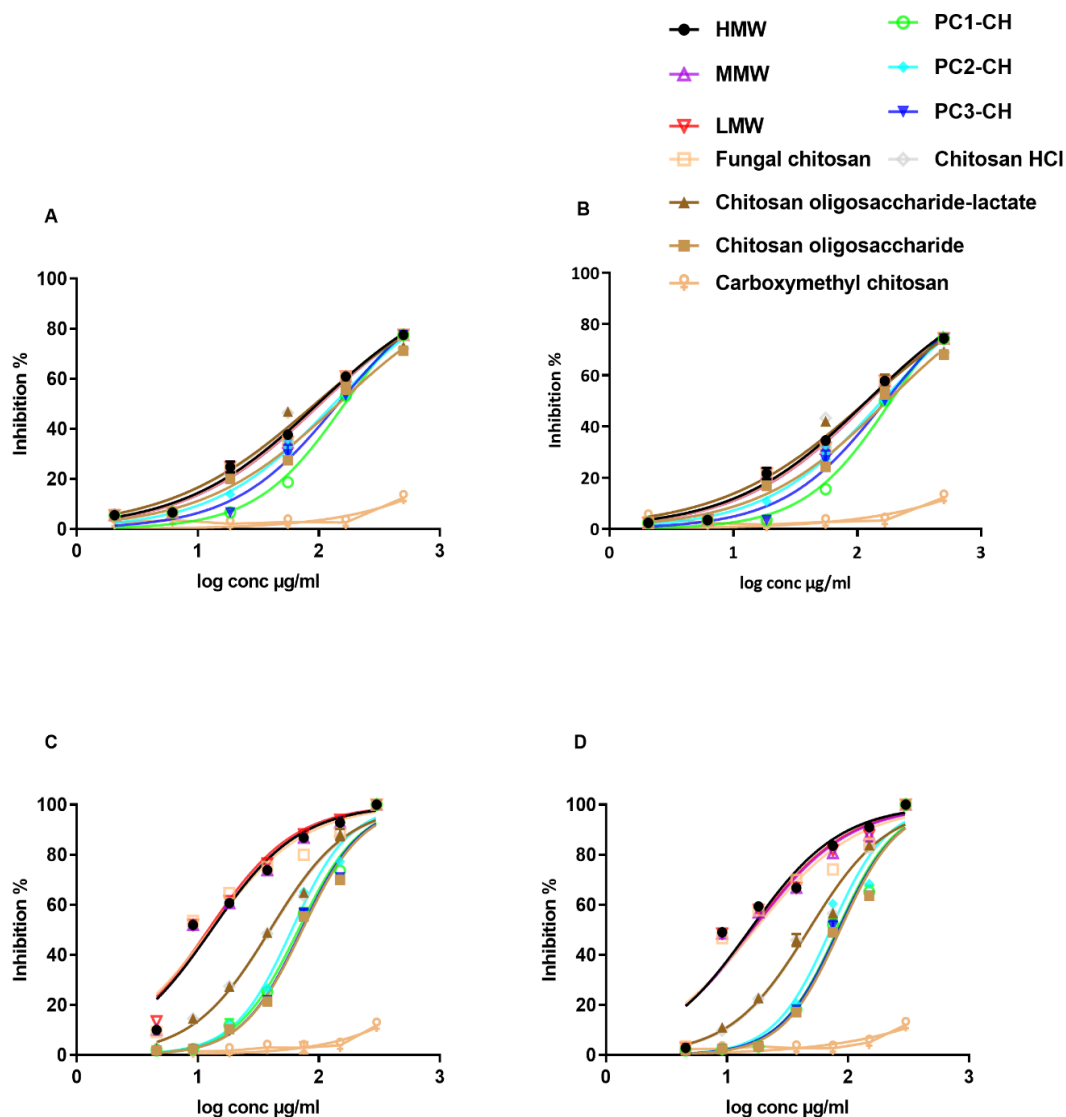


Figure 2.6. Dose-response curves of the activity of chitosan and its derivatives against *Leishmania* amastigotes at two pH values. A: *L. major* at pH=7.5; B: *L. mexicana* at pH = 7.5; C: *L. major* at pH = 6.5; D: *L. mexicana* at pH = 6.5. PEMs were infected with stationary-phase promastigotes and exposed to various concentrations of chitosan and its derivatives, followed by microscopic counting of the number of infected macrophages*. Values are expressed as % inhibition of infection relative to untreated controls. Chitosan and its derivatives are significantly more active in pH 6.5 than in pH 7.5 ($p < 0.05$ by t-test). * Macrophage infection rate was $>80\%$ after 24h. Both RPMI alone pH 6.5 and chitosan solvent did not show any activity against amastigotes.

To allow like-for-like comparison, EC_{50} values were recalculated in terms of molarity using estimated molecular weights (HMW: MW= 342.5 KDa, MMW: MW=250 KDa, LMW: MW= 120 KDa and fungal chitosan MW=130 KDa) at pH = 6.5. Based on molarity (Table 2.7 and 2.8), HMW chitosan was significantly more

active against *L. major* and *L. mexicana* promastigotes and amastigotes and hence used in all subsequent studies. Fig 2.7 observes the morphology of infected macrophages before and after treatment with HMW chitosan is taken by a microscope provided with a digital camera.

Table 2.7. *In vitro* activity of chitosans against promastigotes based on molarity

Compound	pH=6.5*,** <i>L. major</i>		pH=6.5*,** <i>L. mexicana</i>	
	EC ₅₀ μ M	EC ₉₀ μ g/ml	EC ₅₀ μ M	EC ₉₀ μ M
HMW chitosan	0.017 \pm 0.001	0.10 \pm 0.02	0.03 \pm 0.005	0.28 \pm 0.1
MMW chitosan	0.024 \pm 0.001	0.172 \pm 0.03	0.04 \pm 0.005	0.38 \pm 0.1
LMW chitosan	0.05 \pm 0.001	0.33 \pm 0.06	0.08 \pm 0.005	0.7 \pm 0.2
Fungal chitosan	0.05 \pm 0.003	0.31 \pm 0.005	0.08 \pm 0.01	0.5 \pm 0.1
Data expressed as mean \pm SD HMW chitosan is significantly more active against <i>Leishmania</i> promastigotes than other types (p <0.05 by one-way ANOVA)				

Table 2.8. *In vitro* activity of chitosans against amastigotes based on molarity

Compound	pH 6.5* <i>L. major</i>		pH 6.5* <i>L. mexicana</i>	
	EC ₅₀ μ M	EC ₉₀ μ M	EC ₅₀ μ M	EC ₉₀ μ M
HMW chitosan	0.03 \pm 0.01	0.2 \pm 0.05	0.04 \pm 0.005	0.3 \pm 0.08
MMW chitosan	0.05 \pm 0.04	0.32 \pm 0.07	0.06 \pm 0.008	0.5 \pm 0.1
LMW chitosan	0.1 \pm 0.008	0.6 \pm 0.1	0.13 \pm 0.01	0.97 \pm 0.3
Fungal chitosan	0.09 \pm 0.002	0.7 \pm 0.2	0.13 \pm 0.01	1.1 \pm 0.3
Data expressed as mean \pm SD HMW chitosan is significantly more active against <i>Leishmania</i> promastigotes than other types (p <0.05 by one-way ANOVA)				

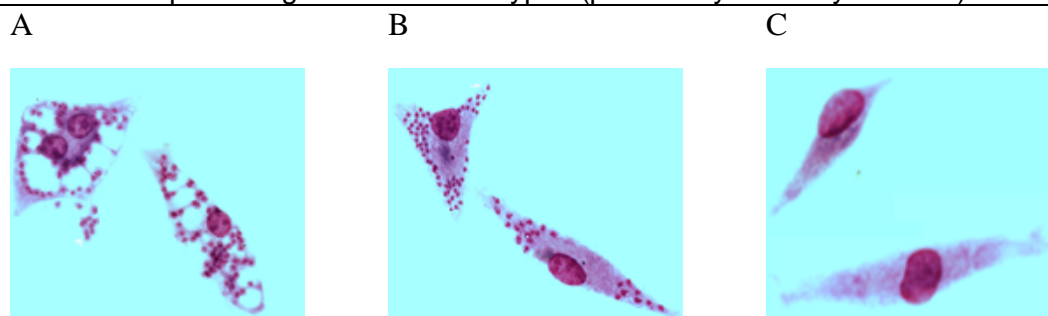


Figure 2.7. Morphology of infected (PEMs) with *L. major* and *L. mexicana* after treatment with HMW chitosan. Slides were fixed with 100% methanol for 5 minutes and stained with 10 % Giemsa for 5 minutes. These figures have been taken by a microscope attached to a digital camera. A: *L. major* infected macrophages before treatment (*L. major* amastigotes with tight vacuoles). B: *L. mexicana* infected macrophages before treatment (*L. mexicana* amastigotes with large vacuoles). C: *L. major* infected macrophages after treatment with HMW chitosan.

2.9.4. Host cell dependence of antileishmanial activity of HMW chitosan and time to kill assay on amastigotes at pH 6.5

We aimed to assess the host cell dependence of anti-leishmanial activity of HMW chitosan and Fungizone by evaluating the *in vitro* activity against *L. major* amastigotes in three different host cells (PEMs, BMMs and THP-1). EC₅₀ and EC₉₀ values of HMW chitosan and Fungizone against amastigotes infecting three different macrophage populations are summarized in Table 2.9. As can be seen, there was a significant difference in the activity of HMW chitosan and Fungizone depending on the type of the host cells ($p < 0.05$ by one-way ANOVA) and both HMW chitosan and Fungizone displayed higher activity in PEMs and BMMs than in differentiated THP-1 cells. The results in Fig 2.8 clearly show that both HMW chitosan and Fungizone had time-dependent effects against intracellular amastigotes in RPMI with pH=6.5.

Table 2.9. HMW chitosan activity against *L. major* amastigotes in three different macrophage cultures after 72 h

Host cell/infection rate % at 24h	HMW chitosan		Fungizone	
	EC ₅₀ µg/ml	EC ₉₀ µg/ml	EC ₅₀ µM	EC ₉₀ µM
PEMs / > 80%	10.31 ± 1.22*	89.07 ± 20.46	0.02 ± 0.004**	0.27 ± 0.07
BMMs / > 80%	14.60 ± 1.79*	145.7 ± 36.2	0.04 ± 0.005**	0.43 ± 0.1
THP-1/ > 80%	24.28 ± 2.87*	200.1 ± 48.8	0.08 ± 0.006**	1.15 ± 0.37
Experiments were conducted in quadruplicate cultures, data expressed as mean +/- SD (experiment was reproduced further two times with confirmed similar data and data not shown)., *, ** statistically significant difference in EC ₅₀ values between the three types of cells (Fungizone and were significantly more active in PEMs and BMMs compared with THP-1 cells) ($p < 0.05$ by an extra sum-of-squares F test) taking into consideration that infection levels were higher in PEMs and THP-1 than BMMs. % infection rate gives the percentage of infected macrophages.. Both pH of 6.5 and chitosan solvent did not show any activity against amastigotes.				

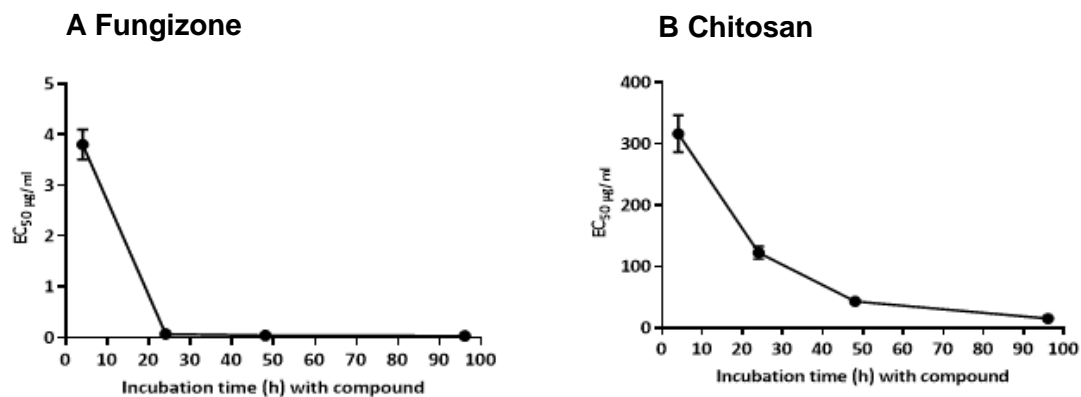
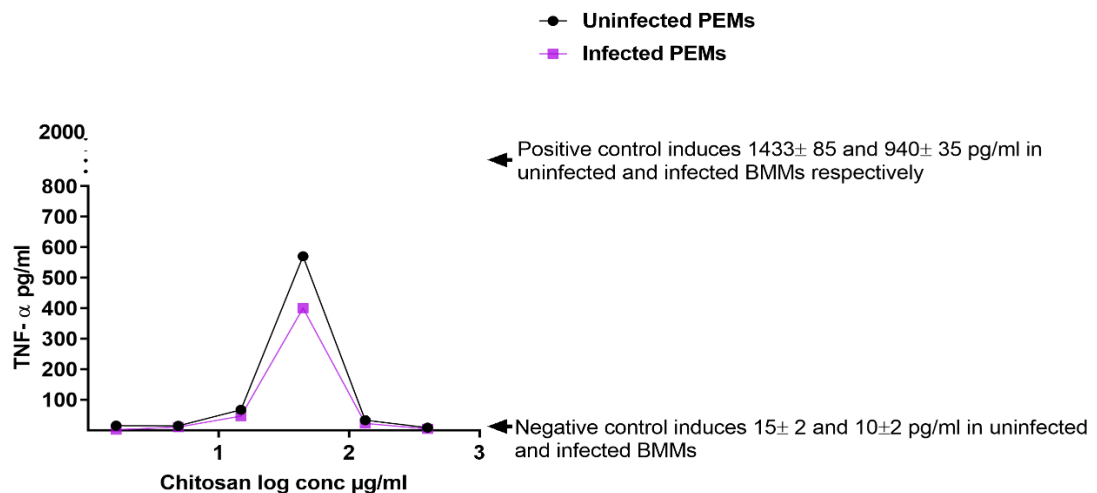
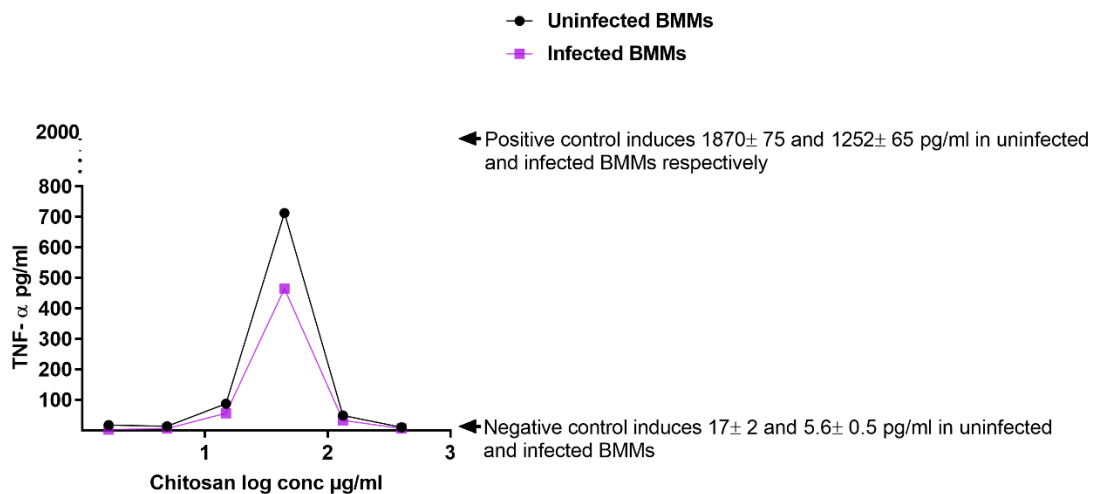


Figure 2.8. Influence of incubation duration on the chitosan and Fungizone activity against *L. major* intracellular amastigotes in BMMs. BMMs were infected with stationary-phase promastigotes and exposed to fixed concentrations of chitosan HMW and Fungizone for 4, 24, 48 and 72 h, followed by microscopic counting of the number of infected macrophages. (A) *In vitro* time-to-kill for Fungizone (B) *In vitro* time-to-kill for chitosan HMW. Results shown are the means \pm SD of quadruplicates and represent one experiment of three performed

2.9.5. Effects of HMW chitosan on the production of TNF- α by uninfected or *L. major* infected macrophages at pH = 6.5

The activation of M1 macrophages by Th1 lymphocyte plays an important role in the control of CL (14, 15, 16) therefore, we measured TNF- α production by macrophages stimulated by HMW chitosan. Following the stimulation by HMW chitosan, the TNF- α production by macrophages (BMMs, PEMs and THP-1) was found to be in a dose-dependent manner in both infected and uninfected cells as shown in Fig 2.9. After 24 h, the levels of TNF- α in the culture fluid of macrophages (both infected and uninfected BMMs, PEMs and THP-1) containing concentrations of HMW chitosan (14.8, 44.4 and 133.3 μ g/ml) was significantly higher than untreated macrophages, with TNF- α being highest at 44.4 μ g/ml chitosan. While at other concentrations (1.64, 4.9 and 400 μ g/ml), HMW chitosan did not stimulate macrophages to produce TNF- α ($p < 0.05$ by t-test). HMW chitosan at concentrations 14.8, 44.4 and 133.3 μ g/ml stimulated uninfected BMMs to produce TNF- α with 87 ± 4.5 - 712 ± 9 - 48 ± 3 pg/ml, uninfected PEMs with 67 ± 5 - 570 ± 8 - 33 ± 3 pg/ml and uninfected THP-1 with 47 ± 3.5 - 412 ± 10 -

22±3 pg/ml respectively and 56± 3.5 - 464± 10 - 32±4 pg/ml, 46± 5 - 400± 7 - 22±4 pg/ml and 36± 2 - 310± 10 - 15±4 pg/ml in *L. major* infected BMMs, PEMs and THP-1 respectively. In other words, HMW chitosan stimulated less amount of TNF- α in *L. major* infected than uninfected macrophages ($p < 0.05$ by t-test) and BMMs produced higher levels of TNF- α after the stimulation in comparison with PEMs and THP-1 ($p < 0.05$ by one-way-ANOVA). Less TNF- α was generated when the chitosan concentration was increased to 133.3 μ g/ml and above. Lipopolysaccharides from *Escherichia coli* O26:B6 (LPS; positive control) stimulated TNF- α production in both uninfected and infected BMMs, PEMs and THP-1 after a 24 h incubation period and at a significantly higher level than chitosan ($p < 0.05$ by t-test). Our results indicated that HMW chitosan activated M1 macrophages.



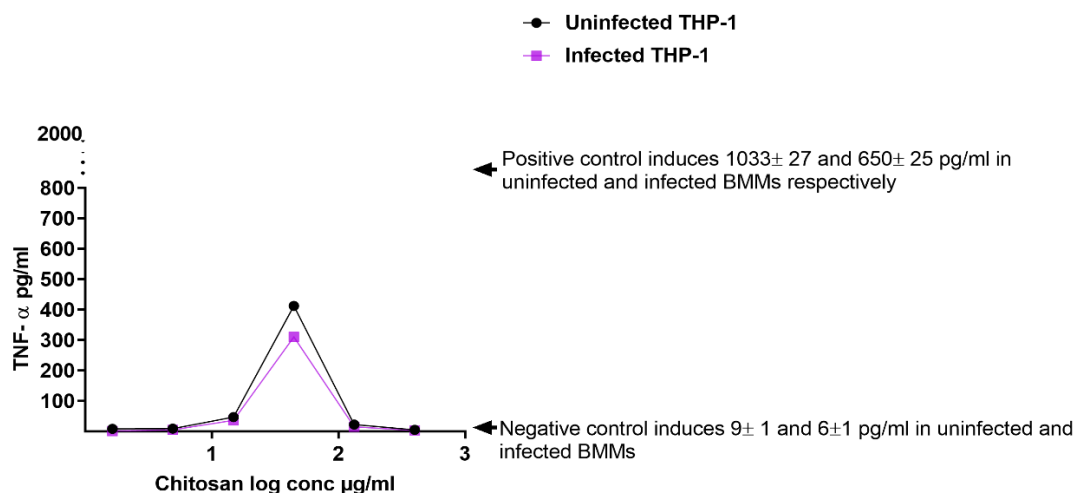


Figure 2.9. TNF- α production in uninfected and *L. major* infected BMIMs, PEMs and THP-1 macrophages* after 24 h of exposure to 1.64, 4.9, 14.8, 44.4, 133.3 and 400 $\mu\text{g/ml}$ of chitosan at pH = 6.5. The dose-response in both uninfected and *L. major* infected macrophages was bell-shaped. TNF- α production was significantly decreased ($p < 0.05$ by t-test) by infecting the cells with *L. major*. TNF- α stimulation was higher with the rank BMIMs, PEMs and THP-1. Experiments were conducted in quadruplicate, data are expressed as mean \pm SD (experiment was reproduced further two times with confirmed similar data and data not shown). Positive control = macrophages treated with LPS 10 $\mu\text{g/ml}$. Negative control = macrophages not exposed to chitosan. *Initial macrophage infection rate was $>80\%$ after 24 h. Chitosan solvent did not cause any TNF- α production.

2.9.6. Effects of HMW chitosan on the production of ROS by macrophages at pH = 6.5

ROS plays an important role in the killing of intracellular amastigotes (14, 15, 16) therefore, we measured ROS production by macrophages stimulated by HMW chitosan. HMW chitosan (at concentrations 14.8, 44.4 and 133.3 $\mu\text{g/ml}$) increased the production of ROS (indicated by H2DCFDA fluorescence) after 4 h of incubation but did not stimulate ROS after 8 h of incubation (Table 2.10). Other concentrations of HMW chitosan (1.64, 4.9 and 400 $\mu\text{g/ml}$) did not stimulate BMIMs, PEMs or THP-1 to produce ROS after 4 h or 8 h of incubation.

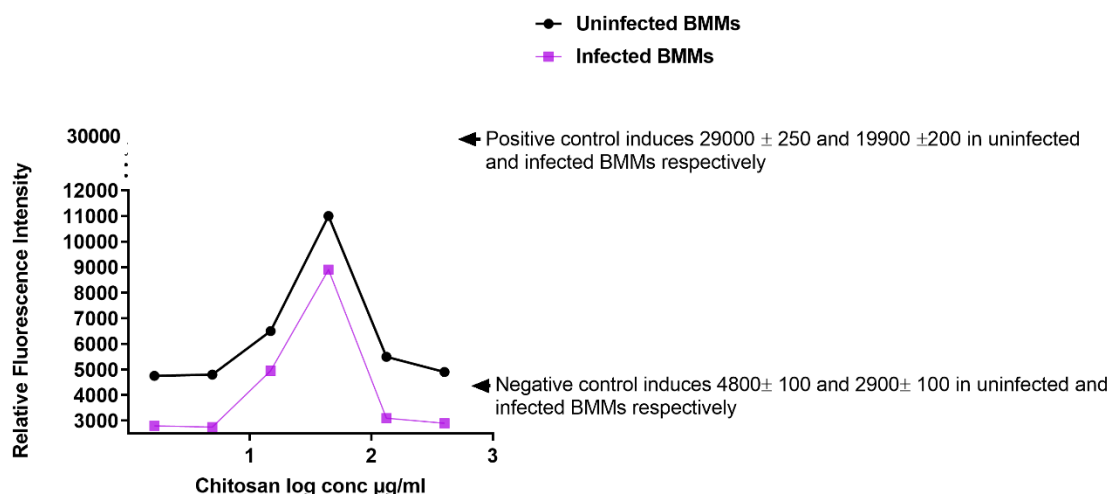
The ROS response in both uninfected and infected BMIMs, PEMs and THP-1 was in bell shaped – similar to that seen with TNF- α . Increasing chitosan concentration (more than 14.8 $\mu\text{g/ml}$) increased ROS production until concentration 44.4 $\mu\text{g/ml}$ (the maximum production of ROS), after which increasing concentration reduced

ROS production. In addition, we showed that ROS production by macrophages was significantly decreased ($p < 0.05$ by t-test) by infecting the cells with *L. major* as shown in Fig 2.10. BMMs produced higher levels of ROS after the stimulation in comparison with PEMs and THP-1 ($p < 0.05$ by one-way-ANOVA).

Table 2.10. ROS production in uninfected and *L. major* infected BMMs after 8 h of exposure to different concentrations of HMW chitosan at pH=6.5

ROS (Relative Fluorescence Intensity) in:		
Chitosan $\mu\text{g/ml}$	Uninfected BMMs	Infected BMMs
1.64	4000 ± 100	2650 ± 100
4.9	3999 ± 200	2550 ± 150
14.81	4020 ± 150	2650 ± 100
44.4	4050 ± 100	2750 ± 200
133.3	4000 ± 200	2564 ± 150
400	3959 ± 100	2400 ± 100
Negative control = BMMs not exposed to chitosan	4750 ± 100	2850 ± 100

Experiments were conducted in quadruplicate, data is expressed as mean \pm SD (experiment was reproduced a further two times with confirmed similar data (not shown). Chitosan solvent alone did not cause any ROS production.



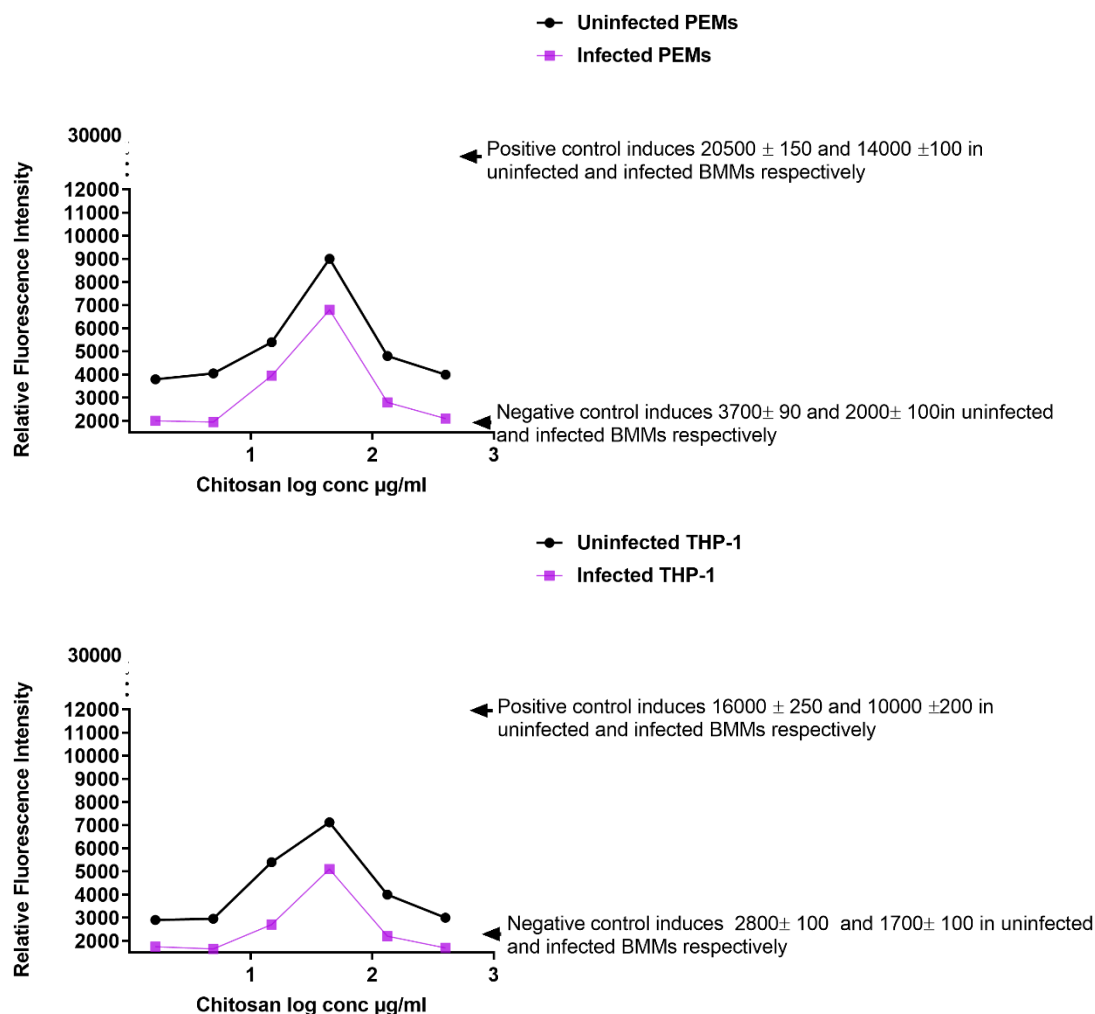


Figure 2.10. ROS production in uninfected and *L. major* infected BMMs, PEMs and THP-1 macrophages * after 4 h of exposure to 1.64, 4.9, 14.8, 44.4, 133.3 and 400 µg/ml of HMW chitosan at pH=6.5. High levels of ROS were induced by both uninfected and *L. major* infected macrophages exposed to HMW chitosan compared to those that were not ($P < 0.05$ by t-test). Maximum production of ROS occurred at 44.4 µg/ml of chitosan. ROS production by *L. major* infected macrophages was significantly lower compared to uninfected cells ($p < 0.05$ by t-test). ROS stimulation was higher with the rank BMMs, PEMs and THP-1. Experiments were conducted in quadruplicate, data is expressed as mean \pm SD (experiment was reproduced a further two times with confirmed similar data (not shown). Positive control = macrophages treated with H_2O_2 25 mM (a known ROS inducer). Negative control = macrophages not exposed to chitosan. *Initial macrophage infection rate was $>80\%$ after 24 h. Chitosan solvent did not cause any ROS production.

We found that HMW chitosan had an *in vitro* stimulatory effect on BMMs ROS production after 4h of incubation. We therefore investigated whether this ROS plays any role in the activity of HMW chitosan against intracellular amastigotes. For these experiments, the 4 h post treatment time point was taken because ROS

peaked at this point in BMMs in response to chitosan treatment at a time when chitosan does not induce NO in BMMs (*ibid*). Scavenging of ROS by the ROS scavenger, 5mM N-acetyl-L-cysteine (NAC), had no significant impact on the activity of chitosan against intracellular amastigotes ($p > 0.05$ by t-test) – see Fig 2.11. ROS scavenger (N-acetyl-L-cysteine (NAC), 5mM) caused a complete scavenging of ROS after 4 h (Table 2.11). and had no cytotoxicity against KB cells or leishmanicidal against *L. major* amastigotes. Even though chitosan stimulated ROS production but this did not play a role in the anti-leishmanial activity of chitosan.

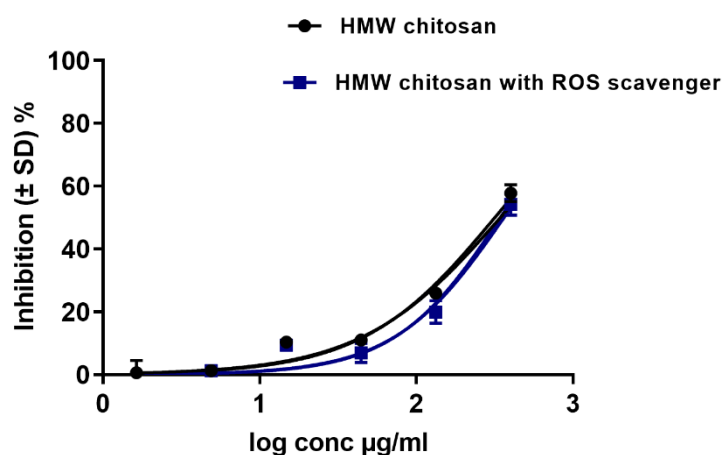


Figure 2.11. Activity of HMW chitosan against *L. major* amastigotes in BMMs* after 4 h, with and without ROS scavenger at pH = 6.5. Infected macrophages were pre-incubated with 5 mM NAC for 2 h, after which HMW chitosan at concentrations 1.64, 4.9, 14.8, 44.4, 133.3 and 400 $\mu\text{g/ml}$ was added and the cells were incubated for a further 4 h. Chitosan activity against intracellular amastigotes was evaluated as described in section (vii). Values are expressed as % inhibition of infection relative to untreated controls. After 4h, there was no significant difference in the anti-leishmanial activity of chitosan after scavenging of ROS ($p > 0.05$ by t-test). Experiments were conducted in quadruplicate, data is expressed as mean \pm SD. Experiment was reproduced further two times with confirmed similar data (not shown). *Initial macrophage infection rate was $>80\%$ after 24 h.

Table 2.11. ROS production in uninfected and *L. major* infected BMMs after exposure to chitosan in the presence of ROS scavenger

Chitosan µg/ml	ROS (Relative Fluorescence Intensity) after 4 h in:	
	Uninfected BMMs pre-treated with ROS scavenger	Infected BMMs pre-treated with ROS scavenger
1.64	4700 ± 200	2850 ± 150
4.9	4800 ± 250	2750 ± 200
14.81	4750 ± 100	2950 ± 150
44.4	4800 ± 100	2750 ± 100
133.3	4900 ± 150	2864 ± 100
400	4950 ± 100	2600 ± 100
Positive control (ROS) = BMMs treated with 25 mM H₂O₂	4800 ± 250	2750 ± 100
Negative control = BMMs not exposed to chitosan or to H₂O₂	4800 ± 100	2900 ± 100
Experiments were conducted in quadruplicate, data is expressed as mean +/- SD (experiment was reproduced a further two times with confirmed similar data (not shown). ROS was measured after 4 h of exposure to HMW chitosan.		

2.9.7. Effects of HMW chitosan on the production of NO by macrophages at pH = 6.5

NO plays an important role in the killing of intracellular amastigotes (14, 15, 16) therefore, we measured NO production by macrophages stimulated by HMW chitosan. We showed that chitosan did not have a stimulatory effect on BMMs, PEMs and THP-1 NO production after 4 h of incubation (Table 2.12). However, after a 24 h incubation, HMW chitosan at pH=6.5 had a stimulatory effect on BMMs, PEMs and THP-1 NO production in a clear bell-shaped dose-dependent manner. HMW chitosan at concentrations 14.8, 44.4 and 133.3 µg/ml induced uninfected BMMs to produce NO with 14.9± 0.3 - 34±1.2 - 11±1 µM, uninfected PEMs with 10.9± 0.4 - 26±1.2 - 8.5±1 µM and uninfected THP-1 with 8.9± 0.2 - 20±1 - 6.1±0.5 µM respectively and 11 ±1- 26 ± 2.5 - 8 ± 1.2 µM, 8 ±1 - 20 ± 2 - 6 ± 1.2 µM and 6± 0.1 - 14±1 - 4.1±0.5 µM in *L. major* infected BMMs, PEMs and THP-1 respectively, NO being highest at 44.4 µg/ml. While other concentrations of HMW chitosan (1.64, 4.9 and 400 µg/ml) did not stimulate macrophages to produce NO after 24 h of incubation. In other words, HMW chitosan stimulated a

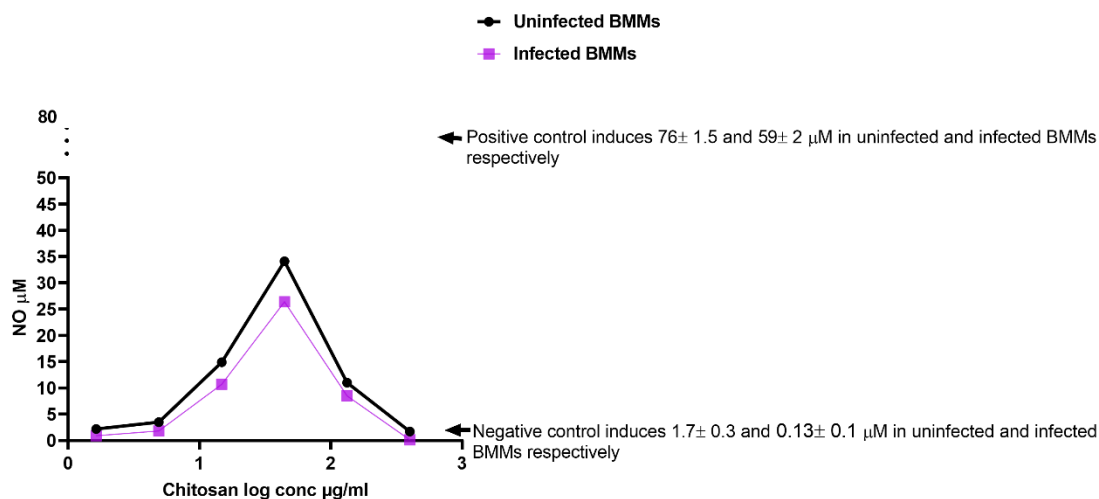
lower quantity of NO in infected than uninfected macrophages ($p < 0.05$ by t-test) and BMMs produced higher levels of NO after the stimulation in comparison with PEMs and THP-1 ($p < 0.05$ by one-way-ANOVA) (Fig 2.12).

LPS caused significantly higher NO production compared to HMW chitosan ($p < 0.05$ by t-test) in both uninfected and infected BMMs, PEMs and THP-1. The levels of NO produced by *L. major* infected BMMs exposed to LPS (positive control) or HMW chitosan were significantly lower than levels produced by uninfected macrophages ($p < 0.05$ by t-test) (Fig 2.12).

Table 2.12. NO production in uninfected and *L. major*-infected BMMs after 4h of exposure to different concentrations of HMW chitosan at pH=6.5

Chitosan $\mu\text{g/ml}$	NO production (μM) in:	
	Uninfected BMMs	Infected BMMs
1.64	0	0
4.9	0	0
14.81	0	0
44.4	0.05 ± 0.01	0
133.3	0.06 ± 0.01	0.05 ± 0.01
400	0.05 ± 0.01	0.04 ± 0.01
Negative control = BMMs not exposed to chitosan	0.07 ± 0.01	0.05 ± 0.01

Experiments were conducted in quadruplicate, data is expressed as mean \pm SD (experiment was reproduced a further two times with confirmed similar data (not shown). Chitosan solvent alone did not cause any NO production.



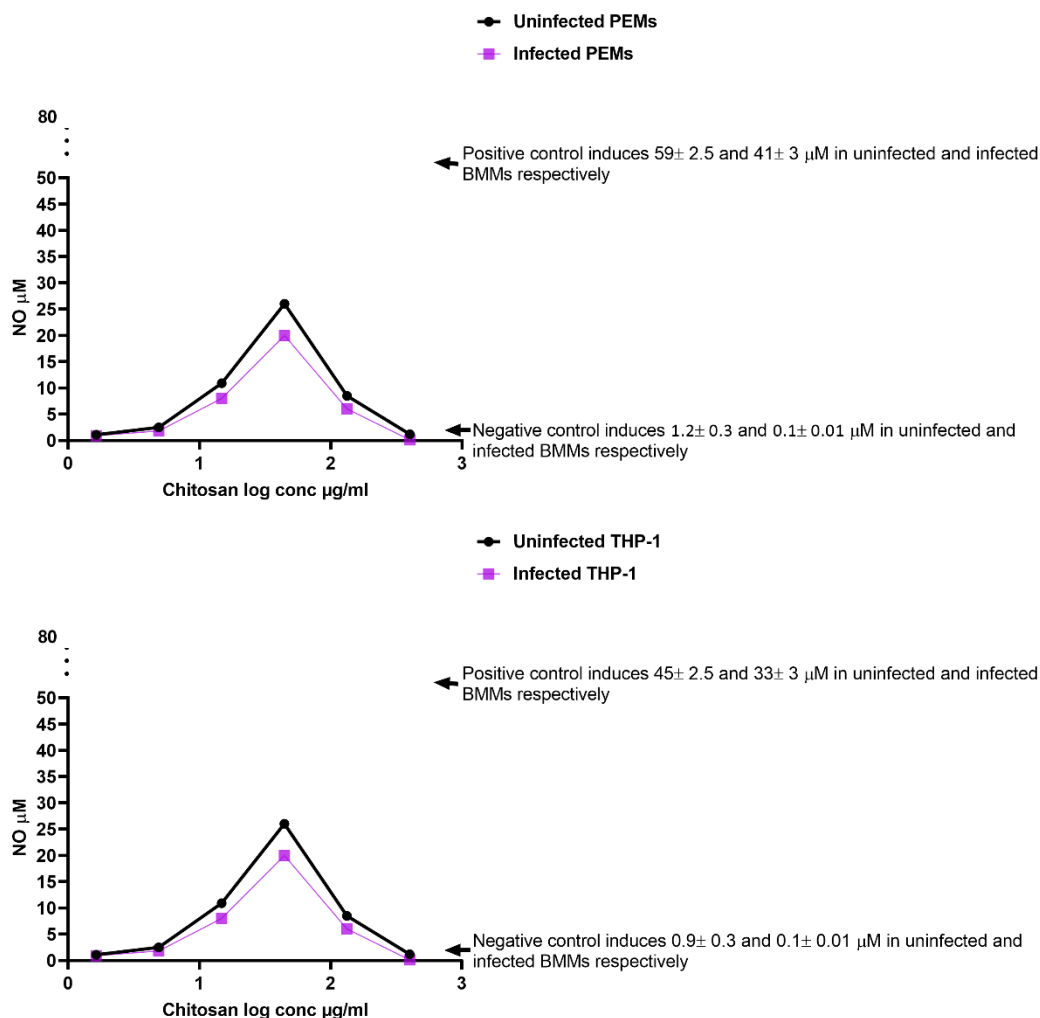


Figure 2.12. NO production in uninfected and *L. major* infected BMMs, PEMs and THP-1 macrophages * after 24 h of exposure to 1.64, 4.9, 14.8, 44.4, 133.3 and 400 µg/ml of chitosan at pH = 6.5. The response in both uninfected and infected macrophages was bell-shaped in relation to chitosan concentration. Maximal production of NO was stimulated by 44.4 µg/ml of chitosan. NO production was significantly decreased ($p < 0.05$ by t-test) when the cells had been infected with *L. major*. NO stimulation was higher with the rank BMMs, PEMs and THP-1. Experiment was conducted in quadruplicate cultures, data expressed as mean \pm SD (experiment was reproduced a further two times with confirmed similar data and data not shown). Positive control = macrophages treated with LPS 10 µg/ml. Negative control = macrophages not exposed to chitosan. *Initial macrophage infection rate was $>80\%$ after 24 h. Chitosan solvent did not cause any NO production.

As HMW chitosan had an *in vitro* stimulatory effect on BMMs NO production after 24h of incubation we investigated further whether NO has any role in the activity of HMW chitosan against intracellular amastigotes. Inhibition of NO production by the NO inhibitor NG-methyl-L-arginine acetate salt (L-NMMA) at 0.4mM, had no

significant influence on the activity of chitosan against intracellular amastigotes ($p > 0.05$ by t-test) (Fig 2.13). The NO inhibitor (L-NMMA, 0.4 mM) caused 90% reduction in NO production (Table 2.13) after 24 h and had no cytotoxicity effects against KB cells and no leishmanicidal against intracellular *L. major* amastigotes. Even though chitosan stimulated NO production but this did not play a role in the anti-leishmanial activity of chitosan.

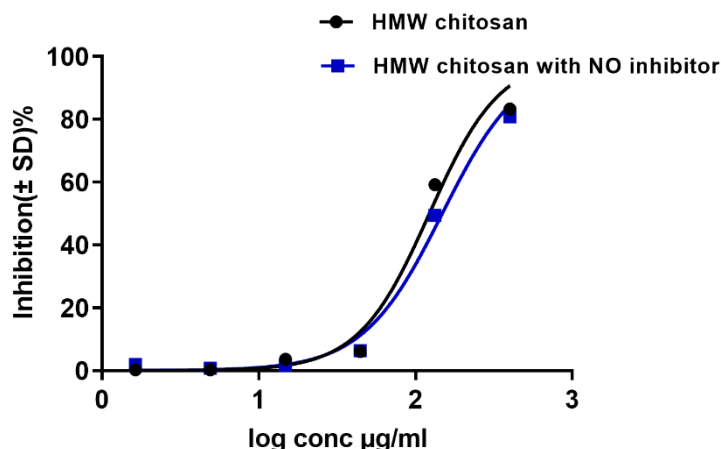


Figure 2.13. Activity of HMW chitosan against *L. major*-infected BMMs* after 24 h in the presence or absence of an NO inhibitor at pH = 6.5. Infected macrophages were pre-incubated with the NO inhibitor L-NMMA (0.4 mM) for 2 h, following which HMW chitosan at concentrations 1.64, 4.9, 14.8, 44.4, 133.3 and 400 $\mu\text{g/ml}$ was added and the cells were incubated for a further 24 h. Chitosan activity against intracellular amastigotes was evaluated as described in section (vii). Values are expressed as % inhibition of infection relative to untreated controls. After 24 h, there was no significant difference in the activity of chitosan after inhibition of NO ($p > 0.05$ by t-test). Experiment was conducted in quadruplicate cultures, data expressed as mean \pm SD. Experiment was reproduced a further two times and confirmed the results (data not shown). *Initial macrophage infection rate was $>80\%$ after 24 h.

Table 2.13. NO production in uninfected and *L. major* infected BMMs after exposure to chitosan in the presence of NO inhibitor at pH=6.5

Chitosan $\mu\text{g/ml}$	NO μM after 24 h in:	
	Uninfected BMMs pre-treated with NO inhibitor	Infected BMMs pre-treated with NO inhibitor
1.64	1.4 ± 0.4	0.15 ± 0.1
4.9	1.5 ± 0.3	0.16 ± 0.1
14.81	1.9 ± 0.5	0.17 ± 0.1
44.4	1.6 ± 0.2	0.15 ± 0.1
133.3	1.2 ± 0.4	0.14 ± 0.1
400	1.0 ± 0.6	0.15 ± 0.1

Positive control (NO) = BMMs treated with 10 µg/ml LPS	1.4 ± 0.3	0.16 ± 0.1
Negative control = BMMs not exposed to chitosan or to LPS	1.7 ± 0.3	0.13 ± 0.1
Experiments were conducted in quadruplicate, data is expressed as mean +/- SD (experiment was reproduced a further two times with confirmed similar data (not shown). NO was measured after 24 h of exposure to HMW chitosan.		

2.9.8. Cellular uptake of HMW chitosan and inhibition of endocytosis

We found that the activation of M1 macrophages by HMW chitosan did not play a role in its activity against intracellular amastigotes therefore, we investigated whether the anti-leishmanial effects of HMW chitosan against intracellular amastigotes after 4 h and 24 h exposure were dependent on the direct activity of chitosan following its entry into the macrophages at pH=6.5. No significant difference was observed in the activity of chitosan against intracellular amastigotes when it was added after prior phagocytosis inhibition with cytochalasin D ($p > 0.05$ by t-test). In contrast, dynasore (an inhibitor of pinocytosis, a clathrin-mediated endocytosis (CME) inhibitor) did significantly affect chitosan mediated parasite killing at pH = 6.5 as shown in Fig. 33 ($p < 0.05$ by t-test). The same activity was seen at pH 7.5. – see Fig 2.14, panel C. We found that cytochalasin caused 94 and 84% phagocytosis inhibition of fluorescent latex beads (Sigma-Aldrich, UK) after 4 h and 24 h respectively and dynasore caused 95 and 90% pinocytosis inhibition of pHrodo™ Red dextran (Mw= 10,000 MW, Thermo Fisher, UK) after 4h and 24h respectively (Table 2.14), The two inhibitors had no activity against intracellular *L. major* amastigotes at the concentrations used. Pinocytosis (CME) played a critical role in the efficacy of HMW chitosan against intracellular amastigotes.

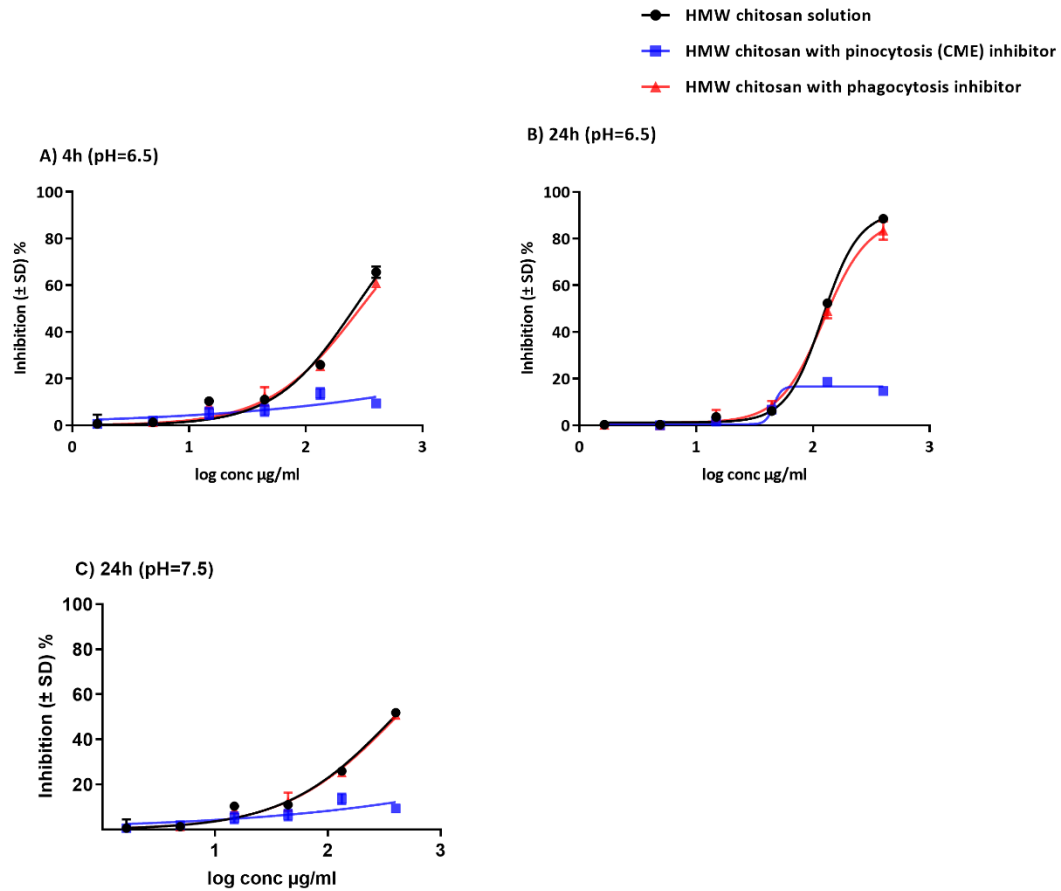


Figure 2.14. Activity of HMW chitosan against *L. major* infected BMMs* after 4 h, pH=6.5 (A), 24 h, pH=6.5 (B) and at 24 h, pH=7.5 with or without phagocytosis inhibitor or pinocytosis (CME) inhibitor. We found that chitosan requires pinocytosis (CME) not phagocytosis by BMMs for killing of *L. major* amastigotes at pH = 6.5 and 7.5. BMMs were infected with stationary-phase promastigotes. Some of the infected macrophages were pre-incubated with cytochalasin D (phagocytosis inhibitor) or dynasore (pinocytosis (CME) inhibitor) and exposed to various concentrations (1.64, 4.9, 14.8, 44.4, 133.3 and 400 $\mu\text{g/ml}$) of chitosan for 4 h and 24 h, followed by microscopic counting of the number of infected macrophages. There was no significant difference in the activity of HMW chitosan after inhibition of phagocytosis ($p > 0.05$ by t-test). While a significant inhibition of chitosan mediated parasite killing occurred in the presence of dynasore at two pH values ($p > 0.05$ by t-test). Values are expressed as % inhibition of infection relative to untreated controls. Experiment was conducted in quadruplicate cultures, data expressed as mean \pm SD. Experiment was reproduced a further two times and confirmed the results (data not shown). *Initial macrophage infection rate was $>80\%$ after 24 h.

Table 2.14. Phagocytosis and pinocytosis by *L. major* infected BMMs in the presence of the uptake inhibitors

Time/Hour	Number of latex beads \pm SD *10 ⁵ /mg protein		Concentration of dextran \pm SD μ g/mg protein	
	Without cytochalasin D	With cytochalasin D	Without dynasore	With dynasore
4	108 \pm 8	6 \pm 1	4.9 \pm 0.5	0.2 \pm 0.1
24	456 \pm 30	73 \pm 8	18.9 \pm 1	1.8 \pm 0.2

Experiments were conducted in triplicate, data is expressed as mean \pm SD (experiment was reproduced a further two times with confirmed similar data (not shown)).

2.9.9. Fluorescence microscopy of the uptake of chitosan by macrophages

Rhodamine-labelled chitosan was used to track the delivery of chitosan to the parasitophorous vacuole (PV) of *Leishmania* infected macrophages. Fig 2.15 illustrates the cellular uptake of chitosan by *L. major*-GFP- or *L. mexicana*-GFP-infected BMMs after 4 h and 24 h rhodamine-labelled chitosan exposure. There was co-localization of chitosan and intracellular amastigotes after 4 h and 24 h with nMDP colour index 0.7 and 1 respectively (see nMDP material and methods). The uptake of chitosan increased in a time-dependent manner. Fig 2.15 (Panels D and E) shows this uptake after 4 h and 24 h respectively, and the accumulation of chitosan in PVs (shown as yellow that indicates co-localization of rhodamine and GFP). Fig 2.15 (Panel F) also shows that the inhibition of pinocytosis (CME) with dynasore prevented the uptake of chitosan with a negative nMDP colour index that represents no co-localization of chitosan and amastigotes. This is also supporting evidence for the uptake by pinocytosis as seen in Fig 2.14.

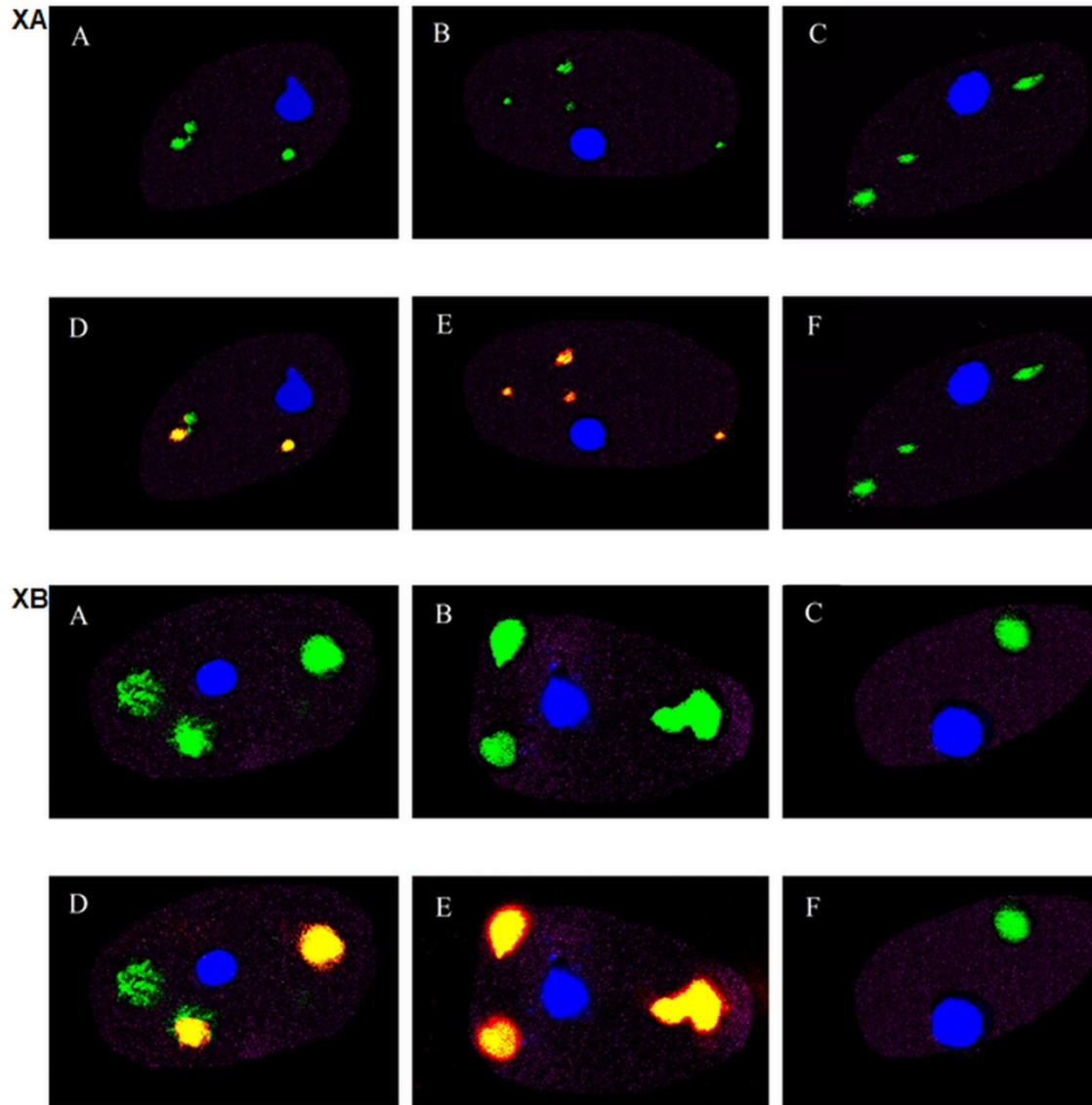


Figure 2.15. Fluorescence microscopy images of the cellular uptake of rhodamine-labelled chitosan over 4 and 24 h at pH=6.5 by BMMs infected with *L. major* (XA) or with *L. mexicana* (XB). Green represents intracellular amastigotes, red represents labelled chitosan and yellow represents merged red chitosan and green *Leishmania*. Panels A-F represent the following: Infected BMMs unexposed to chitosan after 4 h (panel A) or 24 h (panel B); Infected BMMs exposed to chitosan after 4 h (panel D) or 24 h (panel E); Infected BMMs unexposed to chitosan after 24 h (panel C) and Infected BMMs exposed to chitosan and pinocytosis inhibitor (dynasore) after 24 h (panel F)

2.10. Discussion

The literature on the anti-leishmanial activity of chitosan and its derivatives is limited, especially pertaining to its mechanism of action (124, 214, 215). In this study, we assessed the anti-leishmanial activity of various forms of chitosan, including low, medium and high molecular weight chitosan, and chitosan derivatives. Chitosan derivatives are generally produced by chemical modification of the amino or hydroxyl groups of chitosan for the optimization of the physicochemical properties. We found that chitosan and its derivatives had minimal cytotoxicity against KB-cells with LD₅₀ values ≥ 700 $\mu\text{g/ml}$ and other macrophages (PEMs, BMMs and THP-1) at pH 7.5 or 6.5. This data supports previous reports of chitosan's low cytotoxicity against CCRF-CEM (human lymphoblastic leukaemia) and L132 (human embryonic lung) cells with similar LD₅₀ values (173).

We determined that a lower pH 6.5, compared to 7.5, enhanced by 7-20 times the anti-leishmanial activity of chitosan and its derivatives against *L. major* and *L. mexicana* promastigotes and amastigotes. This higher activity of chitosan at the lower pH 6.5 could be due to its greater ionisation (protonation of the amino groups; PKa of chitosan ≈ 6.3). The greater positive charge could increase the chitosan antimicrobial activity by interacting with the negatively charged microbial membrane – in accordance with the first postulated mechanism of antimicrobial activity (124, 174). A higher chitosan activity at lower pH (pH ≈ 5) has previously been reported against *Escherichia coli* and *Salmonella typhimurium* (216, 217). Our study is the first to show the pH dependence of the anti-leishmanial activity of chitosan and its derivatives and could explain why literature reports of the anti-leishmanial activity of chitosan have shown such variability, with EC₅₀ values ranging from 70 to 240 $\mu\text{g/ml}$ against *L. infantum*, *L. amazonensis* and *L. chagasi* promastigotes and amastigotes (122, 127, 129, 191, 218, 219). For example, in one study, the EC₅₀ of chitosan against *L. infantum* amastigotes (in PEMs) in RPMI 1640 medium was 100.81 $\mu\text{g/ml}$, but the pH at which the experiment was conducted was not mentioned (127). Moreover, Malli *et al* (2019) reported that chitosan solution (LMW) showed no activity until 100 $\mu\text{g/ml}$ against *L. major*

promastigotes or amastigotes without mentioning the pH of the experiment(220).

Influence of pH was also seen when the anti-leishmanial activity of chitosan (of the different molecular weights) and chitosan derivatives were compared. While the different chitosans and derivatives showed minor differences in their anti-leishmanial activity at pH 7.5, the derivatives were 3 to 5 times less active than the HMW, MMW, LMW and fungal chitosan at lower pH 6.5. This reduced activity could be due to the lower number of amino groups on the chitosan derivatives (see Fig 2.3). These derivatives are more soluble at a higher pH and have similar activity to chitosan, but at a lower pH the higher protonation of the chitosan improves the anti-leishmanial activity significantly (221, 222). Carboxymethyl chitosan had no anti-leishmanial activity - most of the amino groups on this derivative have been substituted by carboxymethyl moieties making the molecule negatively charged (223) .

HMW, MMW, LMW and fungal chitosan have a wide range of molecular weights. To allow like-for-like comparison, EC₅₀ values were recalculated in terms of molarity using estimated molecular weights (HMW: MW= 342.5 KDa, MMW: MW=250 KDa, LMW: MW= 120 KDa and fungal chitosan MW=130 KDa) at pH = 6.5. Based on molarity (Table 2.7 and 2.8), HMW chitosan was significantly more active against *L. major* and *L. mexicana* promastigotes and amastigotes and further studies were conducted using HMW chitosan. The higher anti-leishmanial activity of HMW chitosan compared to MMW and LMW chitosan mirrors its greater antibacterial activity in another study against *Escherichia coli*, *Pseudomonas aeruginosa* and *Staphylococcus aureus* (224). HMW has a long chain, and therefore more glucosamine units, and possesses more amino groups (Fig 2.3) resulting in more protonated groups (-NH₃⁺) than MMW and LMW(224) which could explain its greater potency.

We also showed that the anti-leishmanial activity of chitosan is significantly greater against *L. major* infected PEMs or BMMs compared to differentiated THP-1 cells in the order PEMs>BMMs>THP-1 cells underlining the need to take the host cell into consideration when conducting similar experiments.

In order to understand the potential anti-amastigote mechanism(s) of chitosan, we investigated whether the activity of HMW chitosan against the intracellular amastigotes was via direct uptake into the host cell and localisation in the parasitophorous vacuole or indirectly via the activation of M1 macrophages,, given that the cellular immune responses in cutaneous leishmaniasis play a critical role in self-cure (225, 226).

The activation of M1 macrophages by Th1 lymphocyte subpopulation, which produces different cytokines, primarily IFN- γ and TNF- α is crucial for the elimination of the intracellular *Leishmania* via the triggering of an oxidative burst and therefore, the host cells increase the production of ROS and NO which are responsible for killing of the parasite (38, 39). We found that HMW chitosan stimulated TNF- α production by macrophages and this would be expected to be an indicator of an M1 macrophage that would have greater leishmanicidal activity. Our results show that chitosan stimulated BMMs, PEMs and THP-1 ROS production with a peak after 4 h and led to a significant increase in the TNF- α and NO production after 24 h in a bell-shaped response. Similar findings have been reported showing that HMW chitosan had *in vitro* stimulatory effect on PEMs (from male rats) NO production (126) and LMW chitosan stimulated RAW264.7 macrophage TNF- α production (184). Another study demonstrated that LMW chitosan induced ROS production in an epithelial, human breast cancer cell line (227). The bell-shaped responses are consistent with a study that showed that chitosan stimulated NO and TNF- α production in peritoneal macrophages in a dose-dependent manner and their levels tended to decrease at higher concentrations of chitosan (320 μ g/ml)(228). This type of response has also been reported previously for tucaresol for both its immunomodulatory and activity against experimental *L. donovani* infections, albeit at lower doses (229). We found that BMMs had high levels expression of TNF- α , NO and ROS and this could be explained as BMMs are more homogenous than PEMs, and they are characterised with their high yield, homogeneity and long lifespan (230).

BMMs were chosen to evaluate if the anti-leishmanial activity of HMW chitosan is through indirect way (through the immunostimulatory effects) or direct way (by the uptake of chitosan by macrophages) or both of them, as these

macrophages are more homogenous than PEMs cells (203). Despite the observed chitosan-induced ROS and NO production there was no evidence that this contributed to the anti-leishmanial activity in our study – the inhibitors we used to mitigate their production had no effect on the ability of chitosan to kill intracellular *Leishmania* amastigotes (Figs 2.11 and 2.13). This led us to investigate the cellular uptake of HMW chitosan and its relationship to the anti-leishmanial activity.

The uptake of the large charged molecule HMW chitosan has not been systematically studied before and there is no clear evidence of its penetrating cell membranes or of its uptake mechanism. Macrophages are known to take up extracellular materials and plasma by endocytosis. Endocytosis mainly occurs via two different cellular uptake mechanisms: pinocytosis or phagocytosis, where pinocytosis is fluid-phase endocytosis and phagocytosis is the process of engulfing large particles (231). Inhibition of pinocytosis (CME) significantly reduced the anti-leishmanial activity of HMW chitosan. Therefore, in our study pinocytosis (CME) was considered to be the main mechanism for the uptake of HMW chitosan by BMMs, indicating a direct anti-leishmanial effect of this molecule against amastigotes. Other researches have also reported pinocytosis as the pathway for the uptake of chitosan of different molecular weights by HEK293 epithelial cells (232). The fluorescence imaging in our study showed that in BMMs HMW chitosan is taken up into the parasitophorous vacuole (PV) where the *Leishmania* amastigotes reside, with the labelled chitosan being internalized within 4 h and increasing up to 24 h later. This scenario is consistent with another study where rhodamine isothiocyanate- chitosan (RITC-chitosan 98-10 K) was found to be directly delivered to the U937 macrophage lysosome after 24 h (233). The accumulation of chitosan in the PV might be due to chitosan's relatively high pKa 6.3, making it more soluble and protonated in the acidic contents of the vacuole. This is consistent with a study using bafilomycin to inhibit acidification and prevent chitosan accumulation within macrophages (233).

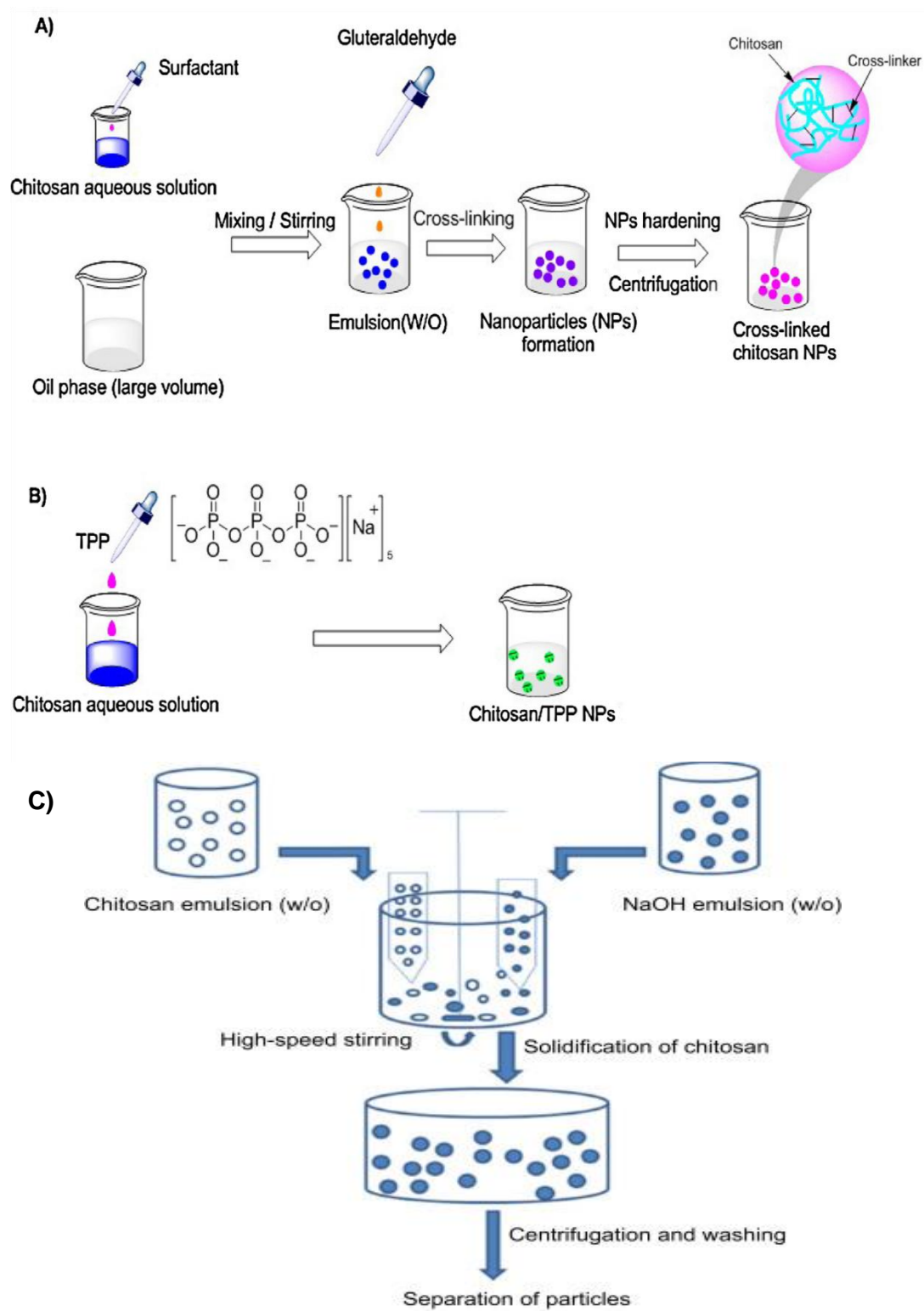
In summary, our studies indicate that chitosan and its water-soluble derivatives showed anti-leishmanial activity against both *L. major* and *L. mexicana* promastigotes and amastigotes in a pH-dependent manner. At pH 6.5 HMW

chitosan is more active than MMW and LMW chitosan and chitosan derivatives, in particular those where the amino groups are substituted. In addition, HMW chitosan activated M1 macrophages, stimulating them to produce NO and ROS. However, the anti-leishmanial activity of chitosan was not due to such immune activation, as an NO inhibitor and a ROS scavenger failed to reduce the anti-leishmanial activity. Instead, the anti-leishmanial activity was related to direct uptake of chitosan into the parasitophorous vacuole by pinocytosis (CME). HMW chitosan demonstrated effective *in vitro* anti-leishmanial activity with minimal cytotoxicity and future work will focus on *in vivo* studies, formulations and routes for drug administration.

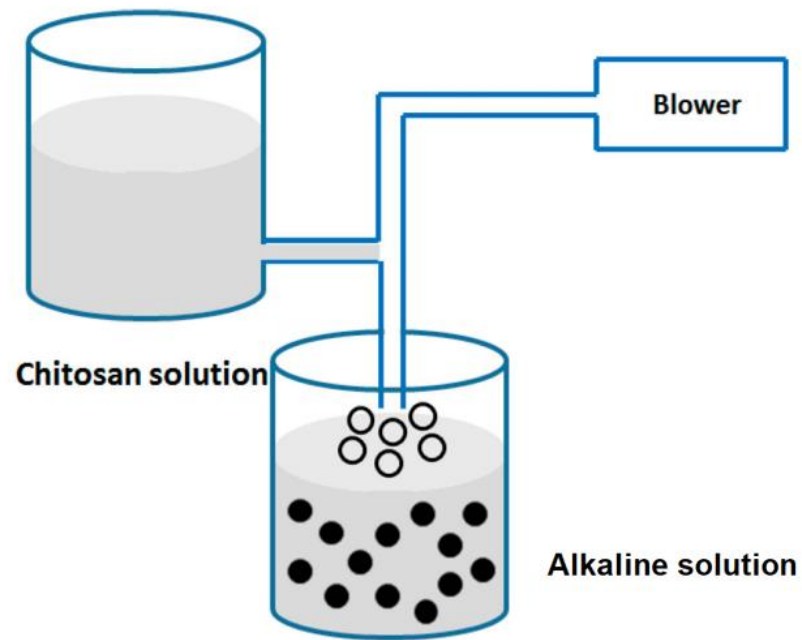
3. Preparation and characterisation of amphotericin B loaded chitosan nanoparticles

3.1. Introduction

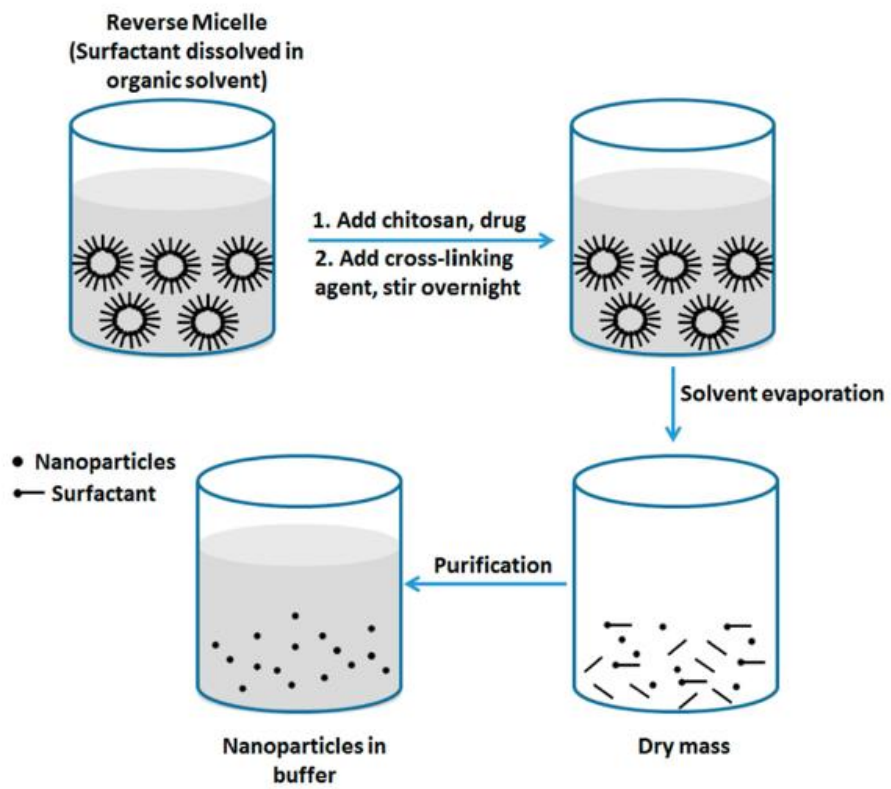
As mentioned in Chapter 1, the polyene antibiotic AmB (a standard treatment for systemic fungal infections) was classified as a second line treatment for VL and MCL, particularly for pentavalent antimonial resistant *Leishmania*. However, the toxic side effects of AmB restrict its use. Great efforts have been spent to develop drug delivery systems (DDs) of AmB, to reduce its toxicity and improve the efficacy of the drug, such as AmBisome®, a liposomal formulation of AmB, which is significantly less toxic than the free drug and is effective against VL and CL and then has been promoted as first line for VL in the Indian subcontinent (ISC), However, the drawbacks are (i) high cost, where donated free of charge by WHO for VL, not for CL and (ii) need for cold chain due to stability guaranteed only up to 25°C (54, 55, 56, 58, 234). Polymeric nanoparticles technology has also gained a great interest in the DDs field, giving opportunities for controlled drug release, drug protection of enzymatic degradation and retention period of drug. We mentioned in Chapter 1 that chitosan nanoparticles are gaining a lot of attention in DDs in the medical field as they are both biodegradable and biocompatible (119). There are different methods for the preparation of chitosan nanoparticles and they are summarised in Fig 3.1.



D)



E)



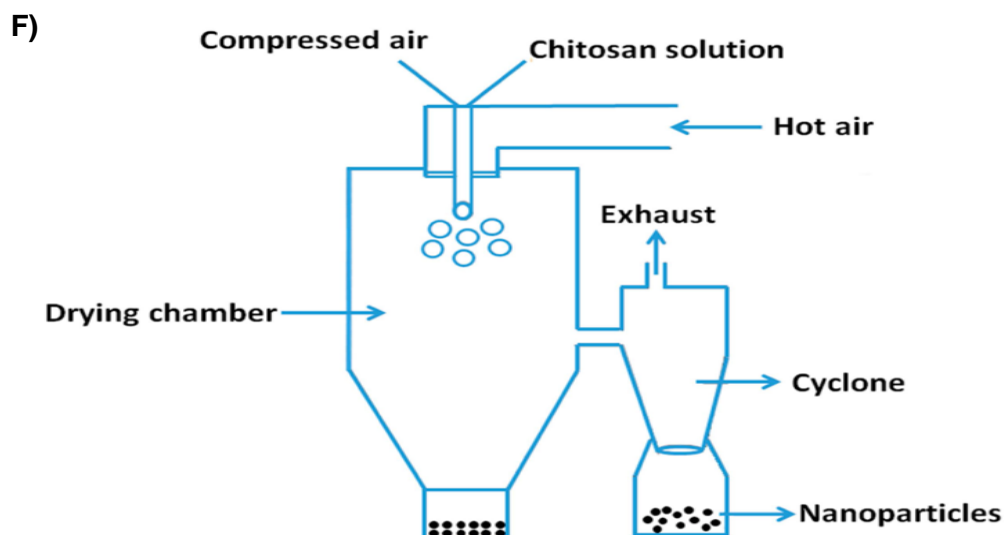


Figure 3.1. Preparation methods of chitosan nanoparticles. (A) Emulsion cross-linking in which chitosan is stabilized by a surfactant and then is emulsified in an oil phase (water-in-oil emulsion) such as chitosan aqueous solution in toluene, using Span 80® as emulsifier) and is then reacted with an appropriate cross linking agent (e.g. formaldehyde, glutaraldehyde, genipin, glyoxal etc.) followed by washing and drying of the nanoparticles, (B) ionotropic gelation which represents the method we used and will be described in details, (C) emulsion-droplet coalescence in which chitosan solution is dispersed in liquid paraffin oil to prepare an emulsion and then sodium hydroxide solution is added to the first emulsion under high speed mixing which produces nanoparticles which are centrifuged and dried, (D) precipitation in which a compressed air nozzle is used to inject chitosan solution into basic organic solvent (sodium hydroxide, NaOH methanol or ethanediamine) , (E) reverse micelles in which a surfactant (e.g. sodium 10 bis (ethyl hexyl) sulfosuccinate or cetyl trimethylammonium bromide) is dissolved into an organic solvent (e.g. n-hexane) to which aqueous chitosan solution is added under continuous stirring. Subsequently, a cross-linking agent (e.g. glutaraldehyde) is added and maintained under stirring overnight, and the organic solvent is removed by evaporation(F) spray drying in which an aqueous acetic acid solution of chitosan is prepared then, drugs are suspended or dissolved in the chitosan solution and then a cross-linking agent (glutaraldehyde or sodium tripolyphosphate). Small droplets are formed upon the atomization and the formation of flowing particles with evaporation of solvent. These techniques except ionotropic gelation frequently require the use of organic solvents or heat, which are undesirable steps and may affect encapsulated drug and may increase cytotoxicity effects (171, 235, 236)

The ionotropic gelation method is described as an easy and simple technique in which, nanoparticles are formed by an electrostatic interaction between the cationic amino groups of chitosan and negatively charged anions of other compounds (such as tripolyphosphate sodium (TPP), dextran sulphate, chondroitin sulphate, etc) with mechanical stirring at room temperature leading to spherical nanoparticles. The use of different pH values of media and ratios

of chitosan and polyanions can result in the synthesis of particles at different sizes and surface charges. This technique has many advantages such as the usage of aqueous condition, low toxicity and not changing the chemistry of the encapsulated drug (120, 237). Moreover, these nanoparticles can be prepared in small and different sizes and charges, they can be used for different routes of administration and offer a sustained drug release (112).

All nanoparticles used in our study were prepared using the inotropic gelation method. Chitosan nanoparticles were prepared via the interaction between the oppositely charged groups of chitosan (positive amino groups) and TPP (polyanions) or dextran sulphate (negative groups) (Fig 3.2, give structure of TPP and dextran sulphate). Dextran sulphate is a biodegradable and biocompatible polysaccharide with a negative charge and is soluble in water. These properties enable dextran sulphate to produce nanoparticles when interacts with positively charged molecules to give positively or negatively charged nanoparticles according to the mass ratios used (238). Because of the biodegradability, biocompatibility and the possibility of dextran to interact with chitosan to produce negative charged nanoparticles, we chose dextran sulphate as a cross-linker.

Tripolyphosphate sodium (TPP) is a popular and commonly used polyanion to prepare chitosan nanoparticles because of its safety (TPP is approved as safe by the FDA; Sec. 182.1810 sodium tripolyphosphate (239)) and gelation properties and furthermore, TPP has a role in the stability of nanoparticles (122, 240). Because of the safety profile and the ability of TPP to interact with chitosan to produce positive charged nanoparticles, we chose TPP as an another cross-linker.

There are several possible mechanisms for drug (AmB) release from chitosan nanoparticles as shown in Fig 3.3 and chitosan nanoparticles show a pH-dependent drug release because of its solubility. Therefore, the aims of this chapter were (i) to produce two types of chitosan nanoparticles containing AmB, one by using TPP to obtain positively charged nanoparticles and the other with dextran sulphate to obtain negatively charged nanoparticles, both with smallest possible sizes. After optimizing the preparation parameters, the

aims were (ii) to characterise the produced blank and AmB loaded nanoparticles in terms, of size, charge, morphology and stability and (iii) to evaluate the amphotericin B loading and drug release from the amphotericin B loaded chitosan TPP or dextran sulphate nanoparticle.

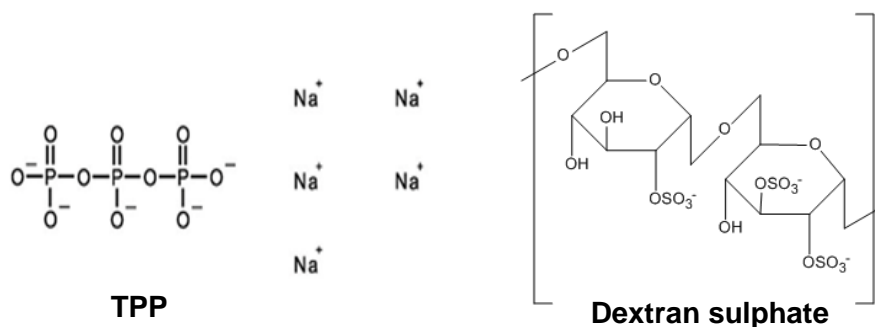


Figure 3.2. Chemical structure of TPP and dextran sulphate (241)

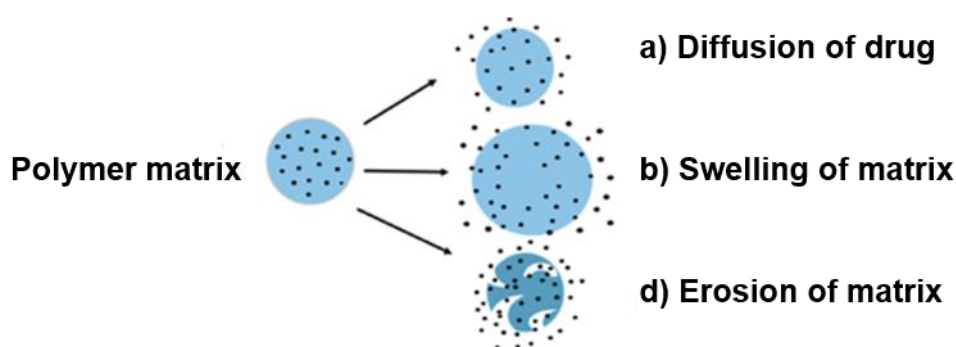


Figure 3.3. Mechanisms of drug release from chitosan nanoparticles. a) In diffusion release, a permeation of the drug is happening through the interior of the matrix of polymer to the near medium, b) in the swelling release, an absorption of water into the polymer is occurred until the dissolving of polymer, c): erosion release which can be homogenous (at the same rate throughout the matrix) and heterogeneous (erosion of the polymer from the surface towards the inner core). Polymer degradation may be due to the surrounding media or the presence of enzymes. (120)

3.2. Material and methods

3.2.1. Preparation of blank chitosan nanoparticles

Nanoparticles were prepared by isotropic gelation by mixing positively charged chitosan with negatively charged TPP or dextran sulphate as shown schematically in Fig 3.4.

- 1- HMW chitosan (MW=310-375 KDa, Sigma, UK) was dissolved at various concentrations (0.33, 1, 3 and 9 mg/ml) in 1% aqueous acetic solution (Sigma, UK). The pH of the resulting chitosan solution was adjusted to pH of 3, 4, 5, 6 and 7 by adding NaOH solution (Sigma, UK) and this enabled investigation into the influence of pH on particles formation.
- 2- The sodium tripolyphosphate (TPP, Mw= 367.85 g/mol, Fisher scientific, US) and dextran sulphate (Mw= 40 kDa, Sigma, UK) solutions were prepared by dissolving TPP or dextran sulphate in double-distilled water at various concentrations
- 3- The nanoparticles were formed at chitosan: TPP or chitosan: dextran sulphate mass ratios of 3:1, 5:1, 10:1, 20:1, 1:1, 1:3, 1:5, 1:10 and 1:20). TPP or dextran sulphate aqueous solution (10 ml) was added dropwise using a 10 ml syringe into the chitosan solution (10ml) under magnetic stirring (Fig 3.4). Directly after adding the TPP or dextran sulphate solution, the nanoparticles suspension was sonicated to reduce the particles size by using a probe sonicator Soniprep 150 (Richmond Scientific Ltd, Lancashire, UK); the diameter of the microprobe was 3mm, operating at an output frequency of 23kHz with an amplitude of 14-16 nm for 15 mins (15 mins was found to be the optimal time after testing for 1, 5, 15 and 20 min) with 1 min rest after every 5 min of sonication to decrease possible overheating of the sample and resulting degradation of the AmB. Subsequently, the nanoparticle suspension

was filtered through a 0.2 μm size syringe filter (Millex, Merck Millipore, UK) to remove aggregates and larger particles. The nanoparticles were concentrated by centrifugation ($8,000 \times g$) using high recovery centrifugal filters (Spin-X UF concentrators, 20 ml, 30 kDa, Corning, UK).

- 4- The nanoparticles suspension was analysed directly by using a Zetaziser (Malvern Instruments Ltd., UK) to determine the size, polydispersity index (PDI) and zeta potential of the nanoparticles. Nanoparticles were then lyophilised using a freeze dryer (Micro Modulyo, Richmond Scientific, UK). In this process, D-mannitol ($M_w = 182.17 \text{ g/mol}$, Sigma, UK) 5% or sucrose ($M_w = 342.3 \text{ g/mol}$, Sigma, UK) 5% v/v was used as a cryoprotectant to protect the nanoparticles from the freezing and desiccation stresses (the stress of freezing and dehydration) (242). After 48 hours, lyophilized nanoparticles were collected, weighed and stored at 4°C for further analysis. The lyophilized blank nanoparticles were white cotton-like substance.

3.2.2. Preparation of AmB loaded chitosan nanoparticles

The optimal parameters determined for producing blank nanoparticles which gave the smallest sizes and PDI (which refers to homogeneity of nanoparticle size (243)) were chosen to prepare the AmB loaded chitosan nanoparticles (Fig 3.4).

- 1- 10 mg of AmB (Purity $\geq 95\%$, Cambridge Bioscience, UK) was dissolved in 0.5 ml of DMSO (high-performance liquid chromatography grade; Fisher Chemical, United Kingdom) and sonicated in a Camlab TransSonic T460/H water bath for 15 min at room temperature.
- AmB is insoluble in water at pH 6 to 7. It is soluble in DMSO (30–40 mg/ml) and in dimethylformamide (2–4 mg/ml). Molecular weight of AmB is 924.08 g/mol and $\log P$ is -0.66 .
- 2- To prepare AmB loaded chitosan-TPP nanoparticles, AmB solution (0.5 ml of 10 mg) was added to 10 ml of TPP solution (6 mg in 10 ml distilled water) and this solution was added dropwise to 10 ml of HMW

chitosan solution (30 mg in 10 ml AC 1%) of pH of 5 under magnetic stirring.

- 3- To prepare AmB loaded chitosan-dextran sulphate nanoparticles, AmB solution (0.5 ml of 10 mg) was added to 10 ml of dextran solution (30 mg in 10 ml double distilled water) and this solution was added dropwise to 10 ml of HMW chitosan solution (10 mg in 10 ml AC 1%) of pH of 5 under magnetic stirring.
- 4- Subsequently, nanoparticle suspension was sonicated directly after adding the gelation material, filtered, purified and freeze dried (using a cryoprotectant) as described for blank nanoparticles in section 3.3.1. The lyophilised AmB loaded nanoparticles were yellow cotton-like material. Each experiment was repeated three times.

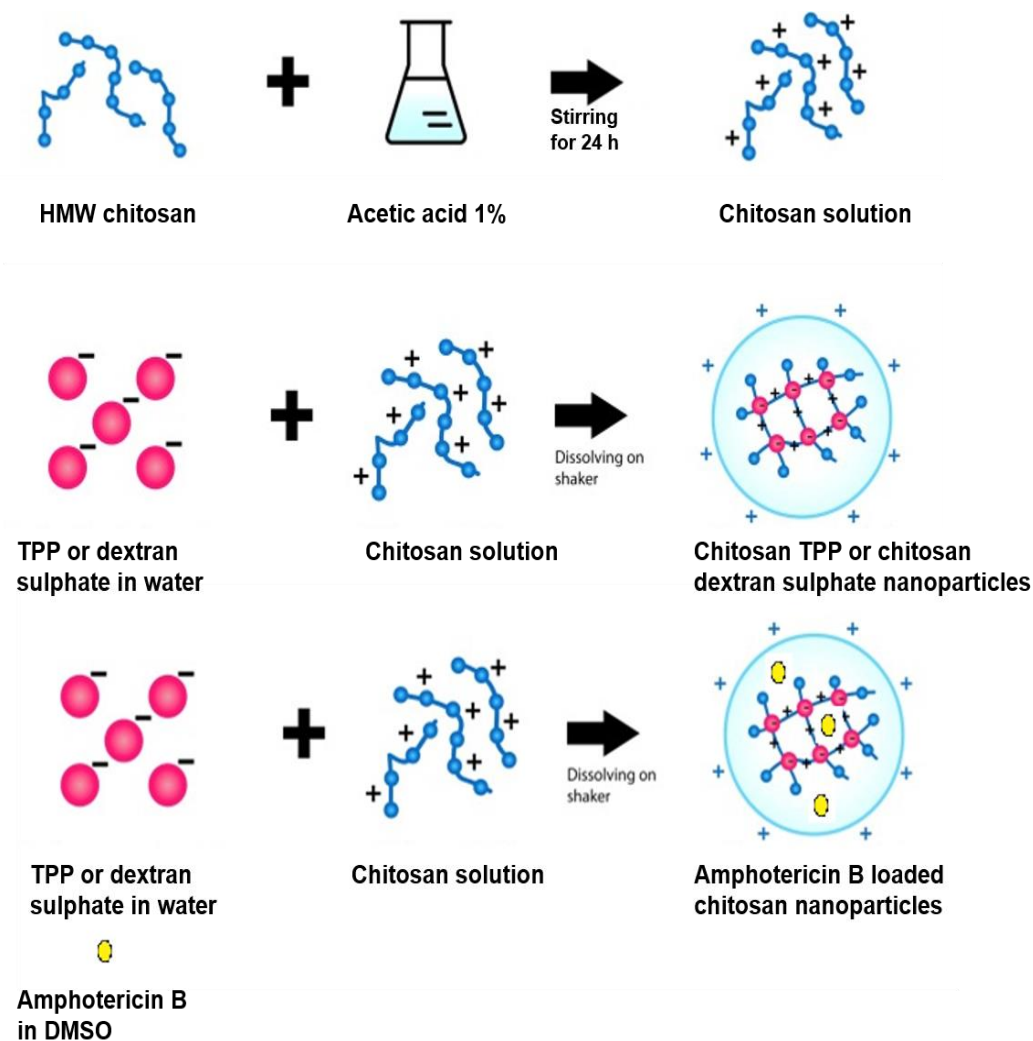


Figure 3.4. Schematic representation for Blank nanoparticles and AmB loaded chitosan nanoparticles with TPP or dextran sulphate (244, 245)

3.2.3. Physicochemical properties of the nanoparticles (size, charge and morphology)

- 1- The size of the nanoparticles was measured by dynamic light scattering (DLS) using a Zetaziser (Malvern Instruments Ltd., UK) with the following parameters: dispersant: water, dispersant refractive indices (RI): 1.33, viscosity (cP):0.8872, material RI: 1.33, temperature (°C):25.0, measurement position (mm):3 and attenuator: 9. The result is expressed as Z-Average (nm) and polydispersity index (PDI). Z - average reflects the intensity weighted mean hydrodynamic size of the particles measured by DLS. PDI represents the distribution of the nanoparticles sizes in the sample (243). DLS is identified as technique for measuring the size and size distribution of molecules and particles which are dispersed or dissolved in liquid and measures hydrodynamic diameter based on the light dispersion properties of samples Tyndall effect (light scattering) and Brownian motion (the random motion of particles suspended in a fluid because of the bombardment by the solvent molecules that surround them). DLS gives the PDI value which reflects the size distribution of the nanoparticles which is classified to monomodal (one population) or plurimodal (several populations) and monodisperse (narrow distribution) or polydisperse (broad distribution) assuming that lower PDI less than 0.4 refers to a homogenous population and 0.1 or less to higher homogeneity in the particle population (246, 247).
- 2- Zeta-potential (representing surface charge of nanoparticles) of the nanoparticles was measured by the Zetaziser with same parameters for the sizing except for measurement position being (mm):2 mm and attenuator:11. Zetaziser measures the zeta potential through the monitoring of the mobility of charged particles on the surface of the nanoparticles by application of an electrical potential (248). Data analysis was performed using the Malvern ZetaSizer software.

Measurements were repeated three times for sizes and 6 times for zeta-potential for each sample.

- 3- The morphology of the nanoparticles was examined using a scanning electron microscopy (SEM, UCL, School of Pharmacy) and a transmission electron microscopy (TEM, UCL, School of Pharmacy)

For the SEM, a fragment of sample was attached to a self-adhesive carbon disc mounted on a 25 mm aluminium stub. The stub was coated with 25 nm of gold using a sputter coater. The stub was then placed into a FEI Quanta 200 FEG SEM for imaging at 5kV accelerating voltage using secondary electron detection (249).

Liquid samples for TEM were dropped with a Pasteur pipette onto a copper grid coated with a carbon/formvar support film. After 15 seconds, a filter paper was blotted off to remove the excess sample. Then a drop of negative stain (1% uranyl acetate) was added and blotted after 15 seconds. The grid was placed into a specimen holder and inserted into a Phillips/FEI CM 120 BioTwin TEM for imaging at 200kV (250).

3.2.4. Stability of nanoparticles regarding size and zeta potential

This stability was evaluated by keeping nanoparticles in distilled water, PBS or RPMI (pH 7.5 or pH 5) and in mouse (BALB/c) plasma (pooled female, BioIVT, UK) in rubber-capped glass vials at temperatures of 4, 34 or 37 °C for 30 days. Particle sizes and zeta-potential were measured after 0, 1, 7 and 30 days.

Stability of dried nanoparticles was identified by resuspending them in water after 0, 1, 7 and 30 days and measuring their size and charge and they were highly stable.

3.2.5. Determination of drug encapsulation efficiency and AmB loading and release

Nanoparticles were prepared as described in section 4-2-2. Following sonication of the suspensions in the probe sonicator and filtration, the AmB

loaded nanoparticle suspension was centrifuged (8,000 x g) to remove the free AmB by using High recovery centrifugal filters (Spin-X UF concentrators, 30 kDa, Corning, UK). Filtrates and supernatants were collected and analysed for AmB concentrations by HPLC as described in section 3.3.6.1. Because of the molecular weight cut-off of the filtration tubes, only the free drug could pass through the membrane. The encapsulation efficiency (EE), drug loading (122) and yield (118) were calculated using the following equations:

$$EE\% = \frac{\text{Mass of total AmB} - \text{mass of free AmB}}{\text{Mass of total AmB}} \times 100$$

$$\text{Drug loading \%} = \frac{\text{Mass of total AmB} - \text{mass of free AmB}}{\text{Mass of chitosan + dextran sulphate or TPP}} \times 100$$

$$\text{Yield \%} = \frac{\text{Mass of nanoparticles after freeze-drying}}{\text{Mass of AmB + chitosan + dextran sulphate or TPP}} \times 100$$

Additionally, the AmB loading was evaluated again after freeze drying by dissolving the yielded yellow powder in DMSO, in acidic pH 3 (by using 1% (v/v) acetic acid), and then by measuring the quantity of AmB by HPLC as described previously in Chapter 3, in section 3.3.6.1. There was no significant difference in the loading value between these two methods, and the data in the thesis will be expressed according to the first method (using High recovery centrifugal filters).

3.2.6. *In vitro* release of AmB

The release of AmB from chitosan-TPP or chitosan-dextran sulphate nanoparticles was evaluated by the dialysis method. One ml of the nanoparticles suspension (1 mg/ml AmB equivalent prepared in double distilled water) was added to either one ml of PBS containing 5% DMSO or

one ml of mouse (BALB/c) plasma (pooled female, BioIVT, UK) containing DMSO (5%) (for the solubility of AmB) (118). Subsequently, this 2 ml was placed in a dialysis bag (molecular mass cut off =12–14 kDa, Sigma, UK) and dialyzed against 50 ml of PBS containing 5% DMSO at pH of 7.5, 6.5 or 5. After immersing the dialysis bag in the release medium, the dialysis set up was left under stirring at 4, 34 or 37 °C for 168 h. The temperatures 4, 34 and 37 °C were chosen to mimic the storage, skin and body temperatures respectively, while pH 5 was chosen to simulate the release in the endosomal compartment of macrophages, pH 7.4 to simulate physiological conditions (251) and pH 6.5 to mimic our *in vitro* study (anti-leishmanial activity) conditions.

After 6, 24, 48, 72, 96, 120, 144 and 168 h the total dialysis medium was replaced with fresh medium to avoid saturation of AmB, (maintaining strict sink conditions throughout the experiment). Release media was processed to quantify the released AmB using HPLC as described in section 3.3.6.1. The results were expressed as a cumulative percentage release of the total amount of AmB (%w/w) versus time according to the equation.

$$\text{Cumulative release (\%)} = \frac{\text{Mass of released AmB at time } t \text{ (mg)}}{\text{Mass of total AmB (1 mg)}} \times 100$$

Mass of released AmB at time *t* is a cumulative amount. For instance, mass of released AmB after 48h is the total amount released at 6, 24 and 48 h.

3.2.6.1. Quantification of AmB by HPLC

AmB was analysed by using a 1260 Infinity Agilent HPLC system. The column and settings used in our study are summarized in Table 3.1 (252). A stock solution of AmB was prepared by dissolving 1 mg of AmB in DMSO. Standard solutions were achieved by diluting this stock solution in PBS containing 5% DMSO.

Table 3.1. HPLC parameters for AmB quantification

HPLC column	Injection volume (µL)	Flow rate (ml/min)	Mobile phase	Detector wavelength nm	Retention time (min)
Phenomenex; Synergi–Hydro RP (250x4.6 mm; 5 µm)	20	1	5mM EDTA•2Na in methanol	450	7.65

3.3. Results

3.3.1. Effects of the initial concentration of chitosan and sonication time on the quality of the nanoparticles

3.3.1.1. Conditions that resulted in poor quality nanoparticles

Precipitation and poor quality of both types of nanoparticles were shown at pH values of 7 and 3 of chitosan solution at all tested conditions. Chitosan solutions at concentrations (0.3 or 9 mg/ml), at all tested pH with different mass ratios and after sonication of the nanoparticles suspension for 1, 5, 15 or 20 mins, gave poor quality nanoparticles with (high PDI>0.8) and with different peaks as seen in Table 3.2. Similarly, chitosan solutions at concentrations (1 or 3 mg/ml) at all pH values with different mass ratios and after sonication of the nanoparticles suspension for 1 or 5 mins produced poor quality nanoparticles (Table 3.2). Finally, chitosan solutions at concentrations (1 or 3 mg/ml) at all pH values with a mass ratio between chitosan and TPP (20:1, 1:1, 1/3, 1:5, 1:10 or 1:20) or a mass ratio between chitosan and dextran sulphate (1:5, 1:10, 1:20, 10:1 or 20:1) and after sonication for 1, 5, 15 or 20 mins caused a precipitation of particles or poor quality nanoparticles with a high PDI of 1.

Table 3.2. Conditions which did not produce good quality nanoparticles

Chitosan mg/ml	pH	Chitosan: TPP or chitosan: dextran sulphate mass ratio	Sonication time mins	Resulted nanoparticles	Related figure
0.3	3, 4, 5, 6 or 7	3:1, 5:1, 10:1, 20:1, 1:1, 1:3, 1:5, 1:10 and 20:1	1, 5, 15 or 20	Poor quality nanoparticles, had a high polydispersity regarding sizes. These samples were deemed not suitable for further study as they might contain large particles or aggregates	3.5, a)
1	3 or 7	3:1, 5:1, 10:1, 20:1, 1:1, 1:3, 1:5, 1:10 and 20:1	1, 5, 15 or 20	Poor quality nanoparticles, had a high polydispersity regarding sizes. These samples were deemed not suitable for further study as they might contain large particles or aggregates	
	4, 5 or 6	3:1, 5:1, 10:1, 20:1, 1:1, 1:3, 1:5, 1:10 and 20:1	1 or 5	Poor quality nanoparticles with high PDI and very large nanoparticles with size≈ 800nm	3.5, b)
	4, 5 or 6	Chitosan: TPP (20:1, 1:1, 1:3, 1:5, 1:10 or 1:20) Chitosan: dextran sulphate (1:5, 1:10, 1:20, 10:1 or 20:1)	15 or 20	A precipitation of particles or poor quality nanoparticles with high PDI of 1	
3	3 or 7	3:1, 5:1, 10:1, 20:1, 1:1, 1:3, 1:5, 1:10 and 20:1	1, 5, 15 or 20	Poor quality nanoparticles, had a high polydispersity regarding sizes. These samples were deemed not suitable for further study as they might contain large particles or aggregates	
	4, 5 or 6	3:1, 5:1, 10:1, 20:1, 1:1, 1:3, 1:5, 1:10 and 20:1	1 or 5	Poor quality nanoparticles with high PDI and very large nanoparticles with size≈ 800nm	3.5, b)
	4, 5 or 6	Chitosan: TPP (20:1, 1:1, 1:3, 1:5, 1:10 or 1:20) Chitosan: dextran sulphate (1:5, 1:10, 1:20, 10:1 or 20:1)	15 or 20	A precipitation of particles or poor quality nanoparticles with high PDI of 1	
9	3, 4, 5, 6 or 7	3:1, 5:1, 10:1, 20:1, 1:1, 1:3, 1:5, 1:10 and 20:1	1, 5, 15 or 20	Poor quality nanoparticles, had a high polydispersity regarding sizes. These samples were deemed not suitable for further study as they might contain large particles or aggregates	3.5, c)
Experiment was reproduced further two times with confirmed similar data					

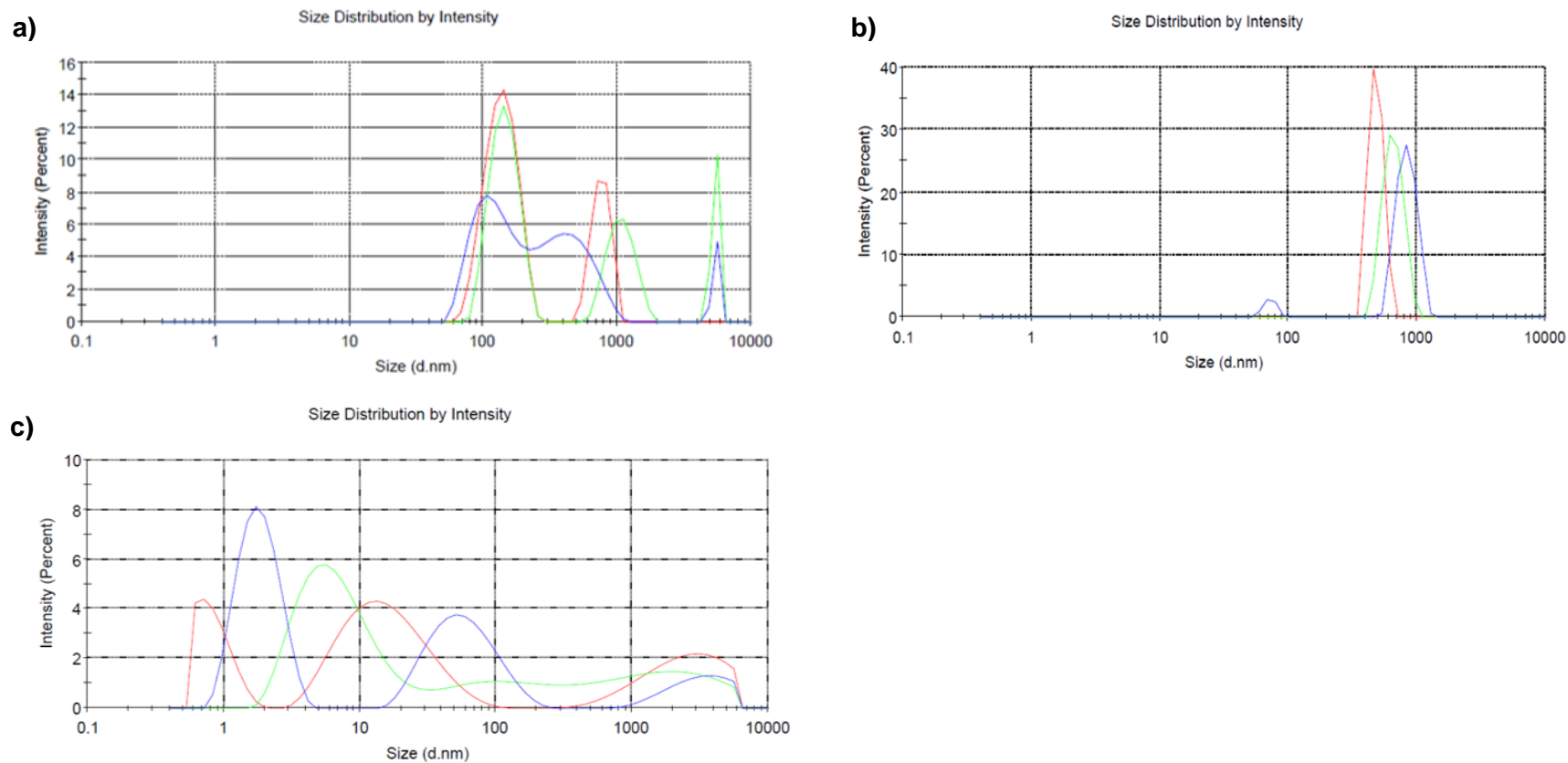


Figure 3.5. Poor quality nanoparticles at different conditions. a) at initial chitosan concentration 0.3 mg/ml and all other different parameters, b) at initial chitosan concentration 1 or 3 mg/ml and sonication for 1 or 5 mins and c) at initial chitosan concentration 9 mg/ml other different parameters. There are several populations of particles, some are small in size e.g. less than 100 nm and some are large about 1 μ m. Each colour represents one measurement as each sample was measured 3 times.

3.3.1.2. Conditions that resulted in good quality nanoparticles

Chitosan solutions at concentrations (1 or 3 mg/ml) at pH (4, 5 or 6) with a mass ratio between chitosan and TPP (3:1, 5:1 or 10:1) or a mass ratio between chitosan and dextran sulphate (1:3, 1:1, 3:1 or 5:1) and after sonication of the nanoparticles suspension for 15 mins gave good quality nanoparticles with (low PDI<0.4) (lower PDI means more homogenous and stable nanoparticles (210)) with one peak; with different Z-Averages according to the conditions that would be discussed later (Fig 3.6 and Fig 3.7). Sonication of the nanoparticles suspension for more than 15 mins (for example 20 mins) produced no significant changes in the quality (PDI) or physicochemical properties (sizes and charges) of the nanoparticles.

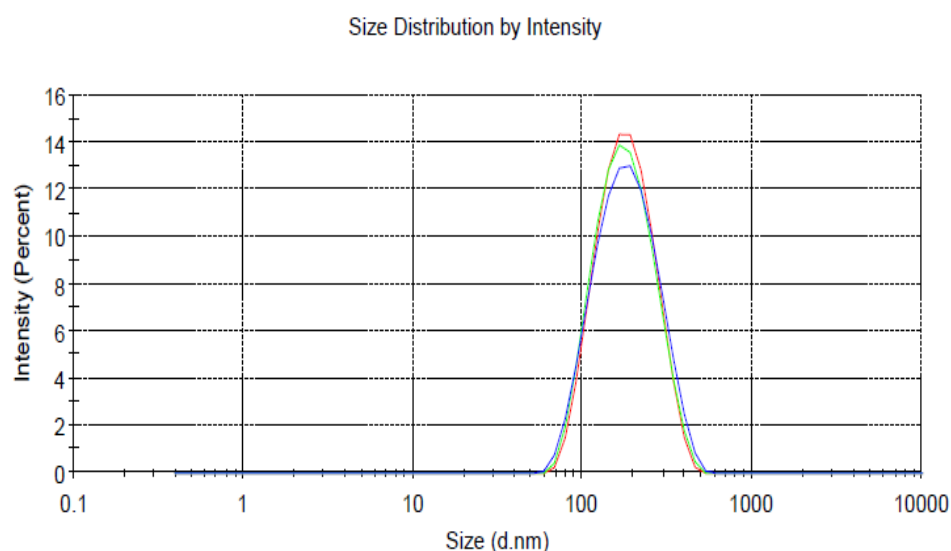


Figure 3.6. Good quality chitosan-dextran sulphate nanoparticles with one peak (one population of nanoparticles at initial chitosan concentration 3 mg/ml and sonication for 15 mins. Chitosan-dextran sulphate nanoparticles (Size = 145.8 nm, PDI =0.2). Each colour represents one measurement as each sample was done in three measurements.

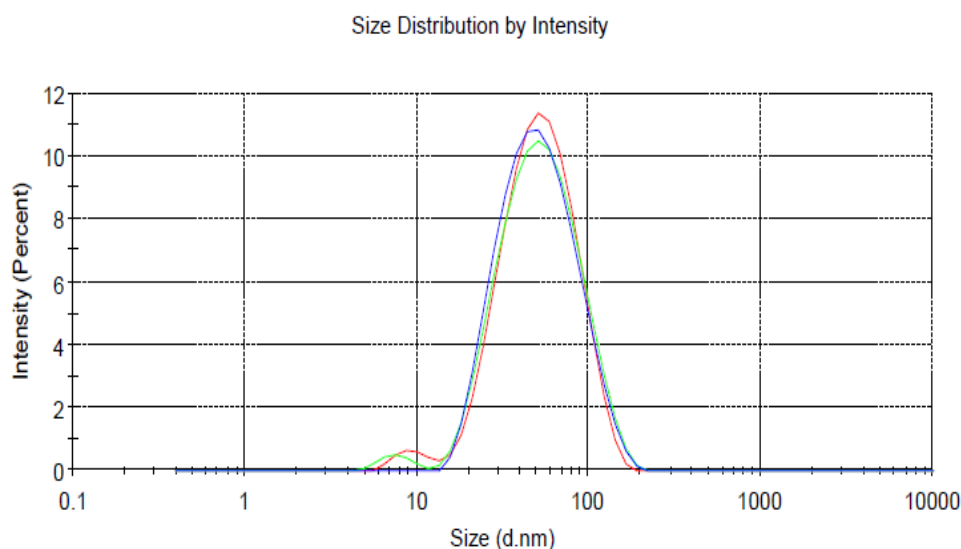


Figure 3.7. Good quality chitosan-TPP nanoparticles with one peak (one population of nanoparticles at initial chitosan concentration 3 mg/ml and sonication for 15 mins. Chitosan – TPP nanoparticles (Size = 43.47 nm, PDI = 0.2). Each colour represents one measurement as each sample was done in three measurements.

Our results indicated that the optimal parameters to obtain good quality nanoparticles (for both types of nanoparticles with TPP or with dextran sulphate) are: initial concentration of chitosan with 1 or 3 mg/ml and sonication time of the nanoparticles suspension for 15 mins as sonicating for more than 15 mins gave same results regarding quality (PDI), size and charge.

3.3.2. Effects of pH of chitosan solution and the mass ratio on the size and charge of good quality nanoparticles

Chitosan and TPP with parameters (chitosan 3 mg/ml at pH 5 and TPP 0.6 mg/ml) produced the smallest and most quality nanoparticles of chitosan-TPP nanoparticles (with lowest PDI, homogenous suspension) with size 48 ± 6 nm, PDI = 0.1 ± 0.03 and positive charge (zeta potential = 32.1 ± 1.2 mv) (Table 3.3). However, chitosan and dextran sulphate with parameters (chitosan 1 mg/ml at pH 5 and dextran sulphate 3 mg/ml) produced the smallest and most quality nanoparticles of chitosan-dextran sulphate nanoparticles with size 145 ± 6 nm, PDI = 0.1 ± 0.05 and negative charge (zeta potential = -15.5 ± 1 mv) (Table 3.4).

Table 3.3. Effect of pH and concentration of chitosan and mass ratio of the reactants on the physicochemical properties of blank chitosan-TPP nanoparticles

Chitosan		TPP		Ch:TPP mass ratio	Ch:TPP Molarity ratio	pH	Particle sizes nm	PDI	Zeta potential mv
mg/ml	μM	mg/ml	μM						
1	0.002	0.3	0.81	3:1	1:405	4	100 ± 9	0.3 ± 0.1	17 ± 1
		0.2	0.53	5:1	1:265		120 ± 8	0.3 ± 0.1	18.9 ± 1
		0.1	0.27	10:1	1:135		170 ± 9	0.3 ± 0.1	19.8 ± 0.9
		0.3	0.81	3:1	1:405	5	95 ± 10	0.3 ± 0.1	13.5±1
		0.2	0.53	5:1	1:265		108 ± 11	0.2 ± 0.05	17.5±0.5
		0.1	0.27	10:1	1:135		169 ± 9	0.3 ± 0.1	19.2±0.3
		0.3	0.81	3:1	1:405	6	135 ± 11	0.2 ± 0.05	11.2±0.2
		0.2	0.53	5:1	1:265		149 ± 12	0.3 ± 0.1	15.5±2
		0.1	0.27	10:1	1:135		190 ± 9	0.2 ± 0.04	17.5±0.9
3	0.008	1	2.72	3:1	1:340	4	141 ± 10	0.2 ± 0.05	23.9 ± 1.2
		0.6	1.6	5:1	1:200		99 ± 6	0.2 ±0.02	34.3 ± 0.9
		0.3	0.81	10:1	1:101		220 ± 15	0.2 ±0.02	44.8 ± 1.9
		1	2.72	3:1	1:340	5	140 ± 9	0.2±0.03	22.9 ± 1.8
		0.6	1.6	5:1	1:200		48 ± 6	0.1 ±0.03	32.1 ± 1.2
		0.3	0.81	10:1	1:101		178 ± 12	0.3±0.02	40.2 ± 1.3
		1	2.72	3:1	1:340	6	174 ± 9	0.1 ±0.05	16.2 ± 1.2
		0.6	1.6	5:1	1:200		155 ± 8	0.2 ± 0.02	18.3 ±1.1
		0.3	0.81	10:1	1:101		340 ± 19	0.3 ± 0.1	18.7 ±1.1
Data expressed as mean +/- SD (experiment was reproduced three times with confirmed similar data). The smallest size and PDI of these nanoparticles were 48 ± 6 nm and 0.1 ± 0.03 with positive surface charge (zeta potential = +32.1 ± 1.2)									

Table 3.4. Effect of pH and concentration of chitosan and mass ratio of the reactants on the physicochemical properties of blank chitosan-dextran sulphate nanoparticles

Chitosan (Ch)		Dextran sulphate(Dx)		Ch:Dx mass ratio	Ch:DX Molarity ratio	pH	sizes nm	PDI	Zeta potential mv
mg/ml	µM	mg/ml	µM						
1	0.002	3	0.075	1:3	1:37.5	4	160 ± 6	0.2 ± 0.05	-17.5 ± 1
		1	0.025	1:1	1:12.5		177 ± 9	0.3 ± 0.1	-8 ± 0.5
		0.3	0.007	3:1	1:3		190 ± 9	0.3 ± 0.1	+6 ± 1
		0.2	0.005	5:1	1:2.5		185 ± 8	0.3 ± 0.1	+8 ± 0.1
		3	0.075	1:3	1:37.5	5	145 ± 6	0.1 ± 0.05	-15.5 ± 1
		1	0.025	1:1	1:12.5		169 ± 9	0.3 ± 0.1	-7 ± 0.7
		0.3	0.007	3:1	1:3		170 ± 5	0.2 ± 0.04	+4 ± 1
		0.2	0.005	5:1	1:2.5		185 ± 8	0.3 ± 0.1	+5 ± 0.1
		3	0.075	1:3	1:37.5	6	230 ± 6	0.2 ± 0.04	-12 ± 1
		1	0.025	1:1	1:12.5		200 ± 6	0.4 ± 0.1	-6 ± 0.5
		0.3	0.007	3:1	1:3		210 ± 7	0.3 ± 0.1	+3 ± 0.5
		0.2	0.005	5:1	1:2.5		220 ± 5	0.4 ± 0.1	+4 ± 1
3	0.008	9	0.225	1:3	1:28	4	340 ± 12	0.3 ± 0.1	-33 ± 7
		3	0.075	1:1	1:9.3		307 ± 12	0.3 ± 0.1	-10 ± 2
		1	0.025	3:1	1:3		332 ± 9	0.2 ± 0.04	+8 ± 2
		0.6	0.015	5:1	1:1.8		303 ± 6	0.4 ± 0.1	+10 ± 3
		9	0.225	1:3	1:28	5	270 ± 10	0.2 ± 0.05	-35 ± 7
		3	0.075	1:1	1:9.3		279 ± 11	0.3 ± 0.1	-15 ± 4
		1	0.025	3:1	1:3		290 ± 11	0.3 ± 0.1	+6 ± 2
		0.6	0.015	5:1	1:1.8		285 ± 10	0.2 ± 0.05	+7 ± 1
		9	0.225	1:3	1:28	6	380 ± 10	0.2 ± 0.05	-39 ± 7
		3	0.075	1:1	1:9.3		400 ± 11	0.3 ± 0.1	-19 ± 4
		1	0.025	3:1	1:3		380 ± 11	0.2 ± 0.05	+3 ± 2
		0.6	0.015	5:1	1:1.8		450 ± 10	0.2 ± 0.03	+4 ± 1

data expressed as mean +/- SD (experiment was reproduced three times with confirmed similar data). The smallest size and PDI of these nanoparticles were 145 ± 6 nm and 0.1 ± 0.05 with negative surface charge (zeta potential = -15.5 ± 1)

3.3.3. Effects of AmB loading and freeze-drying with and without cryoprotectants on physicochemical properties and the morphology of the nanoparticles

- 1- AmB loading increased the size of blank chitosan-TPP and dextran sulphate nanoparticles by 18.75% and 13% respectively. However, such loading did not cause any significant change to the zeta potential and PDI of both types of nanoparticles (Table 3.5) ($p > 0.05$ by t-test). Freeze drying process without the use of a cryoprotectant (sucrose or D-mannitol) resulted in poor quality nanoparticles with various sizes for both blank and AmB loaded chitosan-TPP and chitosan-dextran sulphate nanoparticles. In contrast, the use of sucrose as a cryoprotectant produced good quality nanoparticles and caused 39.5%, 17%, 21% and 6% increase in size for blank chitosan-TPP nanoparticles, blank chitosan-dextran sulphate nanoparticles, loaded AmB chitosan-TPP nanoparticles and loaded AmB chitosan-dextran sulphate nanoparticles respectively and did not lead to a significant difference in the zeta potential or PDI ($p > 0.05$ by t test).
- 2- D-mannitol as a cryoprotectant produced good quality nanoparticles, but caused 108%, 38%, 73% and 15.8% increase in size for blank chitosan-TPP nanoparticles, blank chitosan-dextran sulphate nanoparticles, loaded AmB chitosan-TPP nanoparticles and loaded AmB chitosan-dextran sulphate nanoparticles respectively and did not lead to a significant difference in the zeta potential ($p > 0.05$ by t test). When the two cryoprotectants are compared, sucrose produced significantly smaller nanoparticles with lower PDI for both types of nanoparticles, $p < 0.05$ t-test) (Table 3.5, Fig 3.8).
- 3- The morphological characteristics of blank chitosan-TPP or chitosan-dextran sulphate nanoparticles and AmB loaded nanoparticles were examined using TEM and SEM which showed a spherical structure for both chitosan-TPP or chitosan-dextran sulphate nanoparticles. The

TEM and SEM measured size of the four formulations, which was comparable to values measured by DLS. The incorporation of AmB into the nanoparticles did not change the shape of these nanoparticles, just increased the sizes (Fig 3.9 and Fig 3.10).

Table 3.5. Effect of cryoprotectants used during freeze drying on the physicochemical properties of unloaded and AmB loaded chitosan nanoparticles

			Nanoparticles			
			Chitosan -TPP	AmB loaded chitosan – TPP	Chitosan – dextran sulphate	AmB loaded chitosan – dextran sulphate
Size nm	Before lyophilizing		48 ± 6	57 ± 7	145 ± 6	164 ± 5
	After lyophilization	+ sucrose 5%	67 ± 7	69 ± 8	170 ± 9	174 ± 8
		+ D-mannitol 5%	100 ± 9	99 ± 9	200 ±10	200 ± 6
PDI	Before lyophilizing		0.1 ± 0.01	0.1 ± 0.03	0.15 ± 0.01	0.16 ± 0.01
	After lyophilizing	+ sucrose 5%	0.25 ± 0.05	0.2 ± 0.01	0.29 ± 0.04	0.26 ± 0.01
		+ D-mannitol 5%	0.39 ± 0.07	0.4 ± 0.01	0.42 ± 0.06	0.45 ± 0.05
Zeta potential mv	Before lyophilizing		32.1 ± 1.2	29 ± 2	-15.5 ± 1	-14 ± 2
	After lyophilizing	+ sucrose 5%	28.5 ±1.9	25.5 ± 1	-12.9 ± 3	-11 ± 1
		+ D-mannitol 5%	27 ± 2	24 ± 1	-12.5 ± 2	-12 ± 2
Data expressed as mean +/- SD (experiments were repeated three times with confirmed similar data). Sucrose more effectively protected the nanoparticles in comparison with D-mannitol (p < 0.05 by t-test).						

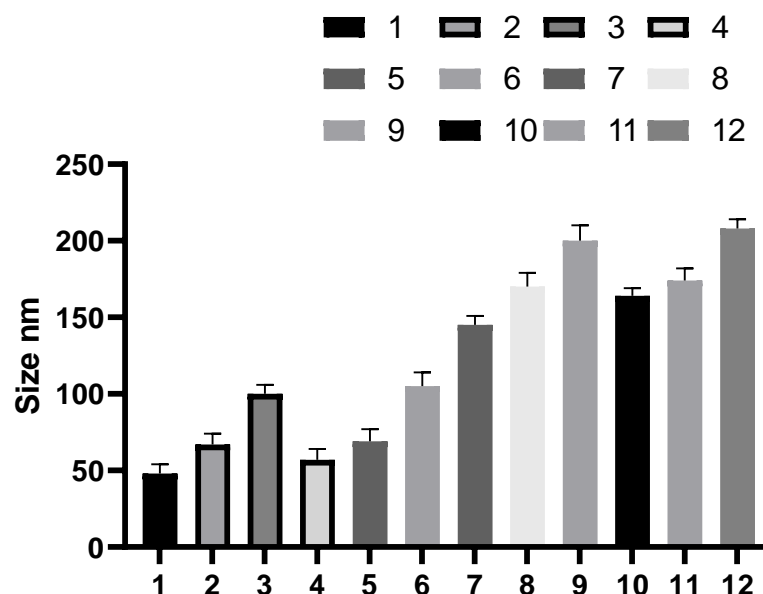


Figure 3.8. Effectiveness of sucrose 5% and D-mannitol 5% as a cryoprotectant for freeze drying of blank and AmB loaded chitosan nanoparticles suspensions. 1: Blank chitosan-TPP nanoparticles before lyophilizing, 2: Blank chitosan-TPP nanoparticles after lyophilizing + sucrose 5%, 3: Blank chitosan-TPP nanoparticles after lyophilizing + D-mannitol 5%, 4: AmB loaded chitosan-TPP nanoparticles before lyophilizing, 5: AmB loaded chitosan-TPP nanoparticles after lyophilizing + sucrose 5%, 6: AmB loaded chitosan-TPP nanoparticles after lyophilizing + D-mannitol 5%, 7: Blank chitosan-dextran nanoparticles before lyophilizing, 8: Blank chitosan-dextran nanoparticles after lyophilizing + sucrose 5%, 9: Blank chitosan-dextran after lyophilizing + D-mannitol 5%, 10: AmB loaded chitosan-dextran nanoparticles before lyophilizing, 11: AmB loaded chitosan-dextran after lyophilizing + sucrose 5%, 12: AmB loaded chitosan-dextran nanoparticles after lyophilizing + D-mannitol 5%. data expressed as mean \pm SD (experiment was reproduced three times with confirmed similar data).

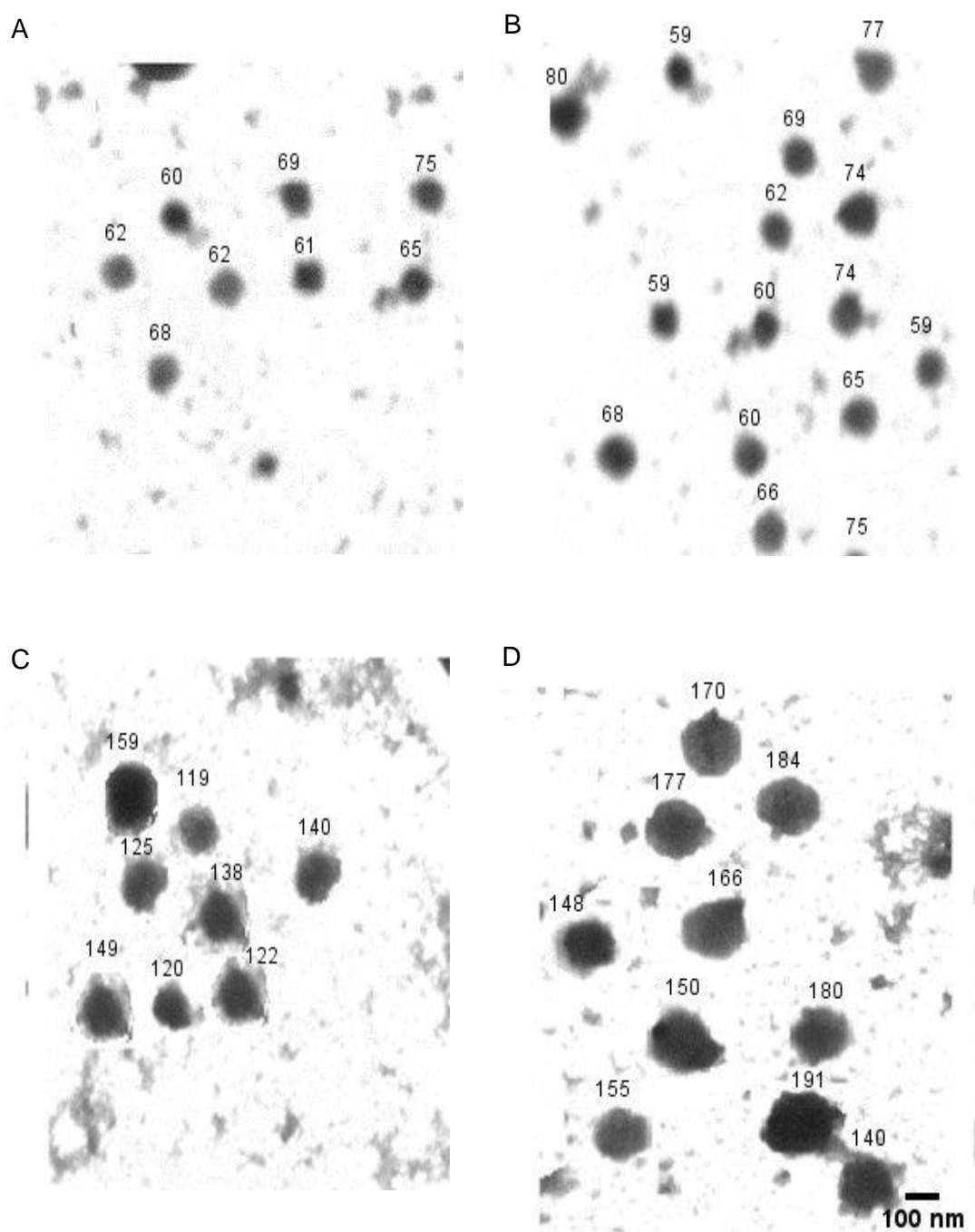


Figure 3.9. TEM micrographs of unloaded and amphotericin B loaded chitosan nanoparticles. A: Unloaded chitosan–TPP nanoparticles, B: AmB loaded chitosan–TPP nanoparticles, C: Unloaded chitosan – dextran sulphate nanoparticles, D: AmB loaded chitosan–dextran sulphate nanoparticles. TEM images indicate the nanoparticles to be spherical. Magnification: 40000x

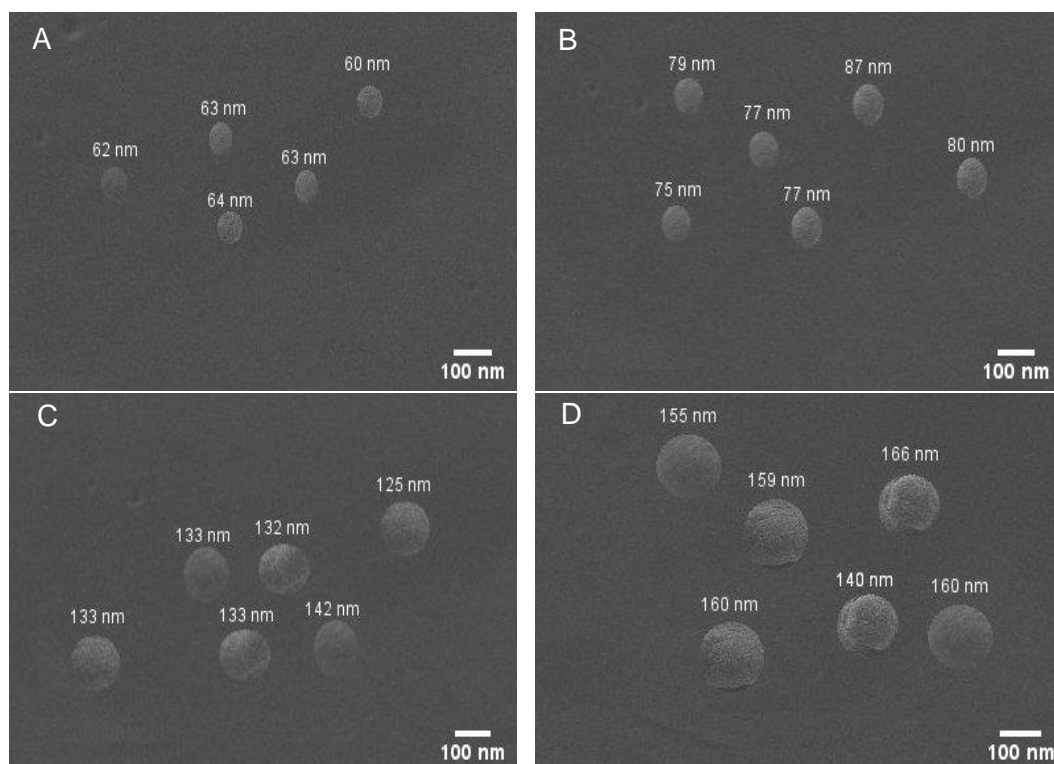


Figure 3.10. SEM micrographs of unloaded and amphotericin B loaded chitosan nanoparticles. A: Unloaded chitosan–TPP nanoparticles, B: AmB loaded chitosan–TPP nanoparticles, C: Unloaded chitosan – dextran sulphate nanoparticles, D: AmB loaded chitosan–dextran sulphate nanoparticles. SEM images indicate the nanoparticles to be spherical and with similar sizes with the zetasizer . Magnification 50000x

3.3.4. Stability of physicochemical properties of AmB loaded chitosan nanoparticles

Both AmB loaded chitosan-TPP and chitosan-dextran sulphate nanoparticles did not show any significant change in their size or zeta potential at temperatures of 4, 34 and 37 °C when incubated in different media (water, PBS or RPMI at pH 7.5 or 6.5) or in mouse (BALB/c) plasma at 4 °C for a period of 30 days which indicated a high stability of these nanoparticles (Tables 3.6 and 3.7, Fig 3.11). Moreover, no significant difference in PDI was identified after 30 days in these different conditions.

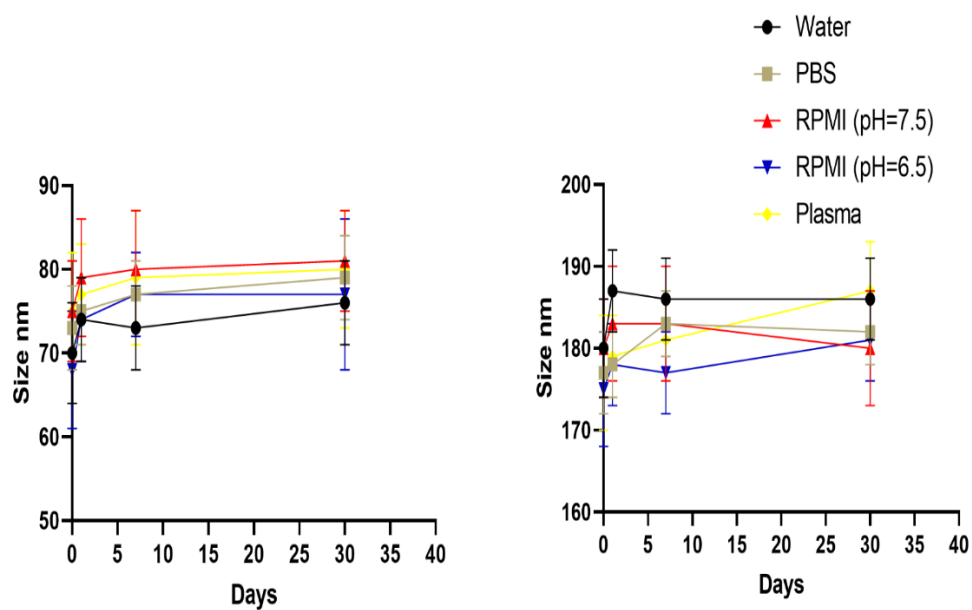


Figure 3.11. Size of AmB loaded chitosan-TPP nanoparticle (A) and AmB loaded chitosan-dextran sulphate nanoparticle (B) in different media over time. The nanoparticles were stable in size after 30 days of storage in different media and temperatures. Data expressed as mean \pm SD (experiment was reproduced three times with confirmed similar data).

Table 3.6. Variations of physicochemical properties of AmB loaded chitosan-TPP nanoparticles in different media upon storage at different temperatures

	<i>Day 0</i>			<i>Day 1</i>			<i>Days 7</i>			<i>Days 30</i>		
	Size nm	PDI	Zeta potential mv	Size nm	PDI	Zeta potential mv	Size nm	PDI	Zeta potential mv	Size nm	PDI	Zeta potential mv
Water at 4, 34 or 37 ° C	70 ± 6	0.1± 0.02	25.5 ± 1	74 ± 5	0.2 ± 0.01	23.4 ± 1	73 ± 5	0.2 ± 0.1	24.0 ± 1	76 ± 5	0.2 ± 0.1	23.9 ± 1
PBS at 4, 34 or 37 ° C	73± 5	0. ± 0.01	23.3 ± 1	75 ± 4	0.1 ± 0.02	22.9 ± 2	77 ± 4	0.2 ± 0.1	22.5 ± 1	79 ± 5	0.2 ± 0.1	21.9 ± 1
RPMI (pH=7.5) at 4, 34 or 37 ° C	75 ± 6	0.2 ± 0.1	24.1± 1	79 ± 7	0.2 ± 0.05	22.9 ± 1	80 ± 7	0.2 ± 0.1	22.8 ± 1	81± 6	0.2± 0.1	22.1 ± 1
RPMI (pH=6.5) at 4, 34 or 37 ° C	68 ± 7	0.1 ± 0.01	32 ± 6	74 ± 5	0.2 ± 0.09	30 ± 4	77 ± 5	0.1 ± 0.1	29 ± 3	77 ± 9	0.2± 0.1	30 ± 3
Plasma at 4 ° C	75 ± 7	0.1 ± 0.01	29 ± 6	77 ± 6	0.2 ± 0.03	30 ± 4	79 ± 8	0.2 ± 0.1	29 ± 3	80 ± 7	0.3 ± 0.1	29 ± 4
data expressed as mean +/- SD (experiment was reproduced three times with confirmed similar data). No significant difference was shown in the size, PDI or zeta potential between two types of the nanoparticles after 30 days storage (p >0.05 by t – test).												

Table 3.7. Variations of physicochemical properties of AmB loaded-chitosan dextran sulphate nanoparticles in different media upon storage at different temperatures

	<i>Day 0</i>			<i>Day 1</i>			<i>Days 7</i>			<i>Days 30</i>		
	Size nm	PDI	Zeta potential mv	Size nm	PDI	Zeta potential mv	Size nm	PDI	Zeta potential mv	Size nm	PDI	Zeta potential mv
Water at 4, 34 or 37 ° C	180 ± 6	0.2± 0.1	-14 ± 5	187 ± 5	0.2± 0.1	-16 ± 5	186 ± 5	0.2± 0.1	-17 ± 5	186 ± 5	0.2± 0.1	-17 ± 5
PBS at 4, 34 or 37 ° C	177 ± 5	0.2 ± 0.1	-15 ± 5	178 ± 4	0.2 ± 0.1	-14 ± 5	183 ± 4	0.2 ± 0.1	-17 ± 5	182 ± 4	0.2 ± 0.1	-17 ± 5
RPMI (pH=7.5) at 4, 34 or 37 ° C	180 ± 6	0.2 ± 0.1	-20 ± 5	183 ± 7	0.2 ± 0.1	-17 ± 5	183 ± 7	0.2 ± 0.1	-19 ± 5	180 ± 7	0.2 ± 0.2	-19 ± 5
RPMI (pH=6.5) at 4, 34 or 37 ° C	175 ± 7	0.2 ± 0.1	-11 ± 5	178 ± 5	0.2 ± 0.1	-14 ± 5	177 ± 5	0.2 ± 0.1	-13 ± 5	181 ± 5	0.2 ± 0.1	-13 ± 5
Plasma at 4 ° C	177 ± 7	0.2 ± 0.1	-15 ± 5	179 ± 5	0.2 ± 0.1	-17 ± 5	181 ± 5	0.3 ± 0.1	-13 ± 5	187 ± 6	0.2 ± 0.1	-14 ± 5
data expressed as mean +/- SD (experiment was reproduced three times with confirmed similar data). No significant difference was shown in the size, PDI or zeta potential between two types of the nanoparticles after 30 days storage (p >0.05 by t – test).												

3.3.5. Nanoparticles loading and encapsulation properties

Both types of nanoparticles had a high encapsulation efficiency of more than 90%. The fluffy yellow yield was more than 90% for both types (Table 3.8). There was no significant difference in AmB loading between chitosan TPP and dextran sulphate nanoparticles ($p>0.05$ by t-test) (Fig 3.12).

Table 3.8. Percentage of AmB loading, encapsulation and yield

Type of nanoparticles	EE %	AmB loading %	Yield %
AmB loaded chitosan-TPP nanoparticles	94 ± 5	26 ± 1	93 ± 6
AmB loaded chitosan-dextran sulphate nanoparticles	92 ± 8	23 ± 2	92 ± 6

data expressed as mean +/- SD (experiment was reproduced three times with confirmed similar data). No significant difference was shown between AmB loaded chitosan-TPP and dextran sulphate nanoparticles ($p>0.05$ by t-test). AmB loaded chitosan-TPP nanoparticles size= 69 ± 8 nm and AmB loaded chitosan-dextran sulphate nanoparticles size= 174 ± 8 nm

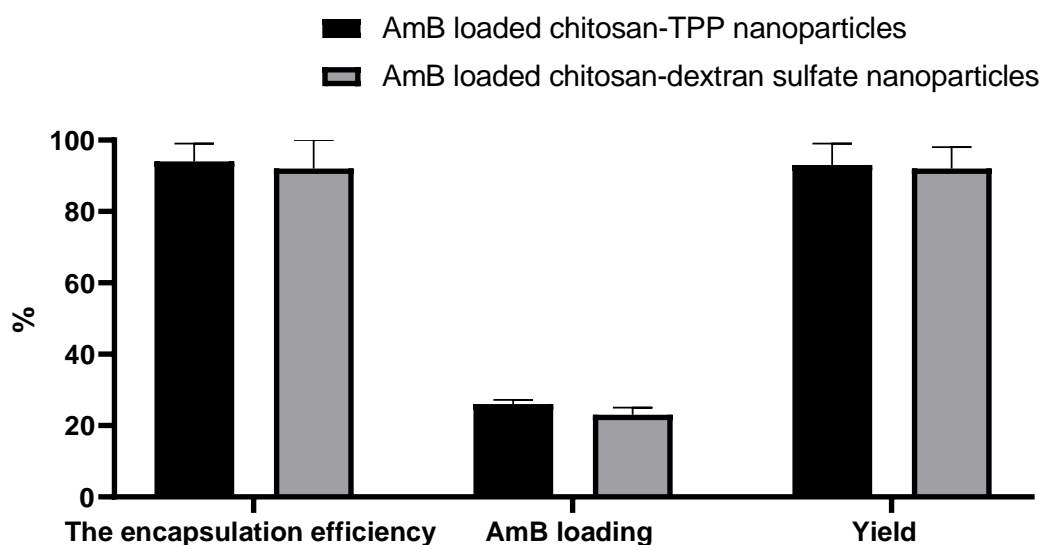


Figure 3.12. Comparison of AmB encapsulation, loading and yield of the two types of nanoparticles. No significant difference was shown between AmB loaded chitosan-TPP and dextran sulphate nanoparticles regarding the encapsulation, loading and yield ($p>0.05$ by t-test). Data expressed as mean +/- SD (experiment was reproduced three times with confirmed similar data). AmB loaded chitosan TPP nanoparticles size= 69 ± 8 nm and AmB loaded chitosan dextran sulphate nanoparticles size= 174 ± 8 nm

3.3.6. *In vitro* release of AmB from the nanoparticles

AmB release from the two types of nanoparticles is shown in Fig 3.13 and Table 3.9. The chitosan-TPP and chitosan-dextran sulphate nanoparticles showed a slow release within 7 days in PBS (at two pH values of 7.5 and 6.5) at three temperatures 4, 34 and 37 ° C and in mouse (BALB/c) plasma at 37 ° C. Chitosan-TPP nanoparticles released AmB significantly quicker than chitosan-dextran sulphate nanoparticles at the different conditions (nanoparticle suspended in plasma or PBS and at different pHs and temperatures) ($p < 0.05$, one-way-ANOVA). Neither AmB loaded chitosan-TPP nanoparticles nor AmB loaded chitosan-dextran sulphate nanoparticles showed any significant difference in the drug release after storing at 34 ° C or 37 ° C ($p > 0.05$ by t -test) (Fig 3.13, Table 3.9). However, the pH influenced the drug release significantly with both types of nanoparticles, showing higher cumulative releases at the lower pH of 5 than at higher pH of 6.5 or 7.5 ($p < 0.05$ by t-test) (Table 3.9 and Fig 3.13).

Table 3.9. *In vitro* cumulative release of AmB from the two formulations at different conditions

Type			6 h %	24 h %	48 h %	72 h %	96 h %	120 h %	144 h %	168 h %
AmB loaded chitosan–dextran sulphate nanoparticles	PBS, pH 7.4	4 °C	0.1 ±0.05	1±0.05	2.2±0.4	5.2±1	7.5±2	9.5±2	11±2	15±2
		34 °C	0.3±0.1	2.5±0.2	5.2±1	8.5±2	10±3	13.5±2	16.4±3	20±3
		37 °C	0.1±0.02	2±0.1	4.4±1	6.9±1	9.1±2	12.5±3	15.5±3	18.5±2
	PBS, pH 6.5	4 °C	0.2±0.02	2±0.2	3.1±1	4.9±1	6.9±1	8.9±1	11.5±2	15.9±2
		34 °C	0.4±0.1	4±0.5	7.3±2	9.2±3	13.1±3	15±2	17.2±4	21.2±2
		37 °C	0.1±0.05	2.9±0.4	5.4±1	7.9±2	10.1±2	12.2±2	16.5±3	19.5±3
	PBS, pH 5	4 °C	0.2±0.05	3.5±1	9.5±2	16.1±4	17.2±3	20.2±3	21.1±4	32.2±4
		34 °C	0.5±0.1	7.5±2	14.5±3	20.9±5	23±4	24.9±3	27.5±4	41.9±5
		37 °C	0.3±0.1	6.5±1	13.5±3	20.1±4	21.2±5	24.2±3	26.1±3	38.2±4
	Plasma	37 °C	0.2±0.05	4.1±1	8.1±1	9.2±2	10.1±2	12±2	14.9±2	22.9±3
AmB loaded chitosan –TPP nanoparticles	PBS, pH 7.4	4 °C	0.5±0.1	5.1±1	9.2±1	11.5±2	13.8±2	15.9±1	18.9±2	22.9±3
		34 °C	1.2±0.3	9.9±2	15.6±2	20.6±3	24.5±5	26±4	28.9±5	32.5±2
		37 °C	1 ±0.2	10 ±2	14.9 ±3	19.5 ±2	23.5 ±5	24.5 ±3	27.5 ±4	31.5 ±5
	PBS, pH 6.5	4 °C	0.3±0.1	4.1±1	10.2±2	12.5±2	15.8±5	17.9±2	19.9±3	24.5±3
		34 °C	1.5±0.3	10.5±2	16.4±4	21.9±4	26.3±5	27.8±3	29.8±5	32.5±3
		37 °C	1.2±0.4	9.8±1	15.2±3	20.2±3	24.1±5	25.6±4	28±4	32.6±2
	PBS, pH 5	4 °C	0.9±0.2	16.5±3	19.8±3	25.5±4	26.2±4	34.5±4	40.2±6	47.5±4
		34 °C	1.5±0.4	21.2±4	27.2±5	31.2±3	34.6±6	39.8±5	41.9±5	50.8±6
		37 °C	1.7±0.4	20.2±3	26.5±6	30.2±4	33.1±4	40.2±5	45.2±5	51.2±6
	Plasma	37 °C	1.7±0.3	11.2±2	14.5±4	20.9±2	25.3±3	27.3±4	29.9±4	33.6±5
AmB solution	PBS, pH 7.4	4 °C	84±2	100±1	0	0	0	0	0	0
		34 °C	85±2	100±2	0	0	0	0	0	0
		37 °C	86±3	100±2	0	0	0	0	0	0
	PBS, pH 6.5	4 °C	83±1	100±1	0	0	0	0	0	0
		34 °C	86±2	100±3	0	0	0	0	0	0
		37 °C	88±4	100±2	0	0	0	0	0	0
		4 °C	84±1	100±2	0	0	0	0	0	0

	PBS, pH	34 ° C	85±1	100±2	0	0	0	0	0	0
	5	37 ° C	87±2	100±2	0	0	0	0	0	0
	Plasma	37 ° C	85±2	100±2	0	0	0	0	0	0
<p>Data expressed as mean +/- SD (experiment was reproduced three times with confirmed similar data). Both types of nanoparticles showed significantly more cumulative release in the low pH of 5 than in higher pH of 6.5 or 7.5 ($p < 0.05$ by t-test). The AmB release from chitosan-TPP nanoparticles was faster than chitosan dextran sulphate nanoparticles ($p < 0.05$ by t – test). AmB loaded chitosan-TPP nanoparticles size= 69 ± 8 nm and AmB loaded chitosan-dextran sulphate nanoparticles size= 174 ± 8 nm</p>										

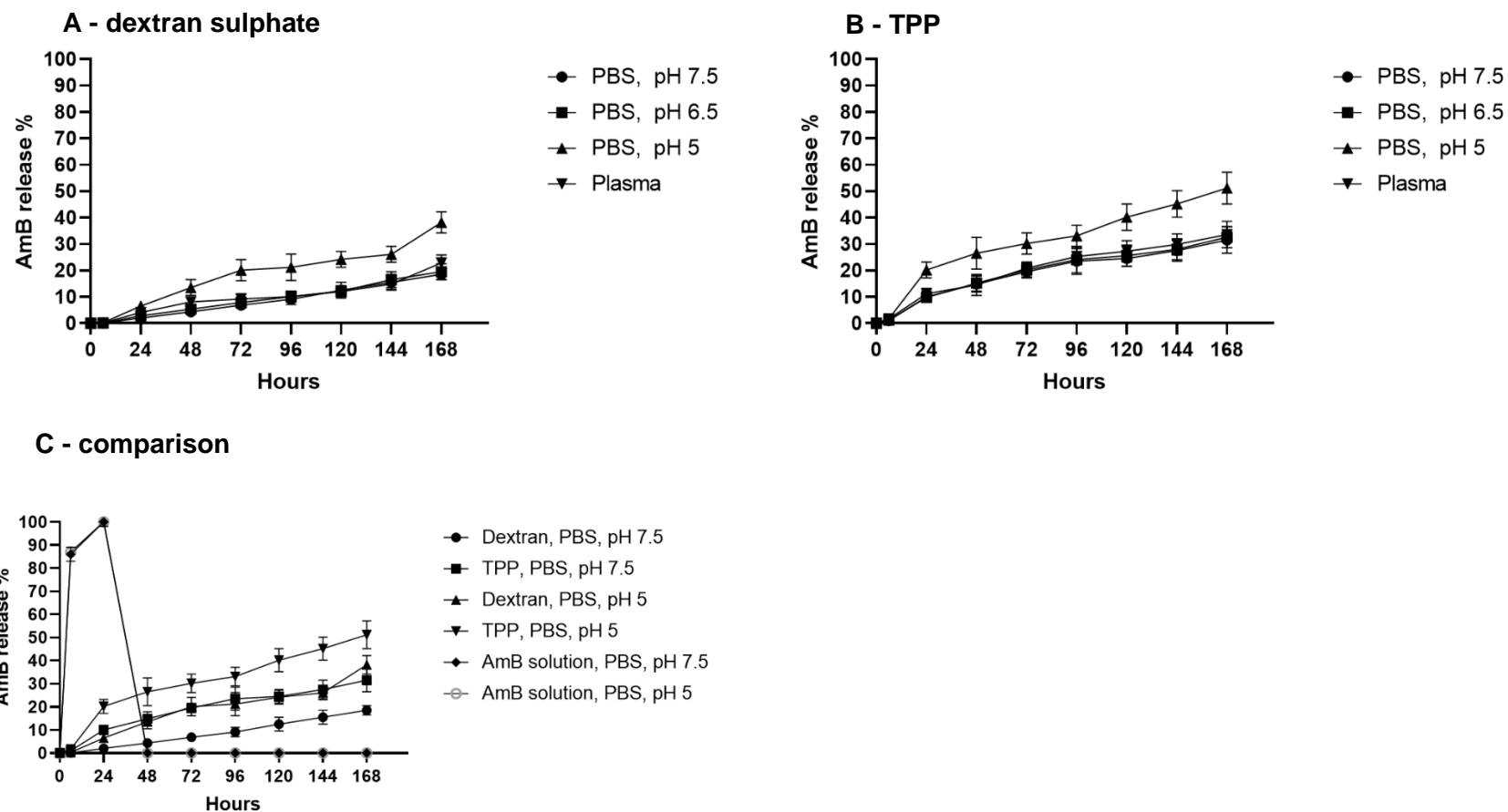


Figure 3.13. *In vitro* release profile of AmB loaded chitosan nanoparticles at 37 ° C. **A:** AmB loaded chitosan-dextran sulphate nanoparticles in PBS (pH of 5, 6.5 or 7.5) and mouse (BALB/c) plasma, **B:** AmB loaded chitosan-TPP nanoparticles in PBS (pH of 5, 6.5 or 7.5) and mouse

(BALB/c) plasma and **C:** comparison of AmB release from AmB solution, AmB loaded chitosan-TPP nanoparticles and AmB loaded chitosan dextran sulphate nanoparticles in PBS at pH 5 and 7.5. Data expressed as mean +/- SD (experiment was reproduced three times with confirmed similar data). AmB loaded chitosan-TPP nanoparticles size= 69 ± 8 nm and AmB loaded chitosan-dextran sulphate nanoparticles size= 174 ± 8 nm

3.4. Discussion

Blank and AmB loaded chitosan-TPP and chitosan-dextran sulphate nanoparticles were successfully produced via the inotropic gelation method. Homogeneously dispersed nanoparticles with different sizes from 50 nm to around 400 nm, with low PDI, and with positive or negative surface charge were synthesised. The effects of experimental conditions and parameters (initial concentration of chitosan, chitosan: TPP or chitosan: dextran sulphate mass ratios, pH of chitosan solution and sonication time) on the physicochemical properties of the nanoparticles (size, PDI and charge) were determined. The aim was to create positively and negatively charged nanoparticles with the smallest size and lowest PDI. The PDI value indicates dispersion homogeneity and the distribution of the nanoparticles sizes in the sample and high PDI means variable ranges of sizes in the sample while lower PDI reflects constantly sized nanoparticles (253). We aimed and succeeded in synthesising the smallest sizes for both types of nanoparticles, as smaller nanoparticles with size 100 nm showed a 2.5-fold higher uptake in Caco-2 cells than larger particles with size 1 μm and a 6-fold higher uptake than particles sized 10 μm (254). Additionally, nanoparticles with small size have exhibited maximum deposition of their content in the skin dermis (after topical application) and small nanoparticles can facilitate macrophage targeting residence in the skin (after intravenous injection) (32, 246, 255, 256). Subsequently, smaller nanoparticles in literatures offered higher uptake rates, more permeability through skin and higher targeting to skin and these properties are substantial in CL treatment.

A paper reported that negatively charged nanoparticles are taken up significantly more than positively charged nanoparticles by Caco-2 epithelial cells (257).

This encouraged us to prepare two types of chitosan nanoparticles (positive and negative charged nanoparticles with smallest possible size).

Influence of reactant mass ratio on the nanoparticles

We indicated that the optimal mass ratio to obtain good quality nanoparticles with smallest size and lowest PDI was 5:1 for chitosan: TPP (at chitosan 3 mg/ml) and this was consistent with literatures (258, 259). It was shown that at this ratio, TPP anions are adequately incorporated into chitosan and as a result, a further boost in the cross-linking and tightening of the chitosan chains within the particle result, which explains the decrease in the nanoparticles sizes, as previously speculated by Masarudin *et al* (2015) (253). Regarding dextran sulphate, a mass ratio 1:3 of chitosan: dextran sulphate (at chitosan 1 mg/ml) gave the smallest nanoparticles size and the lowest PDI and this is similar with another published report published by Tiyafoonchai *et al* (238). As a more concentration of dextran sulphate in comparison with chitosan might increase the level of complexation of the nanoparticles and the chitosan chains can become entangled to a great extent (238, 260).

Influence of initial concentration of chitosan on the nanoparticles

We showed that using a high initial concentration of chitosan (9 mg/ml) led to poor quality and aggregation of nanoparticles and this was in agreement with a previously published report (261). At this high concentration of chitosan, more molecules of chitosan tend to entangle with each other and crosslink with counter ion (TPP) or sulphate groups of dextran sulphate to form larger particles (261) and moreover, this aggregation could be attributed to the higher number of positive groups as these positive groups can make the chitosan chain to stretch because of the intra chitosan chain repulsion (133, 262, 263).

Influence of pH of chitosan solution on the nanoparticles

Additionally, the pH of chitosan solution played an important role in the quality of the nanoparticles. The synthesized nanoparticles were aggregated and of poor quality at pH 3 and pH 7. At pH 3, chitosan is highly protonated with high charge density. While at pH 7, chitosan has a low charge and is partially solubilized. The greater positive charge at pH 3 can make the chitosan chain stretch because of the intra molecular repulsion while at higher pH of 7, there is a large reduction in the protonation degree of the nanoparticles and that large leads to reduce the inter particles electrostatic repulsion among these

nanoparticles. Therefore, there is a higher possibility of the aggregation (133, 262).

Zeta potential of the nanoparticles and the Influence of sonication duration on the nanoparticles

Zeta potential of the nanoparticles increased with increasing concentration and with decreasing pH of the initial chitosan solution used. This increase in zeta potential values could be explained as; the higher concentration of chitosan leads to more total amino groups and consequently more protonated positive $-NH_3^+$ on the surface of the nanoparticles and lower pH of chitosan solution results in more positive amino groups (133, 262). To assess the influence of sonication time on the physicochemical characteristics of nanoparticles, the prepared nanoparticle dispersions were subjected to sonication for 1, 5, 15 and 20 mins. The sonication duration had a critical role in the quality of nanoparticles as sonicating for 15 mins resulted in favoured nanoparticles and this was in accordance with other reports. Too little sonication duration is insufficient to break the aggregation of the nanoparticles and after 20 mins the aggregation cannot be further broken so size and PDI remain constant (264, 265, 266).

The freeze drying process of the nanoparticles

The freeze drying process causes many stresses related to freezing and dehydration and these stresses can destabilize the nanoparticles suspensions and lead to poor quality and aggregation of the nanoparticles (242). This is what we found in our study. Therefore, it is recommended to use protectants for the nanoparticles to protect them from the freeze and dry stress. The most common cryoprotectants used in literatures are sugars as they can form a glassy matrix that can protect the nanoparticles from the mechanical stress and avoid aggregation, so we used D-mannitol and sucrose in our study. We determined that sucrose had a greater protective (2-3 x) effect on both types of nanoparticles than D-mannitol. A similar finding has previously been reported that sucrose is more successful than D-mannitol in protecting the nanoparticles from the lyophilisation (267) possibly due to the fact that sucrose

does not crystallize during lyophilisation process, unlike D-mannitol, as previously reported (242).

Stability of the nanoparticles and their AmB encapsulation and loading properties

We found that blank and AmB loaded chitosan-TPP or chitosan-dextran sulphate nanoparticles were stable in terms of size and zeta potential for 30 days at different temperatures (4, 34 and 37 ° C) and in different media (water, PBS, RPMI and mouse (BALB/c) plasma). Another published report showed that sizes of AmB loaded chitosan-TPP nanoparticles were stable for 6 months in water at 4° C and at room temperature and chitosan-dextran nanoparticles were stable in terms of sizes and zeta potential for 4 weeks (240, 268). The encapsulation efficacy of AmB in both types of nanoparticles was around 90% and similar data was reported for AmB encapsulation in chitosan nanoparticles with TPP (80%) or with chondroitin sulphate (90%) (122, 240). While the loading of AmB was 23% and 26% w/w for chitosan-TPP and chitosan-dextran sulphate nanoparticles respectively with two times more loading in comparison with chitosan chondroitin sulphate nanoparticles (122).

AmB release from the nanoparticles

The release profiles of AmB from AmB solution (as a control) through synthetic membrane was significantly higher than from AmB loaded chitosan-TPP or chitosan-dextran sulphate nanoparticles ($p < 0.05$ by t test). The nature of the complexation agent (TPP or dextran sulphate) did not influence the slow AmB release from both types of nanoparticles in PBS and mouse plasma. The nanoparticles stability in plasma (size and charge) and slow release of AmB in plasma would ensure that AmB does not bind to low density plasma lipoproteins thereby avoiding any potential AmB toxicity. This is consistent with another study of stability of a noncovalent complex of amphotericin B (AmB) with poly(α -glutamic acid) (PGA) in mouse CD/1 serum (118). Both types of chitosan nanoparticles exhibited a pH-dependent AmB release, with a greater release at a low pH of 5 than at higher pH of 7.5. This is likely to be due to the higher solubility of chitosan in acidic media (269).

Drug release from chitosan-TPP nanoparticles was faster than from chitosan-dextran sulphate nanoparticles and this could be explained as chitosan-TPP nanoparticles are significantly smaller than chitosan-dextran sulphate nanoparticle. The resulting larger surface area to volume ratio of chitosan-TPP nanoparticles would allow greater AmB release from the surface of the nanoparticles as more of the drug is closer to the surface (254). The negatively charge of chitosan-dextran sulphate nanoparticles would also play a role in slower release which reported previously of insulin release (270).

3.4.1. Conclusion

In summary, we successfully prepared two different types of AmB loaded chitosan nanoparticles, one smaller size nanoparticle with positive surface charge and the other with larger size and negative charge. The synthesized nanoparticles were able to efficiently encapsulate AmB. Different parameters such as chitosan concentration, chitosan: TPP or chitosan: dextran sulphate mass ratio and chitosan solution pH significantly affected the physicochemical characterization of the nanoparticles. Both positive and negative nanoparticles showed a high stability in terms of size and at different temperatures. As expected, these nanoparticles exhibited a prolonged AmB release. Therefore, they appear to be good candidates for further investigation into their anti-leishmanial activity by different routes of administration.

4. *In vitro* and *in vivo* activity of chitosan formulations in experimental cutaneous leishmaniasis

4.1. Introduction

The intravenous AmB (as mentioned in the introduction) is one of the available second-line drugs for leishmaniasis which acts by forming pores in the cell membrane of *Leishmania* via complexation with ergosterol. However, the use of the conventional deoxycholate amphotericin B (Fungizone) is clinically limited because of the infusion-related side effects such as, fever, nausea, vomiting, rigours and two more serious effects: anaemia and nephrotoxicity (271, 272). A great interest of research to develop the drug delivery system of AmB in leishmaniasis treatment arises. Accordingly, liposomal formulation (AmBisome[®], size= 70-80 nm (272, 273)) with a better tolerated profile and low toxicity issues was developed and approved by FDA for the treatment of VL. It has showed clinical effectivity in CL patients, in multiple doses (3 mg/kg daily for a total of 21 mg/kg) (272, 274). Although AmBisome[®] is on the WHO Essential Medicines List, this formulation has some limitations in terms of the high price (at least 200 USD\$ per vial of 50 mg, is donated by Gilead via WHO for free for VL, not for CL), the need for cold chain, shelf-life related issues, slow infusion and the difficult to access the drug in many countries (170, 275, 276). Moreover, AmBisome[®] has a complex production process and an increase in particles size and a change in the drug content upon storage of AmBisome[®] have been reported (during 72 h of storage) (276, 277).

Other drug delivery systems (DDs) used in the *Leishmania* field encounter some disadvantages summarised in Table 4.1, in addition to accumulation of lipid in liver and spleen caused by the lipidic formulations that may cause pathological conditions (278).

Table 4.1. Disadvantages of different DDs (67, 112, 279, 280, 281, 282, 283, 284)

DDs	Disadvantages
Liposomes	High cost, low stability and using an organic solvent in the preparation
Niosomes	Instability, leaking of entrapped drug and Hydrolysis of encapsulated drugs which limiting the shelf life of the dispersion
Nanodiscs	Lack of size control, using an organic solvent and other drawback is the precipitation under low pH<6
Emulsions	The need to use a high concentration of surfactants and cosurfactant, stability highly influenced by pH and temperatures and desorption of surfactants
Solid lipid nanoparticle	Organic solvent, low drug loading efficiency, fast drug burst release and the possibility of drug expulsion during storage because of the crystalline structure

Polymeric nanoparticles, prepared by ionotropic gelation method (formed by interactions between two oppositely charged molecules), have gained a great interest in the DDs, with advantages over other DDs as their preparation is usually at lower costs, simple, quick ,does not require the use of organic solvents (generally) and the long shelf life of these nanoparticles at room temperature (114)

In Chapter 3, we successfully synthesised two types of AmB loaded nanoparticles (one was positively charged by using TPP and the other was negatively charged by using dextran sulphate) by using ionotropic gelation methods without using any organic solvents. This process was fast, simple and with low cost of 55 USD\$ approx. for 1 g of AmB nanoparticles. These nanoparticles, in contrast to liposomal formulations, showed a high stability in different media (water, PBS, RPMI and mouse (BALB/c) plasma) at different temperatures for a period of 30 days, and they showed a slow drug release in these media. All these characteristics of AmB loaded chitosan nanoparticles (the high stability for a long time in different conditions in terms of size and charge, slow drug release, easy preparation method and low cost etc), made them a suitable candidate for further investigations for CL treatment.

In the literature, chitosan nanoparticles have shown a good activity against a wide range of microbes and are sometimes more active than chitosan solution (MMW and HMW) (Table 4.1). Some studies showed that both chitosan

solution and chitosan nanoparticles have the same antimicrobial mechanism i.e. by interacting with microbial cell membrane or binding with microbial DNA (285). AmB encapsulated in different types of chitosan nanoparticles has been evaluated against leishmaniasis with promising results *in vitro* and *in vivo* and the studies are summarised in Table 4.2. Most of these studies used positively charged nanoparticles with a size greater than 100 nm. In contrast, we decided to investigate smaller nanoparticles (for possible skin permeation, and as smaller size of nanoparticles facilitates a passive transport from blood vessels to tissues when administrated intravenously and can enhance the extravasation in the inflamed lesions on the skin and can facilitates macrophage targeting residence in the skin (255, 256)), with positive charge (when prepared with TPP) or negative charge (when prepared with dextran sulphate) to identify any influence of nanoparticle charge.

Therefore, this chapter aimed to evaluate:

- (i) the *in vitro* activity of blank and amphotericin B loaded chitosan TPP or dextran sulphate nanoparticles against *L. major* and *L. mexicana* promastigotes and amastigotes
- (ii) the *in vivo* anti-leishmanial activity of blank and amphotericin B loaded chitosan TPP or dextran sulphate nanoparticles (through intravenous route) in murine models of CL caused by *L. major*
- (iii) the permeation of these nanoparticles and chitosan solution through BALB/c skin by a Franz diffusion study.

We did not include HMW chitosan solution in the intravenous route of the *in vivo* study as its diluted acid solutions were too viscous and this makes it very difficult and not suitable for mice intravenous route (HMW chitosan viscosity is 800-2000 cP, 1 wt. % in 1% acetic acid) (286, 287).

Table 4.2. Antimicrobial activity of chitosan nanoparticles (285)

Nanoparticles	Microbes	Results
Chitosan nanoparticles (Chitosan, MW 220 KDa)	<i>Staphylococcus aureus</i> <i>Escherichia coli</i>	Chitosan nanoparticles were more effective than chitosan solution and doxycycline(288)
Chitosan nanoparticles (LMW)	<i>Streptococcus mutans</i>	Inhibited biofilm formation (289)
Chitosan-silver nanocomposites (HMW)	<i>Staphylococcus aureus</i>	A synergistic antimicrobial activity between chitosan and silver nanomaterials (290)
Chitosan nanoparticles (Chitosan, MW 310 KDa)	<i>Candida albicans</i>	Chitosan nanoparticles were more active than chitosan with lower MIC ₅₀ (291)
AmB loaded chitosan nanoparticles (LMW)	<i>Candida albicans</i>	Chitosan nanoparticles showed similar activity to AmB with higher corneal penetration(292)

Table 4.3. Anti-leishmanial activity of AmB loaded chitosan nanoparticles

DDS	Preparation method	Nanoparticles properties	Toxicity	Ant-leishmanial activity
Nanoemulsion based chitosan nanocapsule entrapping AmB	First, an oil-in-water (o/w) nanoemulsion was formulated by modified spontaneous emulsification solvent evaporation. Secondly nanocarrier was generated by coating with chitosan deposition on the water-oil surface	Size= 146 ± 9 nm Zeta potential= $+29 \pm 0.8$ mV	AmB DDS was significantly less toxic against the J774A cell line	<i>In vitro</i> : EC ₅₀ for AmB DDS, AmBisome® and Fungizone was 0.19 ± 0.04 , 0.29 ± 0.03 and 0.48 ± 0.05 µg/ml respectively against <i>L. donovani</i> promastigotes <i>In vivo</i> : <i>L. donovani</i> infected hamster model received (i.p.) AmB-loaded formulations at 1 mg/kg on 5 consecutive days. AmB DDS, AmBisome® and Fungizone caused $86 \pm 2\%$, $70 \pm 3\%$ and $56 \pm 4\%$ inhibition of amastigotes in spleen. (219)
Chitosan-coated solid lipid nanoparticles were developed and loaded with amphotericin B	Solvent emulsification-evaporation	Size= 159 ± 25 nm	In mice model, AmB DDS was significantly ten-fold less toxic than pure AmB solution and was safe up to AmB concentration equivalent to 5 mg/kg body weight.	<i>In vitro</i> : EC ₅₀ of AmB DDS, AmBisome® and Fungizone was 0.046 ± 0.02 , 0.157 ± 0.03 and 0.320 ± 0.08 µg/ml respectively against <i>L. donovani</i> amastigotes infecting adherent mouse macrophage cell line J774A.1 (259)
AmB loaded pluronic F127 (PF 127) micelles coated with chitosan	Thin film hydration	Size= 139 ± 3 to 170 ± 53 nm Zeta potential= $+11.0 \pm 2$ to $+53 \pm 5$ mV	AmB DDS was ten-fold less toxic than pure AmB solution against J774A.1 cell	<i>In vitro</i> : EC ₅₀ of AmB DDS, and AmB solution 0.05 and 0.09 µg/ml respectively against <i>L. donovani</i> amastigotes infecting macrophage cell line J774A.1 (293)

AmB loaded chitosan nanoparticles	Inotropic gelation method (between chitosan positively charged and chondroitin sulphate negatively charged)	Size= 136±11 nm Zeta potential= +8.4 to +30.2 mV	Cytotoxicity against murine macrophages of AmB DDS was nearly ten-fold less compared to pure AmB solution	<i>In vitro</i> : EC ₅₀ of AmB DDS and AmB was 1±0 and 0.1±0 respectively (AmB DDS was less active) against <i>L. amazonensis</i> and 0.1±0 and 0.1±0 µg/ml respectively against <i>L. chagasi</i> (AmB DDS had similar activity to AmB). AmB DDS and AmB caused 90% and 89% reduction of <i>L. amazonensis</i> internalized macrophages (%) (122)
AmB loaded chitosan nanoparticles	Inotropic gelation method (between chitosan positively charged and chondroitin sulphate negatively charged)	Size= 136±11 nm Zeta -potential= +8.4 to +30.2 mV	Cytotoxicity against murine macrophages of AmB DDS was nearly ten-fold less compared to pure AmB	<i>In vivo</i> : <i>L. amazonensis</i> infected BALB/c mice received (i.v.) 1 mg of drug/kg daily for 10 days. AmB DDS treated mice showed a smaller lesion size which was sustained up to 30 days after the treatment compared with AmB treated group (83)
AmB loaded chitosan nanoparticles	Phase separation method by mixing chitosan - TPP nanoparticles with AmB solution under stirring for 7 days	Size= 112 nm Zeta potential= +8mV	Mortality in mice received (i.p.) AmB solution 10 mg/kg was 10% while 0% in mice received AmB nanoparticles (10 mg/kg AmB equivalent) every other day for 3 weeks	<i>In vitro</i> : <i>L. major</i> promastigote killing (%): 82% at 20 µg/mL. <i>L. major</i> amastigote killing (%): 78% at 20 µg/mL. <i>In vivo</i> : <i>L. major</i> infected BALB/c mice received (i.p.) AmB nanoparticles of 10 mg/kg while the positive control mice received AmBisome® of 50mg/kg. There was no significant difference in the efficacy of the two formulations and caused 100% reduction of lesion size. (294) and https://www.dovepress.com/comparative-analysis-between-four-model-nanoformulations-of-amphoteric-peer-reviewed-article-IJN

4.2. Material and methods

4.2.1. Preparation of blank and AmB loaded chitosan nanoparticles

All nanoparticles in this study were prepared and characterised as described in Chapter 3 in sections 3-2-1- and 3-2-2-, within the parameters (10 ml of HMW chitosan solution (30 mg in 10 ml AC 1%), 10 mg of AmB (Purity \geq 95%, Cambridge Bioscience, UK) dissolved in 0.5 ml of DMSO (pure AmB), 10 ml of TPP solution (6 mg in 10 ml DS water) or 10 ml of dextran solution (30 mg in 10 ml double distilled water). After freeze drying the nanoparticle suspension, the white (blank nanoparticles) or yellow (AmB loaded nanoparticles) product was reconstituted in double distilled water. After this, these nanoparticles were characterised by size, charge and AmB loading as described in Chapter 3. Additionally, the AmB loading was evaluated again after freeze drying by dissolving the yielded yellow powder in DMSO, in acidic pH 3 (by using 1% (v/v) acetic acid), and then measuring the quantity of AmB by HPLC as described previously in Chapter 3, section 3.3.6.1. There was no significant difference in the loading value between this method and the previously used one in Chapter 3, section 3-2-5- ($p < 0.05$ by t-test).

AmB (Purity \geq 95%, Cambridge Bioscience, UK) dissolved in DMSO at a 10 mM stock and diluter for proper concentrations in RPMI-1640 with 10% HiFCS (pure AmB).

AmBisome[®] (a liposomal formulation of AmB, Gilead Sciences international Ltd, UK) was prepared according to the manufacturer's instructions. Briefly, a suspension of AmB liposome was prepared in cold sterile MilliQ water to obtain an initial concentration of 4 mg/ml. The suspension was shaken and incubated at 65°C for 10 mins and then cooled to room temperature. Further dilution to the required concentration of AmBisome[®] was done with 5% dextrose (w/v) (71).

4.2.2. Red blood cells haemolysis

Blood samples were obtained from two human donors (O⁺) (volunteers, Queen Mary, University of London) drawn directly into EDTA tubes to prevent coagulation. Blood samples were centrifuged at 500 x g for 5 min and the

plasma aspirated and discarded. The remaining red blood cells (RBCs) were then washed three times in buffered saline (10 mM Tris, 150 mM NaCl, pH 7.4) prior to the assay. The RBCs were diluted to a density of 5×10^8 cells/ml and exposed to 1000, 500, 250, 125, 65.5, 31.25, 15.62 and 7.81 $\mu\text{g/ml}$ of chitosan solution (HMW chitosan), blank chitosan-TPP nanoparticles, AmB loaded chitosan-TPP nanoparticles (AmB equivalent), blank chitosan-dextran sulphate nanoparticles, AmB loaded chitosan-dextran sulphate nanoparticles (AmB equivalent) and pure AmB in 96 well plates (200 μl in each well) for 1 h at 37°C . The plate was centrifuged for 5 mins at $500 \times g$ to pellet intact RBCs. 100 μl of supernatant from each well was transferred into a clear, flat-bottomed 96-well plate and cell lysis was determined spectrophotometrically (540 nm). Phosphate buffer was used as a negative control and 20% Triton X-100 was used as a positive control representing 100% haemolysis. The results were expressed as the mean percentage reduction in human red blood cells compared with non-treated control wells, and represented by the 50% haemolytic concentration (RBC_{50}) (295)

4.2.3. *In vitro* cytotoxicity assays

Cytotoxicity of chitosan formulations against KB cells was evaluated at concentrations of 2000, 1000, 500, 250, 125, 65.5, 31.25 and 15.62 $\mu\text{g/ml}$ of blank chitosan-TPP nanoparticles, blank chitosan-dextran sulphate nanoparticles, AmB loaded chitosan-TPP nanoparticles (AmB equivalent) and AmB loaded chitosan-dextran sulphate nanoparticles (AmB equivalent). Cytotoxicity was evaluated in RPMI 1640 at two pH values (at normal pH of RPMI 7.5 and at a lower pH 6.5). Pure AmB, AmBisome[®] and chitosan solution (HMW chitosan) were included in this experiment for comparison. Podophyllotoxin (Sigma, UK) was included as a positive control at a starting concentration of 0.05 μM . Cytotoxicity was evaluated by a cell viability assay using the resazurin sodium salt solution (AlamarBlue, Sigma, UK) as described in Chapter 2, section 2.8.5.

4.2.4. *In vitro* 72-hour activity of chitosan and its derivatives against extracellular *L. major* and *L. mexicana* promastigotes

The activity of chitosan formulations against *L. major* and *L. mexicana* promastigotes was evaluated at concentrations 486, 162, 54, 18, 6, 2, 0.66, 0.22, 0.072, 0.024 and 0.008 µg/ml of blank chitosan-TPP nanoparticles, blank chitosan-dextran sulphate nanoparticles, AmB loaded chitosan-TPP nanoparticles (AmB equivalent) and AmB loaded chitosan-dextran sulphate nanoparticles (AmB equivalent). The anti-leishmanial activity was evaluated in RPMI 1640 at two pH values (7.5 and 6.5). Pure AmB, AmBisome® and chitosan solution (HMW chitosan) were included in this experiment for comparison. See Chapter 2, section 2.8.6 for full details.

4.2.5. *In vitro* 72- hour activity of chitosan and its derivatives against intracellular amastigotes of *L. major* and *L. mexicana*

The activity of chitosan formulations against *L. major* and *L. mexicana* intracellular amastigotes was evaluated at concentrations 486, 162, 54, 18, 6, 2, 0.66, 0.22, 0.072, 0.024 and 0.008 µg/ml of blank chitosan-TPP nanoparticles, blank chitosan-dextran sulphate nanoparticles, AmB loaded chitosan-TPP nanoparticles (AmB equivalent) and AmB loaded chitosan-dextran sulphate nanoparticles (AmB equivalent). The anti-leishmanial activity was evaluated in RPMI 1640 at two pH values (7.5 and 6.5). Pure AmB, AmBisome® and chitosan solution (HMW chitosan) was included in this experiment for comparison. PEMs were used as a macrophage model of intracellular amastigotes. See Chapter 2, section 2.8.7 for full details.

Similarly, **the host cell dependence** of the anti-*L. major* amastigotes activity of chitosan formulations (blank chitosan-TPP nanoparticles, AmB loaded chitosan-TPP nanoparticles and AmB loaded chitosan-dextran sulphate nanoparticles) was evaluated by using two further host cell types (bone marrow macrophages (BMMs) and differentiated THP-1 cells). See Chapter 2, section 2.8.8 for full details.

4.2.6. Evaluation of the *in vivo* anti-leishmanial activity of chitosan formulations

A pre-toxic study of AmB loaded nanoparticles was done before starting the treatment. This toxic study was done by using female BALB/c mice aged 6 to 8 weeks, at 18-20g (Charles River, UK) and these mice were injected intravenously with 100 μ L of AmB loaded chitosan-TPP nanoparticles or AmB loaded chitosan-dextran sulphate nanoparticles starting with concentration 20 mg/kg of AmB and then 2-fold decrease. All mice monitored closely and immediately after administration and then regularly until 48 hours post-dose for two weeks. The safest doses were chosen for the treatment; 5 mg/kg of AmB for AmB loaded chitosan-TPP nanoparticles and 10 mg/kg of AmB loaded chitosan-dextran sulphate nanoparticles.

4.2.6.1. *In vivo* *L. major* model of CL

Female BALB/c mice aged 6 to 8 weeks, at 18-20g, were purchased from Charles River Ltd. These mice were maintained under specific conditions (they were kept in controlled rooms with humidity of 55% and temperature of 26°C and fed water and rodent food ad libitum). *Luciferase-expressing L. major JISH118 (Ppy RE9H+L. major JISH118)* amastigotes were harvested and isolated from mouse skin lesions previously infected with *Leishmania* promastigotes (at a low passage number). Harvested amastigotes were transformed to promastigotes by keeping them at 26°C in Schneider's insect medium + 10% HiFCS. Promastigotes were passaged every week and used at a low passage number (≤ 3) to infect experimental mice due to the potential decrease in virulence with increasing passage number and extended culture (166).

For this study, mice were shaved and then infected with 200 μ L of 4×10^7 of stationary-phase luciferase-expressing *L. major JISH118 (Ppy RE9H+L. major JISH118)* promastigotes subcutaneously on the rump above the tail. After 7 days of infection, small nodules started to be visible at the site of injection and the lesion size was recorded daily by using a digital calliper; 10 days post infection the lesions measured 5 mm approximately in diameter. The infected

mice were allocated in 8 groups (5 mice in each group) with similar average lesion diameters ($P > 0.5$, one-way-ANOVA) after which, the administration of formulations was started as described below:

in vivo experiment 1

- Group 1 Negative control: untreated, uninfected
- Group 2 The positive control group (G2): mice received 10 doses of 100 μ L of paromomycin at a dose of 50 mg/kg intraperitoneally (i.p.) for 10 consecutive days, a regimen with proven efficacy in this CL model (77, 202)
- Group 3 Group 3 (G3): mice received 5 doses of 100 μ L of AmBisome® (size= 70-80 nm) (272, 273), 10 mg/kg intravenously (i.v.) over 10 days, alternate day dosing on days 0, 2, 4, 6, and 8.
- Group 4 Group 4 (G4): mice received 5 doses of 100 μ L of blank chitosan-TPP nanoparticles (equivalent to AmB-loaded) intravenously (i.v.) over 10 days, alternate day dosing
- Group 5 Group 5 (G5): mice received 5 doses of 100 μ L of AmB loaded chitosan-TPP nanoparticles (5 mg/kg of AmB) intravenously (i.v.) over 10 days, alternate day dosing
- Group 6 Group 6 (G6): mice received 5 doses of 100 μ L of blank chitosan-dextran sulphate nanoparticles (equivalent to AmB-loaded) intravenously (i.v.) over 10 days, alternate day dosing
- Group 7 Group 7 (G7): mice received 5 doses of 100 μ L of AmB loaded chitosan-dextran sulphate nanoparticles (10 mg/kg of AmB) intravenously (i.v.) over 10 days, alternate day dosing
- Group 8 Group 8 (G8): mice received 5 doses of 100 μ L of chitosan nanoparticle vehicles (water) intravenously (i.v.) for over 10 days, alternate day dosing

At day 9 (one day after the last dose was administered), the experiment was terminated, mice were humanely killed and skin samples were harvested by surgical removal from the areas containing the localized CL lesion and non-CL-infected skin on the back (control site) of the same mouse (Fig 4.1), stored

at -80°C for further experiments (the biodistribution of AmB and for qPCR and determination of burden). Treatment efficacy was evaluated by measuring the lesion size progression and parasite load (bioluminescence signal).

A second, repeated *in vivo* experiment was conducted with 35 mice were used (*in vivo* experiment 2). This experiment was performed for reproducibility and to study the dose-response effect of AmB loaded chitosan-TPP nanoparticles. Ten days post infection, the lesions measured 5 mm approximately in diameter and mice were allocated to 7 different experimental groups to ensure comparable lesion sizes in each group (5 mice in each group).

Mice were then treated for 10 days, receiving injections containing one of the following regimens:

- Group 1 Control group (G1): untreated, infected mice
- Group 2 The positive control group (G2): mice received 10 doses of 100 µL of paromomycin 50 mg/kg intraperitoneally (i.p.) for 10 consecutive days, a regimen with proven efficacy in this CL model (77, 202)
- Group 3 mice received 5 doses of 100 µL of AmBisome® 10 mg/kg intravenously (i.v.) over 10 days, alternate day dosing on days 0, 2, 4, 6, and 8.
- Group 4 mice received 5 doses of 100 µL of AmB loaded chitosan-TPP nanoparticles (5 mg/kg of AmB) intravenously (i.v.) over 10 days, alternate day dosing
- Group 5 mice received 5 doses of 100 µL of AmB loaded chitosan-TPP nanoparticles (2.5 mg/kg of AmB) intravenously (i.v.) over 10 days, alternate day dosing
- Group 6 mice received 5 doses of 100 µL of AmB loaded chitosan-TPP nanoparticles (1.25 mg/kg of AmB) intravenously (i.v.) over 10 days, alternate day dosing
- Group 7 mice received 5 doses of 100 µL of blank chitosan-TPP nanoparticles (equivalent to 5 mg/kg AmB-loaded) intravenously (i.v.) over 10 days, alternate day dosing

After which the experiment was carried out as previously described.

Both blank and AmB loaded chitosan nanoparticles were suspended in distilled water, characterizes (size, charge, AmB loading) and used freshly for the *in vivo* study.

- Fungizone (a conventional deoxycholate formulation of AmB) was not included in both *in vivo* experiments as controls, because Wijnant *et al* (2017) found that the highest tolerated dose of Fungizone was 1 mg/kg/i.v. (which did not cause acute toxicity to BALB/c mice) and demonstrated that Fungizone (1 mg/kg/QAD for 10 days; i.v.) did not cause a significant reduction in lesion sizes or parasite load in murine (BALB/c) models of *L. major* (170).

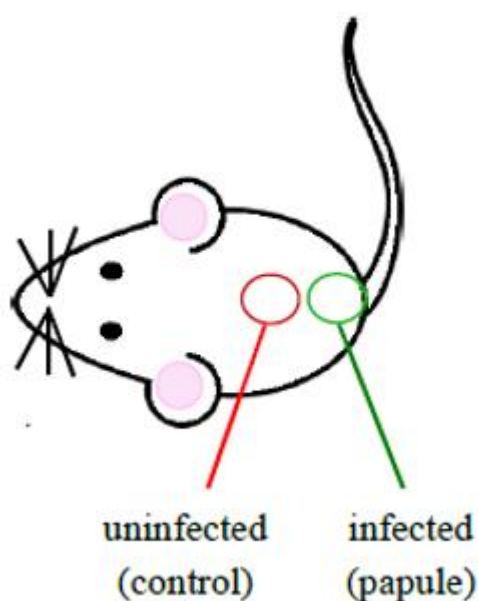


Figure 4.1. Schematic representation of skin samples used in the study (166)

4.2.6.2. Measurement of lesion size

The lesion size was measured daily using digital calipers by determining the width and length of the lesion and then calculating the average (mm). One - way ANOVA with post-hoc Tukey test was performed to analyse the statistical differences between the average diameters per group (166).

4.2.6.3. Measurement of the bioluminescence signal

The luciferase substrate; luciferin (D-Luciferin potassium salt, Xenogen, CA and Gold Biotechnology, St. Louis, MO) was injected (sc) into the mice at 10 mins before the acquiring of bioluminescent signal. After 7 mins of injection, the mice were anaesthetized by inhalation with 3% isoflurane with 100% oxygen at a flow rate of 2.5 l/min until no movement was shown (3 mins approx.). Mice were then imaged and the images were acquired by using a Living Image software (version 4). Emitted photons were gathered by auto acquisition with a charge couple device (CCD) camera (PerkinElmer IVIS Spectrum *In vivo* Imaging System) using the medium resolution (medium binning) mode. A circular region of interest (ROI) encompassing the nodular area on the rump was drawn to quantify the bioluminescence, expressed as radiance and results were expressed in numbers of photons/sec (296).

4.2.6.4. Quantification of AmB in skin samples

Each frozen skin sample was cut into fine, long pieces, weighed and then inserted into microcentrifuge tubes. A spatula of 2 mm zirconium oxide beads (Next Advance, United Kingdom) (about 100 mg) was added with 1 ml of PBS to each tube. After which, the skin sample was homogenised in 3 cycles of 30 seconds of 6800 rpm using a Precellys 24 homogenizer (Bertin Technologies, France) to obtain a smooth homogenate. Then 100 μ l of the homogenate was added to 250 μ l of a mixture of methanol: DMSO (84:16) plus 200 ng/ml tolbutamide (analytical standard; Sigma, United Kingdom) for drug extraction and tolbutamide was used for protein precipitation, in 96-well plates. Then, these 96-well plates were shaken for 10 mins at 200 rpm and centrifuged at 4°C at 6600 rpm for 15 mins. Two hundred microliters of supernatant were stored at -80°C until further analysis for quantification of AmB by HPLC as described previously in Chapter 3, in section 3.3.6.1. A calibration curve for the HPLC was prepared of AmB concentrations in untreated healthy skin homogenate (this homogenate was prepared as described by grinding the skin by using the zirconium oxide beads and the blender, shaking and centrifuging the samples) (170).

4.2.7. Skin permeation study by Franz diffusion cell (FDC) assay

25 female BALB/c mice (6 to 8 weeks old) at 18-20g, were shaved and infected with 200 μ l of 4×10^7 of stationary phase *L. major* JISH118 promastigotes subcutaneously on the rump above the tail. After 7 days of infection small nodules started to be visible at the site of injection and the lesion size was recorded daily by using a digital calliper. Ten days post infection, the lesions measured approximately 5 mm in diameter. The mice were humanely killed and 2 circular discs of skin (infected and uninfected skin- 15mm diameter approximately) were excised per mouse; the infected skin piece containing the *Leishmania* lesion was cut from the dorsal area above the tail and the uninfected piece above the lesion on the higher back of same mouse was collected (Fig 4.1). Forceps were used to gently remove fat and muscle from the skin samples and these samples were stretched carefully on Whatman filter papers. They were then mounted between the donor and receptor compartment of the Franz cell device (Fig 4.2.) and kept in place by a clamp. PBS with 2% hydroxypropyl- β -cyclodextrin (CD, Sigma, UK) was sonicated for 30 mins then added to the receptor compartment (as AmB is soluble in CD at 37 μ g/ml) together with a small magnetic stirrer. The Franz cells were incubated in a warm water bath on a magnetic stirrer plate set at a speed of 800 rpm until the skin reached temperature 34°C. The Franz cells were examined for air bubbles and leakage (166). 100 μ l of each formulation (Pure AmB as a control ($3.96 \pm$ SD mg of amphotericin B/ml), AmB loaded chitosan TPP nanoparticles ($3.93 \pm$ SD mg of amphotericin B/ml)) and AmB loaded chitosan dextran sulphate nanoparticles ($3.84 \pm$ SD mg of amphotericin B/ml)) was applied to each donor compartment. 100 μ l of receptor fluid was taken at regular time intervals and was replaced with 100 μ l of fresh PBS with 2% CD and stored at -80°C to be analysed later by HPLC to quantify AmB. After 24 h the experiment was terminated, and the Franz cells were disassembled. Donor chambers were washed with 1 ml of methanol: DMSO (84:16) which was then stored at -80°C for further AmB analysis by HPLC. A dry cotton swab was used to remove any residual AmB on the surface of skin. This was then stored at -80°C for further quantification of AmB. The skin samples were also stored at -80°C for further experiments. The cumulative amount of drug permeated as a

function of time was plotted and the linear portion of the graph was used to calculate the flux and lag time (Fig 4.14). the permeability coefficient (K_p) was calculated by using Equation 5.

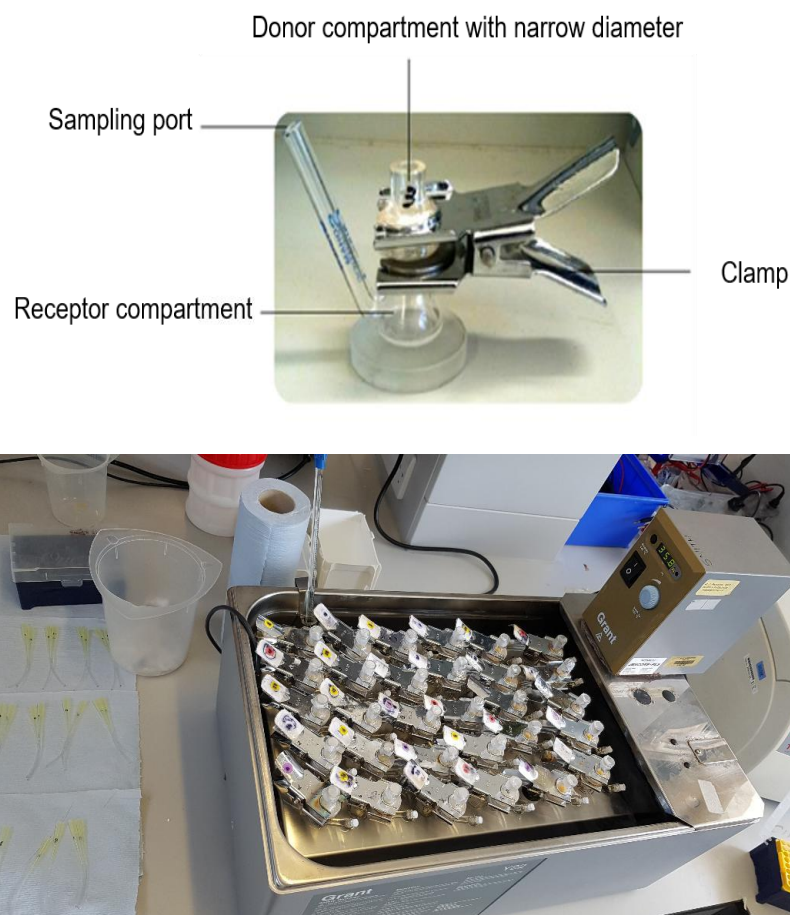


Figure 4.2. Franz diffusion cell used for the permeation studies (166)

4.2.7.1. Quantification of AmB by HPLC

The amount of AmB in the wash was quantified by HPLC using parameters described in Chapter 3 in section 3-2-7- ; standard solutions of AmB were achieved by diluting AmB in methanol: DMSO (84:16) solution.

The amount of AmB in the cotton swab was quantified by HPLC using parameters described in Chapter 3 in section 3-2-7-. Firstly, the cotton swab was soaked in 1 ml of methanol: DMSO (84:16) solution for 24 h and then analysed. For the calibration curve, a dry cotton swab was soaked in 1 ml of

methanol: DMSO (84:16) solution for 24 h and then this solution was used to prepare a standard solution of AmB.

To extract AmB from the skin disc, the skin was homogenised as described below:

Each frozen skin sample was cut into fine, long pieces, weighed and then inserted into microcentrifuge tubes. A spatula-full of 2 mm zirconium oxide beads (Next Advance, United Kingdom) (about 100 mg) was added with 1 ml of PBS to each tube. The skin sample was homogenised in 3 cycles of 30 seconds at 6800 rpm using the Precellys homogeniser (Bertin Technologies) to obtain a smooth homogenate. 100 μ l of homogenate was then added to a 250 μ l of mixture of methanol: DMSO (84:16) plus 200 ng/ml tolbutamide (analytical standard; Sigma, United Kingdom) for drug extraction protein precipitation in 96-well plates. These 96-well plates were shaken for 10 mins at 200 rpm then centrifuged at 4°C at 6600 rpm for 15 mins. 200 μ L of supernatant was stored at -80°C until further analysis for quantification of AmB by HPLC as described previously in Chapter 3. A calibration curve for the HPLC was prepared with AmB concentrations in untreated healthy skin homogenate (this homogenate was prepared as described by grinding the skin using the zirconium oxide beads and the Precellys blender, shaking and centrifuging the samples) (170).

4.2.7.2. Fluorescence microscopy of skin sections post formulation application

To visualise the nanoparticles, formulations with rhodamine-labelled chitosan were prepared in a similar manner to unlabelled particles and then were characterised regarding size and zeta-potential using the Zeta-sizer and applied to infected and uninfected mouse skin using FDC (blank rhodamine-labelled chitosan-TPP nanoparticles equivalent to $3.93 \pm \text{SD}$ mg of amphotericin B/ml loaded in AmB loaded chitosan TPP nanoparticles and blank rhodamine-labelled chitosan-dextran sulphate nanoparticles equivalent to $3.84 \pm \text{SD}$ mg of amphotericin B/ml loaded in AmB loaded chitosan TPP nanoparticles) as described above. After the experiment, the cells were

dismantled and skin tissue fixed in tris-zinc fixative overnight as described by Accart *et al* (2014) (297). After 24 hours the skin samples were embedded in gelatin and immersed in OCT before storage at -80°C. Cryosections of 5 µm were cut using a cryostat (Leica CM1950).

For immunohistochemistry, the sections were defrosted and submerged in PBS (37°C) for 30 minutes to dissolve the gelatine after which they were submerged in PBS for 5 minutes, counterstained with DAPI and mounted in Prolong Gold (Thermofisher Scientific). Sections were examined using a Zeiss Axio Scan Z1 with a x 20 objective.

4.2.8. Statistical analysis.

For the efficacy experiment, ANOVA (1-way for parasite load and intralesional AmB levels, 2-way repeated measures for lesion size) followed by Tukey's multiple comparison test were used. A *P* value of <0.05 was considered statistically significant. All analyses were performed with GraphPad Prism version 7.02.

4.3. Results

4.3.1. Haemolysis activity of chitosan nanoparticles

The haemolytic activity of blank and AmB loaded chitosan TPP or dextran sulphate nanoparticles was clearly observed in a dose-dependent manner as shown in Fig 4.3. Pure AmB was significantly more haemolytic (around 18-fold) than both types of AmB loaded nanoparticles ($p < 0.05$ by an extra sum-of-squares F test) (Table 4.4). On the other hand, AmBisome® is less toxic against RBCs than both types of AmB loaded nanoparticles ($p < 0.05$ by an extra sum-of-squares F test) (Table 4.4).

Table 4.4. *In vitro* haemolytic activity of chitosan formulations after 1h of incubation

Compound	Properties	RBC ₅₀ µg/ml	RBC ₉₀ µg/ml
Amphotericin B (pure AmB)	Purity ≥95%, MW 924.1	11.3 ± 2	40.88 ± 5
AmBisome®	Liposomal AmB, Size= 70-80 nm	525.8 ± 6	1782 ± 8
HMW chitosan	MW=310-375 KDa	810.1 ± 7	3367 ± 9
Blank chitosan-TPP nanoparticles	Size= 67 ± 7 nm, Zeta potential= 28.5 ± 1.9 mv	623.7 ± 6	3639 ± 10
AmB loaded chitosan-TPP nanoparticles	Size= 69 ± 8 nm, Zeta potential= 25.5 ± 1 mv	209.5 ± 5	1129 ± 10
Blank chitosan-dextran sulphate nanoparticles	Size= 170 ± 9 nm, Zeta potential= -12.9 ± 3 mv	621.4 ± 8	3341 ± 16
AmB loaded chitosan-dextran sulphate nanoparticles	Size= 174 ± 8 nm, Zeta potential= -11 ± 1mv	202.8 ± 8	931.4 ± 8

Experiments were conducted in triplicate cultures, data expressed as mean +/- SD (experiment was reproduced further two times with confirmed similar data and data not shown). A statistically significant difference was found in RBC₅₀ values between AmB loaded chitosan nanoparticles and pure AmB ($p < 0.05$ by an extra sum-of-squares F test).

- Chitosan solution ■ Blank chitosan-TPP nanoparticles ▲ AmB loaded chitosan-TPP nanoparticles
- ▼ Blank chitosan-dextran sulphate nanoparticles ◆ AmB loaded chitosan-dextran sulphate nanoparticles
- Pure AmB ■ AmBisome

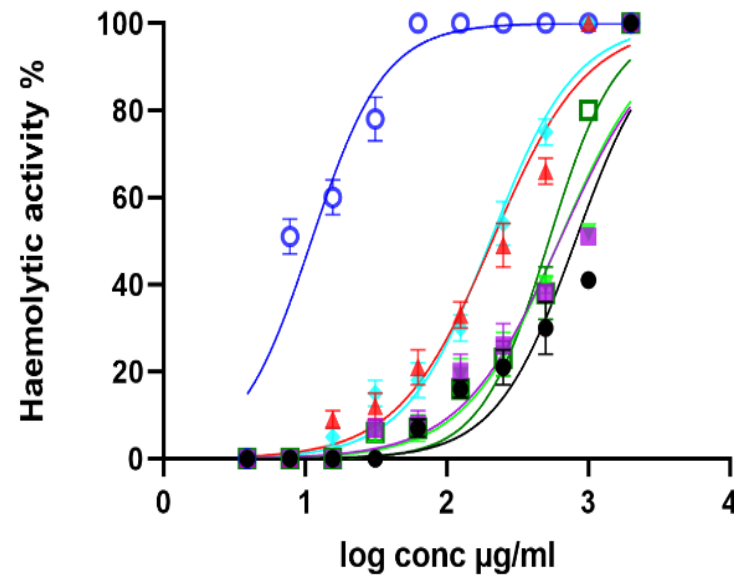


Figure 4.3. Dose-response curves of haemolytic activity of chitosan nanoparticles (blank and AmB loaded nanoparticles) after 1h of incubation. Data are expressed as means \pm SD from triplicates, statistically significant difference in RBC_{50} values between pure AmB and AmB loaded nanoparticles (pure AmB is significantly more toxic AmB loaded nanoparticles) ($P < 0.05$ by an extra sum-of-squares F test)).

4.3.2. Cytotoxicity of blank and AmB loaded chitosan nanoparticles against KB cells in RPMI (pH 7.5 and pH 6.5)

The cytotoxicity of blank and AmB loaded chitosan TPP or dextran sulphate nanoparticles against KB cells was clearly observed in a dose-dependent manner at two pH values (7.5 and 6.5) as shown in Fig 4.4. No significant difference in the cytotoxicity was observed for all formulations at pH of 7.5 and pH of 6.5 (pH did not have an effect on the cytotoxicity) ($p > 0.05$ by t-test) (Table 4.5). Both types of blank chitosan nanoparticles showed a significantly less cytotoxicity than AmB loaded chitosan nanoparticles ($p < 0.05$ by an extra sum-of-squares F test). AmB loaded chitosan TPP or dextran sulphate nanoparticles were significantly less toxic than pure AmB (6-fold less toxic against KB cells) ($p < 0.05$ by an extra sum-of-squares F test). However, no significant difference was observed in the cytotoxicity between AmB loaded nanoparticles and AmBisome® ($p > 0.05$ by an extra sum-of-squares F test) (Table 4.5).

Table 4.5. *In vitro* cytotoxicity of chitosan formulations against KB cells at two pH values after 72h of incubation

Compound	Properties	pH=7.5		pH=6.5	
		LD ₅₀ µg/ml	LD ₉₀ µg/ml	LD ₅₀ µg/ml	LD ₉₀ µg/ml
Podophyllotoxin		0.7 ± 0.03	2 ± 0.3	0.8 ± 0.04	2 ± 0.4
Amphotericin B (pure AmB)	Purity ≥95%, MW 924.1	59 ± 2	228 ± 2	60 ± 2	225 ± 3
AmBisome®	Liposomal AmB, Size= 70-80 nm	401 ± 2	1568 ± 2	401 ± 3	1568 ± 2
HMW chitosan	MW=310- 375 KDa	894 ± 4	2840 ± 3	825 ± 2	2864 ± 2

Blank chitosan-TPP nanoparticles	Size= 67 ± 7 nm, Zeta potential= 28.5 ± 1.9 mv	728 ± 2	2858 ± 4	696 ± 3	2588 ± 4
AmB loaded chitosan-TPP nanoparticles	Size= 69 ± 8 nm, Zeta potential= 25.5 ± 1 mv	356 ± 5	1354 ± 5	348 ± 3	1318 ± 5
Blank chitosan-dextran sulphate nanoparticles	Size= 170 ± 9 nm, Zeta potential= -12.9 ± 3 mv	949 ± 6	2915 ± 6	917 ± 2	2806 ± 1
AmB loaded chitosan-dextran sulphate nanoparticles	Size= 174 ± 8 nm, Zeta potential= -11 ± 1 mv	366 ± 3	1113 ± 3	366 ± 3	1131 ± 4
TPP	MW= 367.864 g/mol	840 ± 8	1400 ± 8	850 ± 8	1500 ± 8
Dextran sulphate	MW= 40 KDa	>1200		>1200	

Experiments were conducted in triplicate cultures, data expressed as mean \pm SD (experiment was reproduced further two times with confirmed similar data and data not shown). Blank or AmB loaded chitosan nanoparticles had a similar toxicity at both pH values (6.5 and 7.5) toward KB-cells ($p > 0.05$ by t-test). A statistically significant difference was found in LD₅₀ (50% lethal dose) values between AmB loaded chitosan nanoparticles and pure AmB ($p < 0.05$ by an extra sum-of-squares F test).

- | | | |
|---|--|---|
| ▲ Pure AmB pH 6.5 | ○ Pure AmB pH 7.5 | ▼ HMW pH 7.5 |
| ◆ AmBisome pH 7.5 | □ AmBisome pH 6.5 | ◇ HMW pH 6.5 |
| ● AmB loaded chitosan-TPP nanoparticles pH 7.5 | ▲ AmB loaded chitosan TPP nanoparticles pH 6.5 | ○ AmB loaded chitosan-dextran sulphate nanoparticles pH 6.5 |
| ■ AmB loaded chitosan-dextran sulphate nanoparticles pH 7.5 | ◆ Blank chitosan-TPP nanoparticles pH 7.5 | ◇ Blank chitosan-TPP nanoparticles pH 6.5 |
| ● Blank chitosan-dextran sulphate nanoparticles pH 7.5 | ● Blank chitosan-dextran sulphate nanoparticles pH 6.5 | |

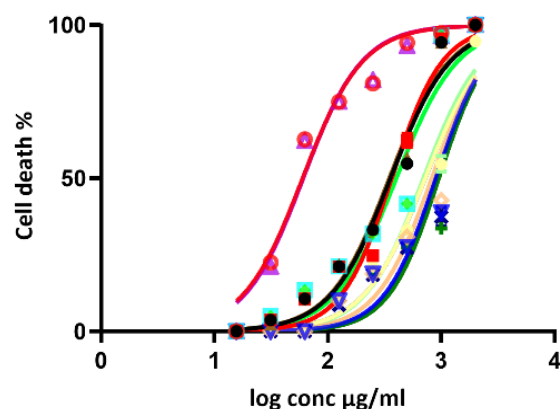


Figure 4.4. Dose-response curves of the cytotoxicity against KB-cells. KB cells were cultured in the presence of different concentrations of chitosan formulations. The toxicity of drugs was measured after 72 hours by measuring the inhibition of metabolic activity. Values are expressed as % inhibition of KB cells relative to untreated controls. Statistically significant difference in LD₅₀ values between pure AmB and AmB loaded nanoparticles against KB-cells (AmB is significantly more toxic AmB loaded nanoparticles) ($P < 0.05$ by an extrasum-of-squares F test)).

4.3.3. Activity of blank and AmB loaded chitosan nanoparticles against *L. major* and *L. mexicana* promastigotes in RPMI (pH 7.5 and pH 6.5)

Both chitosan solution and blank chitosan TPP nanoparticles were significantly more active at lower pH (6.5) than at higher pH (7.5) ($p < 0.05$ by t-test), chitosan solution was more active than blank chitosan-TPP nanoparticles at two pH values ($p < 0.05$ by t-test) (Fig 4.5.). Blank chitosan-dextran sulphate nanoparticles had no activity against *Leishmania* promastigotes up to a concentration of 486 $\mu\text{g/ml}$ at two pH values. At both pH values (7.5 and 6.5) pure AmB, AmB loaded chitosan-TPP nanoparticles and AmB loaded chitosan-dextran sulphate nanoparticles showed a similar anti-promastigote activity without a significant difference in their activity at these two pH values ($p > 0.05$ by t-test). They were significantly more active against *Leishmania* promastigotes than AmBisome® ($p < 0.05$ by an extra sum-of-squares F test) (Table 4.6). *L. major* promastigotes were more sensitive than *L. mexicana* to pure AmB, AmB loaded chitosan-TPP nanoparticles and AmB loaded chitosan-dextran sulphate nanoparticles ($p < 0.05$ by an extra sum-of-squares F test).

Table 4.6. *In vitro* activity of chitosan formulations against promastigotes at two pH values

Compound	Properties	pH=7.5 *				pH=6.5*			
		<i>L. major</i> **		<i>L. mexicana</i> **		<i>L. major</i> **		<i>L. mexicana</i> **	
		EC ₅₀ µg/ml	EC ₉₀ µg/ml	EC ₅₀ µg/ml	EC ₉₀ µg/ml	EC ₅₀ µg/ml	EC ₉₀ µg/ml	EC ₅₀ µg/ml	EC ₉₀ µg/ml
Amphotericin B (pure AmB)	Purity ≥95%, MW 924.1	0.06 ± 0.003	0.3 ± 0.02	0.2 ± 0.004	0.4 ± 0.03	0.06 ± 0.003	0.3 ± 0.02	0.2 ± 0.004	0.4 ± 0.03
AmBisome®	Liposomal AmB, Size= 70-80 nm	1 ± 0.08	7 ± 0.3	1.8 ± 0.1	7 ± 0.07	1.1 ± 0.08	7 ± 0.1	1.9 ± 0.1	7 ± 0.01
HMW chitosan	MW=310-375 KDa	106 ± 7	539 ± 31	141 ± 31	556 ± 5	7.1 ± 0.5	56 ± 4	13.5 ± 0.8	163 ± 27
Blank chitosan-TPP nanoparticles	Size= 67 ± 7 nm, Zeta potential= 28.5 ± 1.9 mv	164 ± 6	443 ± 10	185 ± 10	443 ± 0.8	28 ± 1.5	169 ± 11	38 ± 0.8	173 ± 10
AmB loaded chitosan-TPP nanoparticles	Size= 69 ± 8 nm, Zeta potential= 25.5 ± 1 mv	0.08 ± 0.003	0.5 ± 0.02	0.3 ± 0.02	0.7 ± 0.02	0.06 ± 0.003	0.4 ± 0.02	0.2 ± 0.004	0.4 ± 0.02
Blank chitosan-dextran sulphate nanoparticles	Size= 170 ± 9 nm, Zeta potential= - 12.9 ± 3 mv	No activity up to 486							
AmB loaded chitosan-dextran sulphate nanoparticles	Size= 174 ± 8 nm, Zeta potential= -11 ± 1mv	0.09 ± 0.003	0.4 ± 0.01	0.5 ± 0.02	1 ± 0.07	0.06 ± 0.003	0.3 ± 0.02	0.4 ± 0.02	1.5 ± 0.04
TPP	MW= 367.864 g/mol	No activity up to 486							
Dextran sulphate	MW= 40 KDa	No activity up to 486							

Experiments were conducted in triplicate cultures, data expressed as mean +/- SD (experiment was reproduced further two times with confirmed similar data not shown). *Statistically significant differences were found for the EC₅₀ values of chitosan or blank chitosan-TPP nanoparticles at pH=6.5 and pH=7.5 ($p < 0.05$ by using t-test). ***L. major* promastigotes were significantly more susceptible to pure AmB and AmB loaded chitosan nanoparticles than *L. mexicana* ($p < 0.05$ by an extra sum-of-squares F test)). Pure AmB and AmB loaded chitosan TPP or dextran sulphate nanoparticles had a similar anti-leishmanial activity.

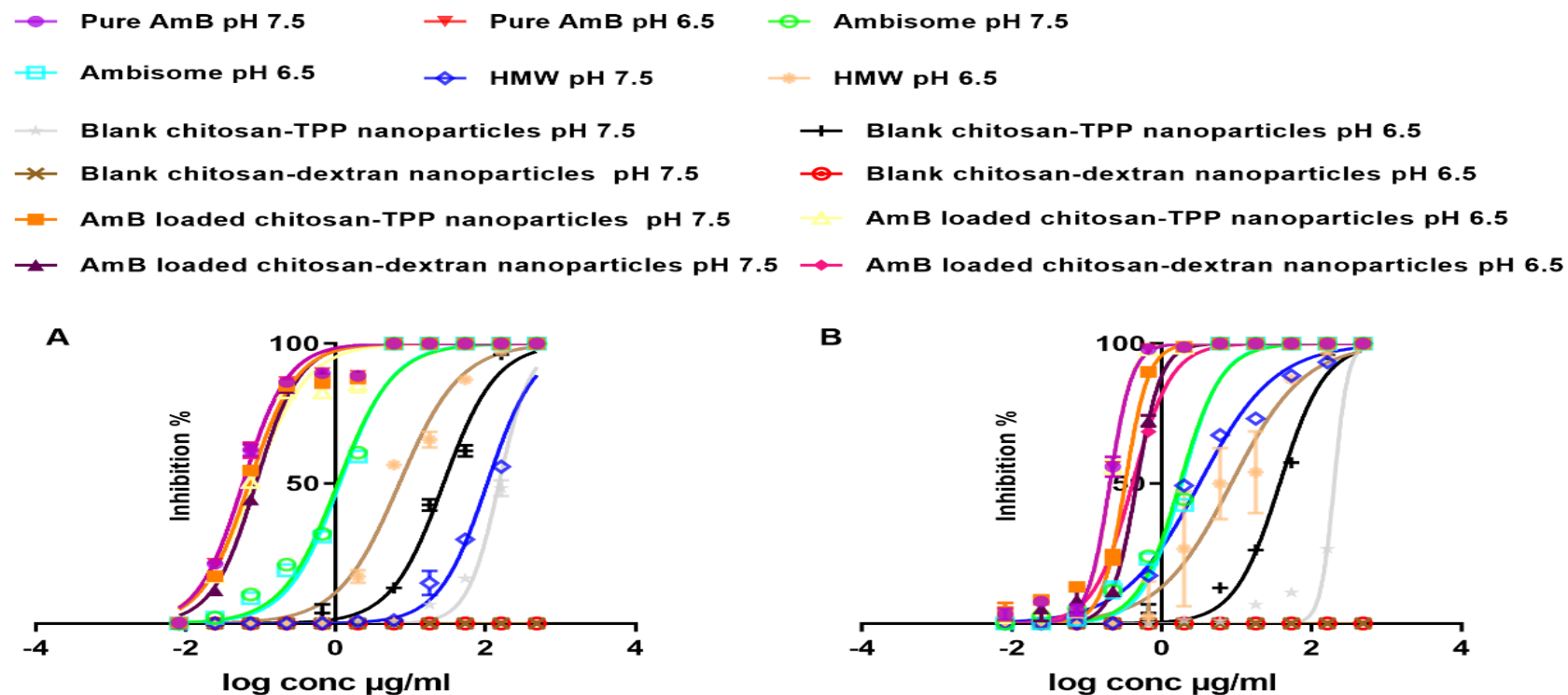


Figure 4.5. Dose-response curves of the activity of blank and AmB loaded chitosan nanoparticles against *Leishmania* promastigotes at two pH values. A: *L. major*; B: *L. mexicana*. Promastigotes were cultured in the presence of different concentrations of chitosan nanoparticles. The activity of drugs was measured after 72h by the resazurin solution. Values are expressed as % inhibition of promastigotes relative to untreated controls. No statistically significant difference was observed in EC₅₀ values of AmB loaded chitosan nanoparticles and pure AmB against *L. mexicana* or *L. major* promastigotes ($p>0.05$ by t-test).

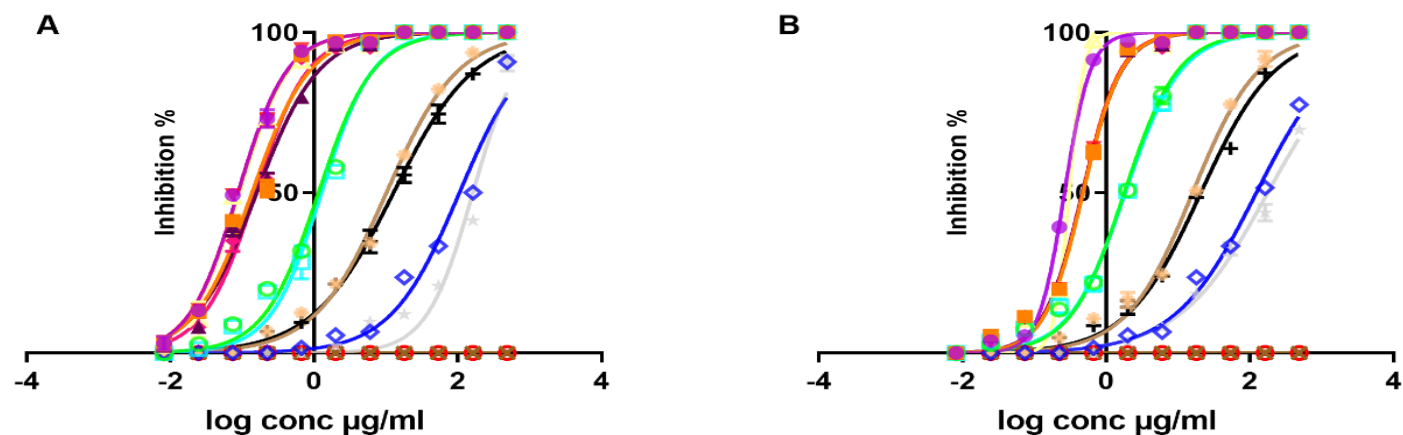
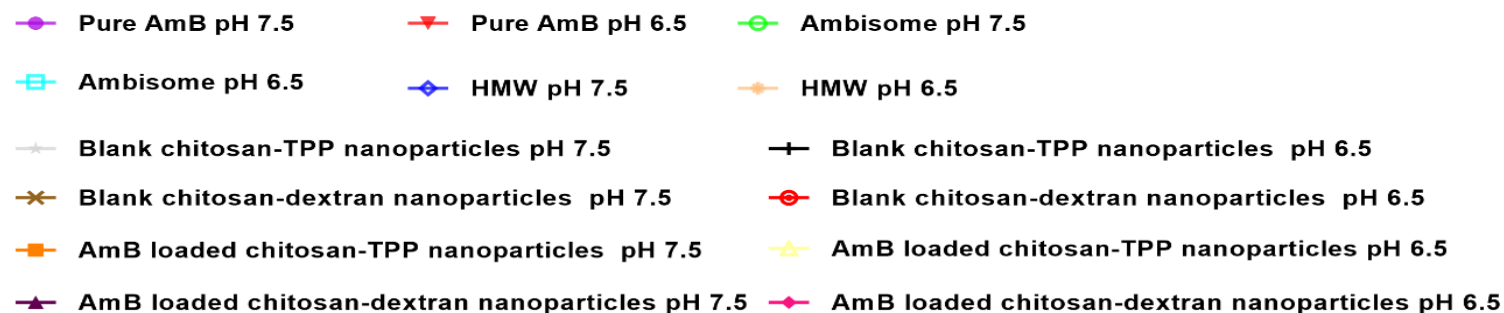
4.3.4. Activity of blank and AmB loaded chitosan nanoparticles against *L. major* and *L. mexicana* amastigotes infecting PEMs

Both chitosan solution and blank chitosan-TPP nanoparticles were significantly more active at lower pH (6.5) than at higher pH (7.5) ($p < 0.05$ by t-test) (Fig 4.6.). Chitosan solution was more effective against amastigotes than blank chitosan-TPP nanoparticles at higher pH of 7.5 ($p < 0.05$ by an extra sum-of-squares F test), However, both have a similar activity against *Leishmania* amastigotes at lower pH of 6.5 ($p > 0.05$ by an extra sum-of-squares F test). Blank chitosan-dextran sulphate nanoparticles had no activity against *Leishmania* amastigotes to concentration up to 486 $\mu\text{g/ml}$ at two pH values. Pure AmB, AmB loaded chitosan-TPP nanoparticles and AmB loaded chitosan-dextran sulphate nanoparticles showed similar anti-amastigotes activity against both *L. major* and *L. mexicana* amastigotes at two pH values (7.5 and 6.5) without a significant difference in their activity at these two pH values ($p > 0.05$ by t-test) and they were significantly more effective against *Leishmania* amastigotes than AmBisome[®] ($p < 0.05$ by an extra sum-of-squares F test). Pure AmB and AmB loaded chitosan-TPP nanoparticles and AmB loaded chitosan-dextran sulphate nanoparticles showed higher anti amastigote activity against *L. major* than *L. mexicana* ($p < 0.05$ by an extra sum-of-squares F test) (Table 4.7).

Table 4.7. *In vitro* activity of chitosan formulations against intracellular amastigotes at two pH values

Compound	Properties	pH=7.5 *				pH=6.5*			
		<i>L. major</i> **		<i>L. mexicana</i> **		<i>L. major</i> **		<i>L. mexicana</i> **	
		EC ₅₀ µg/ml	EC ₉₀ µg/ml	EC ₅₀ µg/ml	EC ₉₀ µg/ml	EC ₅₀ µg/ml	EC ₉₀ µg/ml	EC ₅₀ µg/ml	EC ₉₀ µg/ml
Amphotericin B (pure AmB)	Purity ≥95%, MW 924.1	0.09± 0.003	0.5 ± 0.04	0.3 ± 0.003	0.7 ± 0.02	0.09 ± 0.003	0.5 ± 0.02	0.5 ± 0.04	0.6 ± 0.04
AmBisome®	Liposomal AmB, Size= 70-80 nm	1.2 ± 0.07	8 ± 0.3	1.8 ± 0.08	12 ± 1	1.3 ± 0.08	7 ± 0.1	1.8 ± 0.07	13 ± 1
HMW chitosan	MW=310-375 KDa	105 ± 7	1192± 58	123 ± 5	2206 ± 5	10 ± 0.3	127 ± 5	16 ± 0.7	165 ± 27
Blank chitosan-TPP nanoparticles	Size= 67 ± 7 nm, Zeta potential= 28.5 ± 1.9 mv	162 ± 10	828 ± 43	177 ± 7	4020 ± 352	13 ± 0.5	122 ± 19	21 ± 0.9	284 ± 10
AmB loaded chitosan-TPP nanoparticles	Size= 69 ± 8 nm, Zeta potential= 25.5 ± 1 mv	0.14± 0.009	1 ± 0.09	0.5 ± 0.01	1.8 ± 0.1	0.06 ± 0.003	0.5 ± 0.08	0.3 ± 0.01	1.8 ± 0.02
Blank chitosan-dextran sulphate nanoparticles	Size= 170 ± 9 nm, Zeta potential= -12.9 ± 3 mv	No activity up to 486							
AmB loaded chitosan-dextran sulphate nanoparticles	Size= 174 ± 8 nm, Zeta potential= -11 ± 1mv	0.16± 0.008	1.4 ± 0.02	0.5 ± 0.01	1.8 ± 0.05	0.16 ± 0.007	0.9 ± 0.04	0.4 ± 0.01	1.8 ± 0.05
TPP	MW= 367.864 g/mol	No activity up to 486							
Dextran sulphate	MW= 40 KDa	No activity up to 486							

Experiments were conducted in quadruplicate cultures, data expressed as mean +/- SD (experiment was reproduced further two times with confirmed similar data not shown). *Statistically significant differences were found for the EC₅₀ values of chitosan or blank chitosan TPP nanoparticles at pH=6.5 and pH=7.5 ($p<0.05$ by using t-test). ** *L. major* amastigotes were significantly more susceptible to pure AmB and AmB loaded chitosan nanoparticles than *L. mexicana* ($p<0.05$ by an extra sum-of-squares F test)). Pure AmB, AmB loaded chitosan TPP and dextran sulphate nanoparticles had a similar anti-leishmanial activity.



4.6. Dose-response curves of the activity of blank and loaded chitosan nanoparticles against *Leishmania* amastigotes at two pH values. A: *L. major*; B: *L. mexicana*. PEMs were infected with stationary-phase promastigotes and exposed to various concentrations of chitosan and its derivatives, followed by microscopic counting of the number of infected macrophages*. Values are expressed as % inhibition of infection relative to untreated controls. No statistically significant difference was observed in EC₅₀ values of AmB loaded chitosan nanoparticles and pure AmB against *L. mexicana* or *L. major* amastigotes at pH=6.5 or pH=7.5 ($p>0.05$ by t-test).

4.3.5. Host cell dependence of the anti-leishmanial activity of chitosan nanoparticles at pH of 6.5

EC₅₀ and EC₉₀ values of blank chitosan-TPP nanoparticles, AmB loaded chitosan-TPP nanoparticles and AmB loaded chitosan-dextran sulphate nanoparticles against amastigotes infecting three different macrophage populations are summarized in Table 4.8. There was a significant difference in the activity of chitosan formulations depending on the type of macrophage; as blank chitosan-TPP nanoparticles, AmB loaded chitosan-TPP nanoparticles and AmB loaded chitosan-dextran sulphate nanoparticles were significantly more active against intracellular amastigotes in PEMs and BMMs compared to differentiated THP-1 cells ($p < 0.05$ by an extra sum-of-squares F test) (Table 4.8).

Table 4.8. Activity of chitosan formulations against *L. major* amastigotes in three different macrophage cultures after 72 h at pH of 6.5

	Pure AmB		AmB loaded chitosan-dextran sulphate nanoparticles		AmB loaded chitosan-TPP nanoparticles		blank chitosan-TPP nanoparticles	
Host cell / infection rate % at 24 h	EC ₅₀ µg/ml	EC ₉₀ µg/ml	EC ₅₀ µg/ml	EC ₉₀ µg/ml	EC ₅₀ µg/ml	EC ₉₀ µg/ml	EC ₅₀ µg/ml	EC ₉₀ µg/ml
PEMs / > 80%	0.08 ± 0.01	0.4 ± 0.1	0.08 ± 0.004	0.4 ± 0.1	0.09 ± 0.004	0.5 ± 0.1	12 ± 1	156 ± 9
BMMs / > 80%	0.09 ± 0.02	0.6 ± 0.1	0.09 ± 0.02	0.6 ± 0.1	0.09 ± 0.01	0.5 ± 0.1	14 ± 2	207 ± 14
THP-1 / > 80%	0.2 ± 0.05	3.4 ± 0.4	0.2 ± 0.06	3.3 ± 0.3	0.2 ± 0.06	2.9 ± 0.4	26 ± 4	306 ± 9

Experiments were conducted in quadruplicate cultures, data expressed as mean +/- SD (experiment was reproduced further two times with confirmed similar data and data not shown), statistically significant difference in EC₅₀ as chitosan formulations were significantly more active in PEMs and BMMs compared with THP-1 cells ($p < 0.05$ by an extra sum-of-squares F test). % infection rate gives the percentage of infected macrophages.

4.3.6. *In vivo* anti-leishmanial activity (intravenous route route)

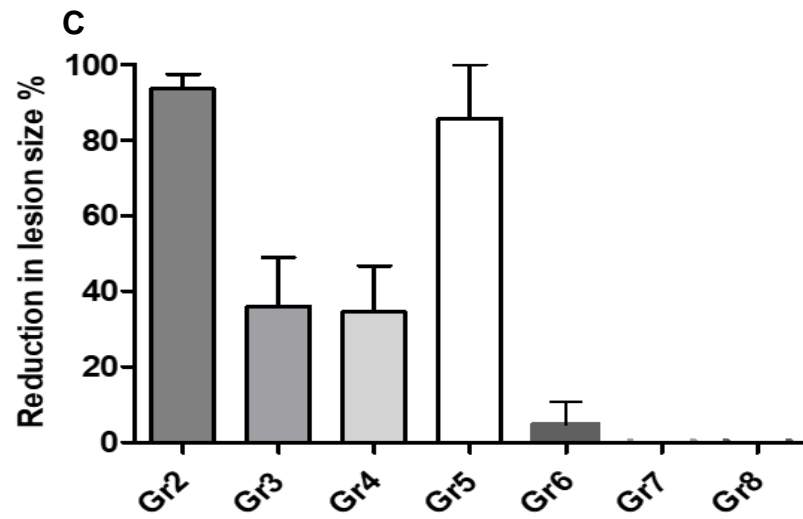
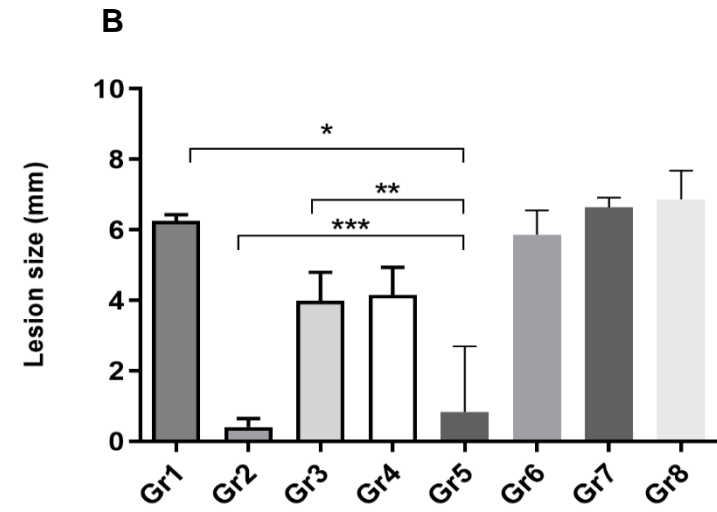
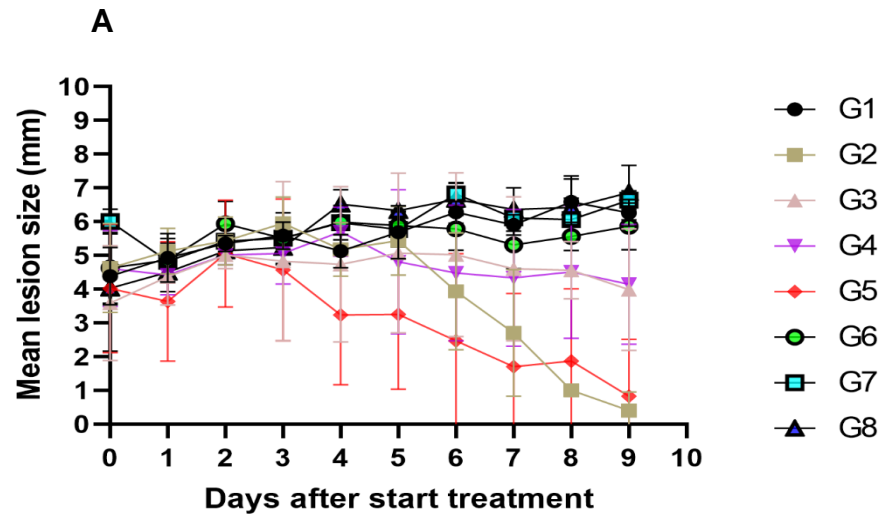
We assessed the efficacy of blank and AmB loaded chitosan nanoparticles (two types) in murine models of CL caused by *L. major*, by analysing the lesion sizes and bioluminescence signal progression among the groups.

4.3.6.1. *In vivo* experiment 1

4.3.6.1.1. Evaluation of the lesion size progression

Fig 4.7. shows the progression of the mean lesion size for each group as a function of time. Blank chitosan-dextran sulphate nanoparticles and nanoparticles vehicles did not cause any reduction in the progression of the lesion size compared to the untreated controls. Both AmBisome® (10 mg/kg/QAD for 10 days; i.v.) and blank chitosan-TPP nanoparticles reduced the lesion size at the end of the treatment with 36% and 34% respectively, reduction compared to the untreated controls without a significant difference in their efficacy ($p>0.05$ by one-way ANOVA). AmB loaded chitosan-TPP nanoparticles (5 mg/kg/QAD for 10 days; i.v.) were the most effective compared with other chitosan formulations and caused a 87% reduction of lesion sizes and was significantly more effective than AmBisome® with 2.4 times greater activity ($p<0.05$ by one-way ANOVA). There was no significant difference in the anti-leishmanial efficacy between AmB loaded chitosan-TPP nanoparticles (5 doses) and paromomycin (50 mg/kg, 10 doses, positive control, 10 doses) with 87% and 93% respectively, reduction of lesion sizes ($p>0.05$ by one-way ANOVA).

Group 7 received one dose of AmB loaded chitosan-dextran sulphate nanoparticles (10 mg/kg, i.v.) for the reason that the day following this dose, mice looked unwell and showed signs of a piloerection and weight loss. Therefore, no more doses were administered. After two days, two mice had died and without any signs of potential CL-related mortality such as severe ulceration, dissemination of the lesion. We just kept monitoring the lesion sizes of the other three mice.

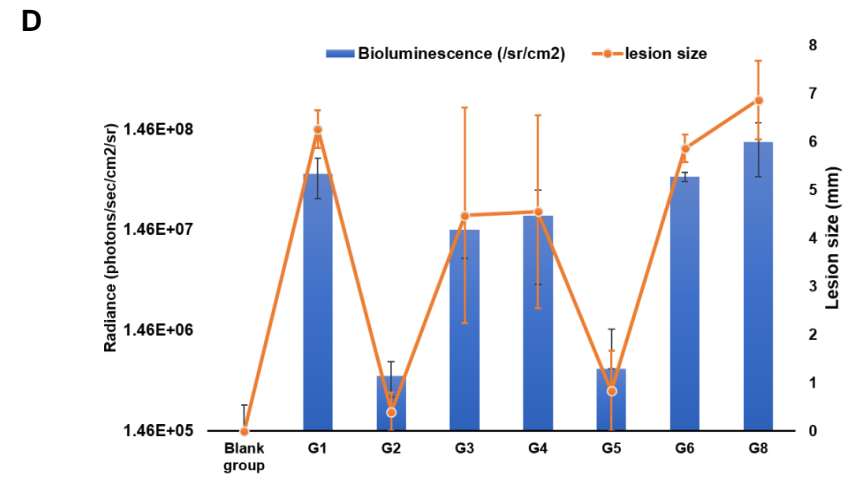
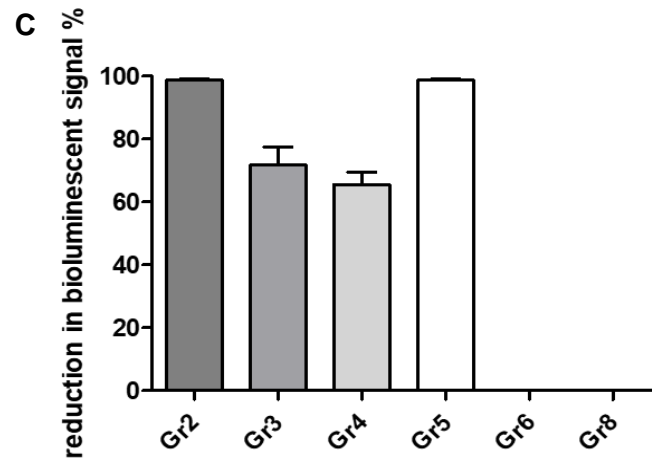
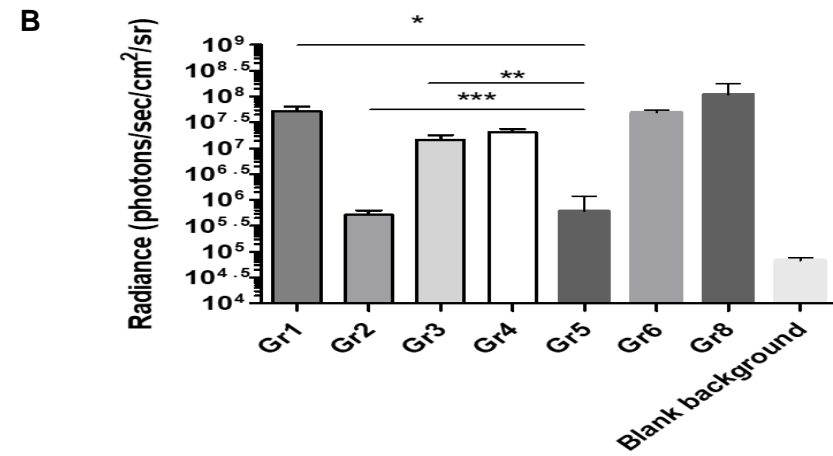
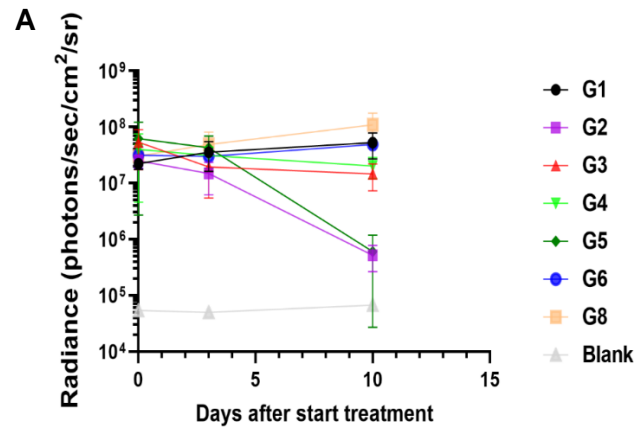


D**E**

Figure 4.7. Amphotericin B nanoparticles efficacy in the lesion cure model in BALB/c mice infected with luciferase-expressing *L. major* parasites. Female BALB/c mice were infected with stationary-phase promastigotes in the rump above the tail (n = 5 per group). At 10 days post-inoculation, animals presenting with CL nodules were dosed with paromomycin (G2) as a positive control (50 mg/kg/QD for 10 days; i.p.), AmBisome® (G3) as a comparison group (10 mg/kg/QAD for 10 days; i.v.), blank chitosan-TPP nanoparticles equivalent to AmB loaded nanoparticles (G4) (QAD for 10 days; i.v.), AmB loaded chitosan-TPP nanoparticles (G5) (5 mg of AmB/kg/QAD for 10 days; i.v.), blank chitosan-dextran sulphate nanoparticles equivalent to AmB loaded nanoparticles (G6) (QAD for 10 days; iv), AmB loaded chitosan-dextran sulphate nanoparticles (G7) (10 mg of AmB/kg/ one dose; i.v.) or the nanoparticles vehicle (G8) (distilled water, QAD for 10 days; i.v.). (G1) represents untreated infected group. During treatment, lesion size was measured daily. The average lesion size represents the mean \pm SD. ANOVA (1 way for parasite load and repeated measures for lesion size) followed by Turkey's multiple-comparison tests was used to compare outcomes among the groups. A p-value < 0.05 was considered statistically significant (*) $p < 0.05$, (**) $p < 0.05$ and (***) $p > 0.05$. (A) represents mean lesion size progression in function of time since the start of treatment, (B) represents the mean lesion size at day 9 (one day after the last dose was administered), (C) represents the % reduction in lesion size compared with G1 (untreated infected group) at day 9, (D) represents images of untreated group on day 9 (lesions are circled) and (E) represents images of G4 on day 9 (infection sites are circled and it is clear the healing effects of treatment on the lesions).

4.3.6.1.2. Evaluation of the parasite load (bioluminescent signal)

Bioluminescence signal progression in all treatment groups is shown in Fig 4.8. The reduction of parasite loads in the skin followed a similar trend of the lesion size with a good correlation between lesion size and bioluminescent signal identified by Pearson correlation coefficients (using GraphPad Prism). AmB loaded chitosan-TPP nanoparticles (5 mg/kg/QAD for 10 days; i.v.) were the most effective compared with other chitosan formulations with 99% reduction in parasite loads (bioluminescent signal) at the end of the treatment compared to the untreated controls and with similar reduction to the Group 2 treated with the positive control (paromomycin, 50 mg/kg, 10 doses; i.p.) ($p > 0.05$ by one-way ANOVA). There was no significant difference between AmBisome® (10 mg/kg/QAD for 10 days; i.v.) and blank chitosan-TPP nanoparticles with 72% and 62% respectively, reduction ($p > 0.05$ by one-way ANOVA). Blank chitosan-dextran sulphate nanoparticles did not cause any reduction in the signal at the end of treatment. We did not image Group 7 as the mice did not look healthy to be anaesthetized and imaged.



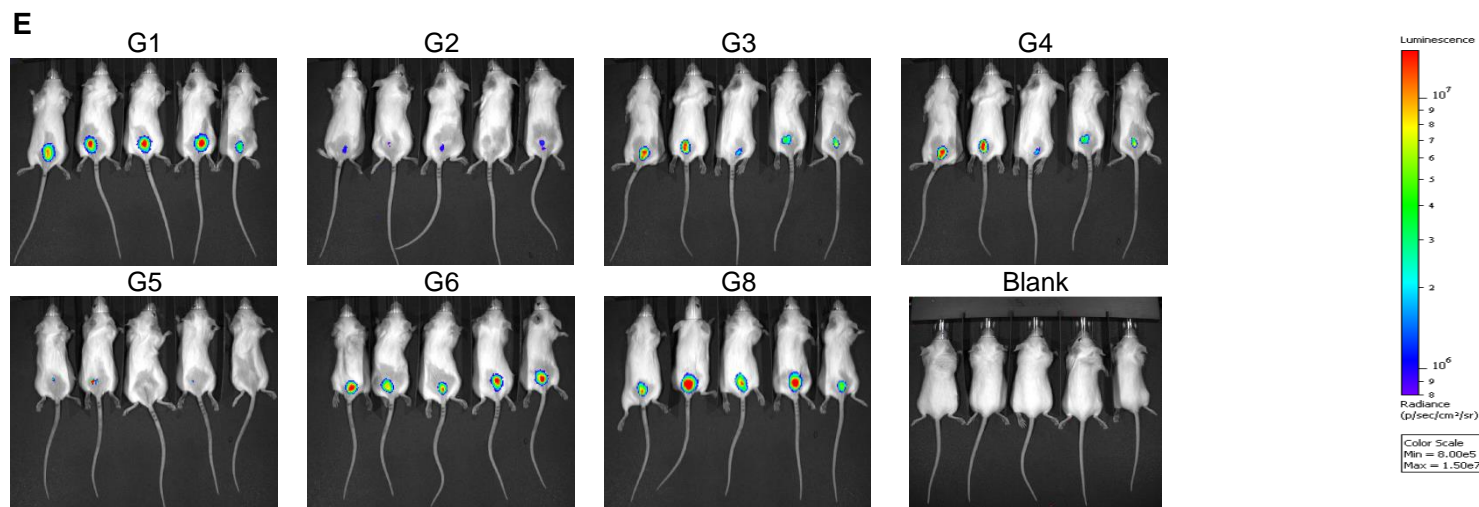


Figure 4.8. Amphotericin B nanoparticles efficacy as measured by the bioluminescence signal (parasite load) at the infection site in BALB/c mice infected with luciferase-expressing *L. major* parasites. Female BALB/c mice were infected with stationary-phase promastigotes in the rump above the tail (n = 5 per group). At 10 days post-inoculation, animals presenting with CL nodules were dosed with paromomycin (G2) as a positive control (50 mg/kg/QD for 10 days; i.p.), AmBisome® (G3) as a comparison group (10 mg/kg/QAD for 10 days; i.v.), blank chitosan-TPP nanoparticles equivalent to AmB loaded nanoparticles (G4) (QAD for 10 days; i.v.), AmB loaded chitosan-TPP nanoparticles (G5) (5 mg of AmB/kg/QAD for 10 days; i.v.), blank chitosan-dextran sulphate nanoparticles equivalent to AmB loaded nanoparticles (G6) (QAD for 10 days; i.v.), or the nanoparticles vehicle (G8) (distilled water, QAD for 10 days; i.v.). (G1) represents untreated infected group. The bioluminescence signal was measured three times: start of treatment, after two doses of treatment and lastly on the day after the administration of the last dose. The data represents the mean \pm standard error. ANOVA (1 way for parasite load and repeated measures for lesion size) followed by Turkey's multiple-comparison tests was used to compare outcomes among the groups. A p-value < 0.05 was considered statistically significant ((*) $p < 0.05$, (**) $p < 0.05$ and (***) $p > 0.05$). (A) represents the bioluminescence signal in function of time since the start of treatment, (B) represents the bioluminescence signal on the day after the administration of the last dose (day 9). (C) represents the % reduction in the signal compared with G1 (untreated infected group) at day 9. (D) represents the correlation between lesion size and the bioluminescence signal on the day after the administration of the last dose and (E) represents the bioluminescent images of mice on day 9 (24 h after the last drug dose administration). Emitted photons were gathered by auto acquisition with a charge couple device (CCD) camera (PerkinElmer IVIS Spectrum *In vivo* Imaging System) using the medium resolution (medium binning) mode.

4.3.6.1.3. Intralesional amphotericin B levels

We measured the levels of the active compound (AmB) within the infected lesion (rump skin) and control skin (uninfected skin, back skin) at the end of the experiment (Fig 4.9.). AmB levels were significantly higher (between 13 and 20-fold) in lesions sites (rump skin) compared to control skin (uninfected skin, back skin) in both Group 3 and Group 5 ($p < 0.05$ by one-way ANOVA). After multiple dosing of either AmBisome® (G3, 10 mg/kg/QAD for 10 days; i.v.) or AmB loaded chitosan-TPP nanoparticles (G5, 5 mg of AmB/kg/QAD for 10 days; i.v.), intralesional AmB levels were significantly lower (6.8-fold) in Group 3 than in Group 5 ($p < 0.05$ by one-way ANOVA). We could not detect any AmB levels as expected in samples from untreated group (G1) and positive control (G2).

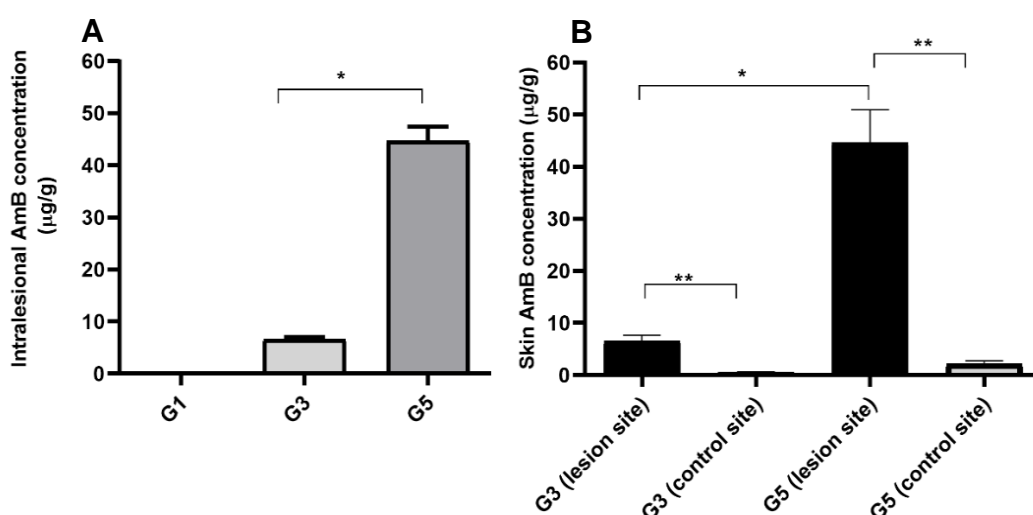


Figure 4.9. Multiple dose skin pharmacokinetics of AmB loaded chitosan-TPP nanoparticles and AmBisome®. *L. major*-infected BALB/c mice received intravenous doses of AmBisome® (G3, 10 mg/kg/QAD for 10 days; i.v.) and AmB loaded chitosan-TPP nanoparticles (G5, 5 mg of AmB/kg/QAD for 10 days; i.v.). 24 hours after the last dosing, AmB levels in skin were determined. The CL lesion was localized on the rump, while the back skin of same mice was used as lesion-free, healthy control site. Each point represents the mean and standard error of the mean (n=5 per group). (A) represents intralesional AmB and (B) represents a comparison between infected and uninfected skin AmB concentration. The data represents the mean \pm standard error. ANOVA followed by Turkey's multiple-comparison tests was used to compare outcomes among the groups. A p-value < 0.05 was considered statistically significant ((* $p < 0.05$ and (** $p < 0.01$)).

4.3.6.2. *In vivo* experiment 2 (dose-response effect)

4.3.6.2.1. Evaluation of the lesion size progression

Fig 4.10. shows the progression of the mean lesion size for each group as a function of time. Our data were similar and reproducible with previous *in vivo* experiment 1 regarding the efficacy of AmB loaded chitosan-TPP nanoparticles (5 mg of AmB/kg/QAD for 10 days; i.v.). In a mouse model of CL caused by *L. major*, AmB loaded chitosan-TPP nanoparticles efficacy showed a dose-response activity in reduction of lesion sizes at doses of 1.25, 2.5 and 5 mg of AmB/kg/QAD for 10 days; i.v., which caused 29%, 40% and 83% respectively, reduction in lesion sizes at the end of the treatment compared to the untreated controls. Similar to *in vivo* experiment 1, there was no significant difference in the efficacy of AmBisome®, blank chitosan-TPP nanoparticles and AmB loaded chitosan-TPP nanoparticles (2.5 AmB/kg/QAD for 10 days; i.v.) with 40%, 35% and 40% respectively, reduction of lesion sizes ($p>0.05$ by one-way ANOVA). Paromomycin (positive control) and AmB loaded chitosan-TPP nanoparticles (5 AmB/kg/QAD for 10 days; i.v.) were the most effective in reduction of lesion sizes and there was no statistically significant difference between the two treated groups with 89% and 83% respectively, reduction of lesion sizes at the end of the treatment compared to the untreated controls ($p>0.05$ by one-way ANOVA).

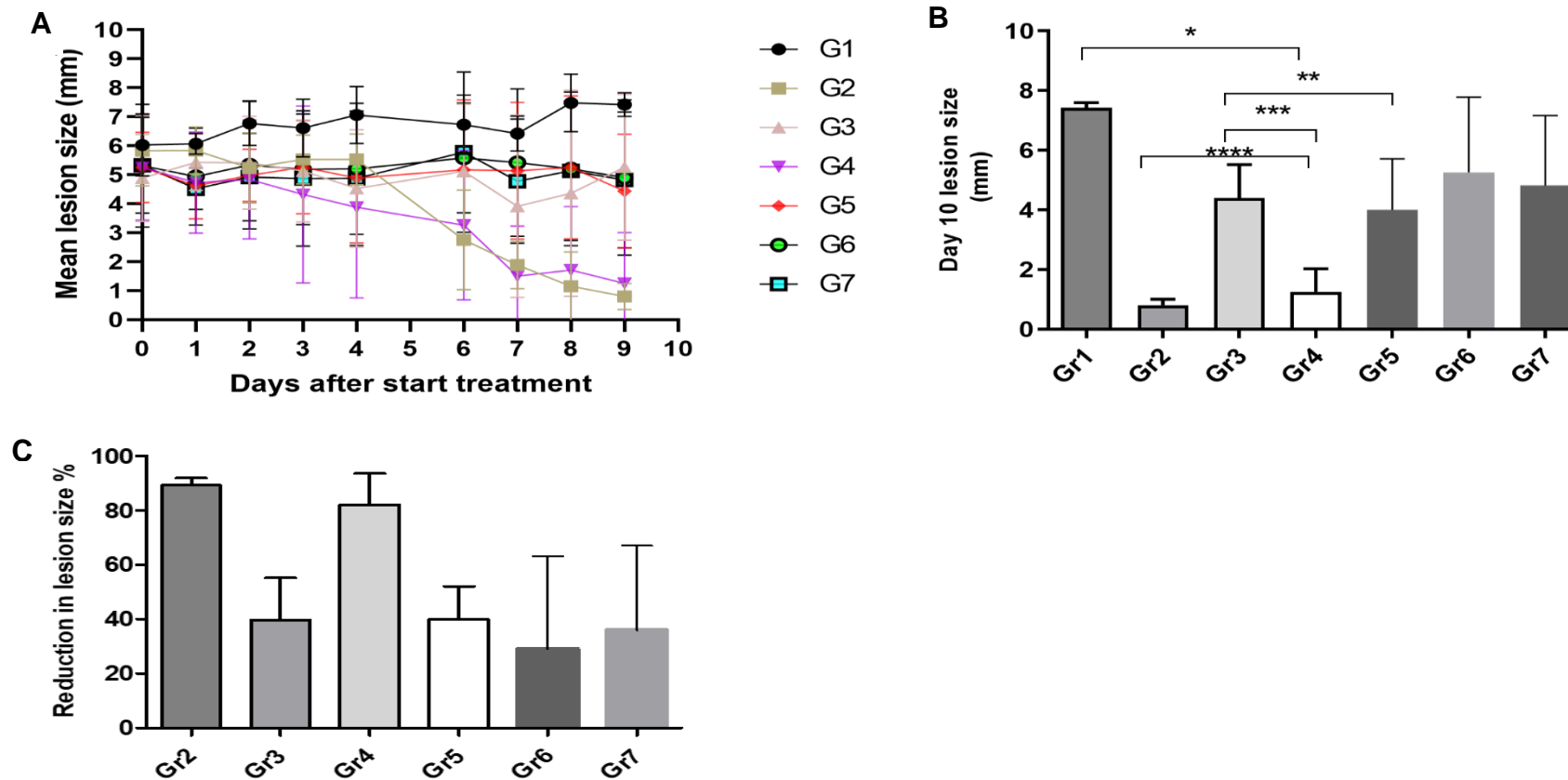


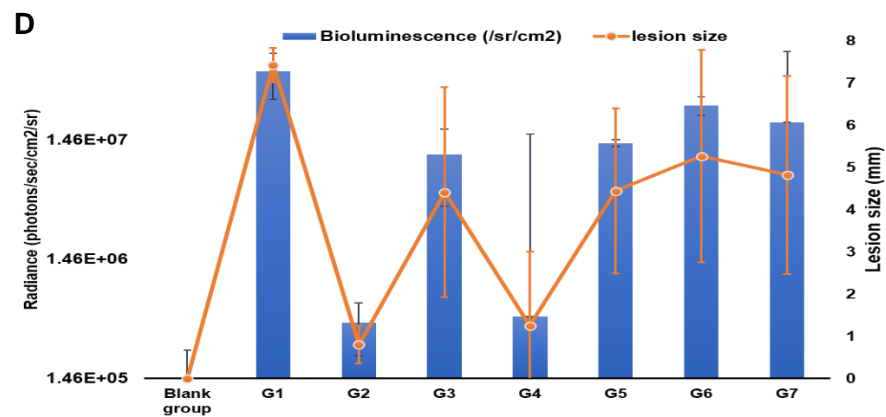
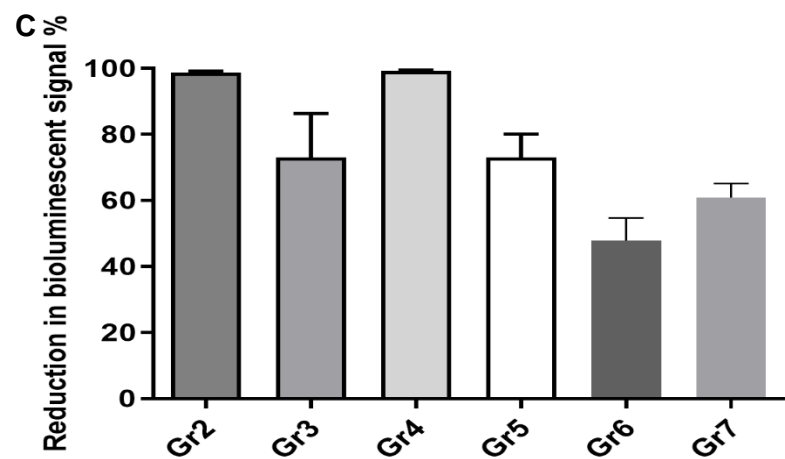
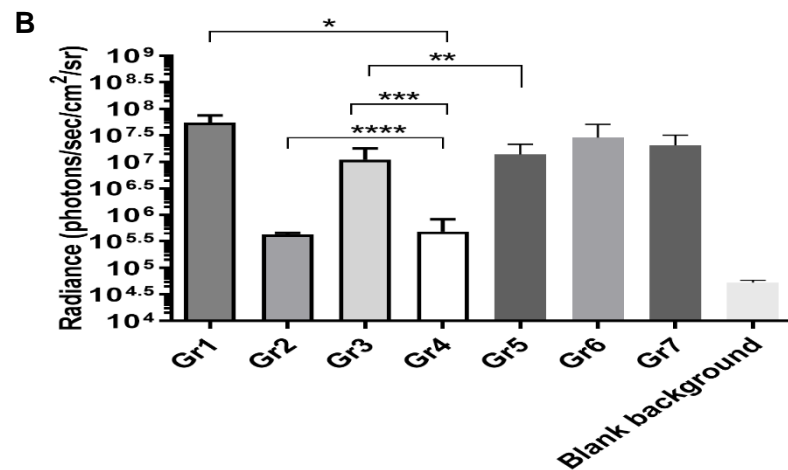
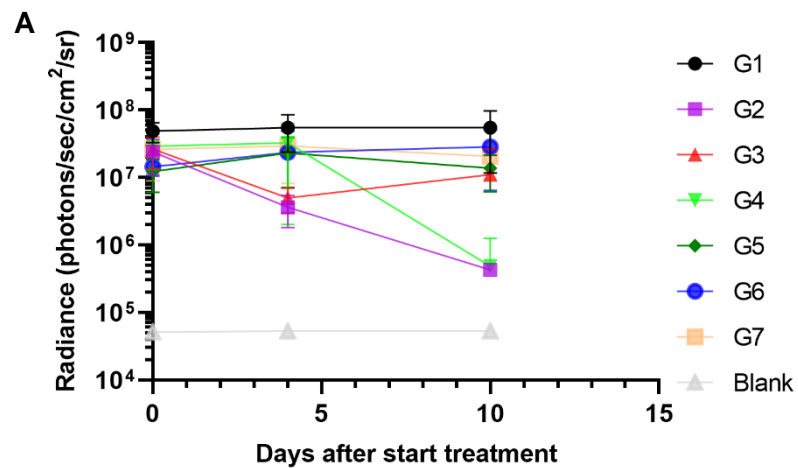
Figure 4.10. Amphotericin B nanoparticles efficacy in the lesion cure model in BALB/c mice infected with luciferase-expressing *L. major* parasites. Female BALB/c mice were infected with stationary-phase promastigotes in the rump above the tail (n = 5 per group). At 10 days post-inoculation, animals presenting with CL nodules were dosed with paromomycin (G2) as a positive control (50 mg/kg/QD for 10 consecutive days; i.p.), AmBisome® (G3) as a comparison group (10 mg/kg/QAD for 10 days; i.v.), AmB loaded chitosan-TPP nanoparticles (G4) (5 mg of AmB/kg/QAD for 10 days; i.v.), AmB loaded chitosan-TPP nanoparticles (G5) (2.5 mg of AmB/kg/QAD for 10 days; i.v.), AmB loaded chitosan-TPP nanoparticles (G6) (1.25 mg of AmB/kg/QAD for 10 days; i.v.) and blank chitosan-TPP nanoparticles equivalent to AmB loaded

nanoparticles (5 mg/kg) (G7) (QAD for 10 days; i.v.). (G1) represents untreated infected group. During treatment, lesion size was measured daily. The average lesion size represents the mean \pm standard error. ANOVA (1 way for parasite load and repeated measures for lesion size) followed by Turkey's multiple-comparison tests was used to compare outcomes among the groups. A p-value < 0.05 was considered statistically significant ((*) $p < 0.05$, (**) $p > 0.05$, (***) $p < 0.05$ and (****) $p > 0.05$). (A) represents mean lesion size progression in function of time since the start of treatment, (B) represents mean lesion size on the day after the administration of the last dose and (C) represents the % reduction in lesion size compared with G1 (untreated infected group) at day 9.

4.3.6.2.2. Evaluation of the parasite load (bioluminescent signal)

Bioluminescence signal progression in all treatment groups is shown in Fig 4.11. The reduction of parasite loads in the skin follows a similar trend of the lesion size with a good correlation between lesion size and bioluminescent signal identified by Pearson correlation coefficients (using GraphPad Prism). In a mouse model of CL caused by *L. major*, AmB loaded chitosan-TPP nanoparticles efficacy showed a dose-response activity in reduction of the parasite loads at doses of 1.25, 2.5, and 5 mg of AmB/kg/QAD for 10 days; i.v., which caused 48%, 75% and 99%, respectively, reduction in parasite loads (bioluminescent signal) at the end of the treatment compared to the untreated controls. Paromomycin and AmB loaded chitosan-TPP nanoparticles (5 mg of AmB/kg/QAD for 10 days; i.v.) were the most effective compounds with 99% reduction of the signal at the end of the treatment.

There was no significant difference in the efficacy of AmBisome® and AmB loaded chitosan-TPP nanoparticles (2.5 AmB/kg/QAD for 10 days; i.v.) in reducing parasite load with 80% and 75% respectively, reduction of bioluminescent signal ($p>0.05$ by one-way ANOVA). Blank chitosan-TPP nanoparticles caused a 65% reduction in parasite loads (bioluminescent signal).



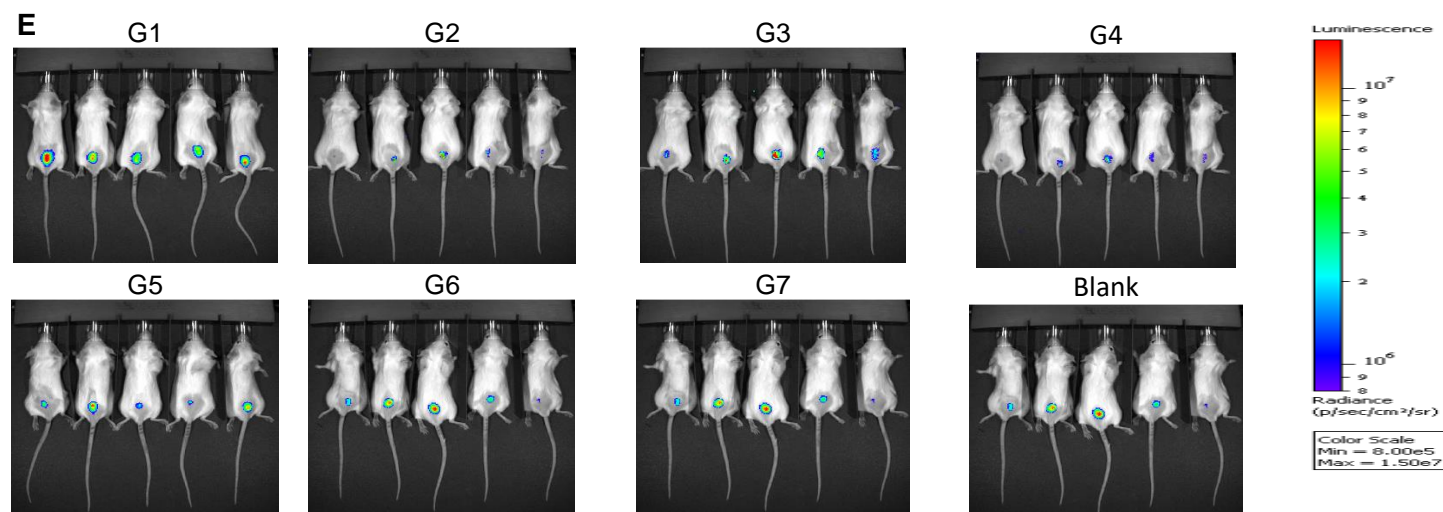


Figure 4.11. Amphotericin B nanoparticles efficacy on the bioluminescence signal (parasite load) at the infection site in BALB/c mice infected with luciferase-expressing *L. major* parasites. Female BALB/c mice were infected with stationary-phase promastigotes in the rump above the tail (n = 5 per group). At 10 days post-inoculation, animals presenting with CL nodules were dosed with paromomycin (G2) as a positive control (50 mg/kg/QD for 10 consecutive days; i.p.), AmBisome® (G3) as a comparison group (10 mg/kg/QAD for 10 days; i.v.), AmB loaded chitosan-TPP nanoparticles (G4) (5 mg of AmB/kg/QAD for 10 days; i.v.), AmB loaded chitosan-TPP nanoparticles (G5) (2.5 mg of AmB/kg/QAD for 10 days; i.v.), AmB loaded chitosan-TPP nanoparticles (G6) (1.25 mg of AmB/kg/QAD for 10 days; i.v.) and blank chitosan-TPP nanoparticles equivalent to AmB loaded nanoparticles (5 mg/kg) (G7) (QAD for 10 days; i.v.). (G1) represents untreated infected group. During treatment, lesion size was measured daily. The bioluminescence signal was measured three times: start of treatment, after two doses of treatment and lastly on the day after the administration of the last dose. The data represents the mean \pm standard error. ANOVA (1 way for parasite load and repeated measures for lesion size) followed by Turkey's multiple-comparison tests was used to compare outcomes among the groups. A p-value < 0.05 was considered statistically significant ((* $p < 0.05$, (** $p > 0.05$, (***) $p < 0.05$ and (****) $p > 0.05$). (A) represents the bioluminescence signal in function of time since the start of treatment, (B) represents mean the bioluminescence signal on the day after the administration of the last dose (day 9), (C) represents the % reduction in the signal compared with G1 (untreated infected group) at day 9. (D) represents the correlation between lesion size and the bioluminescence signal on the day after the administration of the last dose and (E) represents the bioluminescent images of mice on day 9 (24 h after the last drug dose administration). Emitted photons were gathered by auto acquisition with a charge couple device (CCD) camera (PerkinElmer IVIS Spectrum *In vivo* Imaging System) using the medium resolution (medium binning) mode.

4.3.6.2.3. Intralesional amphotericin B levels

We measured the drug levels of the active compound AmB within the infected lesion (rump skin) and control skin (uninfected skin, back skin) at the end of the experiment (Fig 4.12.). After multiple dosing of either AmBisome® (G3) or AmB loaded chitosan-TPP nanoparticles (G4 or G5 or G6), intra-lesional AmB levels were significantly lower (6.7-fold) in Group 3 (received AmBisome® at 10 mg/kg/QAD for 10 days) than in Group 4 (received AmB loaded chitosan-TPP nanoparticles at 5 mg of AmB/kg/QAD for 10 days; i.v.) ($p < 0.05$ by one-way ANOVA). There was no significant difference in the intra-lesional AmB levels between Group 3 and Group 5 (received AmB loaded chitosan-TPP nanoparticles at 2.5 mg of AmB/kg/QAD for 10 days; i.v.) ($p > 0.05$ by one-way ANOVA) and these levels of AmB were significantly higher in these two groups than in Group 6 (received AmB loaded chitosan-TPP nanoparticles at 1.25 mg of AmB/kg/QAD for 10 days; i.v.) ($p < 0.05$ by one-way ANOVA). AmB levels were significantly higher in lesions sites (rump skin) compared to control skin (uninfected skin, back skin) ($p < 0.05$ by one-way ANOVA) for all treated groups with AmB formulations. We could not detect any AmB levels as expected in samples from untreated group (G1) and positive control (G2).

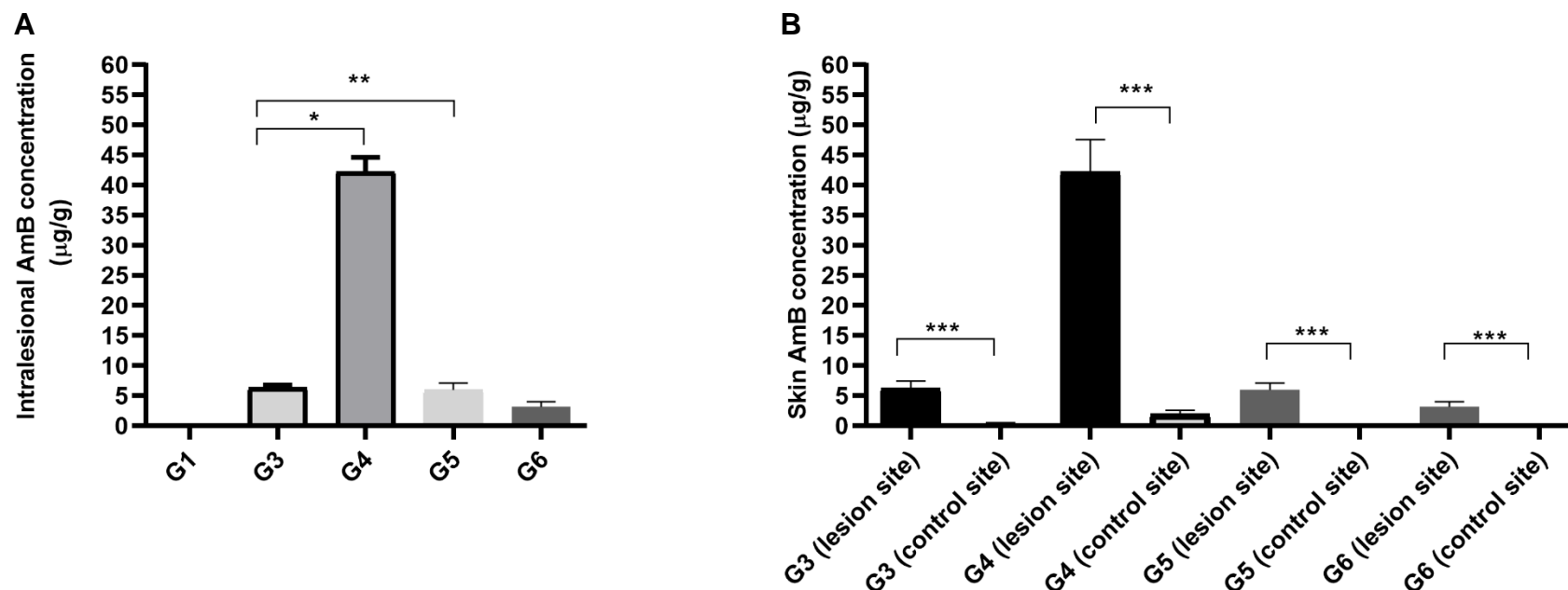


Figure 4.12. Multiple dose skin pharmacokinetics of AmB loaded chitosan-TPP nanoparticles and AmBisome®. *L. major*-infected BALB/c mice received intravenous doses of AmBisome® (G3, 10 mg/kg/QAD for 10 days; i.v.), AmB loaded chitosan-TPP nanoparticles (G4, 5 mg of AmB/kg/QAD for 10 days; i.v.), AmB loaded chitosan-TPP nanoparticles (G5, 2.5 mg of AmB/kg/QAD for 10 days; i.v.) and AmB loaded chitosan-TPP nanoparticles (G6, 1.25 mg of AmB/kg/QAD for 10 days; i.v.). 24 hours after the last dosing, AmB levels in skin were determined. The CL lesion was localized on the rump, while the back skin of same mice used as lesion-free, healthy control site. Each point represents the mean and standard error of the mean (n=5 per group). (A) represents intralesional AmB and (B) represents a comparison between infected and uninfected skin AmB concentration. The data represents the mean \pm standard error. ANOVA followed by Turkey's multiple-comparison tests was used to compare outcomes among the groups. A p-value < 0.05 was considered statistically significant ((*) $p < 0.05$, (**) $p > 0.05$ and (***) $p < 0.05$).

4.3.6.2.4. Dose concentration-response of AmB loaded chitosan-TPP nanoparticles in *L. major*-infected mice

The intralesional AmB levels were related to the dose levels of treatment with AmB loaded chitosan-TPP nanoparticles at concentrations (5 (G4) or 2.5 (G5) or 1.25 (G6) mg of AmB/kg/QAD for 10 days; i.v.) (Fig 4.13.a) and to the response (indicated by lesion size and parasite load) (Fig 4.13.b and 4.13.c, respectively). Fig 3d shows the nonlinear-fit sigmoidal dose-response curve plotting the logarithm of these intralesional AmB levels versus relative reductions in parasite load and lesion size compared to the untreated controls (0 mg/kg). Fig 4.13.e shows the % of relative reduction of lesion size and parasite load related to the doses per kg of AmB.

Correlation was strong between dose concentration and concentration response for relative reduction in parasite load and lesion size (identified by Pearson correlation coefficients (using GraphPad Prism)). We calculated ED₅₀ (The required dose to achieve 50% of maximum effect) and ED₉₀ (The required dose to achieve 90% of maximum effect) after plotting the logarithm of the dose level against percentage response (lesion size or parasite load). ED₅₀ and ED₉₀ were 2.5 and 8.9 mg/kg, respectively for lesion size. ED₅₀ and ED₉₀ were 1.3 and 3.8 mg/kg, respectively for parasite load (bioluminescent signal).

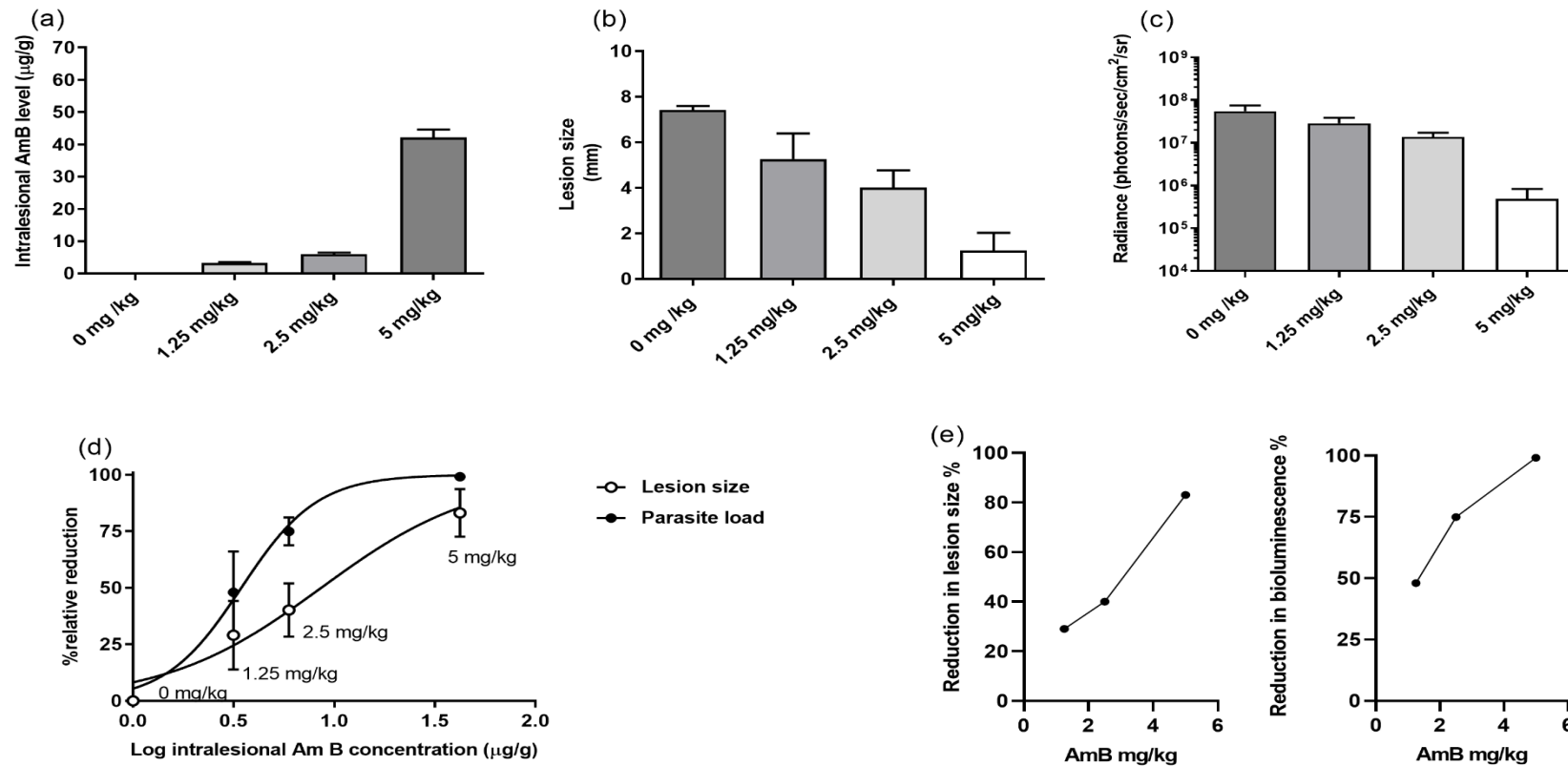


Figure 4.13. Dose concentration-response relationship of AmB loaded chitosan-TPP nanoparticles in experimental CL. *L. major*-infected BALB/c mice received intravenous doses of AmB loaded chitosan-TPP nanoparticles 0 or 1.25 or 2.5 or 5 of AmB/kg/QAD for 10 days ($n = 5$ per group). ; (a) represents the resulting intralesional amphotericin B levels, (b) lesion size, and (c) parasite load on the day after the last dose. (d) Outcomes are linked in a logarithmic-scale dose-response curve plotting drug concentrations against relative reduction in lesion size and parasite load. (e) is the relation between the dose in mg/kg and % of reduction of lesion size and parasite load. Each point represents the means \pm SD ($n=5$ per group). ANOVA followed by Turkey's multiple-comparison tests was used to compare outcomes among the groups. A p-value < 0.05 was considered statistically significant.

4.3.7. *Ex vivo* permeability of *Leishmania*-infected skin in Franz diffusion cells

The permeability of uninfected and *L. major* infected skin for AmB loaded chitosan nanoparticles and fluorescence images of the nanoparticles distribution were evaluated in Franz diffusion cells. The cumulative concentration of AmB from AmB-loaded chitosan-TPP nanoparticles and AmB-loaded chitosan-dextran sulphate nanoparticles in the receptor compartment of Franz diffusion cells permeated as a function of time is shown in Fig 4.14. When applied as solution, pure AmB did not permeate through uninfected or infected skin throughout the 24 h permeation experiment. This was in contrast to the nanoparticle formulations, for which AmB could be detected in the receptor fluid. At the end of the 24 h experiment, both types of AmB loaded chitosan nanoparticles showed approximately a two-fold higher permeation of AmB through infected skin than uninfected skin ($p < 0.05$ by t-test). AmB from AmB loaded chitosan-TPP nanoparticles permeated with almost two times more than from AmB loaded chitosan-dextran sulphate nanoparticles through both uninfected and infected skin ($p < 0.05$ by t-test).

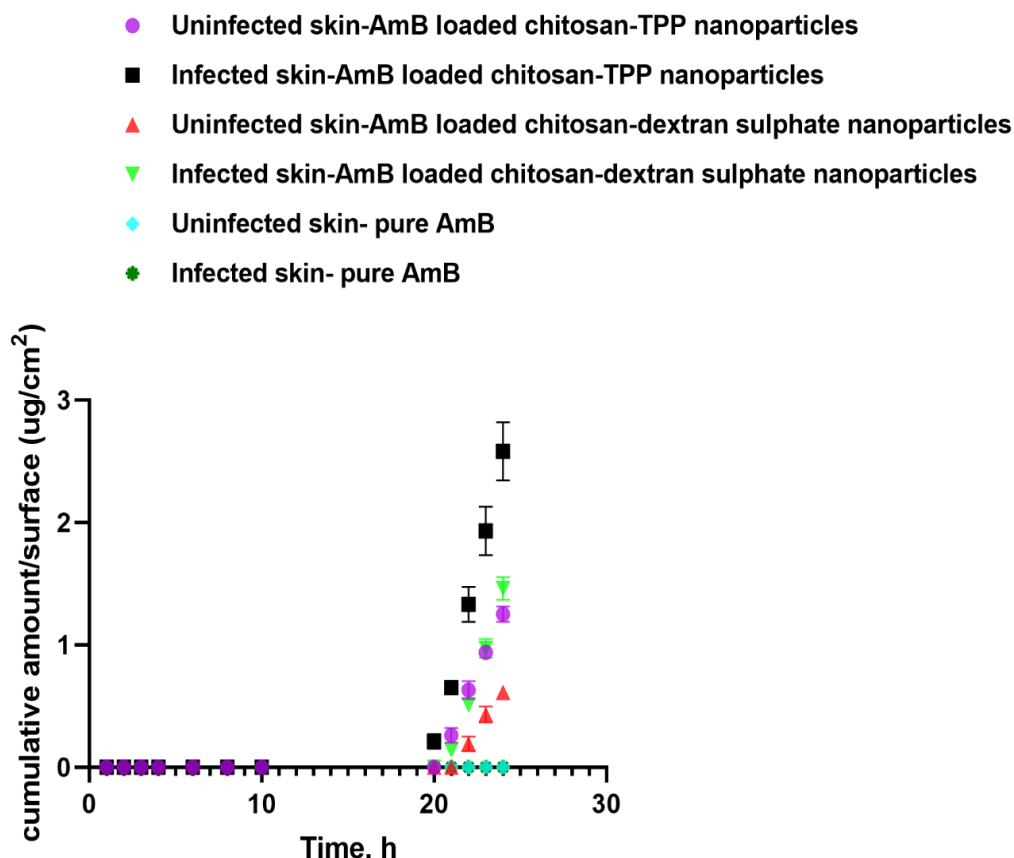


Figure 4.14. The cumulative amount of AmB permeated per surface area ($\mu\text{g}/\text{cm}^2$) through uninfected BALB/c mouse skin ($n=5$) and *L. major* infected BALB/c mouse skin ($n=5$). Infected skin was more permeable to both types of AmB loaded chitosan nanoparticles than uninfected skin ($p<0.05$ by t-test). The use of AmB loaded chitosan-TPP nanoparticles enhanced AmB penetration through both healthy and infected skin in more amount than AmB loaded chitosan-dextran sulphate nanoparticles ($p<0.05$ by t-test).

Lag time, flux and permeability coefficients of the formulations are shown in Table 4. 9. There was no significant difference in the lag time for both types of AmB nanoparticles between uninfected and infected skin ($p>0.05$ by t-test) and no significant difference was observed between AmB loaded chitosan-TPP nanoparticles and AmB loaded chitosan-dextran sulphate nanoparticles ($p>0.05$ by t-test). The flux was 2 times higher for both types of AmB loaded chitosan nanoparticles in infected skin compared to uninfected skin. The permeability coefficient was 1.75 and 2.5 times higher for AmB loaded chitosan-TPP nanoparticles and AmB loaded chitosan-dextran sulphate nanoparticles respectively in infected skin compared with uninfected skin. All the above indicated that *L. major* infection of the skin enhanced the permeation of both types of nanoparticles and the permeation of AmB nanoparticles is slow and poor.

Table 4.9. Flux, lag time and the permeability coefficient (kp) for AmB loaded chitosan nanoparticles

Compounds	Flux ($\mu\text{g}/\text{cm}^2/\text{h}$)		Lag time (h)		Kp (cm/h)	
	Uninfected skin	Infected skin	Uninfected skin	Infected skin	Uninfected skin	Infected skin
AmB loaded chitosan-TPP nanoparticles	0.06 ± 0.002	0.12 ± 0.005	20 ± 0.1	19.8 ± 0.3	$1.8\text{E-}05 \pm 0.05\text{E-}05$	$3.15\text{E-}05 \pm 0.15\text{E-}05$
AmB loaded chitosan-dextran sulphate nanoparticles	0.04 ± 0.002	0.09 ± 0.002	20.5 ± 0.1	20.3 ± 0.02	$0.9\text{E-}05 \pm 0.05\text{E-}05$	$2.3\text{E-}05 \pm 0.06\text{E-}05$
Pure AmB	0				0	

Data expressed as mean \pm SD, n=5. No statistically significant difference of lag time was observed between uninfected and infected skin for both formulations ($p>0.05$ by t-test). Statistically significant differences of flux and kp were observed between uninfected and infected skin for both formulations ($p<0.05$ by t-test).

Table 4.10 shows the distribution of topical AmB from AmB loaded chitosan nanoparticles and pure AmB into healthy and *L. major* infected skin. After the 24 h permeation experiment, more than 90% of pure AmB stayed on the skin without any drug in the receptor fluid. Regarding both types of AmB loaded chitosan nanoparticles only a limited amount of AmB passed through the skin with 0.23% and 0.42% of AmB from applied AmB loaded chitosan-TPP nanoparticles through uninfected and infected skin respectively and 0.12% and 0.28% of AmB from applied AmB loaded chitosan-dextran sulphate nanoparticles through uninfected and infected skin respectively.

Table 4.10. Disposition of topically applied AmB loaded chitosan nanoparticles on healthy and *L. major* infected BALB/ c mice skin using Franz diffusion cells

Applied compounds		Average % recovered of AmB (\pm SD)		P value
		Uninfected skin	<i>L. major</i> infected skin	
Pure AmB	on skin (in wash and cotton swab)	94.65 \pm 2	92.32 \pm 1	>0.05
	in skin (extracted from skin homogenate)	5.35 \pm 0.2	7.68 \pm 0.2	>0.05
	through skin after 24h (in receptor fluid)	0	0	>0.05
AmB loaded chitosan-TPP nanoparticles	on skin (in wash and cotton swab)	69.92 \pm 1	61.49 \pm 1	<0.05
	in skin (extracted from skin homogenate)	29.85 \pm 1	38.09 \pm 0.5	<0.05
	through skin after 24h (in receptor fluid)	0.23 \pm 0.02	0.42 \pm 0.05	<0.05
AmB loaded chitosan-dextran sulphate nanoparticles	on skin (in wash and cotton swab)	81.65 \pm 2	73.14 \pm 2	<0.05
	in skin (extracted from skin homogenate)	18.23 \pm 1	26.58 \pm 1	<0.05
	through skin after 24h (in receptor fluid)	0.12 \pm 0.02	0.28 \pm 0.02	<0.05

The total amount of AmB per Franz diffusion cell recovered at the end of the experiment was considered 100%. The amounts of AmB recovered from the different sites were expressed as a fraction of this amount. The average (\pm SD) percent for 5 infected mice is shown. p values were determined by a t test.

Fluorescence microscopy of skin sections showed no evidence for the penetration of rhodamine labelled chitosan-TPP nanoparticles (size= 72 \pm 7 nm, Zeta potential= 22 \pm 2) or rhodamine labelled chitosan-dextran sulphate nanoparticles (size= 174 \pm 7 nm, Zeta potential= -14 \pm 2) or rhodamine labelled chitosan solution in excised uninfected and *L. major* infected mouse skin. The

microscope study Indicates that the nanoparticles act as drug delivery vehicle and release the AmB rather than permeating alongside the AmB molecules (Fig 4.15).

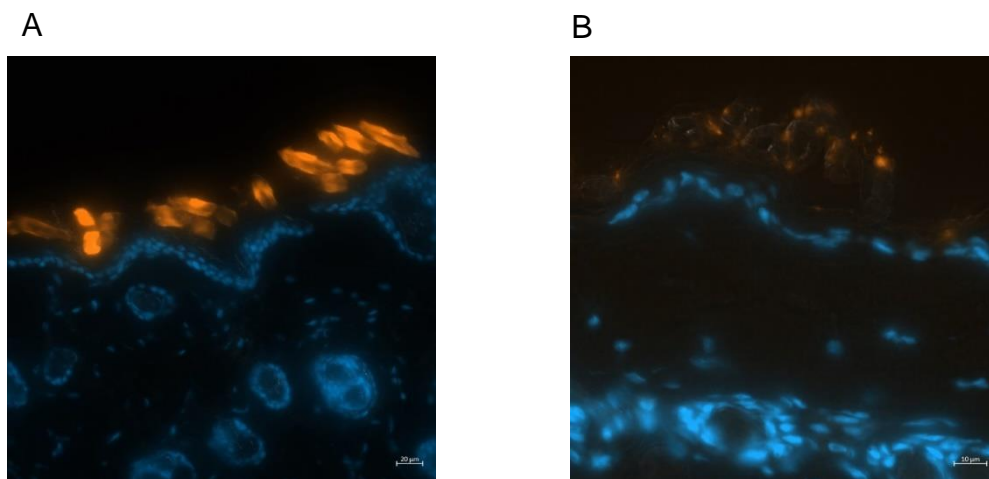


Figure 4.15. Fluorescence images of skin penetration (uninfected and *L. major* infected skin) of blank rhodamine labelled chitosan nanoparticles (A) and rhodamine labelled chitosan solution (B). We found the same scene for both types of nanoparticles and in both uninfected and infected skin. The red signals (refer to rhodamine labelled chitosan) indicated that the three formulations remained on the surface of skin.

4.4. Discussion

***In vitro* haemolytic activity and cytotoxicity of chitosan formulations**

Haemolytic activity of chitosan formulations was determined by using freshly obtained human RBCs (295). Pure AmB showed a serious and significant toxic effect to RBCs after 1h of incubation. Loading the drug into both types of chitosan nanoparticles mitigated these effects, presumably by entrapping and retaining the AmB, allowing for slow release of drug. Similar findings have been reported for blank and AmB loaded chitosan- chondroitin sulphate nanoparticles (122). To evaluate the cytotoxicity of chitosan formulations in more details we found that both types of AmB loaded chitosan nanoparticles were around 6-fold less toxic than pure AmB against KB-cells and there was no significant difference in the cytotoxicity between these AmB loaded chitosan nanoparticles and AmBisome® for same reasons mentioned previously in terms of drug entrapment and slow release. Chitosan solution and blank chitosan nanoparticles (both types) showed a similar cytotoxicity against KB-cells and were significantly less toxic than AmB loaded nanoparticles. This data supports previous reports of less cytotoxicity of AmB loaded chitosan- chondroitin sulphate nanoparticles (136±11 nm, positive charge) compared to pure AmB against murine macrophages and the low toxicity of chitosan solution and blank nanoparticles against murine macrophages (122). Similarly, Jain *et al* reported that chitosan-coated AmB-loaded solid lipid nanoparticles (158.9±7.1 nm, positive charge) showed significantly less toxic effects against macrophages (J774A.1 cells in exponential growth phase) compared to amphotericin B deoxycholate (Fungizone) (259).

***In vitro* anti-leishmanial activity of chitosan formulations**

Consistently with previous data in Chapter 2, lowering pH of RPMI medium from 7.5 to 6.5 increased by 7-20 times, the anti-leishmanial activity of chitosan solution and blank chitosan-TPP nanoparticles against *L. major* and *L. mexicana* promastigotes and amastigotes due to the greater ionisation at lower pH for both chitosan solution and blank chitosan-TPP nanoparticles (positive surface charge). As mentioned in the Chapter 2, increasing the

positive charge could enhance the chitosan antimicrobial activity by interacting with the negatively charged microbial membrane – in accordance with the first postulated mechanism of antimicrobial activity described in the introduction.

Regarding blank chitosan-TPP nanoparticles, they showed less anti-leishmanial activity than chitosan solution against *L. major* and *L. mexicana* promastigotes due to the lower positive charge of these nanoparticles as few numbers of the amino groups have been substituted by TPP groups. On the other hand, blank chitosan-TPP nanoparticles showed similar anti-leishmanial activity to chitosan solution against *L. major* and *L. mexicana* amastigotes at a lower pH due to the significant higher uptake of these nanoparticles by macrophages than chitosan solution (254).

Blank chitosan-dextran sulphate nanoparticles did not present any activity against *L. major* and *L. mexicana* promastigotes and amastigotes at both pH values- these nanoparticles have a negative surface charge as the positive amino groups on chitosan have been substituted by negatively charged sulphate groups.

However, AmB loaded chitosan nanoparticles (both types, positive or negative charged nanoparticles) showed a similar anti-leishmanial activity *L. major* and *L. mexicana* promastigotes and amastigotes at two pH values due to the high activity of AmB and this anti-leishmanial activity was similar to the activity of pure AmB and significantly higher than AmBisome®. Ribeiro *et al* (2014) reported that the anti-leishmanial activity of AmB loaded chitosan-chondroitin sulphate nanoparticles (136±11 nm, positive charge) was similar in comparison to pure AmB against *L. amazonensis* and *L. chagasi* promastigotes with similar EC₅₀ values to our study (83). Additionally, our EC₅₀ values against *L. major* and *L. mexicana* amastigotes were in accordance with another report that found the EC₅₀ values of chitosan-coated AmB-loaded solid lipid nanoparticles (158.9±7.1 nm, positive charge), AmBisome® and Fungizone were 0.022±0.07, 0.086±0.04, and 0.253±0.03 µg/ml, respectively, against *L. donovani* amastigotes infecting mouse macrophage cell line J774A.1 after 72 h of incubation (259).

Ribeiro *et al* (2014) showed that chitosan solution had EC₅₀ values of 66±1 and 71±1 µg/ml and blank chitosan nanoparticles had EC₅₀ values of 52 ±2 and 46 ±6 µg/ml against *L. amazonensis* and *L. chagasi* promastigotes, respectively and these values are different from EC₅₀ values in our study at two pH values (Table 4.8) and this could be explained as Ribeiro *et al* used different *Leishmania* species, 48h incubation of compounds with *Leishmania* and did not mention the pH of the experiment (83).

We were able to develop AmB loaded chitosan-TPP nanoparticles (69 ± 8 nm, positive surface charge) and AmB loaded chitosan-dextran sulphate nanoparticles (170 ± 9 nm, negative surface charge) which showed similar anti-leishmanial activity to pure AmB and higher activity than AmBisome® against promastigotes and amastigotes. These nanoparticles did not show significant haemolytic activity against RBCs and they were 6-fold less cytotoxic against KB-cells than pure AmB. This encouraged us to evaluate their *in vivo* anti-leishmanial activity using the mouse module.

***In vivo* anti-leishmanial activity of chitosan formulations**

We assessed the efficacy of the chitosan formulations in murine models of CL caused by *L. major*, when administrated intravenously.

We evaluated the skin distribution of AmB following intravenous dosing with AmB loaded chitosan-TPP nanoparticles (1.25, 2.5 or 5 mg of AmB/ml/QAD for 10 days; i.v.) and AmBisome® (10 mg/kg/QAD for 10 days; i.v.). AmB accumulated in significant higher levels in the localized lesion compared to those in healthy skin tissue of the same infected mice; revealing the influence of CL skin infection on the drug accumulation. This could be explained by localized inflammatory immune response caused by *L. major* parasites multiplying within dermal macrophages of CL infected skin. Therefore, at the site of infection, the leaky vasculature could enhance permeability and retention effect of the drug and this may promote the local drug accumulation (170, 298) and these small nanoparticles could facilitate extravasation through the leaky capillaries in the inflamed lesion skin while in the healthy skin, the impairment in the extravasation (continuous endothelium with small vessel

pores of 6- to 12-nm diameter) could decrease the drug accumulation (299). Another explanation is because of the immune response to the CL, phagocytic monocytes immigrate from the bloodstream to the infection site (skin lesion) and these cells can act as drug reservoirs (16, 19, 300). Similar finding was reported by Wijnant et (2018) as AmB levels were 5- to 20-fold higher in *L. major* infected BALB/c mice skin than in healthy skin from same infected mice following dosing with AmBisome® or Fungizone.

However, AmB loaded chitosan-TPP nanoparticles (5 mg/ml/QAD for 10 days; i.v.) resulted in significant higher levels of AmB accumulation in infected skin than AmBisome® (10 mg/kg/QAD for 10 days; i.v.). There was no difference in the quantity of AmB in lesion skin following dosing of AmB loaded chitosan-TPP nanoparticles (2.5 mg/ml/QAD for 10 days; i.v.) and AmBisome® (10 mg/kg/QAD for 10 days; i.v.). Similarly, Sarwar *et al* (2017) reported that the oral administration of mannose-anchored thiolated chitosan amphotericin B nanocarriers (400 nm, positive surface charge) resulted in more AmB levels in the systemic circulation and higher pharmacokinetic parameters (AUC, $t_{1/2}$ and C_{max}) in comparison with same dose of AmBisome® or pure amphotericin B (301). Moreover, the same study showed mannose-anchored thiolated chitosan amphotericin B nanocarriers (400 nm, positive surface charge) promoted the cellular uptake of AmB by 70- and 23-fold in comparison to pure AmB and AmBisome®, respectively (301). This could be explained as the chitosan nanoparticles are able to retain the AmB inside the macrophages for the longer period of time compared AmBisome® and AmB and as mentioned that these macrophages could serve as reservoirs for the drug to target the infection site (301).

Blank chitosan-dextran sulphate nanoparticles did not cause any reduction in lesion size or parasite load (bioluminescent signal) of the infected mice. However, blank chitosan-TPP nanoparticles showed a similar activity in regard of lesion size and parasite load (bioluminescent signal) to AmBisome®. Ribeiro *et al* (2014) reported that blank chitosan-chondroitin sulphate nanoparticles (104±11 nm, positive charge) caused a significant reduction in lesion size of *L. amazonensis* infected BALB/c mice, when administrated intravenously (83).

AmB loaded chitosan-TPP nanoparticles (5 mg/ml/QAD for 10 days; i.v.) showed a high effectivity against CL in the mouse module and similar to the positive control (paromomycin, 50 mg/kg/QD for 10 consecutive days; i.p.), and caused a significant reduction on lesion development and parasite load (bioluminescent signal). Additionally, AmB loaded chitosan-TPP nanoparticles (2.5 mg/ml/QAD for 10 days; i.v.) resulted in a similar reduction of lesion size and parasite load (bioluminescent signal) to AmBisome® (10 mg/kg/QAD for 10 days; i.v.). The superior efficacy of AmB loaded chitosan-TPP nanoparticles (5 mg/ml/QAD for 10 days; i.v.) compared to AmBisome® (10 mg/kg/QAD for 10 days; i.v.) could be related to higher intralesional drug concentrations (described previously) and the effectivity of chitosan nanoparticles against CL.

Ribeiro *et al* (2014) reported that AmB loaded chitosan- chondroitin sulphate nanoparticles (136±11 nm, positive charge) caused significant reductions in the lesion size and in the parasite burden of *L. amazonensis* infected BALB/c mice, when administrated intravenously (1 mg/kg/day for 10 days) and were more active than pure AmB at same doses (121).

There was a good correlation between levels of intralesional AmB accumulation and the therapeutic outcomes of AmB loaded chitosan-TPP nanoparticles as the anti-leishmanial activity of AmB has a concentration-dependent response and this due to the concentration-dependency of AmB antimicrobial activity (302) and this consistent with Wijnant *et al* (2018) for AmBisome® in CL mouse module (170).

Chitosan formulations for topical administration – skin penetration

As we mentioned that topical treatment offers several advantages over systemic treatment regarding side effects, the direct target for infected lesions, less need for patient follow up and better compliance by the patients (303, 304, 305, 306). Thus, the aim was to develop topical nanoparticles formulations (positive and negative charged nanoparticles) containing AmB. There are four fundamental factors that control the efficacy of topical treatment of CL:

- (i) The intrinsic efficacy of the compound against *Leishmania*

- (ii) The permeability of the compound through the skin to reach the dermis where the *Leishmania* infected macrophages reside (30)
- (iii) Disposition of the drug in the skin
- (iv) The release of the active compound from formulation in the PV of infected macrophages in the dermis of infected skin (306)

Both AmB chitosan-TPP nanoparticles and AmB chitosan-dextran sulphate nanoparticles showed a high activity against *Leishmania* promastigotes and amastigotes. Therefore, we investigated their *in vitro* permeation characteristics through uninfected and *L. major* infected mice skin using Franz diffusion cells.

By using Franz diffusion cells, pure AmB did not permeate through uninfected or *L. major* infected skin. This is consistent with other reports (307, 308, 309, 310) and this could be explained as AmB is a big molecule (924 g/mol) and is not soluble in water (307).

Briefly to optimise permeation, a given drug should comply with the following physicochemical properties :

- ☐ molecular weight < 500 g/mol
- ☐ log p between 1 – 3
- ☐ aqueous solubility > 1 mg/ml
- ☐ hydrogen bonding groups < 2.

Accordingly AmB is not a a good candidate for topical route, as its molecular weight is > 500 g/mol and log p of AmB is -0.66 and it is not the acceptable range for skin permeation (log P between 1-3) and has 12 H-bond donors and 18 H-bond acceptors (311, 312). This impermeability of AmB through healthy or infected skin clarified the unsuccessful treatment after the topical application of AmB on *L. major* infected mice (313). In addition, AmBisome® (liposomal AmB) was not efficient delivery topical systems for CL (314) and did not present a significant AmB skin deposition, *in vitro* study (Excised human skin from Caucasian female patients) (315).

In vitro permeation study showed a limited and slow permeation of AmB across healthy and infected mice skin when both types of AmB loaded chitosan

nanoparticles applied on the skin samples with a long lag time of about 20 h indicating a long time for the steady state flux to be reached (which indirectly means slow permeation across the stratum corneum). These data were confirmed by imaging the permeation of rhodamine labelled chitosan-TPP nanoparticles and rhodamine labelled chitosan-dextran sulphate nanoparticles across uninfected and *L. major* infected skin using laser microscope which showed that these nanoparticles stayed on the surface of skin. Our results were consistent with other reports; Vogt *et al* reported that most of applied 42–300 nm fluorescent silica nanoparticles stayed in the upper layers of the excised human skin using conventional fluorescence microscopy of skin sections(316).

Try *et al* observed a negligible penetration of poly (L-lactide-co-glycolide) nanoparticles with two sizes 70 and 300 nm in healthy male Swiss mice skin by using confocal laser scanning microscopical examination of skin biopsies while nanoparticles have been visualised in the epidermis in inflamed skin (inflammation induced by the application of oxazolone to develop atopic dermatitis like lesions) (317). Moreover, our data are in agreement with the study of Campbell *et al* who reported no penetration of fluospheres nanoparticles (carboxy-modified, fluorescent, polystyrene nanoparticles with three sizes 20, 100 and 200 nm) through pig skin and these nanoparticles remained in the top layers of the stratum corneum after 16 h of the application in Franz diffusion cells by using a laser scanning confocal microscopy (318). Similar observation regarding the limited permeation of chitosan nanoparticles was noticed by Nair *et al*, that curcumin-encapsulated chitosan nanoparticles with sizes ranged from 167.3 ± 3.8 nm to 251.5 ± 5.8 nm had a slow permeation and with low amounts using Franz diffusion cells through Strat-M® membrane (Strat-M is made of polyester sulfone arranged as multiple layers mimicking the skin structure including a tough outer layer manufactured by Merck) and the cumulative amount of curcumin permeated at 72 h was 34.3 ± 1.6 $\mu\text{g cm}^{-2}$ and 27.7 ± 1.7 $\mu\text{g cm}^{-2}$ for nanoparticles with sizes 251.5 and 167.3nm , respectively (319) . Malli *et al* (2019) reported that the topical application of chitosan-Coated Poly (isobutyl cyanoacrylate) (size=187nm , zeta potential =53.8 mv) nanoparticles (prepared by anionic emulsion

polymerization method) gelified by pluronic F127 daily for 3 consecutive weeks to BALB/c mice infected with *L. major*, resulted in partial and not complete healing of lesion and could be due to a physical effect of the F127 hydrogel (220).

AmB loaded chitosan nanoparticles offered more permeation of AmB through infected than uninfected skin when applied topically and this was consistent with another report that showed more permeation of caffeine and ibuprofen through *L. major* infected than uninfected BALB/c mouse skin, using Franz diffusion cells (166). The same study reported no permeation of paromomycin sulphate through uninfected mice skin while a high permeation through *L. major* infected skin was observed using Franz diffusion cells (166). This could be explained as CL lesions cause a damage to the skin barrier and this alteration in skin could enhance the penetration of nanoparticles (320). Moreover, *Leishmania* infected skin is characterised by the presence of abundant inflammatory cells in the infection site and this could disarrange the consistency of the epidermal and dermal skin layers and by ulceration and necrosis (307, 310, 321). Trans-epidermal water loss (TEWL) was significantly higher in *L. major* infected skin and this reduced the barrier function of the skin and subsequently increased the accumulation of fluid in the interstitial spaces cause an oedema that could enhance the permeation of water-soluble compounds (307).

AmB loaded chitosan-TPP nanoparticles (size= 68 ± 7 nm, Zeta potential= 30 ± 2) presented more permeation of AmB than AmB loaded chitosan-dextran sulphate nanoparticles (size= 168 ± 7 nm, Zeta potential= -15.5 ± 2). Similarly, Try *et al* reported a higher penetration of smaller poly(L-lactide-co-glycolide) nanoparticles (70nm) than bigger ones (300 nm) in healthy male Swiss mice skin and could be explained as smaller sized nanoparticles can penetrate for more distance compared with bigger ones (317).

Another explanation of this higher penetration as the positive surface charge of chitosan-TPP nanoparticles could interact with negative charges in the skin and confirm close contact with the skin and make an occlusive barrier that enhance the hydration and this facilitates the nanoparticles permeation through the skin (322, 323).

All of the above regarding the limited and slow permeation of AmB from AmB loaded nanoparticles made these nanoparticles unsuitable candidates for topical administration. On this basis we did not pursue *in vivo* evaluation of the antileishmanial activity of topical route of these formulations.

In conclusion, AmB loaded chitosan-TPP nanoparticles showed efficient, stability properties and target oriented drug delivery system in an experimental model cutaneous leishmaniasis when administered by the i.v. route, these nanoparticles were significantly more active than AmBisome[®] against the murine model (female BALB/c mice) of *L. major* even with lower doses of these nanoparticles. AmB loaded chitosan-TPP nanoparticles can specifically target the CL lesions more than AmBisome as they resulted in a higher concentration of AmB in the lesion sites in comparison to AmBisome[®]. However, Franz diffusion cell studies showed poor drug permeation into and through the skin of both types of AmB loaded chitosan nanoparticles suggesting that these formulations are not an appropriate candidate for topical treatment for CL. Our results indicate the need for more extensive studies using the intravenous route using different *Leishmania* species, different mammalian models and further extensive toxicity studies. Finally, skin samples from the *in vivo* study are stored for qPCR determination of parasite load and this work fell beyond the time line of this project.

5. Comparison of *in vitro* static and dynamic culture systems to evaluate the macrophages functions and the anti-leishmanial efficacy of chitosan formulations **

** research in this chapter was performed in collaboration with Alec O'Keeffe, who showed in a published paper (I am one of the co-authors) that the infection of macrophages by *L. major* was significantly reduced under slow medium flow and faster medium flow (to match the interstitial fluid flow rate in human skin) compared to macrophages under static conditions. The replication of *Leishmania* amastigotes and two functions of macrophages (phagocytosis and macropinocytosis) were also reduced under two media perfusion conditions, see publication, Appendix 2 (Paper 1).

Alec O'Keeffe completed his PhD on the development of novel predictive 2D and 3D *in vitro* models for ant-leishmanial drug testing, studying the activity and accumulation of anti-leishmanial drugs under these different flow conditions. Some of his results are included in the discussion for reference.

5.1. Media perfusion system: an introduction

The important effects of fluid flow (blood flow, interstitial flow, etc) on cell signalling and morphogenesis have been widely recognized. Cells in the mammalian body are residing in highly complex microenvironments and encounter many signals that vary in time and space. Tissues are in direct contact with moving body fluids, which encompass the haemolymphatic system, the digestive system and cerebrospinal fluid. These fluids play a significant role in the body cells such as the provision and delivery of nutrients, oxygen, cell signalling components and the removal of waste. The flow of blood and other bodily fluids within the body exerts mechanical stress on cells (324). Different rates of body fluid flow have been recorded, from fast plasma flow of 9.8 ml/min in the portal vein of the rat (325) to slow rates of 0.19 μ l/min of interstitial fluid drainage from rat brains (326). 20% of the human body's mass is estimated to be made up of interstitial fluid which is in all tissues, including skin; derived from the normal leakage of plasma from blood vessels

and has a similar structure to that of blood plasma (327). *Leishmania* amastigotes reside and survive in the phagolysosome of mammalian macrophages and in CL, these infected macrophages are exposed to interstitial fluid in the skin. The flow of interstitial fluid in uninfected human skin has been recorded to be in the order of 0.1–2 $\mu\text{m/s}$ but this flow in CL infected skin has not been determined (327, 328, 329).

Most *in vitro* studies, in the *Leishmania* field (on drug discovery, host cell transport and immunology), have been conducted on macrophages in static culture, typically using 4-, 12-, 16-, 24-, 48-, and 96-well plates with a culture medium overlay. This static system does not provide the mechanical stress, and O_2 tension, amongst other things, to that of cells within a mammalian body (98). Consequently, a static system has a major limitation when evaluating cellular parameters *in vitro*, such as infection rate, drug activity, and macrophage functions such as phagocytosis and pinocytosis, offering a poor mechanistic understanding and predictive value (98, 324). Increasing the complexity of a culture system could produce, potentially, a more biologically relevant system. Additionally, the issues surrounding the use of animal models in terms of welfare, time and cost constraints, and the limits of non-human models in predicting outcomes in humans, make developing a more predictive *in vitro* culture system a high priority (324).

A first step is transforming static cultures systems to flow systems where the culture medium constantly flows, to imitate the flow conditions in the mammalian body (330). Microfluidic (Fig 5.1.) and macrofluidic systems (Fig 5.2.) are the main two types of media perfusion systems to conduct *in vitro* assays.

Many “microbioreactor” systems have been described for cell culture which range from laminar flow, membrane systems to rotating vessel systems. Most of these bioreactors require the use of particular seeding methods with narrow dimensional specifications (331, 332, 333). Microfluidic systems can be adjusted to mimic physiological conditions and deliver nutrients, dissolved gases and remove waste products. The advantage of a microfluidic system is, that less reagents are used overall helping to lower experimental costs.

However, microfluidic systems do have a number of disadvantages – they are typically very small and require significant technical ability and care when setting up (98). In microfluidic systems, just a few thousand cells can be seeded on the tiny culture surface (0.5–0.8 mm²) and this low number of seeded cells cannot predict precisely the *in vivo* pathophysiology. Another drawback of these systems includes the “edge effect” in which a high proportion of cultured cells will be located on the outer circumference of the chamber. These cells will be organised differently as medium evaporates at a higher rate at the edges compared to the central area of the chamber, affecting cell seeding. An uneven cell layer can skew the results (334). Another disadvantage, when using micro systems, is that small hydrophobic molecules can be adsorbed by the material that either the chamber system or the connecting tubes are composed of (335, 336). A micro system will also have a high surface area to volume ratio and surface adsorption which will cause an increase in metabolic consumption rates and depletion of nutrition for the cells (335, 336, 337). Air bubble formation can pose problems within these systems, disrupting flow and affecting shear stress (338).

Macrofluidic systems (for example, Quasi Vivo, Kirkstall Ltd, Fig 5.2) offer many advantages over microfluidic systems - a higher volume of liquid is used which eases the preparation of low concentration compounds without wasting compounds through dilution. These systems can keep the shear stress consistently similar to the shear stress in most physiological environments (324). Moreover, macrofluidic systems can run for a longer time than micro system cultures and have a lower surface area to volume ratio, overcoming the major disadvantage of high metabolic consumption seen in micro systems (324).

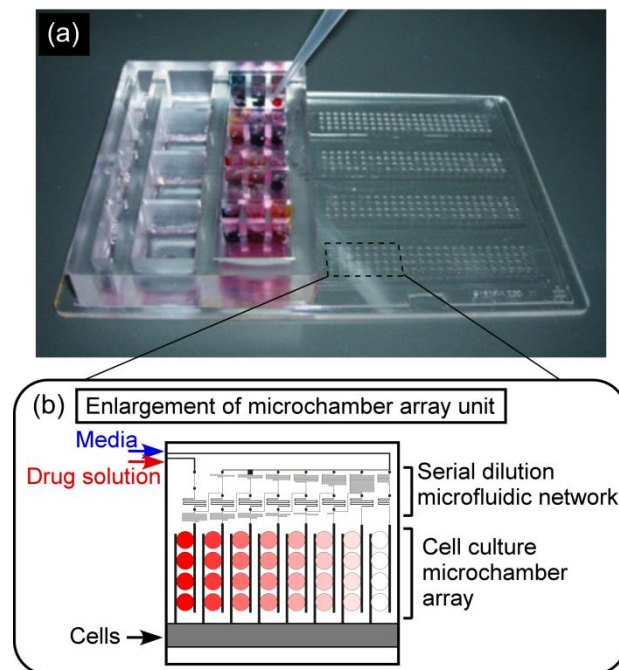


Figure 5.1. Microfluidic system (A) The integrated perfusion culture micro-chamber array chip. (B) Enlarged view of a micro-chamber array unit (339).

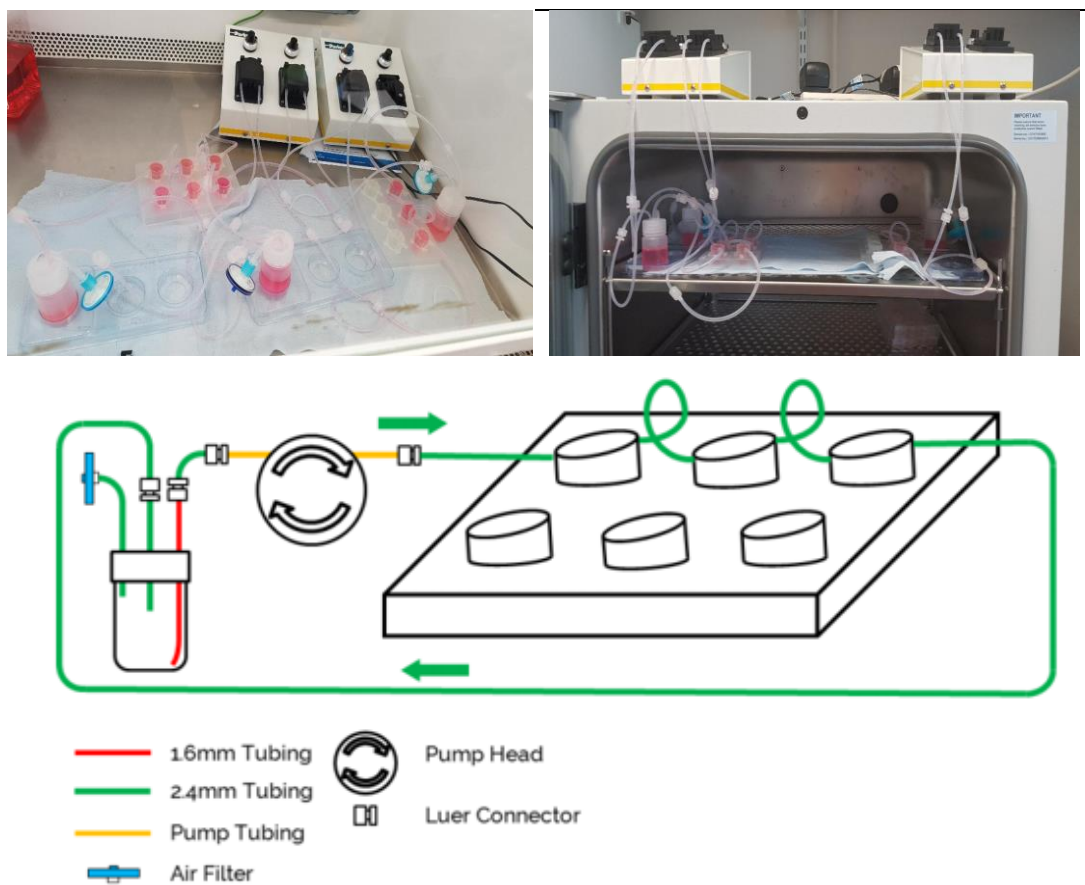


Figure 5.2. Kirkstall LTD. Quasi Vivo 900 media perfusion system in use circulating RPMI 1640 media(340).

Our study used QV900, as described by O'Keeffe A *et al* (2018) with two flow rates, in which one rate mimics the interstitial tissue flow rate in the skin. Modelling of the flow rate at the cell surface and O₂ tension was made by a collaboration between The London School of Hygiene & Tropical Medicine (Alec O'Keeffe and Simon L Croft) and University of Glasgow (Lauren Hyndman and Sean McGinty) (100).

Here, this Chapter describes the impact of flow on host cell phagocytosis and macropinocytosis and how increasing the complexity of *in vitro* model influences the anti-leishmanial activity of chitosan formulations (chitosan solution, blank chitosan-TPP -nanoparticles and AmB loaded chitosan-TPP nanoparticles) against intracellular *L. major* amastigotes, these formulations showed a high *in vitro* activity against *L. major* amastigotes using static culture system (Chapter 4)

5.2. Material and methods

Kirkstall Ltd (Rotherham, UK), established in 2006 by Dr J Malcolm Wilkinson in 2006, has developed cell culture technology into a commercially available inter-connected cell culture system, known as Quasi Vivo®, by introducing flow into the cell cultures to increase physiological relevance and create more confidence in the data produced. The Quasi Vivo system includes QV500 (an individual chamber system) and QV900 and their specifications are summarised in Table 5.1.

Table 5.1. Specifications of QV500 and QV900 media perfusion system(340, 341, 342)

	Features	
	QV500	QV900
Chamber width	15 mm internal	15 mm internal
Chamber depth	10 mm from culture surface to top of chamber base	22 mm
Materials	Chamber: PDMS Tubing: Tygon Luers and reservoir bottle: Polypropylene	Chamber: Base: Altuglas SG7 – Acrylic Resin Lids: Melifex M8706 – Styrene TEP Tubing: Tygon/PTFE & FEP Luers and reservoir bottle: Polypropylene
Overall dimensions	23 mm height x 37 mm diameter	23 mm height x 37 mm diameter
Diameter of tubing	Inlet: 1/16" ID Outlet: 3/32" ID	Inlet: 1/16" ID Outlet: 3/32" ID
Volume of chamber	2 ml	4 ml

5.2.1. Preparation of chitosan solution and blank and AmB loaded chitosan nanoparticles

All nanoparticles in this study were prepared and characterised as described in chapter 3 in sections 3-2-1- and 3-2-2-. After freeze drying the nanoparticle

suspension, the white (blank nanoparticles) or yellow (AmB loaded nanoparticles) product was reconstituted in double distilled water (ddH₂O). The nanoparticles were then characterised by size, charge and AmB loading (see Chapter 3). A solution of HMW chitosan was prepared by dissolving 1 g in 100 ml of 1% (v/v) acetic acid solution at room temperature with continuous stirring for 24 hours until a clear solution was obtained. The pH of the solution was adjusted to ~ pH 6 by adding sodium hydroxide 2N (NaOH, Sigma, UK) solution using a pH meter (Orion Model 420A). The chitosan solutions were autoclaved (121 °C; 15 mins).

5.2.2. QV900 and media perfusion system

QV900 is a 6-chamber optical tray which can be connected together in any combination, providing a high degree of flexibility and the potential to culture cells in a defined set of conditions. QV900 is more suited to high-throughput testing than QV500. A 3D printed block (9mm) composed of Nylon 12 (Kirkstall Ltd) can be added to the chamber which will alter the depth of the chambers and can be used to adjust the level of oxygen and flow rates, the cells are subjected to. A peristaltic pump (Parker Hannifin, UK), external to the CO₂ incubator, continuously circulated culture media through the system is used. A constant flow rate of 360 µl/min of culture media was used. The cells (infected or uninfected macrophages) were cultured either at the base of a perfusion chamber or raised on 9 mm high inserts. This resulted in a cell surface flow rate of 1.33×10^{-9} at the base of the chamber or 1.17×10^{-7} (m/s) on an insert which is in line within the reported range for interstitial flow in the human skin (100).

5.2.3. Macrophages

Macrophages were plated on 12mm round glass coverslips (Bellco, US) placed in 24 well plates (Corning, UK) at a density of 4×10^5 cells per well in RPMI-1640 media (PEMs and THP-1) or DMEM (BMMs) supplemented with 10% (v/v) HiFCS.

- THP-1 cells were incubated in RPMI 1640 plus 10% (v/v) HiFCS and 20 ng/ml phorbol 12-myristate 13-acetate (PMA; Sigma, UK) at 37°C

and 5% CO₂ for 72 h to induce maturation transformation of these monocytes into adherent macrophages.

5.2.4. Infection of macrophages by *L. major* promastigotes

Macrophages 4 x 10⁵/ml in RPMI-1640 media (PEMs and THP-1) or DMEM (BMMs) medium supplemented with 10% (v/v) HiFCS were plated in 24 well plates (Corning, UK) (1 ml per well) on 12mm round glass coverslips (Bellco, US) placed in 24 well and incubated for 24 hours at 37 °C in 5 % CO₂. After 24 hours, wells were washed by fresh culture medium to remove non-adherent cells. After washing, stationary phase *L. major* (MHOM/SA/85/JISH118) promastigotes were added into the wells at a ratio of 5:1 (5 parasites: 1 host). Plates were incubated for another 24 hours at 34 °C in 5 % CO₂. Subsequently, free parasites were removed by washing with the medium. One infected coverslip slide was fixed with 100 % methanol for 5 minutes and stained with 10 % Giemsa for 5 minutes. The number of infected macrophages per 100 macrophages was microscopically counted. If the initial infection was higher than 80 %, the assay was suitable for the experiments. Subsequently, two thirds of the glass coverslips were transferred to the media perfusion system (at the base of chamber or on the 9 mm insert) and maintained under flow conditions at a flow speed of 360 µl/min for 72 hours. The remaining coverslips were used for the static control.

5.2.5. Measurement of macrophage functions.

5.2.5.1. Phagocytosis

Phagocytosis by macrophages (PEMs, BMMs and THP-1) was initially evaluated using 0.5, 1 and 2 µm diameter fluorescent red labelled latex beads (carboxylate-modified polystyrene) (Sigma-Aldrich, UK) (343, 344). 2 µm beads were eventually selected as they showed maximal signal. Macrophages were infected with *L. major* promastigotes, then transferred to the three flow conditions as described above. To each well, 2µm beads (9.12 x 10⁷ latex beads/ml) were added and the cells were incubated for 0.5, 1, 2, 4 and 24 hours at 34 °C under the three different flow conditions. The experiment was terminated by washing the cells 4 times with ice-cold PBS pH 7.4 to remove

non-internalized latex beads, followed by the addition of 1 ml of 0.5% Triton X100 in 0.2 M NaOH to lyse the cells. Phagocytosis was quantified by the analysis of the cell lysate using a fluorescence plate reader (Spectramax M3, at excitation and emission wavelengths set at 575 and 610 nm), calibrated with standard solutions containing different number of latex beads in a cell lysate mixture. Uptake was expressed as the number of latex beads associated per mg of cellular protein, the protein content of the cell lysate being measured using a Micro BCA protein kit (Thermo Fisher, UK) assay as per supplier's instructions. For control studies, 1 µg/ml cytochalasin D was used as a phagocytosis inhibitor (Sigma-Aldrich, UK) by incubation with macrophages for 2 hours prior to addition of the latex beads. Phagocytosis was completely inhibited after 0.5, 1, 2 and 4 hours of incubation with cytochalasin D and 90% after 24 hours.

5.2.5.2. Macropinocytosis

Macropinocytosis was measured using a fluorescence-labeled dextran dye (pHrodo Red dextran, average molecular weight of dextran 10,000 MW, Thermo Fisher, UK) (345). This dye has a pH-sensitive fluorescence emission that increases in intensity with increasing acidity while exhibiting a minimal fluorescence at neutral pH. Macrophages (PEMs, BMMs and THP-1) were infected with *L. major* promastigotes and then transferred to the three flow conditions as described above. Macrophages were washed 3 x by Live Cell Imaging Solution (Thermofisher, UK) and the cells were returned to RPMI 1640 + 10% hiFCS containing 40 µg/ml pHrodo Red dextran (1 ml for each well) and incubated at 34 °C / 5% CO₂ for 0.5, 1, 2, 4 and 24 hours under the three different flow conditions. At each time point, the cells were washed with Live Cell Imaging Solution and macropinocytosis was analysed by a Spectramax M3 at excitation and emission wavelengths set at 560 and 585 nm respectively. Chlorpromazine hydrochloride 10 µg/ml, a known inhibitor (Sigma-Aldrich, UK), was used as a control and was incubated with macrophages for 2 hours prior to addition of fluorescence-labeled dextran dye. Macropinocytosis was completely inhibited after 0.5, 1, 2 and 4 hours of incubation with chlorpromazine hydrochloride and by 90% after 24 hours.

5.2.6. Evaluation of the anti-leishmanial activity of chitosan solutions, blank and AmB loaded chitosan TPP nanoparticles in the media perfusion system at pH 6.5

PEMs were infected with *L. major* promastigotes, then transferred to the three flow conditions as described above. This experiment was conducted at pH 6.5. After 72 hours, the coverslips were fixed using methanol and stained with Giemsa and drug activity was evaluated by microscopically counting the number of infected and uninfected cells per 100 macrophages comparing with the control (Fig 5.3.) (324). The anti-leishmanial activity of compounds was expressed as percentage reduction in infected macrophages compared to untreated control wells.

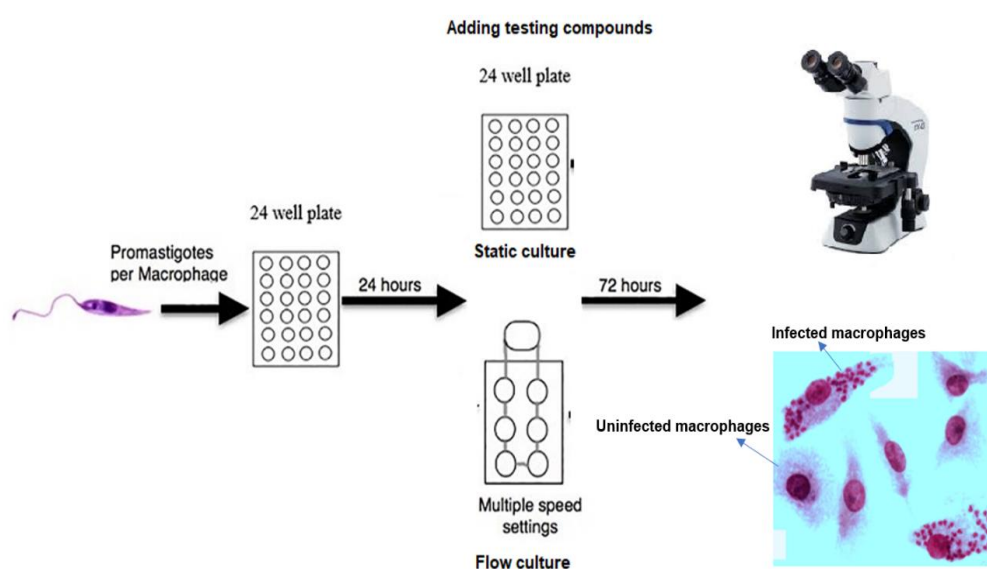


Figure 5.3. Schematic overview of evaluation of the anti-leishmanial activity in static and flow culture systems.

5.3. Results

As previously mentioned, O'Keeffe A *et al* (2018) have described the Quasi Vivo QV900 macro-perfusion system and briefly, found that a $85 \pm 3\%$ infection rate of macrophages at 72 hours in static cultures decreased to $62 \pm 5\%$ for cultures under slow medium flow and $55 \pm 3\%$ under fast medium flow and media perfusion also decreased amastigote replication and both macrophage phagocytosis (by $44 \pm 4\%$ under slow flow and $57 \pm 5\%$ under fast flow compared with the static condition) and macropinocytosis (by $40 \pm 4\%$ under slow flow and $62 \pm 5\%$ under fast flow compared with the static condition). Mathematical and computational modelling were used to estimate the effect of speed of medium flow on infection rate, shear stress and oxygen concentration. For further details see publication Annex 1.

5.3.1. Macrophage functions

5.3.1.1. Phagocytosis.

Phagocytosis of latex beads by uninfected and infected macrophages (PEMs, BMMs or THP-1) showed a clear time dependent response (Fig 5.4.), with phagocytosis increasing with duration of incubation. Phagocytosis was significantly higher in infected cells (infection rate of $> 80\%$) compared to uninfected ones after 24 hours under static conditions ($p < 0.05$ by t-test) (Table 5.2 and Fig 5.4). PEMs and BMMs showed significantly higher phagocytosis of latex beads than THP-1 ($p < 0.05$ by one- way ANOVA).

Table 5.2. Phagocytosis of fluorescent latex beads (2 μ m) by uninfected and infected PEMs, BMMs and THP-1 in static culture system.

Number of latex beads \pm SD *10 ⁵ /mg protein						
Uninfected cells - static system				infected cells - static system		
Time/Hour	PEMs	BMMs	THP-1	PEMs	BMMs	THP-1
0.5	2.42 \pm 0.2	2.3 \pm 0.2	1 \pm 0.2	3.45 \pm 0.04	3 \pm 0.04	1.8 \pm 0.04
1	6.93 \pm 0.8	6.2 \pm 0.8	5.2 \pm 0.8	11.56 \pm 0.02	10.9 \pm 0.02	8 \pm 0.02
2	61.18 \pm 1.5	60 \pm 1	41 \pm 1	76.58 \pm 0.4	74 \pm 0.2	59 \pm 0.2
4	106.74 \pm 7.7	95 \pm 5	66 \pm 5	142.96 \pm 3.9	139 \pm 2	90 \pm 2
24	421.27 \pm 30	396 \pm 27	265 \pm 27	530 \pm 30	519 \pm 25	398 \pm 22

Experiments were conducted in triplicate cultures, data expressed as mean \pm SD (experiment was reproduced further two times with confirmed similar data not shown). Phagocytosis was significantly higher ($p < 0.05$ by t-test) in infected macrophages compared to uninfected ones. Phagocytosis was significantly higher ($p < 0.05$ by t-test) in infected macrophages compared to uninfected ones. Initial macrophage infection rate was $>80\%$ after 24 h.

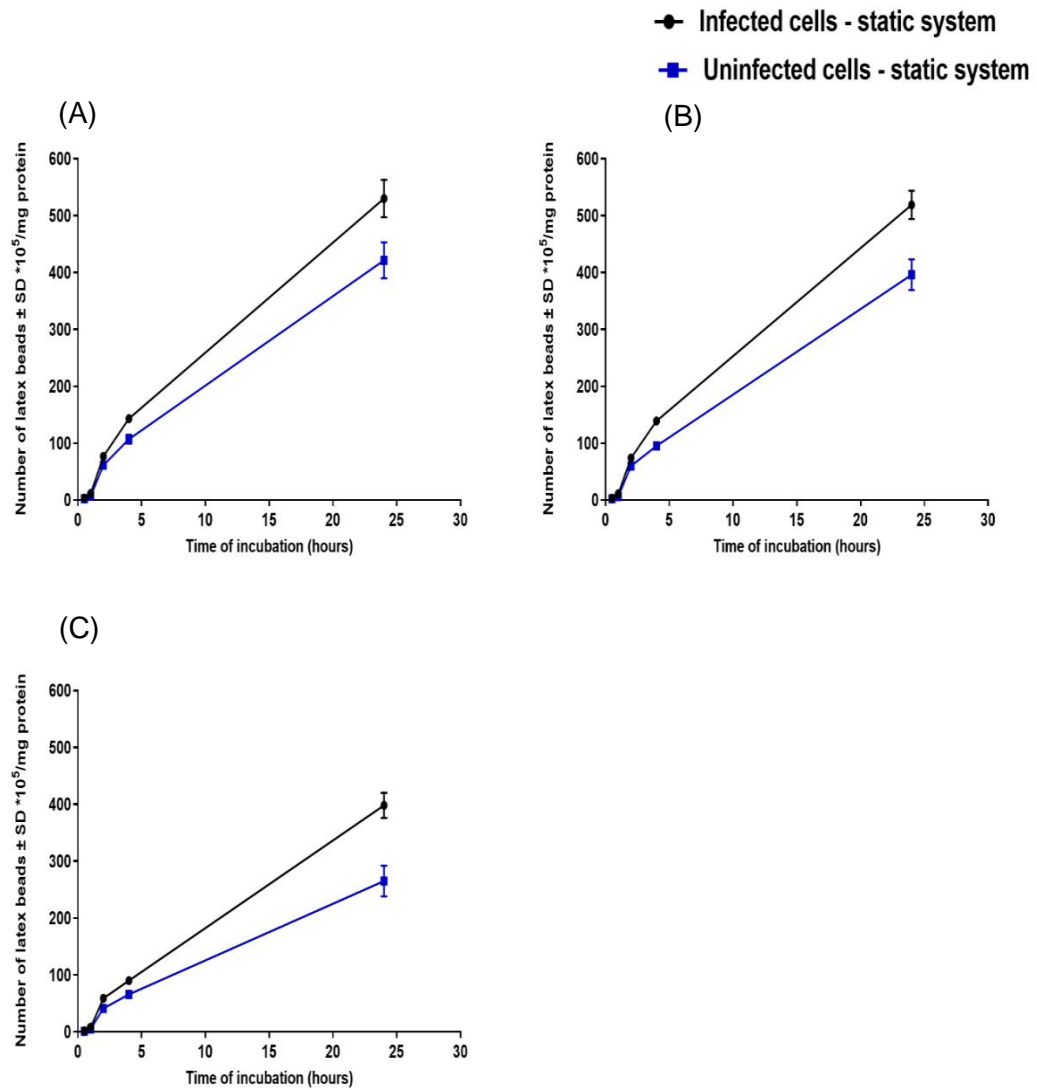


Figure 5.4. Phagocytosis of fluorescent latex beads (2 μ m) by uninfected and infected PEMs (A), BMMs (B) and THP-1 (C) in static culture system. There is a significant increase in phagocytosis by infected macrophages compared to uninfected ones ($p < 0.05$ by t-test). The data show means \pm standard deviations (SD), $N = 3$. Infection rate was $> 80\%$.

After which, the effects of media perfusion systems on phagocytosis function of *L. major*- infected macrophages were evaluated. Flow conditions caused a significant reduction in phagocytosis by infected macrophages as shown in Fig 5.5 - after 24 h of incubation, phagocytosis had significantly decreased from $530 \pm 30 \times 10^5$, $519 \pm 30 \times 10^5$ and $398 \pm 22 \times 10^5$ beads/mg protein by PEMs, BMMs and THP-1, respectively in static cultures to $304 \pm 32 \times 10^5$, $299.9 \pm 24 \times 10^5$ and $200 \pm 30 \times 10^5$ beads/mg protein by PEMs, BMMs and THP-1, respectively at slow flow speed (1.45×10^{-9} m/s) and this phagocytosis decreased more at faster flow speed (1.23×10^{-7} m/s) to $231 \pm 28 \times 10^5$, $227.6 \pm 25 \times 10^5$ and $144 \pm 18 \times 10^5$ beads/mg protein by PEMs, BMMs and THP-1, respectively ($p < 0.05$ by one-way ANOVA) (Table 5.3).

Table 5.3. Phagocytosis of fluorescent latex beads (2 μm) by infected PEMs, BMMs and THP-1 in the three culture systems (static, slow flow rate 1.45×10^{-9} m/s and fast flow rate 1.23×10^{-7} m/s).

Number of latex beads \pm SD $\times 10^5/\text{mg}$ protein									
infected cells - static system			Infected cells - 1.45×10^{-9} m/s			Infected cells - 1.23×10^{-7} m/s			
Time/Hour	PEMs	BMMs	THP-1	PEMs	BMMs	THP-1	PEMs	BMMs	THP-1
0.5	3.45 ± 0.04	3 ± 0.04	1.8 ± 0.04	1.06 ± 0.02	1 ± 0.02	1 ± 0.02	0.54 ± 0.1	0.45 ± 0.1	0.3 ± 0.1
1	11.56 ± 0.02	10.9 ± 0.02	8 ± 0.02	6.59 ± 0.1	5.9 ± 0.1	3 ± 0.1	3.92 ± 0.06	3.89 ± 0.06	1.5 ± 0.06
2	76.58 ± 0.4	74 ± 0.3	59 ± 0.2	40.24 ± 0.4	39 ± 0.25	22 ± 0.25	28.18 ± 0.2	27 ± 0.2	15 ± 0.2
4	142.96 ± 3.9	139 ± 3	90 ± 2	75.92 ± 5.5	73.9 ± 5	49 ± 1	53.55 ± 4.9	50 ± 4	33 ± 3
24	530.05 ± 32.9	519 ± 30	398 ± 22	303.88 ± 27.5	299.9 ± 24	200 ± 30	231.11 ± 30	227.6 ± 25	144 ± 18

Experiments were conducted in triplicate cultures, data expressed as mean \pm SD (experiment was reproduced further two times with confirmed similar data not shown). Flow conditions caused a significant reduction in phagocytosis by infected macrophages ($p > 0.05$ by one-way ANOVA). Initial macrophage infection rate was $>80\%$ after 24 h.

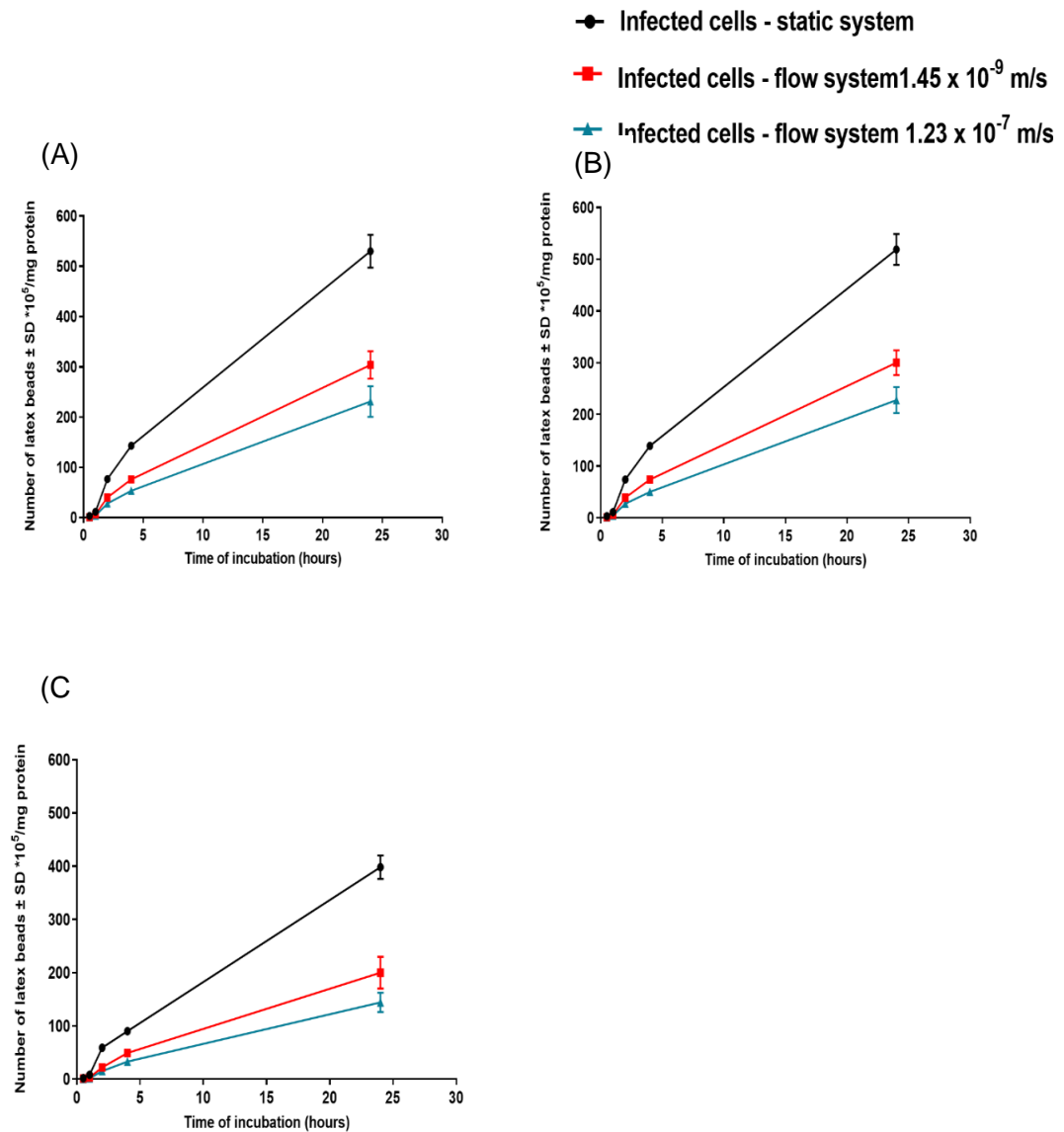


Figure 5.5. Phagocytosis of fluorescent latex beads (2 μ m) by infected PEMs (A), BMMs (B) and THP-1 (C) in the three culture systems (static, slow flow rate 1.45×10^{-9} m/s and fast flow rate 1.23×10^{-7} m/s). Phagocytosis is significantly higher in static than in flow system ($p < 0.05$ by one-way ANOVA). The data are means \pm standard deviations (SD), N = 3. Infection rate > 80%.

5.3.1.2. Macropinocytosis

Macropinocytosis of pHrodo Red dextran by uninfected and infected macrophages (PEMs, BMMs or THP-1) showed a clear time dependent response with macropinocytosis increasing with duration of incubation (Fig 5.6.). Macropinocytosis was significantly increased in infected macrophages,

from 19.02 ± 1.1 , 16.5 ± 1.1 and 8 ± 1.1 $\mu\text{g}/\text{mg}$ protein of pHrodo Red dextran by uninfected PEMs, BMMs and THP-1, respectively to 25.3 ± 0.9 , 23 ± 0.8 and 13.5 ± 0.8 $\mu\text{g}/\text{mg}$ protein of pHrodo Red dextran in infected PEMs, BMMs and THP-1, respectively after 24h in static conditions ($p < 0.05$ by t-test) (Table 5.4).

Table 5.4. Macropinocytosis of pHrodo™ Red dextran by uninfected and infected PEMs, BMMs and THP-1 in static culture system.

Concentration of dextran \pm SD $\mu\text{g}/\text{mg}$ protein						
Time/Hour	Uninfected cells - static system			infected cells - static system		
	PEMs	BMMs	THP-1	PEMs	BMMs	THP-1
0.5	0.43 ± 0.01	0.3 ± 0.01	0.15 ± 0.01	0.92 ± 0.1	0.6 ± 0.1	0.3 ± 0.1
1	1.28 ± 0.3	1.1 ± 0.3	0.55 ± 0.3	2.8 ± 0.2	2.2 ± 0.1	1.6 ± 0.1
2	2.77 ± 0.5	2.5 ± 0.5	0.99 ± 0.5	3.78 ± 0.5	3.4 ± 0.3	1.8 ± 0.3
4	4.83 ± 0.9	4.1 ± 0.9	2.5 ± 0.9	7.1 ± 0.8	5.9 ± 0.7	3.9 ± 0.7
24	19.02 ± 1.1	16.5 ± 1.1	8 ± 1.1	25.3 ± 0.9	23 ± 0.8	13.5 ± 0.8

Experiments were conducted in triplicate cultures, data expressed as mean \pm SD (experiment was reproduced further two times with confirmed similar data not shown). Macropinocytosis was significantly higher ($p < 0.05$ by t-test) in infected macrophages compared to uninfected ones. Macropinocytosis was significantly higher ($p < 0.05$ by t-test) in infected macrophages compared to uninfected ones. Initial macrophage infection rate was $>80\%$ after 24 h.

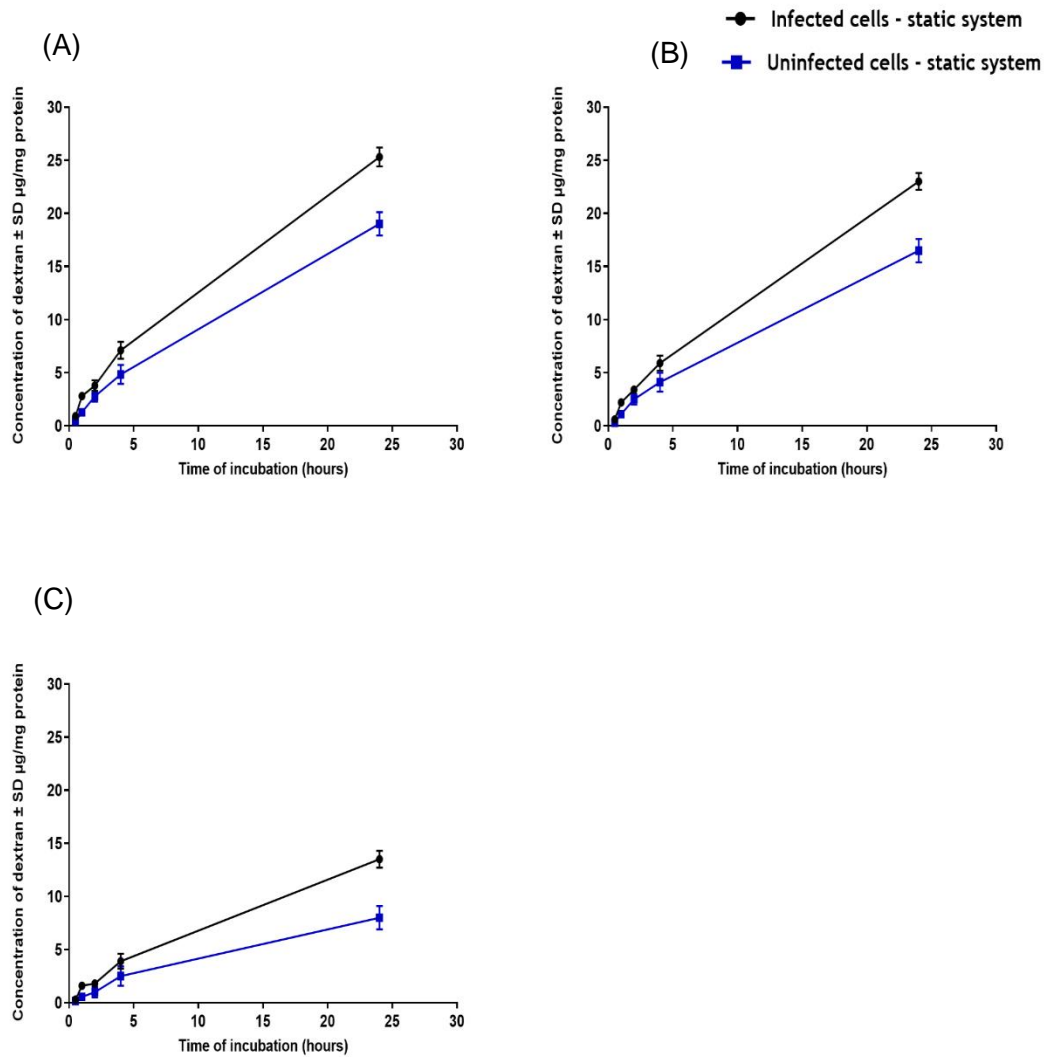


Figure 5.6. Macropinocytosis of pHrodo Red dextran by uninfected and infected PEMs (A), BMMs (B) and THP-1 (C) in static culture system. There is a significant increase in macropinocytosis by infected PEMs compared to uninfected ones ($p < 0.05$ by t- test). The data are means \pm standard deviations (SD), $N = 3$. Infection rate was $> 80\%$.

After which, the effects of media perfusion systems on macropinocytosis function of *L. major*- infected macrophages were evaluated. Macropinocytosis was significantly reduced under flow conditions (Fig 5.7.), with higher speed of culture medium flow causing the greatest reduction, as after 24 hours of incubation with pHrodo Red dextran, macropinocytosis was reduced from 25.3 ± 0.9 , 23 ± 0.8 and 13.5 ± 0.8 µg of pHrodo Red dextran /mg protein by PEMs, BMMs and THP-1, respectively under static to 15.1 ± 1 , 14.99 ± 0.3 and 9 ± 0.3 µg/mg protein by PEMs, BMMs and THP-1, respectively under low flow (1.45×10^{-9} m/s) and more reduction occurred by higher flow (1.23×10^{-7} m/s) to

9.54 \pm 1.2, 9 \pm 1 and 5.5 \pm 1 by PEMs, BMMs and THP-1 μ g/mg protein, respectively (p <0.05 by one-way ANOVA) (Table 5.5).

Table 5.5. Macropinocytosis of pHrodo™ Red dextran by infected PEMs, BMMs and THP-1 at the three culture systems (static, slow flow rate 1.45×10^{-9} m/s and fast flow rate 1.23×10^{-7} m/s).

Concentration of dextran \pm SD $\mu\text{g}/\text{mg}$ protein									
Time/Hour	infected cells - static system			Infected cells - 1.45×10^{-9} m/s			Infected cells - 1.23×10^{-7} m/s		
	PEMs	BMMs	THP-1	PEMs	BMMs	THP-1	PEMs	BMMs	THP-1
0.5	0.92 ± 0.1	0.6 ± 0.1	0.3 ± 0.1	0.29 ± 0.01	0.2 ± 0.01	0 ± 0.01	0 ± 0.0	0 ± 0.02	0 ± 0.02
1	2.8 ± 0.2	2.2 ± 0.1	1.6 ± 0.1	0.68 ± 0.5	0.55 ± 0.5	0.25 ± 0.5	0.13 ± 0.06	0.1 ± 0.05	0 ± 0.05
2	3.78 ± 0.5	3.4 ± 0.3	1.8 ± 0.3	1.75 ± 0.5	1.5 ± 0.5	0.7 ± 0.5	1.32 ± 0.2	1.1 ± 0.1	0.35 ± 0.1
4	7.1 ± 0.8	5.9 ± 0.7	3.9 ± 0.7	3.17 ± 0.9	3 ± 0.7	1.5 ± 0.7	2.29 ± 0.7	2 ± 0.55	0.9 ± 0.5
24	25.3 ± 0.9	23 ± 0.8	13.5 ± 0.8	15.1 ± 1	14.9 ± 0.3	9 ± 0.3	9.54 ± 1.2	9 ± 1	5.5 ± 1

Experiments were conducted in triplicate cultures, data expressed as mean \pm SD (experiment was reproduced further two times with confirmed similar data not shown). Flow conditions caused a significant reduction in macropinocytosis by infected macrophages ($p > 0.05$ by one-way ANOVA). Initial macrophage infection rate was $>80\%$ after 24 h.

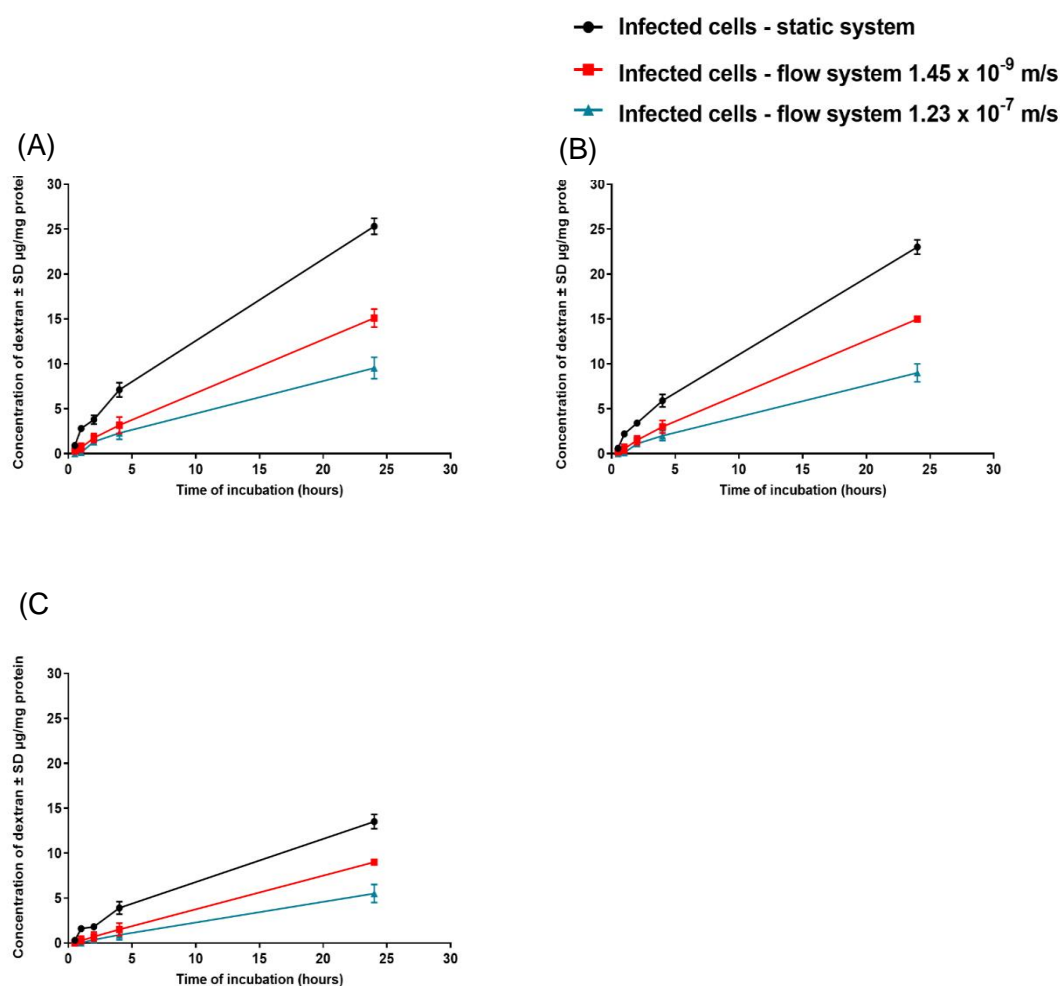


Figure 5.7. Macropinocytosis of pHrodo Red dextran by infected PEMs (A), BMMs (B) and THP-1 (C) at the three culture systems (static, slow flow rate 1.45×10^{-9} m/s and fast flow rate 1.23×10^{-7} m/s). Macropinocytosis is significantly higher in static than in flow systems ($p < 0.05$ by one-way ANOVA). The data are means \pm standard deviations (SD), $N = 3$. Infection rate was > 80 .

5.3.2. Effects of media perfusion system on the anti-leishmanial activity of chitosan formulations

Dose-dependent anti-leishmanial activity (Fig 5.8.) was observed for all formulations (chitosan solution, blank chitosan-TPP nanoparticles and AmB loaded chitosan-TPP nanoparticles) across two media velocities and static culture. In the 72 h assays, the data showed that the addition of media perfusion reduced the anti-leishmanial activity of these three chitosan formulations. Chitosan solution, blank chitosan-TPP nanoparticles and AmB loaded chitosan-TPP nanoparticles showed a significantly higher activity in static culture (flow of 0 m/s) than in the QV900 system both at the base of the chamber (flow of 1.45×10^{-9} m/s) and on an insert (flow of 1.23×10^{-7} m/s)

($p < 0.05$ by an extra sum-of-squares F test). The three formulations, chitosan solution, blank chitosan-TPP nanoparticles and AmB loaded chitosan-TPP nanoparticles, were 2.08 times, 2 times and 4 times respectively, more active against intracellular *L. major* amastigotes in static culture in comparison with the flow of 1.45×10^{-9} m/s. Similarly, increasing the velocity of culture media from flow of 1.45×10^{-9} m/s to flow of 1.23×10^{-7} m/s by using the insert reduced the activity of chitosan solution, blank chitosan-TPP nanoparticles and AmB loaded chitosan-TPP nanoparticles against *L. major* amastigotes by 2.4 times, 1.8 times and 2.75 times respectively (Table 5.6). Regarding pure AmB, we did not find a significant difference in EC_{50} values between the three culture systems ($p > 0.05$ by an extra sum-of-squares F test). In contrast, a significant difference was observed in EC_{90} values of pure AmB as increasing the media perfusion decreased the effectivity of AmB against 90% of amastigotes ($p < 0.05$ by an extra sum-of-squares F test) (Table 5.6).

Table 5.6. *In vitro* activity of chitosan solution and nanoparticles against *L. major* amastigotes in RPMI medium (pH=6.5) at different flow rates

Compound	Static- 0 m/s		Flow - 1.45×10^{-9} m/s		Flow - 1.23×10^{-7} m/s	
	EC_{50}	EC_{90}	EC_{50}	EC_{90}	EC_{50}	EC_{90}
	$\mu\text{g/ml}$					
Chitosan solution	10.9 ± 1	165 ± 5	22.7 ± 1	230 ± 15	55.3 ± 2	455 ± 9
Blank chitosan-TPP nanoparticles	14.6 ± 4	241 ± 26	29.3 ± 3	299 ± 35	53.7 ± 4	459 ± 69
AmB loaded chitosan-TPP nanoparticles	0.1 ± 0.01	1 ± 0.1	0.4 ± 0.01	2.5 ± 0.1	1.1 ± 0.02	3.5 ± 0.3
AmB solution (Pure)	0.09 ± 0.01	0.5 ± 0.02	0.1 ± 0.01	0.9 ± 0.1	0.1 ± 0.02	1.5 ± 0.1

Experiments were conducted in triplicate cultures, data expressed as mean \pm SD (experiment was reproduced further two times with confirmed similar data not shown). *Statistically significant differences were found for the EC_{50} values of chitosan solution, blank chitosan-TPP nanoparticles and AmB loaded chitosan-TPP nanoparticles at static culture (flow of 0 m/s), flow of 1.45×10^{-9} m/s and flow of 1.23×10^{-7} m/s ($p < 0.05$ by an extra sum-of-squares F test). Initial macrophage infection rate was $>80\%$ after 24 h.

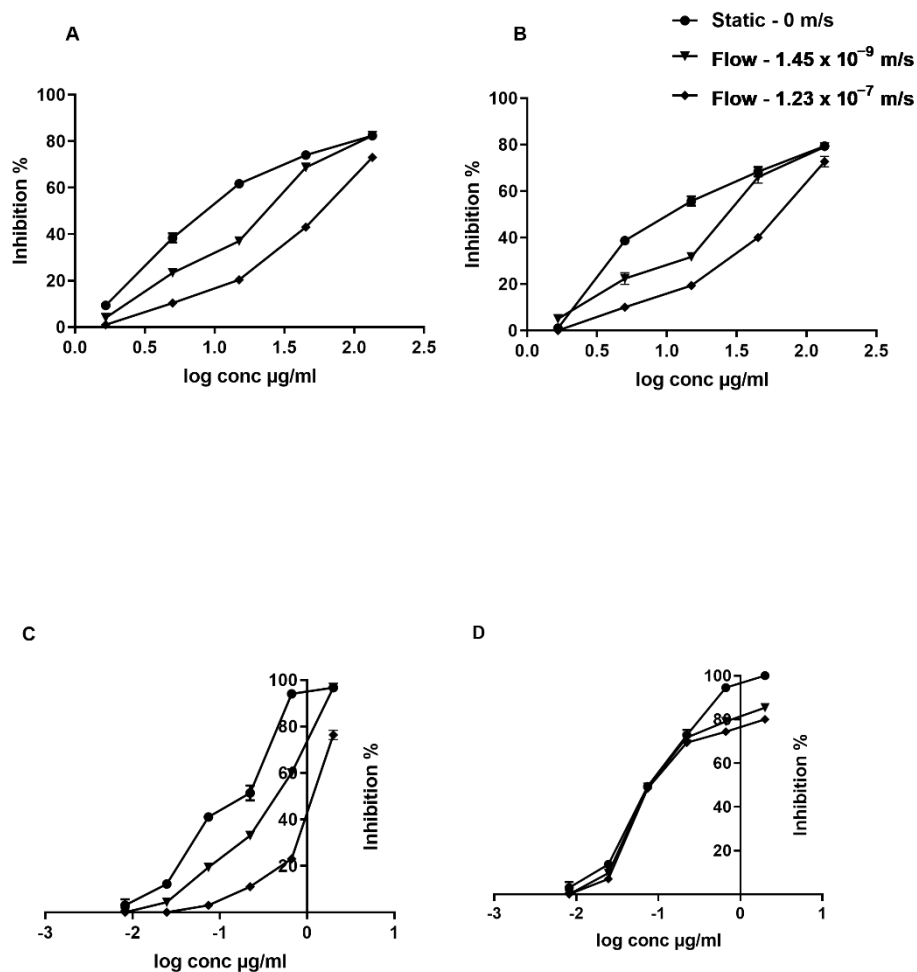


Figure 5.8. Dose-response curve of the activity of chitosan solution (A), blank chitosan-TPP nanoparticles (B), AmB loaded chitosan-TPP nanoparticles (C) and AmB solution (pure) (D) against *L. major* amastigotes infecting PEMs in pH=6.5 under different flow conditions. Quasi Vivo QV900 system has been used as a flow culture system. Values are expressed as % amastigotes inhibition relative to untreated controls. Data are representative of one experiment in triplicate cultures, data is expressed as mean \pm SD (experiment was reproduced further two times with confirmed similar data and data not shown).

5.4. Discussion

The QV900 culture flow system was used to overcome some fundamental limitations of *in vitro* static culture system when investigating cellular responses and anti-leishmanial activity of compounds and formulations. Static culture systems are unable to provide dynamic chemical or physical stimuli to cells, such as concentration gradients, flow, pressure, or mechanical stress caused by movement of fluids around them, which are physiologically relevant (100).

This study found a significant increase in cell functions (phagocytosis and macropinocytosis) in *L. major*-infected macrophages (PEMs, BMMs and THP-1) compared to uninfected cells - consistent with results described elsewhere, for example macrophages infected with either *L. donovani* or *L. mexicana* had greater pinocytic rates than uninfected macrophages, as measured by a fluorescent probe (fluorescein isothiocyanate dextran) (204). Similar observations have been reported with RAW 264.7 macrophages infected with *L. major* showing increased uptake of fluorescently labelled liposomes (204). This might be due to morphological changes of the infected cells or the parasitic infection may alter both the metabolic activity of the macrophages and their ability to ingest particulate material (346).

This study found that PEMs and BMMs showed significantly higher phagocytosis and macropinocytosis than THP-1, and this could be explained as BMMs and PEMs are more homogenous than THP-1, and they are characterised with their homogeneity and long lifespan (230).

We evaluated the effects of media perfusion rates on host cell phagocytosis and macropinocytosis. We found that phagocytosis and macropinocytosis were significantly decreased by media flow and increasing the media flow speed caused a further reduction in the uptake. This is consistent with previous reports of decreased uptake of fluorescein isothiocyanate (FITC)-poly (ethylene glycol) diacrylate particles (200 nm diameter) by human umbilical vein endothelial cells in a dynamic cell culture system exposed to shear stress

of 10 dynes/cm² compared to the uptake in static cultures (347). Similar findings were also seen with a lower cellular uptake of solid silica particles (350 nm) by RAW 264.7 macrophages under dynamic condition compared to the uptake in static cultures (348). One explanation given was that the static system conditions might cause a sedimentation of the latex beads on the cell surface or exposure to higher concentrations of pHrodo Red dextran resulting in a local increase in their concentrations (349). In contrast, medium flow prevents such localization of materials with subsequently reduced uptake (350).

We also showed that the media perfusion system had a significant influence on the anti-leishmanial activity of chitosan solution, blank chitosan-TPP nanoparticles and AmB loaded chitosan-TPP nanoparticles- increasing the flow rates caused a significant decrease in their activity. Similarly, O'Keeffe reported that the anti-leishmanial activity of miltefosine and paromomycin against *L. major* amastigotes was reduced under these two flow rates (high and slow) (324).

This decrease in the anti-leishmanial activity of chitosan formulations under flow system could be attributed to a number of factors: (i) in a static system, waste products (because of catabolic and xenobiotic metabolism) accumulate in the culture medium and can cause an oxidative stress and lead to the loss of cellular function and viability during the culture time *in vitro*. On the other hand, culture under dynamic conditions can overcome these issues by the distribution of nutrients, waste products, and tested substances within the cell culture (351, 352, 353). (ii) It has been reported that static system conditions can cause a sedimentation of the drug on the cell surface resulting in a local increase in the drug concentrations (Fig 5.9). However, a flow method for the exposure of cells to the drugs can overcome this problem and leads to homogenous dispersion of the drugs and prevention of sedimentation (351, 352, 353).

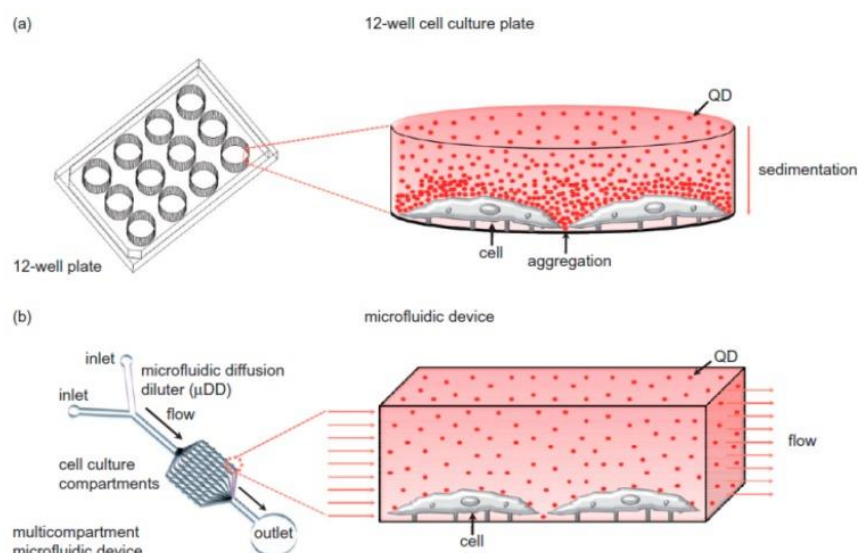


Figure 5.9. Sedimentation under a) static conditions, b) homogeneous distribution of drugs under flow conditions(353)

(iii) The effects of the two media perfusion conditions used in our study on the accumulation of anti-leishmanial drugs (amphotericin B and miltefosine) have been previously reported by O’Keeffe *et al* (2017) - the accumulation of both drugs was significantly higher in the static system compared to the media perfusion system (Fig 5.10) , after 24 hours and this could be due to a reduction in the rate of drug uptake (324).

The study described here also showed that cell uptake (phagocytosis and micropinocytosis) is reduced significantly by the application of flow compared with static culture conditions. Therefore, this reduction in drug accumulation and macrophage functions (phagocytosis and micropinocytosis) are contributing factor to the reduced anti-leishmanial activity seen (Fig 5.5, 5.7 and 5.8)

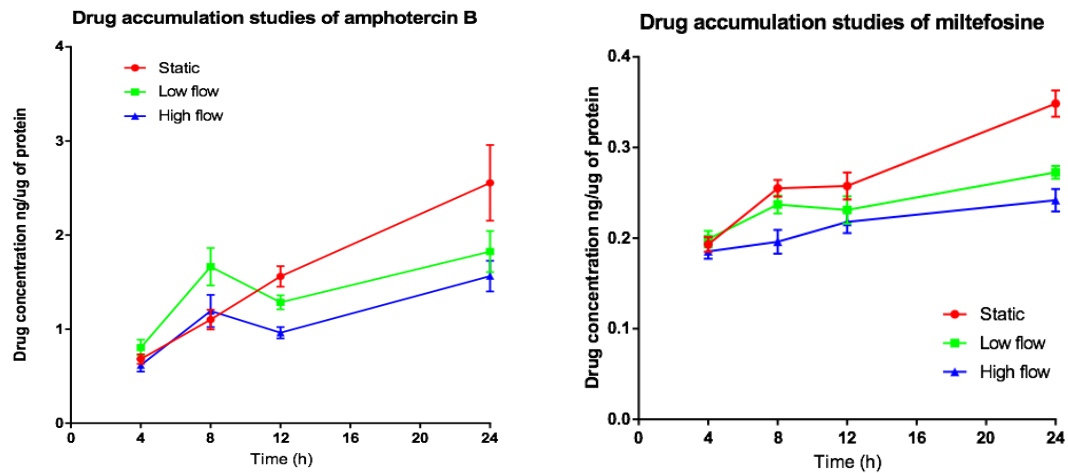


Figure 5.10. Accumulation of amphotericin B (left) and miltefosine (right) in peritoneal macrophages at three culture systems using the QV900 over time. Static and two flow rates (1.33×10^{-9} at the base of the chamber or 1.17×10^{-7} (m/s) on an insert) (324)

Broussou *et al* (2019) reported *in vitro* time-kill studies for a combination of amikacin and vancomycin against *Staphylococcus aureus* in static conditions and dynamic conditions (fluctuating antibiotic concentrations, by using A Hollow-Fibre model (Fig 5.11)) and reported a significant difference in the efficacy of the combination between static and dynamic conditions (354).

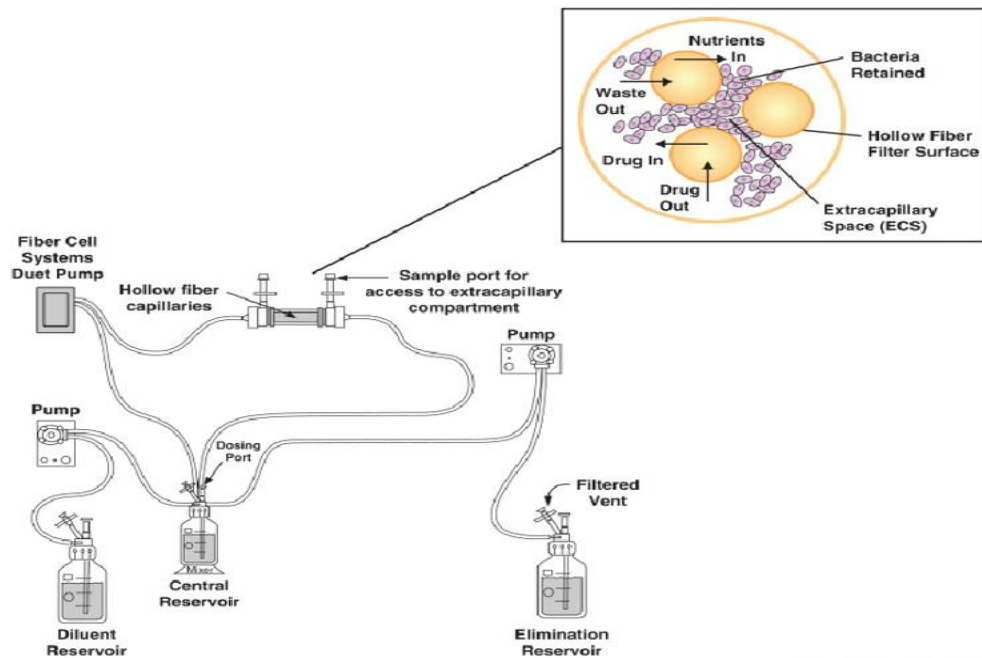


Figure 5.11. A Hollow-Fibre model (355)

Both EC_{50} and EC_{90} values of AmB loaded chitosan-TPP nanoparticles against intracellular amastigotes significantly increased as the speed of media

perfusion increases and this pattern was not obvious when comparing EC₅₀ values of pure AmB however, the EC₉₀ values diminished with increasing flow rate. Similar finding was reported by O'Keeffe *et al* (2017) in terms of EC₅₀ and EC₉₀ values of AmB solution at these three culture systems, could be due to the high activity of AmB against *Leishmania* amastigotes (324).

The difference between AmB nanoparticles and AmB solution (EC₉₀ values, at three culture systems) could be due to that nanoparticles are uptaken at higher rates compared with solution and therefore a significant less amount of AmB nanoparticles entered the macrophages under flow system compared with AmB solution (353).

In conclusion, in the media perfusion culture system, flow speed was observed to influence the anti-leishmanial activities of the tested formulations. This could influence the development of new drugs for cutaneous leishmaniasis particularly by considering the possible higher flow rates in inflammatory sites. The collateral effects of flow on pathogen replication rate and on host cell metabolism, as indicated by reduction in phagocytosis and macropinocytosis, introduces new avenues of research and how these models could be used in studies on immune response and drug and vaccine discovery. This combined experimental and modelling approach permits future hypothesis testing and development of more complex/advanced/predictive models for drug discovery and development.

6. General discussion

6.1. Discussion and conclusion

Although cutaneous leishmaniasis (CL) is not fatal, it does have a significant impact on the health and well-being impact of those infected. The large numbers involved, in at least 149 tropical and sub-tropical countries, have a detrimental impact on the economy of low- and middle-income countries where this disease is found (356, 357).

The available therapies for CL have acknowledged limitations which include adverse side effects/toxicity, are poorly tolerated, variable effectiveness against *Leishmania* species and are expensive in terms of both cost of drugs and care and other associated costs. Despite the clear need, new treatments for CL have not been forthcoming (51, 52). Drug discovery is a long and costly process which can take 10 to 20 years from a molecule to a usable drug, with an associated investment of a possible 2.6 billion USD\$ before a new active compound is identified, developed for clinical applications and brought to the market (358, 359). CL could be regarded as one of the more neglected of the NTDs, typified by a general lack of interest in pursuing and funding drug development, both by Pharma and other actors, for this disease. Some anti-leishmanial drugs developed for VL that are in the current pipeline may be considered for the treatment of CL in the future (360).

One of the strategies to address the barriers of high cost and long developmental time-lines is the employment of drug delivery systems with an already known effective drug with established clinical activity. Drug delivery systems give an opportunity to manage the solubility and other pharmacokinetic parameters of a drug, such as bioavailability, half-life and biodistribution, and can serve to protect a drug from degradation. All this can result in both reducing toxicity and enhancing efficacy.

Amphotericin B (AmB), a polyene antibiotic, is considered the second most common treatment for leishmaniasis and is very effective against different *Leishmania* species experimentally, but its clinical use is limited due to its

inherent acute toxicity. AmB is one of the most-studied drugs for the development of new drug delivery strategies in the field of leishmaniasis (118, 361).

One of these promising drug delivery systems is AmBisome® (a liposomal formulation of AmB) which is effective against VL and CL. AmBisome® is less toxic than free AmB and the clinically used amphotericin B deoxycholate formulations (Fungizone®) and is recommended by the World Health Organization for the treatment of VL (60). AmBisome® has some limitations which include (i) the high cost (200 \$ per vial of 50 mg, and is donated free for VL in endemic countries, not for CL), (ii) is the need for a cold chain (unstable over 25°C) and (iii) some renal toxicity and infusion-related reactions. In a recent study of CL and MCL in travellers coming back from both Old- and New-World countries AmBisome® treatment showed only 63% positive outcome and 53% of them experienced renal toxicity and infusion-related reactions (59) and (iv) higher rates of relapse have been observed in immunocompetent patients with VL treated with AmBisome® (60, 61).

There is an urgent need for new treatments which can eliminate the parasites, improve the healing process, are safe, reliable and also field-adaptable for use in diverse healthcare systems.

Chitosan has shown promising features in effective therapeutic delivery systems due to its cationic structure, biocompatibility, biodegradability, controlled drug release, mucoadhesive, wound healing and antimicrobial properties. Both chitosan in solution and nanoparticles showed interesting antimicrobial and antileishmanial activity with variable effective values across different published studies. These properties make chitosan an appropriate candidate for further studies to evaluate its suitability for the treatment of CL.

In Chapter 2, pH was demonstrated to play a critical role in the anti-leishmanial activity of chitosan and its derivatives (except carboxymethyl chitosan which showed no activity at both pH values), as all showed a higher anti-leishmanial effectivity at a lower pH. To date, there is no literature available on the anti-leishmanial activity of all of these derivatives or on the role of pH on the anti-leishmanial activity of chitosan. In this chapter, HMW chitosan demonstrated

a higher anti-leishmanial activity against *L. major* and *L. mexicana* promastigotes and amastigotes than other types and derivatives of chitosan. Accordingly, HMW chitosan was chosen for further studies. After which, the aim was to investigate whether the anti-leishmanial efficacy of HMW chitosan is related to indirect activity (through the activation of macrophages M1 pro-inflammatory phenotype) or via a direct way (through direct uptake of chitosan into the parasitophorous vacuole (PV) where the *Leishmania* amastigotes reside). Interestingly, it was shown that HMW chitosan acted by direct effect on the intracellular amastigotes; this has not been reported previously in any other literatures.

The results pointed towards the possibility of using HMW chitosan as a drug delivery component for CL treatment, harnessing the benefits of both anti-leishmanial activity of chitosan itself and to improve the therapeutic window of AmB (enhancing AmB anti-leishmanial activity and reducing its toxicity). AmB encapsulated in different types of chitosan nanoparticles has shown a promising *in vitro* and *in vivo* anti-leishmanial activity, see Table 4.3. Most of these studies used positively charged nanoparticles with a size greater than 100 nm. Therefore, in Chapter 3, we endeavoured to prepare two types of AmB-loaded chitosan nanoparticles; a positively charged type with TPP and a negatively charged type with dextran sulphate with the smallest possible sizes. The goal was to obtain the smallest sizes in an attempt to improve the topical delivery of AmB into the dermal layer of the skin. On the other hand, smaller nanoparticles when administrated intravenously, show a higher permeation through body membranes compared to larger nanoparticles, and smaller size of nanoparticles facilitates a passive transport from blood vessels to tissues (255).

The nanoparticle preparation parameters were optimised and two types of spherical blank and AmB loaded nanoparticles using the inotropic gelation method were successfully produced. One type of chitosan nanoparticles with a positive charge by using TPP as a crosslinker and this resulted in blank chitosan-TPP nanoparticles (size= 67 ± 7 nm, zeta potential= 28.5 ± 1.9 mv) and AmB loaded chitosan-TPP nanoparticles (size= 69 ± 8 nm, zeta potential= 25.5 ± 1 mv). The other type with a negative charge by using dextran sulphate

as a crosslinker and this resulted in blank chitosan-dextran sulphate nanoparticles (size= 170 ± 9 nm, zeta potential= -12.9 ± 3 mv) and AmB loaded chitosan-dextran sulphate nanoparticles (size= 174 ± 8 nm, zeta potential= -11 ± 1 mv). Also, the importance of using cryoprotectants and the advantage of sucrose over D-mannitol in protecting the nanoparticles were identified during the freeze drying process. Then, the encapsulation efficacy and AmB loading were approximately 90% and 25%, respectively of both types of nanoparticles. In addition, these nanoparticles showed a high stability in terms of size and charge, in different conditions (different media (water, PBS, RPMI and mouse plasma) and at different temperatures (4, 34 or 37 ° C)). Both types of nanoparticles displayed a slow release of AmB in PBS or mouse plasma. All previous promising properties of our nanoparticles made them suitable candidates for further studies in terms of evaluating the anti-leishmanial efficacy of blank chitosan nanoparticles or AmB loaded chitosan nanoparticles (as delivery vehicles) and the possibility of using them in CL mouse model either topically or intravenously.

The fourth chapter investigated the anti-leishmanial activity of chitosan formulations *in vitro* and *in vivo*. Firstly, both types of blank nanoparticles showed neither a significant haemolytic activity against human RBCs nor cytotoxicity against KB-cells. With regard to AmB loaded chitosan nanoparticles, both produced around 18-fold less haemolytic activity and 6-fold less toxicity against KB cells than pure AmB. Blank, positively surfaced charged, nanoparticles showed an *in vitro* activity against *L. major* and *L. mexicana* promastigotes and amastigotes at two pH's of 7.5 and 6.5, with a higher activity at the lower pH. Encouragingly, AmB loaded chitosan-TPP nanoparticles and AmB loaded chitosan-dextran sulphate nanoparticles presented a similar anti-leishmanial activity to pure AmB against *L. major* and *L. mexicana* promastigotes and amastigotes, and a higher activity than AmBisome®. The little *in vitro* cytotoxicity and high effectivity against *in vitro* *Leishmania* parasites led to the evaluation of the anti-leishmanial activity of chitosan formulations *in vivo* *L. major* model of CL via the intravenous route of administration. A safe dosing regimen was established in BALB/c mice of AmB loaded chitosan-TPP nanoparticles and AmB loaded chitosan-dextran

sulphate nanoparticles via i.v. route - 5 mg/kg (AmB equivalent) and 10 mg/kg (AmB equivalent), respectively. Promisingly, AmB loaded chitosan-TPP nanoparticles (5 mg of AmB/kg/QAD for 10 days, i.v.) showed a higher *in vivo* anti-leishmanial effectivity than AmBisome® (10 mg of AmB/kg/QAD for 10 days, i.v) and was similar to the activity of paromomycin used as the positive control (50 mg/kg/QD for 10 consecutive days; i.p.) in terms of reducing lesion size and bioluminescence signal (parasite load). This anti-leishmanial activity of AmB loaded chitosan-TPP nanoparticles was in a dose-response manner. Levels of AmB within the infected lesion (rump skin) and control skin (uninfected skin, back skin) were assessed at the end of the experiment and a good correlation between the doses of AmB loaded chitosan-TPP nanoparticles and the intralesional AmB and the relative reduction in parasite load and lesion size was found. Additionally, AmB loaded chitosan-TPP nanoparticles resulted in higher drug accumulation in the lesions in comparison with a higher dose of AmBisome®. Parasite load was determined via *in vivo* imaging (by using bioluminescent *L. major* strain) and compared with untreated controls. Previous studies have strongly correlated parasite load determined by both quantitative PCR and bioluminescent signal (199). qPCR determination of parasite load will be determined on the harvested and stored tissues from this study – this work fell beyond the time line of this project. To conclude, AmB loaded chitosan-TPP nanoparticles were more stable than AmBisome® and had a more sustainable drug release than AmBisome (The release of AmB was 5% from AmB loaded chitosan-TPP nanoparticles and 75% from AmBisome® (362) in 24 h). Moreover, AmB loaded chitosan-TPP nanoparticles were significantly more active than AmBisome® against *L. major* in mice even though with lower doses of these nanoparticles than AmBisome®.

The possibility of using these nanoparticles as topical formulations was evaluated. The permeability of the nanoparticles (blank and AmB loaded nanoparticles) through uninfected and *L. major* infected mouse skin performing *in vitro* Franz cell diffusion studies was determined. Both types of nanoparticles acted as a drug delivery vehicle and released the AmB rather than permeating alongside the AmB molecules. For both types of

nanoparticles, AmB permeation was limited and slow, but interestingly higher in infected skin than uninfected, albeit in low concentrations (Kat ref). These outcomes in the permeation study indicate the poor suitability of these particular formulations as credible topical formulations to treat CL.

The effect of media perfusion on macrophage functions and on the anti-leishmanial activity of chitosan formulations was assessed in Chapter 5 in an attempt to simulate some of the more complex interactions between the parasite and macrophages in the mammalian host. For this purpose, a QV900 media perfusion system was used, as described by O'Keeffe *et al* (2017), with similar flow rates to mimic the interstitial tissue flow rate in the skin. Media perfusion significantly decreased both phagocytosis and macropinocytosis of different types of macrophages (PEMs, THP-1 and BMMs). This described how the additional complexity of each *in vitro* model could improve the predictivity of the assay and how drug properties based on static assays can give rise to misleading data. The aim of this perfusion model was to develop a more predictive *in vitro* model (compared to the current static 2D one), which could ultimately lead to a reduction in animal use and save both time and expenditure evaluating poor compounds. Interestingly, the anti-leishmanial activity of chitosan formulations was significantly less in the media perfusion systems compared to the static culture system.

6.2. Future work

AmB loaded chitosan-TPP nanoparticles were effective in the murine model (female BALB/c mice) of *L. major*, when administrated intravenously.

Many parts are associated with the scale-up of these nanoparticles from bench to the market. For instance, nature of material, procedure of nanoparticle development, cost, *in vivo* biodegradability of nanoparticles and acceptability of finished product both by clinicians and patients. On account of their economic feasibility, AmB loaded chitosan-TPP nanoparticles are better because they are made of chitosan and TPP whose production scale up is significantly less expensive than phospholipids in liposomal AmB.

The evaluation of anti-leishmanial activity of AmB loaded chitosan-TPP nanoparticles *in vivo* using a New World species (for example *L. mexicana*) might be of interest for future work. Assessment of the activity of these nanoparticles in other models of *Leishmania* infection, such as self-curing model would be interesting (363) . Further extensive toxicity studies in animals would also be required.

The therapeutic index of these nanoparticles could be improved by either loading two active drugs into the nanoparticles, e.g. miltefosine (or other known active anti-leishmanials) and AmB, or by using a combination of therapy, e.g. using these nanoparticles via the i.v. route and other topical treatment (including thermotherapy or cryotherapy or paromomycin ointment) or other commercially available drugs. Both of these ways could develop more effective, lower-dose, and shorter treatments. It would be interesting to evaluate the *in vitro* and *in vivo* efficacy of AmB loaded chitosan-TPP nanoparticles in the treatment of VL. Another important experiment would be evaluating the distribution of the nanoparticles among different organs and study their uptake by lymphocytes, APCs and neutrophils.

7. References

1. Reithinger R, Dujardin JC, Louzir H, Pirmez C, Alexander B, Brooker S. 2007. Cutaneous leishmaniasis. *Lancet Infect Dis* 7:581-96.
2. Steverding D. 2017. The history of leishmaniasis. *Parasit Vectors* 10:82.
3. De Luca PM, Macedo ABB. 2016. Cutaneous Leishmaniasis Vaccination: A Matter of Quality. *Frontiers in immunology* 7:151-151.
4. Burza S, Croft SL, Boelaert M. 2018. Leishmaniasis. *The Lancet* 392:951-970.
5. Salam N, Al-Shaqha WM, Azzi A. 2014. Leishmaniasis in the middle East: incidence and epidemiology. *PLoS neglected tropical diseases* 8:e3208-e3208.
6. Du R, Hotez PJ, Al-Salem WS, Acosta-Serrano A. 2016. Old World Cutaneous Leishmaniasis and Refugee Crises in the Middle East and North Africa. *PLoS neglected tropical diseases* 10:e0004545-e0004545.
7. Alvar J, Croft S, Olliaro P. 2006. Chemotherapy in the Treatment and Control of Leishmaniasis, p 223-274. *In* Molyneux DH (ed), *Advances in Parasitology*, vol 61. Academic Press.
8. Torres-Guerrero E, Quintanilla-Cedillo M, Ruiz-Esmenjaud J, Arenas R. 2017. Leishmaniasis: a review [version 1; peer review: 2 approved]. *F1000Research* 6.
9. Esch KJ, Petersen CA. 2013. Transmission and epidemiology of zoonotic protozoal diseases of companion animals. *Clin Microbiol Rev* 26:58-85.
10. Lievin-Le Moal V, Loiseau PM. 2016. Leishmania hijacking of the macrophage intracellular compartments. *Febs j* 283:598-607.
11. Regli IB, Passelli K, Hurrell BP, Tacchini-Cottier F. 2017. Survival Mechanisms Used by Some Leishmania Species to Escape Neutrophil Killing. *Front Immunol* 8:1558.
12. Bailey MS, Lockwood DN. 2007. Cutaneous leishmaniasis. *Clin Dermatol* 25:203-11.
13. CDC. Parasites - Leishmaniasis.
14. Gupta G, Oghumu S, Satoskar AR. 2013. Mechanisms of immune evasion in leishmaniasis. *Adv Appl Microbiol* 82:155-84.
15. da Silva Santos C, Brodskyn CI. 2014. The Role of CD4 and CD8 T Cells in Human Cutaneous Leishmaniasis. *Front Public Health* 2:165.
16. Scott P, Novais FO. 2016. Cutaneous leishmaniasis: immune responses in protection and pathogenesis. *Nat Rev Immunol* 16:581-92.
17. Kemp M, Hey AS, Kurtzhals JA, Christensen CB, Gaafar A, Mustafa MD, Kordofani AA, Ismail A, Kharazmi A, Theander TG. 1994. Dichotomy of the human T cell response to Leishmania antigens. I. Th1-like response to Leishmania major promastigote antigens in individuals recovered from cutaneous leishmaniasis. *Clinical and experimental immunology* 96:410-415.
18. Kemp M, Hey AS, Bendtzen K, Kharazmi A, Theander TG. 1994. Th1-Like Human T-Cell Clones Recognizing Leishmania gp63 Inhibit Leishmania major in Human Macrophages. *Scandinavian Journal of Immunology* 40:629-635.
19. Scorza BM, Carvalho EM, Wilson ME. 2017. Cutaneous Manifestations of Human and Murine Leishmaniasis. *Int J Mol Sci* 18.
20. Wanasen N, Xin L, Soong L. 2008. Pathogenic role of B cells and antibodies in murine Leishmania amazonensis infection. *Int J Parasitol* 38:417-29.
21. McGwire BS, Satoskar AR. 2014. Leishmaniasis: clinical syndromes and treatment. *Qjm* 107:7-14.
22. Aronson N, Herwaldt BL, Libman M, Pearson R, Lopez-Velez R, Weina P, Carvalho EM, Ephros M, Jeronimo S, Magill A. 2016. Diagnosis and Treatment of Leishmaniasis: Clinical Practice Guidelines by the Infectious Diseases Society of

- America (IDSA) and the American Society of Tropical Medicine and Hygiene (ASTMH). *Clinical Infectious Diseases* 63:e202-e264.
23. Aronson N, Herwaldt BL, Libman M, Pearson R, Lopez-Velez R, Weina P, Carvalho E, Ephros M, Jeronimo S, Magill A. 2017. Diagnosis and Treatment of Leishmaniasis: Clinical Practice Guidelines by the Infectious Diseases Society of America (IDSA) and the American Society of Tropical Medicine and Hygiene (ASTMH). *The American journal of tropical medicine and hygiene* 96:24-45.
 24. Markle WH, Makhoul K. 2004. Cutaneous leishmaniasis: recognition and treatment. *Am Fam Physician* 69:1455-60.
 25. Alvar J, Arana B. 2018. I. Appraisal of Leishmaniasis Chemotherapy, Current Status and Pipeline Strategies Chapter 1 Leishmaniasis, Impact and Therapeutic Needs, p 1-23, Drug Discovery for Leishmaniasis doi:10.1039/9781788010177-00001. The Royal Society of Chemistry.
 26. Haldar AK, Sen P, Roy S. 2011. Use of Antimony in the Treatment of Leishmaniasis: Current Status and Future Directions. *Molecular Biology International* 2011:23.
 27. Goodwin LG. 1995. Pentostam® (sodium stibogluconate); a 50-year personal reminiscence. *Transactions of the Royal Society of Tropical Medicine and Hygiene* 89:339-341.
 28. WHO. 2010. Control of the leishmaniasis: report of a meeting of the WHO Expert Committee on the Control of Leishmaniasis. Geneva, 22-26 March 2010. World Health Organization. .
 29. Sharquie KE, Al-Talib KK, Chu AC. 1988. Intralesional therapy of cutaneous leishmaniasis with sodium stibogluconate antimony. *Br J Dermatol* 119:53-7.
 30. Garnier T, Croft SL. 2002. Topical treatment for cutaneous leishmaniasis. *Curr Opin Investig Drugs* 3:538-44.
 31. Gonzalez U, Pinart M, Reveiz L, Alvar J. 2008. Interventions for Old World cutaneous leishmaniasis. *Cochrane Database Syst Rev* doi:10.1002/14651858.CD005067.pub3: Cd005067.
 32. Frezard F, Demicheli C, Ribeiro RR. 2009. Pentavalent antimonials: new perspectives for old drugs. *Molecules* 14:2317-36.
 33. Berman JD, Chulay JD, Hendricks LD, Oster CN. 1982. Susceptibility of clinically sensitive and resistant *Leishmania* to pentavalent antimony in vitro. *Am J Trop Med Hyg* 31:459-65.
 34. Allen S, Neal RA. 1989. The in vitro Susceptibility of Macrophages Infected with Amastigotes of *Leishmania* spp. to Pentavalent Antimonial Drugs and Other Compounds with Special Relevance to Cutaneous Isolates, p 711-720. *In* Hart DT (ed), *Leishmaniasis: The Current Status and New Strategies for Control* doi:10.1007/978-1-4613-1575-9_88. Springer US, Boston, MA.
 35. Wyllie S, Cunningham ML, Fairlamb AH. 2004. Dual action of antimonial drugs on thiol redox metabolism in the human pathogen *Leishmania donovani*. *J Biol Chem* 279:39925-32.
 36. Krauth-Siegel RL, Comini MA. 2008. Redox control in trypanosomatids, parasitic protozoa with trypanothione-based thiol metabolism. *Biochim Biophys Acta* 1780:1236-48.
 37. Sereno D, Holzmüller P, Mangot I, Cuny G, Ouaisi A, Lemesre JL. 2001. Antimonial-mediated DNA fragmentation in *Leishmania infantum* amastigotes. *Antimicrobial agents and chemotherapy* 45:2064-2069.
 38. Sudhandiran G, Shaha C. 2003. Antimonial-induced increase in intracellular Ca²⁺ through non-selective cation channels in the host and the parasite is responsible for apoptosis of intracellular *Leishmania donovani* amastigotes. *J Biol Chem* 278:25120-32.

39. Herman JD, Gallalee JV, Best JM. 1987. Sodium stibogluconate (pentostam) inhibition of glucose catabolism via the glycolytic pathway, and fatty acid β -oxidation in *leishmania mexicana* amastigotes. *Biochemical Pharmacology* 36:197-201.
40. Frézard F, Demicheli C, Ribeiro RR. 2009. Pentavalent Antimonials: New Perspectives for Old Drugs. *Molecules* 14:2317-2336.
41. Vakil NH, Fujinami N, Shah PJ. 2015. Pharmacotherapy for leishmaniasis in the United States: focus on miltefosine. *Pharmacotherapy* 35:536-45.
42. Dorlo TP, Balasegaram M, Beijnen JH, de Vries PJ. 2012. Miltefosine: a review of its pharmacology and therapeutic efficacy in the treatment of leishmaniasis. *J Antimicrob Chemother* 67:2576-97.
43. Soto J, Arana BA, Toledo J, Rizzo N, Vega JC, Diaz A, Luz M, Gutierrez P, Arboleda M, Berman JD, Junge K, Engel J, Sindermann H. 2004. Miltefosine for new world cutaneous leishmaniasis. *Clin Infect Dis* 38:1266-72.
44. Escobar P, Matu S, Marques C, Croft SL. 2002. Sensitivities of *Leishmania* species to hexadecylphosphocholine (miltefosine), ET-18-OCH₃ (edelfosine) and amphotericin B. *Acta Trop* 81:151-7.
45. Croft SL, Seifert K, Yardley V. 2006. Current scenario of drug development for leishmaniasis. *Indian J Med Res* 123:399-410.
46. Moreira RA, Mendanha SA, Fernandes KS, Matos GG, Alonso L, Dorta ML, Alonso A. 2014. Miltefosine increases lipid and protein dynamics in *Leishmania amazonensis* membranes at concentrations similar to those needed for cytotoxicity activity. *Antimicrob Agents Chemother* 58:3021-8.
47. Rakotomanga M, Blanc S, Gaudin K, Chaminade P, Loiseau PM. 2007. Miltefosine affects lipid metabolism in *Leishmania donovani* promastigotes. *Antimicrob Agents Chemother* 51:1425-30.
48. Uberall F, Oberhuber H, Maly K, Zaknun J, Demuth L, Grunicke HH. 1991. Hexadecylphosphocholine inhibits inositol phosphate formation and protein kinase C activity. *Cancer Res* 51:807-12.
49. Lucas A, Kim Y, Rivera-Pabon O, Chae S, Kim DH, Kim B. 2010. Targeting the PI3K/Akt cell survival pathway to induce cell death of HIV-1 infected macrophages with alkylphospholipid compounds. *PLoS One* 5.
50. Saint-Pierre-Chazalet M, Ben Brahim M, Le Moyec L, Bories C, Rakotomanga M, Loiseau P. 2009. Membrane sterol depletion impairs miltefosine action in wild-type and miltefosine-resistant *Leishmania donovani* promastigotes. *The Journal of antimicrobial chemotherapy* 64:993-1001.
51. Yardley V, Croft SL. 1997. Activity of liposomal amphotericin B against experimental cutaneous leishmaniasis. *Antimicrobial agents and chemotherapy* 41:752-756.
52. Mesa-Arango AC, Scorzoni L, Zaragoza O. 2012. It only takes one to do many jobs: Amphotericin B as antifungal and immunomodulatory drug. *Frontiers in microbiology* 3:286-286.
53. Dupont B. 2002. Overview of the lipid formulations of amphotericin B. *J Antimicrob Chemother* 49 Suppl 1:31-6.
54. Meyerhoff A. 1999. U.S. Food and Drug Administration approval of AmBisome (liposomal amphotericin B) for treatment of visceral leishmaniasis. *Clin Infect Dis* 28:42-8; discussion 49-51.
55. Yardley V, Croft SL. 2000. A comparison of the activities of three amphotericin B lipid formulations against experimental visceral and cutaneous leishmaniasis. *Int J Antimicrob Agents* 13:243-8.
56. Sara Gaspani BM. 2013. Access to liposomal generic formulations: beyond AmBisome and Doxil/Caelyx. *Generics and Biosimilars Initiative Journal (GaBI Journal)* 2:60-2.

57. Tiuman TS, Santos AO, Ueda-Nakamura T, Filho BP, Nakamura CV. 2011. Recent advances in leishmaniasis treatment. *Int J Infect Dis* 15:e525-32.
58. WHO. 2016. WHO and Gilead Sciences extend collaboration against visceral leishmaniasis.
59. Guery R, Henry B, Martin-Blondel G, Rouzaud C, Cordoliani F, Harms G, Gangneux JP, Foulet F, Bourrat E, Baccard M, Morizot G, Consigny PH, Berry A, Blum J, Lortholary O, Buffet P. 2017. Liposomal amphotericin B in travelers with cutaneous and muco-cutaneous leishmaniasis: Not a panacea. *PLoS Negl Trop Dis* 11:e0006094.
60. Lanza JS, Pomel S, Loiseau PM, Frezard F. 2019. Recent advances in amphotericin B delivery strategies for the treatment of leishmaniases. *Expert Opin Drug Deliv* 16:1063-1079.
61. Burza S, Mahajan R, Sinha PK, van Griensven J, Pandey K, Lima MA, Sanz MG, Sunyoto T, Kumar S, Mitra G, Kumar R, Verma N, Das P. 2014. Visceral leishmaniasis and HIV co-infection in Bihar, India: long-term effectiveness and treatment outcomes with liposomal amphotericin B (AmBisome). *PLoS Negl Trop Dis* 8:e3053.
62. Ramos H, Valdivieso E, Gamargo M, Dagger F, Cohen BE. 1996. Amphotericin B kills unicellular leishmanias by forming aqueous pores permeable to small cations and anions. *J Membr Biol* 152:65-75.
63. Saha AK, Mukherjee T, Bhaduri A. 1986. Mechanism of action of amphotericin B on *Leishmania donovani* promastigotes. *Mol Biochem Parasitol* 19:195-200.
64. Anderson TM, Clay MC, Cioffi AG, Diaz KA, Hisao GS, Tuttle MD, Nieuwkoop AJ, Comellas G, Maryum N, Wang S, Uno BE, Wildeman EL, Gonen T, Rienstra CM, Burke MD. 2014. Amphotericin forms an extramembranous and fungicidal sterol sponge. *Nat Chem Biol* 10:400-6.
65. Jahn B, Rampp A, Dick C, Jahn A, Palmer M, Bhakdi S. 1998. Accumulation of amphotericin B in human macrophages enhances activity against *Aspergillus fumigatus* conidia: quantification of conidial kill at the single-cell level. *Antimicrob Agents Chemother* 42:2569-75.
66. Lin SH, Medoff G, Kobayashi GS. 1977. Effects of amphotericin B on macrophages and their precursor cells. *Antimicrob Agents Chemother* 11:154-60.
67. Romero EL, Morilla MJ. 2008. Drug delivery systems against leishmaniasis? Still an open question. *Expert Opin Drug Deliv* 5:805-23.
68. McGwire BS. 2014. Treatment Modalities for Cutaneous and Visceral Leishmaniasis, p 77-90. *In* Satoskar A, Durvasula R (ed), *Pathogenesis of Leishmaniasis: New Developments in Research* doi:10.1007/978-1-4614-9108-8_6. Springer New York, New York, NY.
69. Sundar S, Chatterjee M. 2006. Visceral leishmaniasis - current therapeutic modalities. *Indian J Med Res* 123:345-52.
70. Kip AE, Schellens JHM, Beijnen JH, Dorlo TPC. 2018. Clinical Pharmacokinetics of Systemically Administered Antileishmanial Drugs. *Clin Pharmacokinet* 57:151-176.
71. Wijnant G J, Murdan S, Croft S L. 2018. New pharmacokinetic and PK/PD drug development methodologies for cutaneous leishmaniasis. PhD. London School of Hygiene and Tropical medicine
72. Minodier P, Parola P. 2007. Cutaneous leishmaniasis treatment. *Travel Med Infect Dis* 5:150-8.
73. CDC. 2018. Diagnosis and treatment of leishmaniasis: clinical practice guidelines by the Infectious Diseases Society of America (IDSA) and the American Society of Tropical Medicine and Hygiene (ASTMH). Centers for Disease Control and Prevention,

74. Kariyawasam R, Challa P, Lau R, Boggild AK. 2019. Susceptibility testing of *Leishmania* spp. against amphotericin B and fluconazole using the Sensititre™ YeastOne™ YO9 platform. *BMC Infectious Diseases* 19:593.
75. Charlton RL, Rossi-Bergmann B, Denny PW, Steel PG. 2018. Repurposing as a strategy for the discovery of new anti-leishmanials: the-state-of-the-art. *Parasitology* 145:219-236.
76. el-On J, Cawich F, Evans DA, Weinrauch L. 1993. Topical treatment of cutaneous leishmaniasis in Belize: in vitro and in vivo studies with *Leishmania mexicana*. *Int J Parasitol* 23:121-7.
77. el-On J, Hamburger AD. 1987. Topical treatment of New and Old World cutaneous leishmaniasis in experimental animals. *Trans R Soc Trop Med Hyg* 81:734-7.
78. Maarouf M, Lawrence F, Croft SL, Robert-Gero M. 1995. Ribosomes of *Leishmania* are a target for the aminoglycosides. *Parasitol Res* 81:421-5.
79. Maarouf M, Lawrence F, Brown S, Robert-Gero M. 1997. Biochemical alterations in paromomycin-treated *Leishmania donovani* promastigotes. *Parasitol Res* 83:198-202.
80. DNDi. Drugs for neglected diseases: a failure of the market and a public health failure? <https://www.dndi.org/2001/media-centre/scientific-articles/scientific-articles-neglected-diseases/drugs-for-neglected-diseases-a-failure-of-the-market-and-a-public-health-failure/>. Accessed 28th July 2019.
81. Asilian A, Sadeghinia A, Faghihi G, Momeni A. 2004. Comparative study of the efficacy of combined cryotherapy and intralesional meglumine antimoniate (Glucantime) vs. cryotherapy and intralesional meglumine antimoniate (Glucantime) alone for the treatment of cutaneous leishmaniasis. *Int J Dermatol* 43:281-3.
82. Salmanpour R, Razmavar MR, Abtahi N. 2006. Comparison of intralesional meglumine antimoniate, cryotherapy and their combination in the treatment of cutaneous leishmaniasis. *Int J Dermatol* 45:1115-6.
83. Ribeiro TG, Franca JR, Fuscaldi LL, Santos ML, Duarte MC, Lage PS, Martins VT, Costa LE, Fernandes SO, Cardoso VN, Castilho RO, Soto M, Tavares CA, Faraco AA, Coelho EA, Chavez-Fumagalli MA. 2014. An optimized nanoparticle delivery system based on chitosan and chondroitin sulfate molecules reduces the toxicity of amphotericin B and is effective in treating tegumentary leishmaniasis. *Int J Nanomedicine* 9:5341-53.
84. Croft SL, Olliaro P. 2011. Leishmaniasis chemotherapy--challenges and opportunities. *Clin Microbiol Infect* 17:1478-83.
85. Convit J, Ulrich M, Zerpa O, Borges R, Aranzazu N, Valera M, Villarroel H, Zapata Z, Tomedes I. 2003. Immunotherapy of American cutaneous leishmaniasis in Venezuela during the period 1990–1999. *Transactions of The Royal Society of Tropical Medicine and Hygiene* 97:469-472.
86. Tripathi P, Jaiswal AK, Dube A, Mishra PR. 2017. Hexadecylphosphocholine (Miltefosine) stabilized chitosan modified Ampholipospheres as prototype co-delivery vehicle for enhanced killing of *L. donovani*. *Int J Biol Macromol* 105:625-637.
87. Brito G, Dourado M, Polari L, Celestino D, Carvalho LP, Queiroz A, Carvalho EM, Machado PRL, Passos S. 2014. Clinical and immunological outcome in cutaneous leishmaniasis patients treated with pentoxifylline. *The American journal of tropical medicine and hygiene* 90:617-620.
88. Santos JB, de Jesus AR, Machado PR, Magalhaes A, Salgado K, Carvalho EM, Almeida RP. 2004. Antimony plus recombinant human granulocyte-macrophage colony-stimulating factor applied topically in low doses enhances healing of

- cutaneous Leishmaniasis ulcers: a randomized, double-blind, placebo-controlled study. *J Infect Dis* 190:1793-6.
89. Pedrique B, Strub-Wourgaft N, Some C, Olhagro P, Trouiller P, Ford N, Pécoul B, Bradol J-H. 2013. The drug and vaccine landscape for neglected diseases (2000–2013;11): a systematic assessment. *The Lancet Global Health* 1:e371-e379.
 90. Ashburn TT, Thor KB. 2004. Drug repositioning: identifying and developing new uses for existing drugs. *Nat Rev Drug Discov* 3:673-83.
 91. Blessy M, Patel RD, Prajapati PN, Agrawal YK. 2014. Development of forced degradation and stability indicating studies of drugs-A review. *J Pharm Anal* 4:159-165.
 92. Silva SY, Rueda LC, Lopez M, Velez ID, Rueda-Clausen CF, Smith DJ, Munoz G, Mosquera H, Silva FA, Buitrago A, Diaz H, Lopez-Jaramillo P. 2006. Double blind, randomized controlled trial, to evaluate the effectiveness of a controlled nitric oxide releasing patch versus meglumine antimoniate in the treatment of cutaneous leishmaniasis [NCT00317629]. *Trials* 7:14.
 93. Abazid N, Jones C, Davies CR. 2012. Knowledge, attitudes and practices about leishmaniasis among cutaneous leishmaniasis patients in Aleppo, Syrian Arab Republic. *East Mediterr Health J* 18:7-14.
 94. Ruoti M, Oddone R, Lampert N, Orué E, Miles MA, Alexander N, Rehman AM, Njord R, Shu S, Brice S, Sinclair B, Krentel A. 2013. Mucocutaneous leishmaniasis: knowledge, attitudes, and practices among paraguayan communities, patients, and health professionals. *Journal of tropical medicine* 2013:538629-538629.
 95. Yardley V, Koniordou M. 2018. II. Methodologies and Medicinal Chemistry Strategies to Discover and Develop New TreatmentsChapter 4 Drug Assay Methodology in Leishmaniasis: From the Microplate to Image Analysis, p 55-76, Drug Discovery for Leishmaniasis doi:10.1039/9781788010177-00055. The Royal Society of Chemistry.
 96. Martin J, Cantizani J, Peña I. 2018. Chapter 5 The Pursuit of Novel Anti-leishmanial Agents by High-throughput Screening (HTS) of Chemical Libraries, p 77-100, Drug Discovery for Leishmaniasis doi:10.1039/9781788010177-00077. The Royal Society of Chemistry.
 97. Gupta S. 2011. Visceral leishmaniasis: experimental models for drug discovery. *Indian J Med Res* 133:27-39.
 98. Mazzei D, Guzzardi MA, Giusti S, Ahluwalia A. 2010. A low shear stress modular bioreactor for connected cell culture under high flow rates. *Biotechnol Bioeng* 106:127-37.
 99. Pampaloni F, Reynaud EG, Stelzer EH. 2007. The third dimension bridges the gap between cell culture and live tissue. *Nat Rev Mol Cell Biol* 8:839-45.
 100. O'Keeffe A, Hyndman L, McGinty S, Riezk A, Murdan S, Croft SL. 2019. Development of an in vitro media perfusion model of Leishmania major macrophage infection. *PLoS One* 14:e0219985.
 101. Yardley V, Croft SL. 1999. Chapter 93 - Animal Models of Cutaneous Leishmaniasis, p 775-781. In Zak O, Sande MA (ed), *Handbook of Animal Models of Infection* doi:<https://doi.org/10.1016/B978-012775390-4/50232-3>. Academic Press, London.
 102. Mears ER, Modabber F, Don R, Johnson GE. 2015. A Review: The Current In Vivo Models for the Discovery and Utility of New Anti-leishmanial Drugs Targeting Cutaneous Leishmaniasis. *PLoS Negl Trop Dis* 9:e0003889.
 103. Nwaka S, Ramirez B, Brun R, Maes L, Douglas F, Ridley R. 2009. Advancing Drug Innovation for Neglected Diseases—Criteria for Lead Progression. *PLOS Neglected Tropical Diseases* 3:e440.

104. Nagata N, Marriott D, Harkness J, Ellis JT, Stark D. 2012. Current treatment options for *Dientamoeba fragilis* infections. *International journal for parasitology Drugs and drug resistance* 2:204-215.
105. Allen U. 2010. Antifungal agents for the treatment of systemic fungal infections in children. *Paediatrics & child health* 15:603-615.
106. Sundar S, Olliaro PL. 2007. Miltefosine in the treatment of leishmaniasis: Clinical evidence for informed clinical risk management. *Therapeutics and clinical risk management* 3:733-740.
107. Nwaka S, Ridley RG. 2003. Virtual drug discovery and development for neglected diseases through public-private partnerships. *Nat Rev Drug Discov* 2:919-28.
108. Pecoul B. 2004. New drugs for neglected diseases: from pipeline to patients. *PLoS Med* 1:e6.
109. Caridha D, Vesely B, van Bocxlaer K, Arana B, Mowbray CE, Rifati S, Uliana S, Regura R, Kreishman-Deitrick M, Sciotti R, Buffet P, Croft SL. 2019. Route map for the discovery and pre-clinical development of new drugs and treatments for cutaneous leishmaniasis. *Int J Parasitol Drugs Drug Resist* doi:10.1016/j.ijpddr.2019.06.003.
110. Klug DM, Gelb MH, Pollastri MP. 2016. Repurposing strategies for tropical disease drug discovery. *Bioorganic & Medicinal Chemistry Letters* 26:2569-2576.
111. DNDi. TOWARDS A NEW GENERATION OF TREATMENTS FOR LEISHMANIASIS. https://www.dndi.org/wp-content/uploads/2018/12/DNDi_Leishmaniasis_2018.pdf. Accessed 28th of July 2019.
112. Yasinzaï M, Khan M, Nadhman A, Shahnaz G. 2013. Drug resistance in leishmaniasis: current drug-delivery systems and future perspectives. *Future Med Chem* 5:1877-88.
113. Gutiérrez V, Seabra AB, Reguera RM, Khandare J, Calderón M. 2016. New approaches from nanomedicine for treating leishmaniasis. *Chemical Society Reviews* 45:152-168.
114. Shaw CD, Carter KC. 2014. Drug delivery: lessons to be learnt from *Leishmania* studies. *Nanomedicine (Lond)* 9:1531-44.
115. Sousa-Batista A, Rossi-Bergmann B. 2018. Nanomedicines for Cutaneous Leishmaniasis doi:10.5772/intechopen.75750.
116. New RR, Chance ML. 1980. Treatment of experimental cutaneous leishmaniasis by liposome-entrapped Pentostam. *Acta Trop* 37:253-6.
117. de Carvalho RF, Ribeiro IF, Miranda-Vilela AL, de Souza Filho J, Martins OP, Cintra e Silva Dde O, Tedesco AC, Lacava ZG, Bao SN, Sampaio RN. 2013. Leishmanicidal activity of amphotericin B encapsulated in PLGA-DMSA nanoparticles to treat cutaneous leishmaniasis in C57BL/6 mice. *Exp Parasitol* 135:217-22.
118. Mohamed-Ahmed AH, Les KA, Seifert K, Croft SL, Brocchini S. 2013. Noncovalent complexation of amphotericin-B with Poly(alpha-glutamic acid). *Mol Pharm* 10:940-50.
119. Quintanar-Guerrero D, Allemann E, Fessi H, Doelker E. 1998. Preparation techniques and mechanisms of formation of biodegradable nanoparticles from preformed polymers. *Drug Dev Ind Pharm* 24:1113-28.
120. Mohammed MA, Syeda JTM, Wasan KM, Wasan EK. 2017. An Overview of Chitosan Nanoparticles and Its Application in Non-Parenteral Drug Delivery. *Pharmaceutics* 9.
121. Ribeiro TG, Franca JR, Fuscaldi LL, Santos ML, Duarte MC, Lage PS, Martins VT, Costa LE, Fernandes SOA, Cardoso VN, Castilho RO, Soto M, Tavares CAP, Faraco AAG, Coelho EAF, Chávez-Fumagalli MA. 2014. An optimized nanoparticle delivery system based on chitosan and chondroitin sulfate molecules reduces the toxicity of

- amphotericin B and is effective in treating tegumentary leishmaniasis. *International journal of nanomedicine* 9:5341-5353.
122. Ribeiro TG, Chávez-Fumagalli MA, Valadares DG, França JR, Rodrigues LB, Duarte MC, Lage PS, Andrade PHR, Lage DP, Arruda LV, Abánades DR, Costa LE, Martins VT, Tavares CAP, Castilho RO, Coelho EAF, Faraco AAG. 2014. Novel targeting using nanoparticles: an approach to the development of an effective anti-leishmanial drug-delivery system. *International journal of nanomedicine* 9:877-890.
 123. Ali A, Ahmed S. 2018. A review on chitosan and its nanocomposites in drug delivery. *International Journal of Biological Macromolecules* 109:273-286.
 124. Goy RC, Britto Dd, Assis OBG. 2009. A review of the antimicrobial activity of chitosan. *Polímeros* 19:241-247.
 125. Sarkar K, Xue Y, Sant S. 2017. Host Response to Synthetic Versus Natural Biomaterials, p 81-105. *In* Corradetti B (ed), *The Immune Response to Implanted Materials and Devices: The Impact of the Immune System on the Success of an Implant* doi:10.1007/978-3-319-45433-7_5. Springer International Publishing, Cham.
 126. Peluso G, Petillo O, Ranieri M, Santin M, Ambrosic L, Calabró D, Avallone B, Balsamo G. 1994. Chitosan-mediated stimulation of macrophage function. *Biomaterials* 15:1215-1220.
 127. Pujals G, Sune-Negre JM, Perez P, Garcia E, Portus M, Tico JR, Minarro M, Carrio J. 2008. In vitro evaluation of the effectiveness and cytotoxicity of meglumine antimoniate microspheres produced by spray drying against *Leishmania infantum*. *Parasitol Res* 102:1243-7.
 128. Salah- Tazdaït R, Tazdaït D, Harrat Z, Eddaikra N, Abdi N, Mameri N. 2015. Antiparasite Activity of Chitosan. *Proceedings of 2015 International Conference on Chemical, Metallurgy and Environmental Engineering (CMAEE 2015)* doi:10.17758/UR.U0615223.
 129. Hoseini MH, Moradi M, Alimohammadian MH, Shahgoli VK, Darabi H, Rostami A. 2016. Immunotherapeutic effects of chitin in comparison with chitosan against *Leishmania* major infection. *Parasitol Int* 65:99-104.
 130. Zhang H, Oh M, Allen C, Kumacheva E. 2004. Monodisperse chitosan nanoparticles for mucosal drug delivery. *Biomacromolecules* 5:2461-8.
 131. Sinha VR, Singla AK, Wadhawan S, Kaushik R, Kumria R, Bansal K, Dhawan S. 2004. Chitosan microspheres as a potential carrier for drugs. *Int J Pharm* 274:1-33.
 132. Hussain Z, Katas H, Amin MC, Kumulosasi E, Sahudin S. 2013. Antidermatitic perspective of hydrocortisone as chitosan nanocarriers: an ex vivo and in vivo assessment using an NC/Nga mouse model. *J Pharm Sci* 102:1063-75.
 133. Grenha A, Seijo B, Remunan-Lopez C. 2005. Microencapsulated chitosan nanoparticles for lung protein delivery. *Eur J Pharm Sci* 25:427-37.
 134. Papadimitriou SA, Achilias DS, Bikiaris DN. 2012. Chitosan-g-PEG nanoparticles ionically crosslinked with poly(glutamic acid) and tripolyphosphate as protein delivery systems. *Int J Pharm* 430:318-27.
 135. Dash M, Chiellini F, Ottenbrite RM, Chiellini E. 2011. Chitosan—A versatile semi-synthetic polymer in biomedical applications. *Progress in Polymer Science* 36:981-1014.
 136. Zambito Y, Di Colo G. 2003. Preparation and in vitro evaluation of chitosan matrices for colonic controlled drug delivery. *J Pharm Pharm Sci* 6:274-81.
 137. Park S-H, Chun M-K, Choi H-K. 2008. Preparation of an extended-release matrix tablet using chitosan/Carbopol interpolymer complex. *International Journal of Pharmaceutics* 347:39-44.

138. reddy, Ramanji, Dhachinamoorthi D, Kothapalli Bannoth C. 2010. Independent release behavior of Glipizide matrix release tablets containing chitosan and xanthan gum. *International Journal of Pharmaceutical and Biological Research*.
139. Shah S. 2009. Formulation and in-Vitro evaluation of mesalamine matrix tablets using chitosan for colonic drug delivery. *Journal of Pharmacy Research*.
140. Tozaki H, Komoike J, Tada C, Maruyama T, Terabe A, Suzuki T, Yamamoto A, Muranishi S. 1997. Chitosan capsules for colon-specific drug delivery: improvement of insulin absorption from the rat colon. *J Pharm Sci* 86:1016-21.
141. Phromsopha T, Baimark Y. 2010. Chitosan Microparticles Prepared by the Water-in-Oil Emulsion Solvent Diffusion Method for Drug Delivery. *Biotechnology* 9.
142. Silva CM, Ribeiro AJ, Figueiredo M, Ferreira D, Veiga F. 2006. Microencapsulation of hemoglobin in chitosan-coated alginate microspheres prepared by emulsification/internal gelation. *The AAPS journal* 7:E903-E913.
143. Kumbhar SG, Kulkarni AR, Aminabhavi M. 2002. Crosslinked chitosan microspheres for encapsulation of diclofenac sodium: effect of crosslinking agent. *J Microencapsul* 19:173-80.
144. Kotadiya R, Patel V, Patel H, Koradia H. 2009. Effect of cross-linking on physicochemical properties of chitosan mucoadhesive microspheres: A factorial approach. *International Journal of Green Pharmacy* 3.
145. He P, Davis SS, Illum L. 1999. Chitosan microspheres prepared by spray drying. *International Journal of Pharmaceutics* 187:53-65.
146. Tokumitsu H, Ichikawa H, Fukumori Y. 1999. Chitosan-Gadopentetic Acid Complex Nanoparticles for Gadolinium Neutron-Capture Therapy of Cancer: Preparation by Novel Emulsion-Droplet Coalescence Technique and Characterization. *Pharmaceutical Research* 16:1830-1835.
147. Gan Q, Wang T. 2007. Chitosan nanoparticle as protein delivery carrier--systematic examination of fabrication conditions for efficient loading and release. *Colloids Surf B Biointerfaces* 59:24-34.
148. Van Der Lubben IM, Konings FA, Borchard G, Verhoef JC, Junginger HE. 2001. In vivo uptake of chitosan microparticles by murine Peyer's patches: visualization studies using confocal laser scanning microscopy and immunohistochemistry. *J Drug Target* 9:39-47.
149. van der Lubben IM, Kersten G, Fretz MM, Beuvery C, Coos Verhoef J, Junginger HE. 2003. Chitosan microparticles for mucosal vaccination against diphtheria: oral and nasal efficacy studies in mice. *Vaccine* 21:1400-8.
150. De Campos AM, Sanchez A, Alonso MJ. 2001. Chitosan nanoparticles: a new vehicle for the improvement of the delivery of drugs to the ocular surface. Application to cyclosporin A. *Int J Pharm* 224:159-68.
151. Wang K, He Z. 2002. Alginate-konjac glucomannan-chitosan beads as controlled release matrix. *International Journal of Pharmaceutics* 244:117-126.
152. Bhardwaj V, Shukla VK, Goyal N, Malviya R, Sharma PK. 2010. Formulation and Evaluation of Different Concentration Chitosan based Periodontal Film of Ofloxacin. *Journal of Pharmacy Research*.
153. Dhanikula AB, Panchagnula R. 2004. Development and characterization of biodegradable chitosan films for local delivery of Paclitaxel. *The AAPS journal* 6:e27-e27.
154. Ohya Y, Takei T, Kobayashi H, Ouchi T. 1993. Release behaviour of 5-fluorouracil from chitosan-gel microspheres immobilizing 5-fluorouracil derivative coated with polysaccharides and their cell specific recognition. *J Microencapsul* 10:1-9.
155. Palmer BC, DeLouise LA. 2016. Nanoparticle-Enabled Transdermal Drug Delivery Systems for Enhanced Dose Control and Tissue Targeting. *Molecules* 21.

156. Espuelas S, Schwartz J, Moreno E. 2016. Chapter 11 - Nanoparticles in the Topical Treatment of Cutaneous Leishmaniasis: Gaps, Facts, and Perspectives, p 135-155. *In* Hamblin MR, Avci P, Prow TW (ed), *Nanoscience in Dermatology* doi:<https://doi.org/10.1016/B978-0-12-802926-8.00011-2>. Academic Press, Boston.
157. Wijnant GJ, Van Bocxlaer K, Fortes Francisco A, Yardley V, Harris A, Alavijeh M, Murdan S, Croft SL. 2018. Local Skin Inflammation in Cutaneous Leishmaniasis as a Source of Variable Pharmacokinetics and Therapeutic Efficacy of Liposomal Amphotericin B. *Antimicrob Agents Chemother* 62.
158. Tan Q, Liu W, Guo C, Zhai G. 2011. Preparation and evaluation of quercetin-loaded lecithin-chitosan nanoparticles for topical delivery. *Int J Nanomedicine* 6:1621-30.
159. Biagini G, Bertani A, Muzzarelli R, Damadei A, DiBenedetto G, Belligolli A, Riccotti G, Zucchini C, Rizzoli C. 1991. Wound management with N-carboxybutyl chitosan. *Biomaterials* 12:281-286.
160. Stone CA, Wright H, Clarke T, Powell R, Devaraj VS. 2000. Healing at skin graft donor sites dressed with chitosan. *Br J Plast Surg* 53:601-6.
161. Azad AK, Sermsintham N, Chandkrachang S, Stevens WF. 2004. Chitosan membrane as a wound-healing dressing: characterization and clinical application. *J Biomed Mater Res B Appl Biomater* 69:216-22.
162. Valentine R, Athanasiadis T, Moratti S, Hanton L, Robinson S, Wormald PJ. 2010. The efficacy of a novel chitosan gel on hemostasis and wound healing after endoscopic sinus surgery. *Am J Rhinol Allergy* 24:70-5.
163. Kim DG, Jeong YI, Choi C, Roh SH, Kang SK, Jang MK, Nah JW. 2006. Retinol-encapsulated low molecular water-soluble chitosan nanoparticles. *Int J Pharm* 319:130-8.
164. Hasanovic A, Zehl M, Reznicek G, Valenta C. 2009. Chitosan-tripolyphosphate nanoparticles as a possible skin drug delivery system for aciclovir with enhanced stability. *J Pharm Pharmacol* 61:1609-16.
165. Chaiyasan W, Srinivas SP, Tiyafoonchai W. 2013. Mucoadhesive chitosan-dextran sulfate nanoparticles for sustained drug delivery to the ocular surface. *J Ocul Pharmacol Ther* 29:200-7.
166. Van Bocxlaer K, Murdan S, Croft S L , Yardley V. 2015. CUTANEOUS LEISHMANIASIS -SKIN BARRIER PROPERTIES AND DRUG DELIVERY STRATEGIES-. PhD. School of Pharmacy.
167. Lau WM, Ng KW. 2017. Finite and Infinite Dosing, p 35-44 doi:10.1007/978-3-662-53270-6_3.
168. Williams A. 2003. *Transdermal and Topical Drug Delivery from Theory to Clinical Practice*. Pharmaceutical Press.
169. Mitragotri S, Anissimov YG, Bunge AL, Frisch HF, Guy RH, Hadgraft J, Kasting GB, Lane ME, Roberts MS. 2011. Mathematical models of skin permeability: an overview. *Int J Pharm* 418:115-29.
170. Wijnant GJ, Van Bocxlaer K, Yardley V, Harris A, Murdan S, Croft SL. 2018. Relation between Skin Pharmacokinetics and Efficacy in AmBisome Treatment of Murine Cutaneous Leishmaniasis. *Antimicrob Agents Chemother* 62.
171. Kashyap P, Xiang X, Heiden P. 2015. Chitosan nanoparticle based delivery systems for sustainable agriculture. *International Journal of Biological Macromolecules* 77:36-51.
172. Nejati Hafdani F, Sadeghinia N. 2011. A review on application of chitosan as a natural antimicrobial. *World Academy of Science, Engineering and Technology* 74:257-261.
173. Kean T, Thanou M. 2010. Biodegradation, biodistribution and toxicity of chitosan. *Adv Drug Deliv Rev* 62:3-11.

174. Cheung RC, Ng TB, Wong JH, Chan WY. 2015. Chitosan: An Update on Potential Biomedical and Pharmaceutical Applications. *Mar Drugs* 13:5156-86.
175. Senel S, McClure SJ. 2004. Potential applications of chitosan in veterinary medicine. *Adv Drug Deliv Rev* 56:1467-80.
176. FDA. 20002. GRAS Notices.
177. Yong SK, Shrivastava M, Srivastava P, Kunhikrishnan A, Bolan N. 2015. Environmental Applications of Chitosan and Its Derivatives, p 1-43. *In* Whitacre DM (ed), *Reviews of Environmental Contamination and Toxicology Volume 233* doi:10.1007/978-3-319-10479-9_1. Springer International Publishing, Cham.
178. Alves NM, Mano JF. 2008. Chitosan derivatives obtained by chemical modifications for biomedical and environmental applications. *International Journal of Biological Macromolecules* 43:401-414.
179. Shukla SK, Mishra AK, Arotiba OA, Mamba BB. 2013. Chitosan-based nanomaterials: A state-of-the-art review. *International Journal of Biological Macromolecules* 59:46-58.
180. C. Goy R, Britto D, B. G. Assis O. 2009. A Review of the Antimicrobial Activity of Chitosan. *Polimeros-ciencia E Tecnologia - POLIMEROS* 19.
181. Hadwiger LA, Kendra DF, Fristensky BW, Wagoner W. 1986. Chitosan Both Activates Genes in Plants and Inhibits RNA Synthesis in Fungi, p 209-214. *In* Muzzarelli R, Jeuniaux C, Gooday GW (ed), *Chitin in Nature and Technology* doi:10.1007/978-1-4613-2167-5_28. Springer US, Boston, MA.
182. Porporatto C, Bianco ID, Riera CM, Correa SG. 2003. Chitosan induces different L-arginine metabolic pathways in resting and inflammatory macrophages. *Biochem Biophys Res Commun* 304:266-72.
183. Ravindranathan S, Koppolu BP, Smith SG, Zaharoff DA. 2016. Effect of Chitosan Properties on Immunoreactivity. *Marine drugs* 14:91.
184. Wu N, Wen ZS, Xiang XW, Huang YN, Gao Y, Qu YL. 2015. Immunostimulative Activity of Low Molecular Weight Chitosans in RAW264.7 Macrophages. *Mar Drugs* 13:6210-25.
185. Lopez-Moya F, Colom-Valiente MF, Martinez-Peinado P, Martinez-Lopez JE, Puellas E, Sempere-Ortells JM, Lopez-Llorca LV. 2015. Carbon and nitrogen limitation increase chitosan antifungal activity in *Neurospora crassa* and fungal human pathogens. *Fungal Biol* 119:154-69.
186. Sahariah P, Benediktssdottir BE, Hjalmarsdottir MA, Sigurjonsson OE, Sorensen KK, Thygesen MB, Jensen KJ, Masson M. 2015. Impact of chain length on antibacterial activity and hemocompatibility of quaternary N-alkyl and n,n-dialkyl chitosan derivatives. *Biomacromolecules* 16:1449-60.
187. Kong M, Chen XG, Xing K, Park HJ. 2010. Antimicrobial properties of chitosan and mode of action: a state of the art review. *Int J Food Microbiol* 144:51-63.
188. McAdams TA, Miller WM, Papoutsakis ET. 1997. Variations in culture pH affect the cloning efficiency and differentiation of progenitor cells in ex vivo haemopoiesis. *Br J Haematol* 97:889-95.
189. Fernandes AC, Soares DC, Saraiva EM, Meyer-Fernandes JR, Souto-Padron T. 2013. Different secreted phosphatase activities in *Leishmania amazonensis*. *FEMS Microbiol Lett* 340:117-28.
190. Xu W, Xin L, Soong L, Zhang K. 2011. Sphingolipid degradation by *Leishmania major* is required for its resistance to acidic pH in the mammalian host. *Infect Immun* 79:3377-87.
191. Bahrami S, Esmaeilzadeh S, Zarei M, Ahmadi F. 2015. Potential application of nanochitosan film as a therapeutic agent against cutaneous leishmaniasis caused by *L. major*. *Parasitol Res* 114:4617-24.

192. Esboei BR, Mohebbali M, Mousavi P, Fakhar M, Akhoundi B. 2018. Potent antileishmanial activity of chitosan against Iranian strain of *Leishmania major* (MRHO/IR/75/ER): In vitro and in vivo assay. *J Vector Borne Dis* 55:111-115.
193. Abdollahimajd F, Moravvej H, Dadkhahfar S, Mahdavi H, Mohebbali M, Mirzadeh H. 2019. Chitosan-based biocompatible dressing for treatment of recalcitrant lesions of cutaneous leishmaniasis: A pilot clinical study. *Indian J Dermatol Venereol Leprol* doi:10.4103/ijdv.IJDVL_189_18.
194. Tiera MJ, Qiu XP, Bechaouch S, Shi Q, Fernandes JC, Winnik FM. 2006. Synthesis and characterization of phosphorylcholine-substituted chitosans soluble in physiological pH conditions. *Biomacromolecules* 7:3151-6.
195. Szczepanska J, Pawlowska E, Synowiec E, Czarny P, Rekas M, Blasiak J, Szaflik JP. 2011. Protective effect of chitosan oligosaccharide lactate against DNA double-strand breaks induced by a model methacrylate dental adhesive. *Medical science monitor : international medical journal of experimental and clinical research* 17:BR201-BR208.
196. Naveed M, Phil L, Sohail M, Hasnat M, Baig MMFA, Ihsan AU, Shumzaid M, Kakar MU, Mehmood Khan T, Akabar MD, Hussain MI, Zhou Q-G. 2019. Chitosan oligosaccharide (COS): An overview. *International Journal of Biological Macromolecules* 129:827-843.
197. Tzaneva D, Simitchiev A, Petkova N, Nenov V, Stoyanova A, Denev P. 2017. Synthesis of Carboxymethyl Chitosan and its Rheological Behaviour in Pharmaceutical and Cosmetic Emulsions. *Journal of Applied Pharmaceutical Science* 7:70-78.
198. Seifert K, Escobar P, Croft SL. 2010. In vitro activity of anti-leishmanial drugs against *Leishmania donovani* is host cell dependent. *J Antimicrob Chemother* 65:508-11.
199. Van Bocxlaer K, Caridha D, Black C, Vesely B, Leed S, Sciotti RJ, Wijnant G-J, Yardley V, Braillard S, Mowbray CE, Ioset J-R, Croft SL. 2019. Novel benzoxaborole, nitroimidazole and aminopyrazoles with activity against experimental cutaneous leishmaniasis. *International Journal for Parasitology: Drugs and Drug Resistance* doi:<https://doi.org/10.1016/j.ijpddr.2019.02.002>.
200. Barros LM, Duarte AE, Morais-Braga MF, Waczuk EP, Vega C, Leite NF, de Menezes IR, Coutinho HD, Rocha JB, Kamdem JP. 2016. Chemical Characterization and Trypanocidal, Leishmanicidal and Cytotoxicity Potential of *Lantana camara* L. (Verbenaceae) Essential Oil. *Molecules* 21.
201. Callahan HL, Portal IF, Bensinger SJ, Grogil M. 1996. *Leishmania* spp: temperature sensitivity of promastigotes in vitro as a model for tropism in vivo. *Exp Parasitol* 84:400-9.
202. Wijnant GJ, Van Bocxlaer K, Yardley V, Murdan S, Croft SL. 2017. Efficacy of Paromomycin-Chloroquine Combination Therapy in Experimental Cutaneous Leishmaniasis. *Antimicrob Agents Chemother* 61.
203. Zhao YL, Tian PX, Han F, Zheng J, Xia XX, Xue WJ, Ding XM, Ding CG. 2017. Comparison of the characteristics of macrophages derived from murine spleen, peritoneal cavity, and bone marrow. *J Zhejiang Univ Sci B* 18:1055-1063.
204. Chang KP. 1980. Endocytosis of *Leishmania*-infected macrophages. Fluorometry of pinocytotic rate, lysosome-phagosome fusion and intralysosomal pH, p 231-234. Elsevier/North-Holland Biomedical Press., Amsterdam, The.
205. Antoine JC, Prina E, Jouanne C, Bongrand P. 1990. Parasitophorous vacuoles of *Leishmania amazonensis*-infected macrophages maintain an acidic pH. *Infect Immun* 58:779-87.
206. Miguel DC, Yokoyama-Yasunaka JK, Andreoli WK, Mortara RA, Uliana SR. 2007. Tamoxifen is effective against *Leishmania* and induces a rapid alkalinization of

- parasitophorous vacuoles harbouring *Leishmania (Leishmania) amazonensis* amastigotes. *J Antimicrob Chemother* 60:526-34.
207. Foresi N, Correa N, Amenta M, Arruebarrena Di Palma A, Creus C, Lamattina L. 2016. Detection of Nitric Oxide and Determination of Nitrite Concentrations in *Arabidopsis thaliana* and *Azospirillum brasilense*. *Bio-protocols* 6:e1765.
 208. Dutta D, Donaldson JG. 2012. Search for inhibitors of endocytosis: Intended specificity and unintended consequences. *Cell Logist* 2:203-208.
 209. Kruth HS, Jones NL, Huang W, Zhao B, Ishii I, Chang J, Combs CA, Malide D, Zhang WY. 2005. Macropinocytosis is the endocytic pathway that mediates macrophage foam cell formation with native low density lipoprotein. *J Biol Chem* 280:2352-60.
 210. Michael DR, Ashlin TG, Davies CS, Gallagher H, Stoneman TW, Buckley ML, Ramji DP. 2013. Differential regulation of macropinocytosis in macrophages by cytokines: implications for foam cell formation and atherosclerosis. *Cytokine* 64:357-61.
 211. O'Keeffe A, Hyndman L, McGinty S, Riezk A, Murdan S, Croft SL. 2019. Development of an in vitro media perfusion model of *Leishmania major* macrophage infection. *PLoS one* 14:e0219985-e0219985.
 212. Jaskolski F, Mulle C, Manzoni OJ. 2005. An automated method to quantify and visualize colocalized fluorescent signals. *J Neurosci Methods* 146:42-9.
 213. Valiante S, Falanga A, Cigliano L, Iachetta G, Busiello RA, La Marca V, Galdiero M, Lombardi A, Galdiero S. 2015. Peptide gH625 enters into neuron and astrocyte cell lines and crosses the blood-brain barrier in rats. *Int J Nanomedicine* 10:1885-98.
 214. Balicka-Ramisz A, Wojtasz-Pajak A, Pilarczyk B, Ramisz A, Laurans L. 2005. Antibacterial and antifungal activity of chitosan, vol 2.
 215. Shanmugam A, Kathiresan K, Nayak L. 2015. Preparation, characterization and antibacterial activity of chitosan and phosphorylated chitosan from cuttlebone of *Sepia kobeensis* (Hoyle, 1885). *Biotechnology reports (Amsterdam, Netherlands)* 9:25-30.
 216. Ardila N, Daigle F, Heuzey MC, Ajji A. 2017. Effect of Chitosan Physical Form on Its Antibacterial Activity Against Pathogenic Bacteria. *J Food Sci* 82:679-686.
 217. Tsai GJ, Su WH. 1999. Antibacterial activity of shrimp chitosan against *Escherichia coli*. *J Food Prot* 62:239-43.
 218. Salah- Tazdaït R, Tazdaït D, Harrat Z, Eddaïkra N, Abdi N, Mammeri N. 2015. Antiparasite Activity of Chitosan doi:10.17758/UR.U0615223.
 219. Asthana S, Jaiswal AK, Gupta PK, Pawar VK, Dube A, Chourasia MK. 2013. Immunoadjuvant chemotherapy of visceral leishmaniasis in hamsters using amphotericin B-encapsulated nanoemulsion template-based chitosan nanocapsules. *Antimicrob Agents Chemother* 57:1714-22.
 220. Malli S, Pomel S, Ayadi Y, Delomenie C, Da Costa A, Loiseau P, Bouchemal K. 2019. Topically applied Chitosan-Coated Poly(isobutylcyanoacrylate) Nanoparticles are Active Against Cutaneous Leishmaniasis by Accelerating Lesion Healing and Reducing the Parasitic Load. *ACS Applied Bio Materials* doi:10.1021/acsabm.9b00263.
 221. Sahariah P, Masson M. 2017. Antimicrobial Chitosan and Chitosan Derivatives: A Review of the Structure-Activity Relationship. *Biomacromolecules* 18:3846-3868.
 222. Seyfarth F, Schliemann S, Elsner P, Hipler UC. 2008. Antifungal effect of high- and low-molecular-weight chitosan hydrochloride, carboxymethyl chitosan, chitosan oligosaccharide and N-acetyl-d-glucosamine against *Candida albicans*, *Candida krusei* and *Candida glabrata*. *International Journal of Pharmaceutics* 353:139-148.
 223. Qiu M, Wu C, Ren G, Liang X, Wang X, Huang J. 2014. Effect of chitosan and its derivatives as antifungal and preservative agents on postharvest green asparagus. *Food Chem* 155:105-11.

224. Jeon Y-J, Park P-J, Kim S-K. 2001. Antimicrobial effect of chitooligosaccharides produced by bioreactor. *Carbohydrate Polymers* 44:71-76.
225. Green SJ, Scheller LF, Marletta MA, Seguin MC, Klotz FW, Slayter M, Nelson BJ, Nacy CA. 1994. Nitric oxide: cytokine-regulation of nitric oxide in host resistance to intracellular pathogens. *Immunol Lett* 43:87-94.
226. Tokura S, Tamura H, Azuma I. 1999. Immunological aspects of chitin and chitin derivatives administered to animals. *Exs* 87:279-92.
227. Salehi F, Behboudi H, Kavoosi G, Ardestani SK. 2017. Chitosan promotes ROS-mediated apoptosis and S phase cell cycle arrest in triple-negative breast cancer cells: evidence for intercalative interaction with genomic DNA. *RSC Advances* 7:43141-43150.
228. Li H, Shi B, Yan S, Zhao T, Li J, Guo X. 2014. Effects of Chitosan on the Secretion of Cytokines and Expression of Inducible Nitric Oxide Synthase mRNA in Peritoneal Macrophages of Broiler Chicken. *Brazilian Archives of Biology and Technology* 57:466-471.
229. Smith AC, Yardley V, Rhodes J, Croft SL. 2000. Activity of the Novel Immunomodulatory Compound Tucaresol against Experimental Visceral Leishmaniasis. *Antimicrobial Agents and Chemotherapy* 44:1494-1498.
230. Wang C, Yu X, Cao Q, Wang Y, Zheng G, Tan TK, Zhao H, Zhao Y, Wang Y, Harris D. 2013. Characterization of murine macrophages from bone marrow, spleen and peritoneum. *BMC Immunol* 14:6.
231. Soldati T, Schliwa M. 2006. Powering membrane traffic in endocytosis and recycling. *Nat Rev Mol Cell Biol* 7:897-908.
232. Hoemann CD, Guzman-Morales J, Tran-Khanh N, Lavallee G, Jolicoeur M, Lavertu M. 2013. Chitosan rate of uptake in HEK293 cells is influenced by soluble versus microparticle state and enhanced by serum-induced cell metabolism and lactate-based media acidification. *Molecules* 18:1015-35.
233. Fong D, Gregoire-Gelinas P, Cheng AP, Mezheritsky T, Lavertu M, Sato S, Hoemann CD. 2017. Lysosomal rupture induced by structurally distinct chitosans either promotes a type 1 IFN response or activates the inflammasome in macrophages. *Biomaterials* 129:127-138.
234. WHO. 2014. National Strategic Guideline on Kala-azar

Elimination Program in Nepal

2014

235. Wang Y, Li P, Truong-Dinh Tran T, Zhang J, Kong L. 2016. Manufacturing Techniques and Surface Engineering of Polymer Based Nanoparticles for Targeted Drug Delivery to Cancer. *Nanomaterials (Basel, Switzerland)* 6:26.
236. Jayasuriya AC. 2017. 8 - Production of micro- and nanoscale chitosan particles for biomedical applications, p 185-209. *In* Jennings JA, Bumgardner JD (ed), *Chitosan Based Biomaterials Volume 1* doi:<https://doi.org/10.1016/B978-0-08-100230-8.00008-X>. Woodhead Publishing.
237. Rajalakshmi R, Muzib Y, Aruna U, Vinesha V, Rupangada V, Krishna Moorthy SB. 2014. Chitosan Nanoparticles—An Emerging Trend In Nanotechnology. *International Journal of Drug Delivery* 6:204-229.
238. Tiyafoonchai W, Limpeanchob N. 2007. Formulation and characterization of amphotericin B-chitosan-dextran sulfate nanoparticles. *Int J Pharm* 329:142-9.
239. FDA. 2018. FOOD AND DRUGS.
240. Krishnan RA, Pant T, Sankaranarayan S, Stenberg J, Jain R, Dandekar P. 2018. Protective nature of low molecular weight chitosan in a chitosan–Amphotericin B

- nanocomplex – A physicochemical study. *Materials Science and Engineering: C* 93:472-482.
241. Cho Y, Shi R, Borgens R. 2010. Chitosan nanoparticle-based neuronal membrane sealing and neuroprotection following acrolein-induced cell injury. *Journal of biological engineering* 4:2.
 242. Abdelwahed W, Degobert G, Stainmesse S, Fessi H. 2006. Freeze-drying of nanoparticles: Formulation, process and storage considerations. *Advanced Drug Delivery Reviews* 58:1688-1713.
 243. Debnath SK, Saisivam S, Debanth M, Omri A. 2018. Development and evaluation of Chitosan nanoparticles based dry powder inhalation formulations of Prothionamide. *PLOS ONE* 13:e0190976.
 244. Ai J-w, Liao W, Ren Z-l. 2017. Enhanced anticancer effect of copper-loaded chitosan nanoparticles against osteosarcoma cancer. *RSC Adv* 7.
 245. Varshosaz J, Arbabi B, Pestehchian N, Saberi S, Delavari M. 2018. Chitosan-titanium dioxide-glucantime nanoassemblies effects on promastigote and amastigote of *Leishmania major*. *Int J Biol Macromol* 107:212-221.
 246. Danaei M, Dehghankhold M, Ataei S, Hasanzadeh Davarani F, Javanmard R, Dokhani A, Khorasani S, Mozafari MR. 2018. Impact of Particle Size and Polydispersity Index on the Clinical Applications of Lipidic Nanocarrier Systems. *Pharmaceutics* 10.
 247. Gaumet M, Vargas A, Gurny R, Delie F. 2008. Nanoparticles for drug delivery: The need for precision in reporting particle size parameters. *European Journal of Pharmaceutics and Biopharmaceutics* 69:1-9.
 248. Soppimath KS, Aminabhavi TM, Kulkarni AR, Rudzinski WE. 2001. Biodegradable polymeric nanoparticles as drug delivery devices. *Journal of Controlled Release* 70:1-20.
 249. Raimi-Abraham B, Moffat J, Belton P, Barker S, Craig D. 2014. Generation and Characterization of Standardized Forms of Trehalose Dihydrate and Their Associated Solid-State Behavior. *Crystal Growth & Design* 14.
 250. Fernando O, Tagalakis AD, Awwad S, Brocchini S, Khaw PT, Hart SL, Yu-Wai-Man C. 2018. Development of Targeted siRNA Nanocomplexes to Prevent Fibrosis in Experimental Glaucoma Filtration Surgery. *Mol Ther* 26:2812-2822.
 251. Zhao X, Liu L, Li X, Zeng J, Jia X, Liu P. 2014. Biocompatible Graphene Oxide Nanoparticle-Based Drug Delivery Platform for Tumor Microenvironment-Responsive Triggered Release of Doxorubicin. *Langmuir* 30:10419-10429.
 252. Pierfrancesco Lanzilotti SMAGB. 2017. Investigation into deformable vesicles for topical drug delivery. PhD. UCL, School of Pharmacy.
 253. Masarudin MJ, Cutts SM, Evison BJ, Phillips DR, Pigram PJ. 2015. Factors determining the stability, size distribution, and cellular accumulation of small, monodisperse chitosan nanoparticles as candidate vectors for anticancer drug delivery: application to the passive encapsulation of [(14)C]-doxorubicin. *Nanotechnol Sci Appl* 8:67-80.
 254. Rizvi SAA, Saleh AM. 2018. Applications of nanoparticle systems in drug delivery technology. *Saudi Pharmaceutical Journal* 26:64-70.
 255. Ferrari R, Sponchioni M, Morbidelli M, Moscatelli D. 2018. Polymer nanoparticles for the intravenous delivery of anticancer drugs: the checkpoints on the road from the synthesis to clinical translation. *Nanoscale* 10:22701-22719.
 256. Griffin JI, Wang G, Smith WJ, Vu VP, Scheinman R, Stitch D, Moldovan R, Moghimi SM, Simberg D. 2017. Revealing Dynamics of Accumulation of Systemically Injected Liposomes in the Skin by Intravital Microscopy. *ACS Nano* 11:11584-11593.

257. Du XJ, Wang JL, Iqbal S, Li HJ, Cao ZT, Wang YC, Du JZ, Wang J. 2018. The effect of surface charge on oral absorption of polymeric nanoparticles. *Biomater Sci* 6:642-650.
258. Jain A, Thakur K, Sharma G, Kush P, Jain UK. 2016. Fabrication, characterization and cytotoxicity studies of ionically cross-linked docetaxel loaded chitosan nanoparticles. *Carbohydr Polym* 137:65-74.
259. Jain V, Gupta A, Pawar VK, Asthana S, Jaiswal AK, Dube A, Chourasia MK. 2014. Chitosan-assisted immunotherapy for intervention of experimental leishmaniasis via amphotericin B-loaded solid lipid nanoparticles. *Appl Biochem Biotechnol* 174:1309-1330.
260. Chen Y, Mohanraj VJ, Wang F, Benson HA. 2007. Designing chitosan-dextran sulfate nanoparticles using charge ratios. *AAPS PharmSciTech* 8:E98.
261. Hussain Z, Sahudin S. 2016. Preparation, characterisation and colloidal stability of chitosan-tripolyphosphate nanoparticles: Optimisation of formulation and process parameters. *International Journal of Pharmacy and Pharmaceutical Sciences* 8:297-308.
262. Gan Q, Wang T, Cochrane C, McCarron P. 2005. Modulation of surface charge, particle size and morphological properties of chitosan-TPP nanoparticles intended for gene delivery. *Colloids Surf B Biointerfaces* 44:65-73.
263. Hu B, Pan C, Sun Y, Hou Z, Ye H, Zeng X. 2008. Optimization of fabrication parameters to produce chitosan-tripolyphosphate nanoparticles for delivery of tea catechins. *J Agric Food Chem* 56:7451-8.
264. Tang ESK, Huang M, Lim LY. 2003. Ultrasonication of chitosan and chitosan nanoparticles. *International Journal of Pharmaceutics* 265:103-114.
265. Hussain Z, Sahudin S. 2015. Preparation, characterisation and colloidal stability of chitosan-tripolyphosphate nanoparticles: Optimisation of formulation and process parameters.
266. Esmaeilzadeh E, Faramarzi M, Amini MA, Rouholamini Najafabadi A, Rezayat M, Amani A. 2012. Effects of processing parameters on particle size of ultrasound prepared chitosan nanoparticles: An Artificial Neural Networks Study. *Pharmaceutical development and technology* 17:638-47.
267. Dave R PR, Patel J and Chauhan H. 2012. Effect of cryoprotectant on lyophilisation of doxorubicin –HCl loaded chitosan nanoparticles *INTERNATIONAL JOURNAL OF PHARMACY & LIFE SCIENCES* 3:1769 - 1772.
268. Chaiyasan W, Srinivas SP, Tiyafoonchai W. 2015. Crosslinked chitosan-dextran sulfate nanoparticle for improved topical ocular drug delivery. *Molecular vision* 21:1224-1234.
269. Yuan Z, Ye Y, Gao F, Yuan H, Lan M, Lou K, Wang W. 2013. Chitosan-graft-beta-cyclodextrin nanoparticles as a carrier for controlled drug release. *Int J Pharm* 446:191-8.
270. Gatti THH, Eloy JO, Ferreira LMB, Silva ICd, Pavan FR, Gremião MPD, Chorilli M. 2018. Insulin-loaded polymeric mucoadhesive nanoparticles: development, characterization and cytotoxicity evaluation. *Brazilian Journal of Pharmaceutical Sciences* 54.
271. Tonin FS, Steimbach LM, Borba HH, Sanches AC, Wiens A, Pontarolo R, Fernandez-Llimos F. 2017. Efficacy and safety of amphotericin B formulations: a network meta-analysis and a multicriteria decision analysis. *J Pharm Pharmacol* 69:1672-1683.
272. Wijnant GJ, Van Bocxlaer K, Yardley V, Harris A, Alavijeh M, Silva-Pedrosa R, Antunes S, Mauricio I, Murdan S, Croft SL. 2018. Comparative efficacy, toxicity and biodistribution of the liposomal amphotericin B formulations Fungisome((R)) and

- AmBisome((R)) in murine cutaneous leishmaniasis. *Int J Parasitol Drugs Drug Resist* 8:223-228.
273. Tollemar J, Klingspor L, Ringdén O. 2001. Liposomal amphotericin B (AmBisome) for fungal infections in immunocompromised adults and children. *Clinical Microbiology and Infection* 7:68-79.
 274. Wortmann G, Zapor M, Ressler R, Fraser S, Hartzell J, Pierson J, Weintrob A, Magill A. 2010. Liposomal Amphotericin B for Treatment of Cutaneous Leishmaniasis. *The American Journal of Tropical Medicine and Hygiene* 83:1028-1033.
 275. Gaspari S. Access to liposomal generic formulations: beyond AmBisome and Doxil/Caelyx doi:10.5639/gabij.2013.0202.022. Pro Pharma Communications International.
 276. Zia Q, Mohammad O, Rauf MA, Khan W, Zubair S. 2017. Biomimetically engineered Amphotericin B nano-aggregates circumvent toxicity constraints and treat systemic fungal infection in experimental animals. *Scientific Reports* 7:11873.
 277. Jain JP, Kumar N. 2010. Development of amphotericin B loaded polymersomes based on (PEG)(3)-PLA co-polymers: Factors affecting size and in vitro evaluation. *Eur J Pharm Sci* 40:456-65.
 278. Ghasemiyeh P, Mohammadi Samani S. 2018. Solid lipid nanoparticles and nanostructured lipid carriers as novel drug delivery systems: Applications, advantages and disadvantages. *Research in pharmaceutical sciences* 13:288-303.
 279. Md U, Ghuge P, Jain B. 2017. Niosomes: A Novel Trend of Drug Delivery. *European Journal of Biomedical and Pharmaceutical sciences (EJBPS)*.
 280. Ravula T, Ramadugu SK, Di Mauro G, Ramamoorthy A. 2017. Bioinspired, Size-Tunable Self-Assembly of Polymer–Lipid Bilayer Nanodiscs. *Angewandte Chemie International Edition* 56:11466-11470.
 281. Azrini N, Elgharbawy A, Rezaei S, Samsudin N, Mohd H. 2019. processes Nanoemulsions: Factory for Food, Pharmaceutical and Cosmetics. *Processes* 7.
 282. Gupta PK, Bhandari N, Shah H, Khanchandani V, Keerthana R, Nagarajan V, Hiremath L. 2019. An Update on Nanoemulsions Using Nanosized Liquid in Liquid Colloidal Systems doi:10.5772/intechopen.84442.
 283. Kathe N, Henriksen B, Chauhan H. 2014. Physicochemical characterization techniques for solid lipid nanoparticles: principles and limitations. *Drug Development and Industrial Pharmacy* 40:1565-1575.
 284. Ghasemiyeh P, Mohammadi-Samani S. 2018. Solid lipid nanoparticles and nanostructured lipid carriers as novel drug delivery systems: applications, advantages and disadvantages. *Research in pharmaceutical sciences* 13:288-303.
 285. Landriscina A, Rosen J, Friedman AJ. 2015. Biodegradable chitosan nanoparticles in drug delivery for infectious disease. *Nanomedicine* 10:1609-1619.
 286. Yong Z, Huo M, Zhou J, Yu D, Wu Y. 2009. Potential of amphiphilically modified low molecular weight chitosan as a novel carrier for hydrophobic anticancer drug: Synthesis, characterization, micellization and cytotoxicity evaluation. *Carbohydrate Polymers* 77:231-238.
 287. Garg P, Kumar S, Pandey S, Seonwoo H, Choung P-H, Koh J, Chung JH. 2013. Triphenylamine coupled chitosan with high buffering capacity and low viscosity for enhanced transfection in mammalian cells, in vitro and in vivo. *Journal of Materials Chemistry B* 1:6053-6065.
 288. Qi L, Xu Z, Jiang X, Hu C, Zou X. 2004. Preparation and antibacterial activity of chitosan nanoparticles. *Carbohydrate Research* 339:2693-2700.
 289. Chavez de Paz LE, Resin A, Howard KA, Sutherland DS, Wejse PL. 2011. Antimicrobial effect of chitosan nanoparticles on streptococcus mutans biofilms. *Appl Environ Microbiol* 77:3892-5.

290. Potara M, Jakab E, Damert A, Popescu O, Canpean V, Astilean S. 2011. Synergistic antibacterial activity of chitosan-silver nanocomposites on *Staphylococcus aureus*. *Nanotechnology* 22:135101.
291. Ing LY, Zin NM, Sarwar A, Katas H. 2012. Antifungal activity of chitosan nanoparticles and correlation with their physical properties. *Int J Biomater* 2012:632698.
292. Zhou W, Wang Y, Jian J, Song S. 2013. Self-aggregated nanoparticles based on amphiphilic poly(lactic acid)-grafted-chitosan copolymer for ocular delivery of amphotericin B. *Int J Nanomedicine* 8:3715-28.
293. Singh PK, Pawar VK, Jaiswal AK, Singh Y, Srikanth CH, Chaurasia M, Bora HK, Raval K, Meher JG, Gayen JR, Dube A, Chourasia MK. 2017. Chitosan coated PluronicF127 micelles for effective delivery of Amphotericin B in experimental visceral leishmaniasis. *Int J Biol Macromol* 105:1220-1231.
294. Zadeh Mehrizi T, Shafiee Ardestani M, Haji Molla Hoseini M, Khamesipour A, Mosaffa N, Ramezani A. 2018. Novel Nanosized Chitosan-Betulinic Acid Against Resistant *Leishmania* Major and First Clinical Observation of such parasite in Kidney. *Scientific reports* 8:11759-11759.
295. Au - Evans BC, Au - Nelson CE, Au - Yu SS, Au - Beavers KR, Au - Kim AJ, Au - Li H, Au - Nelson HM, Au - Giorgio TD, Au - Duvall CL. 2013. Ex Vivo Red Blood Cell Hemolysis Assay for the Evaluation of pH-responsive Endosomolytic Agents for Cytosolic Delivery of Biomacromolecular Drugs. *JoVE* doi:doi:10.3791/50166:e50166.
296. Wijnant G-J, Croft S, de la Flor R, Alavijeh M, Yardley V, Braillard S, Mowbray C, Van Bocxlaer K. 2019. Pharmacokinetics and pharmacodynamics of the nitroimidazole DNDI-0690 in mouse models of cutaneous leishmaniasis. *Antimicrobial Agents and Chemotherapy* doi:10.1128/AAC.00829-19.
297. Accart N, Sergi F, Rooke R. 2014. Revisiting fixation and embedding techniques for optimal detection of dendritic cell subsets in tissues. *J Histochem Cytochem* 62:661-71.
298. Weinkopff T, Konradt C, Christian DA, Discher DE, Hunter CA, Scott P. 2016. *Leishmania* major Infection-Induced VEGF-A/VEGFR-2 Signaling Promotes Lymphangiogenesis That Controls Disease. *Journal of immunology (Baltimore, Md : 1950)* 197:1823-1831.
299. Sarin H. 2010. Physiologic upper limits of pore size of different blood capillary types and another perspective on the dual pore theory of microvascular permeability. *Journal of angiogenesis research* 2:14-14.
300. Nylen S, Eidsmo L. 2012. Tissue damage and immunity in cutaneous leishmaniasis. *Parasite Immunol* 34:551-61.
301. Sarwar HS, Sohail MF, Saljoughian N, Rehman AU, Akhtar S, Nakhman A, Yasinzaï M, Gendelman HE, Satoskar AR, Shahnaz G. 2018. Design of mannosylated oral amphotericin B nanoformulation: efficacy and safety in visceral leishmaniasis. *Artif Cells Nanomed Biotechnol* 46:521-531.
302. Lestner JM, Howard SJ, Goodwin J, Gregson L, Majithiya J, Walsh TJ, Jensen GM, Hope WW. 2010. Pharmacokinetics and pharmacodynamics of amphotericin B deoxycholate, liposomal amphotericin B, and amphotericin B lipid complex in an in vitro model of invasive pulmonary aspergillosis. *Antimicrob Agents Chemother* 54:3432-41.
303. Aguiar MG, Pereira AMM, Fernandes AP, Ferreira LAM. 2010. Reductions in Skin and Systemic Parasite Burdens as a Combined Effect of Topical Paromomycin and Oral Miltefosine Treatment of Mice Experimentally Infected with *Leishmania*.

- &em>amazonensis. Antimicrobial Agents and Chemotherapy 54:4699.
304. Shio MT, Paquet M, Martel C, Bosschaerts T, Stienstra S, Olivier M, Fortin A. 2014. Drug Delivery by Tattooing to Treat Cutaneous Leishmaniasis. Scientific Reports 4:4156.
 305. Carneiro G, Aguiar MG, Fernandes AP, Ferreira LA. 2012. Drug delivery systems for the topical treatment of cutaneous leishmaniasis. Expert Opin Drug Deliv 9:1083-97.
 306. Van Bocxlaer K, Yardley V, Murdan S, Croft SL. 2016. Topical formulations of miltefosine for cutaneous leishmaniasis in a BALB/c mouse model. J Pharm Pharmacol 68:862-72.
 307. Van Bocxlaer K, Yardley V, Murdan S, Croft SL. 2016. Drug permeation and barrier damage in Leishmania-infected mouse skin. J Antimicrob Chemother 71:1578-85.
 308. Manosroi A, Kongkaneramt L, Manosroi J. 2004. Stability and transdermal absorption of topical amphotericin B liposome formulations. International Journal of Pharmaceutics 270:279-286.
 309. Santos CM, de Oliveira RB, Arantes VT, Caldeira LR, de Oliveira MC, Egito ES, Ferreira LA. 2012. Amphotericin B-loaded nanocarriers for topical treatment of cutaneous leishmaniasis: development, characterization, and in vitro skin permeation studies. J Biomed Nanotechnol 8:322-9.
 310. Cangussu SD, Souza CC, Campos CF, Vieira LQ, Afonso LC, Arantes RM. 2009. Histopathology of Leishmania major infection: revisiting L. major histopathology in the ear dermis infection model. Mem Inst Oswaldo Cruz 104:918-22.
 311. Lipinski CA, Lombardo F, Dominy BW, Feeney PJ. 2001. Experimental and computational approaches to estimate solubility and permeability in drug discovery and development settings. Adv Drug Deliv Rev 46:3-26.
 312. Dolores RS, Maria PB, Andreas GS, Juan JT, Ijeoma FU. 2013. Amphotericin B Formulations – The Possibility of Generic Competition. Pharmaceutical Nanotechnology 1:250-258.
 313. El-On J, Jacobs GP, Witztum E, Greenblatt CL. 1984. Development of topical treatment for cutaneous leishmaniasis caused by Leishmania major in experimental animals. Antimicrobial agents and chemotherapy 26:745-751.
 314. Rossi-Bergmann B, Falcão CAB, Zanchetta B, Badra Bentley MVL, Santana MHA. 2011. Performance of Elastic Liposomes for Topical Treatment of Cutaneous Leishmaniasis, p 181-196. In Beck R, Guterres S, Pohlmann A (ed), Nanocosmetics and Nanomedicines: New Approaches for Skin Care doi:10.1007/978-3-642-19792-5_9. Springer Berlin Heidelberg, Berlin, Heidelberg.
 315. Perez AP, Altube MJ, Schilrreff P, Apezteguia G, Celes FS, Zacchino S, de Oliveira CI, Romero EL, Morilla MJ. 2016. Topical amphotericin B in ultradeformable liposomes: Formulation, skin penetration study, antifungal and antileishmanial activity in vitro. Colloids Surf B Biointerfaces 139:190-8.
 316. Vogt A, Rancan F, Ahlberg S, Nazemi B, Choe CS, Darvin ME, Hadam S, Blume-Peytavi U, Loza K, Diendorf J, Eppler M, Graf C, Ruhl E, Meinke MC, Lademann J. 2014. Interaction of dermatologically relevant nanoparticles with skin cells and skin. Beilstein J Nanotechnol 5:2363-73.
 317. Try C, Moulari B, Beduneau A, Fantini O, Pin D, Pellequer Y, Lamprecht A. 2016. Size dependent skin penetration of nanoparticles in murine and porcine dermatitis models. Eur J Pharm Biopharm 100:101-8.
 318. Campbell CS, Contreras-Rojas LR, Delgado-Charro MB, Guy RH. 2012. Objective assessment of nanoparticle disposition in mammalian skin after topical exposure. J Control Release 162:201-7.

319. Nair RS, Morris A, Billa N, Leong CO. 2019. An Evaluation of Curcumin-Encapsulated Chitosan Nanoparticles for Transdermal Delivery. *AAPS PharmSciTech* 20:69.
320. Moreno E, Schwartz J, Fernandez C, Sanmartin C, Nguewa P, Irache JM, Espuelas S. 2014. Nanoparticles as multifunctional devices for the topical treatment of cutaneous leishmaniasis. *Expert Opin Drug Deliv* 11:579-97.
321. Beil WJ, Meinardus-Hager G, Neugebauer DC, Sorg C. 1992. Differences in the onset of the inflammatory response to cutaneous leishmaniasis in resistant and susceptible mice. *J Leukoc Biol* 52:135-42.
322. Taveira SF, Nomizo A, Lopez RF. 2009. Effect of the iontophoresis of a chitosan gel on doxorubicin skin penetration and cytotoxicity. *J Control Release* 134:35-40.
323. He W, Guo X, Xiao L, Feng M. 2009. Study on the mechanisms of chitosan and its derivatives used as transdermal penetration enhancers. *Int J Pharm* 382:234-43.
324. O'Keeffe A, Murdan S, Croft SL. 2017. DEVELOPMENT OF NOVEL PREDICTIVE 2D AND 3D IN VITRO MODELS FOR ANTI-LEISHMANIAL DRUG TESTING. PhD. London School of Hygiene and Tropical Medicine
325. Davies B, Morris T. 1993. Physiological Parameters in Laboratory Animals and Humans. *Pharmaceutical Research* 10:1093-1095.
326. Szentistvanyi I, Patlak CS, Ellis RA, Cserr HF. 1984. Drainage of interstitial fluid from different regions of rat brain. *Am J Physiol* 246:F835-44.
327. Swartz MA, Fleury ME. 2007. Interstitial flow and its effects in soft tissues. *Annu Rev Biomed Eng* 9:229-56.
328. Dafni H, Israely T, Bhujwalla ZM, Benjamin LE, Neeman M. 2002. Overexpression of vascular endothelial growth factor 165 drives peritumor interstitial convection and induces lymphatic drain: magnetic resonance imaging, confocal microscopy, and histological tracking of triple-labeled albumin. *Cancer Res* 62:6731-9.
329. Haessler U, Teo JC, Foretay D, Renaud P, Swartz MA. 2012. Migration dynamics of breast cancer cells in a tunable 3D interstitial flow chamber. *Integr Biol (Camb)* 4:401-9.
330. Martin Y, Vermette P. 2005. Bioreactors for tissue mass culture: design, characterization, and recent advances. *Biomaterials* 26:7481-503.
331. Fu Q, Wu C, Shen Y, Zheng S, Chen R. 2008. Effect of LIMK2 RNAi on reorganization of the actin cytoskeleton in osteoblasts induced by fluid shear stress. *J Biomech* 41:3225-8.
332. Morelli S, Salerno S, Rende M, Lopez LC, Favia P, Procino A, Memoli B, Andreucci VE, d'Agostino R, Drioli E, De Bartolo L. 2007. Human hepatocyte functions in a galactosylated membrane bioreactor. *Journal of Membrane Science* 302:27-35.
333. Martin I, Wendt D, Heberer M. 2004. The role of bioreactors in tissue engineering. *Trends Biotechnol* 22:80-6.
334. Reynolds PM, Holzmann Rasmussen C, Hansson M, Dufva M, Riehle MO, Gadegaard N. 2018. Controlling fluid flow to improve cell seeding uniformity. *PLOS ONE* 13:e0207211.
335. Toepke MW, Beebe DJ. 2006. PDMS absorption of small molecules and consequences in microfluidic applications. *Lab Chip* 6:1484-6.
336. Halldorsson S, Lucumi E, Gomez-Sjoberg R, Fleming RMT. 2015. Advantages and challenges of microfluidic cell culture in polydimethylsiloxane devices. *Biosens Bioelectron* 63:218-231.
337. McBeath R, Pirone DM, Nelson CM, Bhadriraju K, Chen CS. 2004. Cell shape, cytoskeletal tension, and RhoA regulate stem cell lineage commitment. *Dev Cell* 6:483-95.
338. Zheng W, Wang Z, Zhang W, Jiang X. 2010. A simple PDMS-based microfluidic channel design that removes bubbles for long-term on-chip culture of mammalian cells. *Lab Chip* 10:2906-10.

339. Shinji Sugiura KN, Toshiyuki Kanamori and Kiyoshi Ohnuma. 2016. Application of Microfluidics in Stem Cell Culture. *ew Applications in Biology, Energy, and Materials Sciences* doi:DOI: 10.5772/64714.
340. Anonymous. Kirkstall Ltd QV900 information page. <http://www.kirkstall.com/qv900/>. Accessed 11/09/2019.
341. . Kirkstall Ltd QV500 information page. <http://www.kirkstall.com/qv500/>. Accessed 11/09/2019.
342. . Kirkstall Ltd QV600 information page. <http://www.kirkstall.com/qv600/>. Accessed 11/09/2019.
343. Huang M, Khor E, Lim LY. 2004. Uptake and cytotoxicity of chitosan molecules and nanoparticles: effects of molecular weight and degree of deacetylation. *Pharm Res* 21:344-53.
344. Lemaire S, Mingeot-Leclercq MP, Tulkens PM, Van Bambeke F. 2014. Study of macrophage functions in murine J774 cells and human activated THP-1 cells exposed to oritavancin, a lipoglycopeptide with high cellular accumulation. *Antimicrob Agents Chemother* 58:2059-66.
345. Xu M, Liu K, Swaroop M, Porter FD, Sidhu R, Firnkes S, Ory DS, Marugan JJ, Xiao J, Southall N, Pavan WJ, Davidson C, Walkley SU, Remaley AT, Baxa U, Sun W, McKew JC, Austin CP, Zheng W. 2012. δ -Tocopherol reduces lipid accumulation in Niemann-Pick type C1 and Wolman cholesterol storage disorders. *The Journal of biological chemistry* 287:39349-39360.
346. Treiger Borborema SE, Schwendener RA, Osso Junior JA, de Andrade Junior HF, do Nascimento N. 2011. Uptake and antileishmanial activity of meglumine antimoniate-containing liposomes in Leishmania (Leishmania) major-infected macrophages. *International Journal of Antimicrobial Agents* 38:341-347.
347. Journey P, Agarwal R, Singh V, Choi D, Roy K, Sreenivasan SV, Shi L. 2017. Unique size and shape-dependent uptake behaviors of non-spherical nanoparticles by endothelial cells due to a shearing flow. *Journal of Controlled Release* 245:170-176.
348. Yazdimamaghani M, Barber ZB, Hadipour Moghaddam SP, Ghandehari H. 2018. Influence of Silica Nanoparticle Density and Flow Conditions on Sedimentation, Cell Uptake, and Cytotoxicity. *Molecular Pharmaceutics* 15:2372-2383.
349. Ahmad Khanbeigi R, Kumar A, Sadouki F, Lorenz C, Forbes B, Dailey LA, Collins H. 2012. The delivered dose: Applying particokinetics to in vitro investigations of nanoparticle internalization by macrophages. *Journal of Controlled Release* 162:259-266.
350. Mahto SK, Yoon TH, Rhee SW. 2010. A new perspective on in vitro assessment method for evaluating quantum dot toxicity by using microfluidics technology. *Biomicrofluidics* 4.
351. Li Z, Cui Z. 2014. Three-dimensional perfused cell culture. *Biotechnol Adv* 32:243-54.
352. Sambale F, Stahl F, Bahnemann D, Scheper T. 2015. In vitro toxicological nanoparticle studies under flow exposure. *Journal of Nanoparticle Research* 17:298.
353. McCormick SC, Kriel FH, Ivask A, Tong Z, Lombi E, Voelcker NH, Priest C. 2017. The Use of Microfluidics in Cytotoxicity and Nanotoxicity Experiments. *Micromachines* 8:124.
354. Broussou DC, Toutain PL, Woehrle F, El Garch F, Bousquet-Melou A, Ferran AA. 2019. Comparison of in vitro static and dynamic assays to evaluate the efficacy of an antimicrobial drug combination against *Staphylococcus aureus*. *PLoS One* 14:e0211214.
355. Velkov T, Bergen PJ, Lora-Tamayo J, Landersdorfer CB, Li J. 2013. PK/PD models in antibacterial development. *Current Opinion in Microbiology* 16:573-579.

356. Okwor I, Uzonna J. 2016. Social and Economic Burden of Human Leishmaniasis. *Am J Trop Med Hyg* 94:489-93.
357. Reithinger R, Dujardin J-C, Louzir H, Pirmez C, Alexander B, Brooker S. 2007. Cutaneous leishmaniasis. *The Lancet Infectious Diseases* 7:581-596.
358. Sosa N, Capitan Z, Nieto J, Nieto M, Calzada J, Paz H, Spadafora C, Kreishman-Deitrick M, Kopydlowski K, Ullman D, McCarthy WF, Ransom J, Berman J, Scott C, Grogl M. 2013. Randomized, double-blinded, phase 2 trial of WR 279,396 (paromomycin and gentamicin) for cutaneous leishmaniasis in Panama. *Am J Trop Med Hyg* 89:557-563.
359. Neal RA. 1968. The effect of antibiotics of the neomycin group on experimental cutaneous leishmaniasis. *Ann Trop Med Parasitol* 62:54-62.
360. Caridha D, Vesely B, van Bocxlaer K, Arana B, Mowbray CE, Rafati S, Uliana S, Reguera R, Kreishman-Deitrick M, Sciotti R, Buffet P, Croft SL. 2019. Route map for the discovery and pre-clinical development of new drugs and treatments for cutaneous leishmaniasis. *Int J Parasitol Drugs Drug Resist* doi:10.1016/j.ijpddr.2019.06.003.
361. Les K, Ahmed A, Balan S, Choi J-w, Martin D, Yardley V, Powell K, Godwin A, Brocchini S. 2013. Poly(methacrylic acid) complexation of amphotericin B to treat neglected diseases. *Polym Chem* 5.
362. Tang J, Srinivasan S, Yuan W, Ming R, Liu Y, Dai Z, Noble CO, Hayes ME, Zheng N, Jiang W, Szoka FC, Schwendeman A. 2019. Development of a flow-through USP 4 apparatus drug release assay for the evaluation of amphotericin B liposome. *Eur J Pharm Biopharm* 134:107-116.
363. Mears ER, Modabber F, Don R, Johnson GE. 2015. A Review: The Current In Vivo Models for the Discovery and Utility of New Anti-leishmanial Drugs Targeting Cutaneous Leishmaniasis. *PLOS Neglected Tropical Diseases* 9:e0003889.

8. Appendix

8.1. Appendix 1: Validation of HPLC methods

Table 8.1. HPLC validation parameters

Parameter	Value
Accuracy	100.15 ± 0.22
Slope	108.11
Intercept	0.31
Linearity range	0.5-300 µg/ml
SE of intercept	0.2
SD of intercept	0.52
LOD (limit of detection) = $3.3 \times (\text{SD of intercept/Slope})$	0.015 µg/ml
LOQ (limit of quantification) = $10 \times (\text{SD of intercept/Slope})$	0.048 µg/ml

- Precision

Accuracy can be defined as the degree to which a measured value conforms to the true value. In pharmaceutical analysis, an assay is said to be accurate if the mean result is the same as the true value. On the other hand, precision is described as the variability of a set of measurements. Unlike accuracy, this does not provide any indication of the closeness of the obtained results from the true value. High precision is indicative of low variability in measurements usually demonstrated by low standard deviation values. This is usually reported as a percentage relative standard deviation.

$$(\%RSD): \text{SD/Drug} \times 100$$

The precision of the method was determined by repeatability (intra-day) and intermediate precision (inter-day). Repeatability was determined by performing three repeated analysis of the same standard solution on the same day, under the same experimental conditions. The intermediate precision of the HPLC methods was assessed by carrying out the analysis on three different days (inter-day). For each drug, the percentage relative standard

deviation (%RSD) and the percentage recovery of the standard solutions are reported for each drug.

Table 8.2. The precision of AmB HPLC assay

Standard concentration µg/ml	Intra-day calculated concentration (µg/ml)	Inter-day Calculated concentration (µg/ml)	Intra-day % RSD	Inter-day % RSD
300	300.03± 0.21	300.33± 0.15	0.05	0.07
100	99.91± 0.16	100.10± 0.17	0.17	0.16
33.3	33.26± 0.05	33.29± 0.04	0.11	0.14
11.1	11.10± 0.09	11.27± 0.14	1.26	0.81
3.7	3.71± 0.02	3.70± 0.05	1.28	0.41
1.23	1.24± 0.02	1.23± 0.02	1.24	1.24
0.4	0.39± 0.02	0.4± 0.02	5.25	3.88

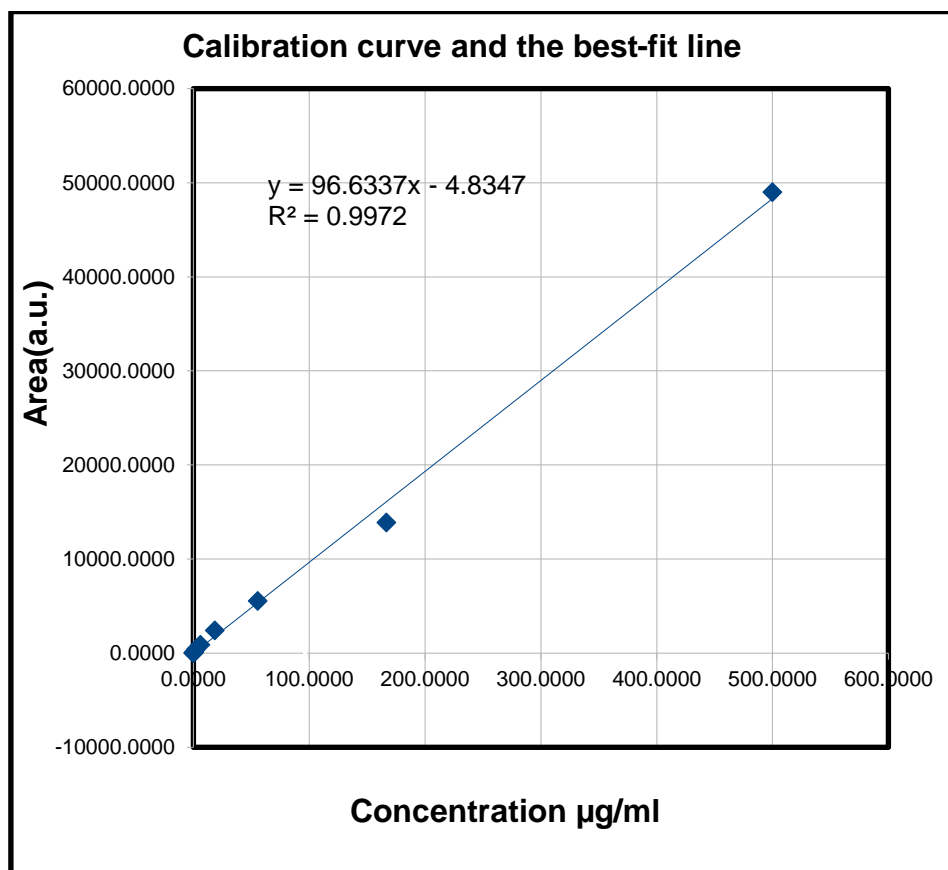
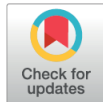


Figure Calibration curve of amphotericin B

8.2. Appendix 2: Paper 1



OPEN ACCESS

Citation: O'Keeffe A, Hyndman L, McGinty S, Riezk A, Murdan S, Croft SL (2019) Development of an *in vitro* media perfusion model of *Leishmania major* macrophage infection. PLoS ONE 14(7): e0219985. <https://doi.org/10.1371/journal.pone.0219985>

Editor: Farhat Afrin, Taibah University, SAUDI ARABIA

Received: January 8, 2019

Accepted: July 4, 2019

Published: July 24, 2019

Copyright: © 2019 O'Keeffe et al. This is an open access article distributed under the terms of the [Creative Commons Attribution License](https://creativecommons.org/licenses/by/4.0/), which permits unrestricted use, distribution, and reproduction in any medium, provided the original author and source are credited.

Data Availability Statement: All data is available at the University College School of Pharmacy Data Repository at: <https://doi.org/10.5522/04/8075312.v1>.

Funding: This work was supported by Biotechnology and Biological Sciences Research Council [grant number BB/M009513/1] to AOK, SC; Kirkstall Ltd., UK to SM, LH; Engineering and Physical Sciences Research Council (EP/M506539/1 and EP/M508056/1) to SM, LH; Alan & Kathie Stross Summer Fellowship to LH; Dr Hadwen Trust

RESEARCH ARTICLE

Development of an *in vitro* media perfusion model of *Leishmania major* macrophage infection

Alec O'Keeffe^{1,2}, Lauren Hyndman³, Sean McGinty³, Alaa Riezk¹, Sudaxshina Murdan², Simon L. Croft^{1*}

1 Department of Infection and Immunology, London School of Hygiene and Tropical Medicine, London, United Kingdom, **2** Department of Pharmaceutics, UCL School of Pharmacy, University College London, London, United Kingdom, **3** Division of Biomedical Engineering, University of Glasgow, Glasgow, United Kingdom

* simon.croft@lshtm.ac.uk

Abstract

Background

In vitro assays are widely used in studies on pathogen infectivity, immune responses, drug and vaccine discovery. However, most *in vitro* assays display significant differences to the *in vivo* situation and limited predictive properties. We applied medium perfusion methods to mimic interstitial fluid flow to establish a novel infection model of *Leishmania* parasites.

Methods

Leishmania major infection of mouse peritoneal macrophages was studied within the Quasi Vivo QV900 macro-perfusion system. Under a constant flow of culture media at a rate of 360 µl/min, *L. major* infected macrophages were cultured either at the base of a perfusion chamber or raised on 9mm high inserts. Mathematical and computational modelling was conducted to estimate medium flow speed, shear stress and oxygen concentration. The effects of medium flow on infection rate, intracellular amastigote division, macrophage phagocytosis and macropinocytosis were measured.

Results

Mean fluid speeds at the macrophage cell surface were estimated to be 1.45×10^{-9} m/s and 1.23×10^{-7} m/s for cells at the base of the chamber and cells on an insert, respectively. *L. major* macrophage infection was significantly reduced under both media perfusion conditions compared to cells maintained under static conditions; a $85 \pm 3\%$ infection rate of macrophages at 72 hours in static cultures compared to $62 \pm 5\%$ for cultures under slow medium flow and $55 \pm 3\%$ under fast medium flow. Media perfusion also decreased amastigote replication and both macrophage phagocytosis (by $44 \pm 4\%$ under slow flow and $57 \pm 5\%$ under fast flow compared with the static condition) and macropinocytosis (by $40 \pm 4\%$ under slow flow and $62 \pm 5\%$ under fast flow compared with the static condition) as measured by uptake of latex beads and pHrodo Red dextran.

to LH; Medical Research Council Confidence in Concept award (number IF MC-PC_13069) to SC, AOK. The funders had no role in study design, data collection and analysis, decision to publish, or preparation of the manuscript.

Competing interests: SM and LH gratefully acknowledge a financial donation from Kirkstall Ltd. This does not alter our adherence to PLOS ONE policies on sharing data and materials.

Conclusions

Perfusion of culture medium in an *in vitro* *L. major* macrophage infection model (simulating *in vivo* lymphatic flow) reduced the infection rate of macrophages, the replication of the intracellular parasite, macrophage phagocytosis and macropinocytosis with greater reductions achieved under faster flow speeds.

Introduction

Traditional cell culture methods typically rely on either immortalized cell lines or primary isolated cells grown in designed nutritious media on non-physiological substrates, such as functionalized plastic and glass. Although these methods have been at the core of *in vitro* studies on many basic biological processes, they provide a limited platform owing to both their inadequate representation of key physiological characteristics and their relevance to disease models [1]. One area that is often overlooked in cell culture models is the transport and movement of nutrients around cells, which occurs through fluid flow in the body. This could impact on the growth and survival of pathogens in intracellular models as infection is reliant on nutrients provided by the host cell and cell-cell interactions. Within the mammalian body, rates of fluid flow vary from the rapid plasma flow of 9.8 ml/min in the portal vein of the rat [2] to the slower 0.19 μ l/min rate of interstitial fluid drainage from rat brains [3]. Interstitial fluid in tissues, including skin, arises from the normal leakage of plasma from blood vessels and has a composition that is similar to that of blood plasma [4]. It is estimated that up to 20% of the body's mass is made up of interstitial fluid [4].

Leishmaniasis is an infectious disease caused by protozoa parasites of the genus *Leishmania*, which have two distinct life cycle stages: an extracellular motile promastigote form in the sand-fly vector and an intracellular amastigote form that survives and multiplies in the phagolysosomal compartment of mammalian macrophages [5]. Two predominant forms of the disease result from infection by *Leishmania* parasites, the potentially fatal visceral leishmaniasis (VL) and the self-curing, but disfiguring, cutaneous leishmaniasis (CL). Although macrophages of the liver and spleen infected with *Leishmania donovani*, the cause of VL, are exposed to plasma flow rates, in the skin sites of infection in CL, infected macrophages are exposed to interstitial fluid. While the exact speed of interstitial fluid flow through the CL lesion is not known, measurements have shown that interstitial fluid flow in uninfected human skin is of the order of 0.1–2 μ m/s [4,6,7]. Most *in vitro* studies on invasion, infection, immunology and drug discovery within the *Leishmania* field have so far been performed using macrophages grown under static culture conditions [8–10]. To simulate some of the more complex interactions between the parasite and macrophages in the host we selected the Quasi Vivo 900 media perfusion system (QV900) with a 6-chamber optical tray, to enable the imaging of cultures *in situ* at a flow rate similar to that of interstitial fluid. Here we describe the effect of media perfusion on the infection of mouse peritoneal macrophages with *Leishmania major* and use mathematical modelling to estimate the flow speed, shear stress and oxygen tension at the host cell surface. In addition, we have determined the impact of flow on intracellular amastigote division, and host cell phagocytosis and macropinocytosis.

Material and methods

Media perfusion system

Quasi Vivo media perfusion systems (Kirkstall Ltd, Rotherham, UK) were selected as they enable the direct observation of infected cells exposed to different medium perfusion rates and

the continuous monitoring of infection. The Quasi Vivo systems include the QV500, an individual chamber system, and the QV900, a six chamber optical tray which permits connecting of chambers in series. We selected the QV900 given that it is more suited to high-throughput testing. Mathematical and computational modelling of the QV500 [11] has shown that the speed of media at the surface of cells cultured at the base of the chambers is within the range of interstitial fluid flow rates [4,6,7] in humans for a flow rate of 360 μ l/min. However, the QV900 chambers differ in geometry and in particular are significantly deeper, having a depth of 22 mm compared with 12 mm in the QV500. As a result of this difference in chamber geometry, the fluid environment in the QV900 is markedly different from that in the QV500 at the same flow rate. Therefore, we inserted a 3D printed block composed of Nylon 12 (Kirkstall Ltd) in selected chambers to enable us to study cells cultured at different depths in the QV900 chamber. Mathematical and computational modelling (see sections below) were utilized to calculate the insert height that would ensure the cell surface flow speeds would fall within the reported range for interstitial flow in the skin. All six chambers of the QV900 were connected in series with the last three of the chambers containing inserts. A peristaltic pump (Parker Hannifin, UK), external to the CO₂ incubator, continuously circulated culture media through the system.

Modelling fluid flow and oxygen transport in the QV900 system

COMSOL Multiphysics, a commercially available finite element analysis software, was used to perform simulations in this study. Initial modelling focused on single chamber studies to establish the size of the insert required to achieve the desired cell surface flow speeds. Subsequently, simulations were conducted for six chambers connected in series, matching the experiments. Fig 1 illustrates the computational domains for cells placed at the base of the chamber (left) and on a 9mm insert (right). Note that in both cases the chambers are identical in dimensions, but since there is assumed to be no fluid flow beneath the insert, the depth of this computational domain is reduced.

The fluid flow was modelled using the Navier-Stokes equations, assuming that the media is an incompressible Newtonian fluid. The transport of oxygen throughout the media was modelled by convection and diffusion. The cells were assumed to reside at the base of each computational domain on circular coverslips of diameter 12mm. Oxygen consumption by the cells was described using Michaelis-Menten kinetics and implemented through a flux boundary condition. The equations and parameter values used in the simulations are detailed in the supplementary material (S1 File).

Culture systems

Leishmania parasites. *L. major* (MHOM/SA/85/JISH118) amastigotes were obtained and isolated from mouse skin lesions. They were allowed to transform to promastigotes and were maintained in Schneider's insect medium (Sigma Aldrich, UK) supplemented with 10% heat inactivated foetal calf serum (HiFCS) (Harlan, UK) at 26°C. The parasites were routinely passaged through BALB/c mice (Charles River, UK) and low passage number promastigotes (< passage number 3) were used for experiments as infectivity has been shown to decrease with time of parasite cultivation [12].

All animal experiments were conducted under license (project license 70/6997 or X20014A54) in accordance with UK Home Office approval, EU regulations, EU directive 2010/63/EU. Protocols followed in these studies for the isolation of peritoneal macrophages was approved by the LSHTM Animal Welfare and Ethics Review Board. The mice are housed in green line I.V.C.s, 5 mice per cage, with access to food and water ad libitum. At all stages the 3Rs (replacement, reduction and refinement) were taken into consideration.

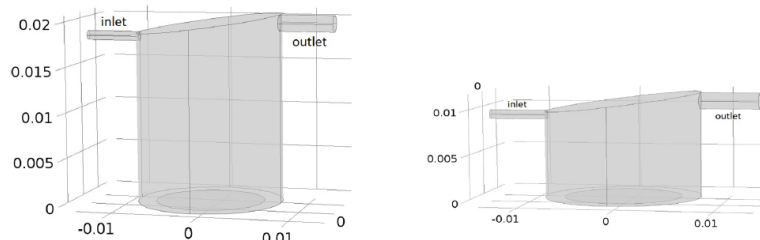


Fig 1. Left: Idealized 3D geometry of a single QV900 chamber. This represents the computational domain for the case where the cells are placed at the base of the chamber. Right: Computational domain for cells placed on a 9mm insert. Note that length scales are in m.

<https://doi.org/10.1371/journal.pone.0219985.g001>

Macrophages. Mouse peritoneal macrophages (PEM) were isolated from CD-1 mice (Charles River, Margate, UK) by abdominal lavage [13] with RPMI-1640 medium containing 1% penicillin and 1% streptomycin (Sigma, UK).

THP1 cells (ATCC TIB-202, UK) were maintained in RPMI-1640 containing 10% HiFCS (Harlan, UK) and passaged by a 1:10 split weekly.

Infection of macrophages by *L. major* promastigotes. Macrophages were plated on 12mm round glass coverslips (Bellco, US) placed in 24 well plates (Corning, UK) at a density of 4×10^5 cells per well in RPMI-1640 media supplemented with 10% HiFCS. The plates were incubated at 37°C in 5% CO₂ for 24 hours. *L. major* stationary phase promastigotes were counted and dilutions of different concentrations of parasite (2×10^5 to 6×10^7) were pre-prepared in media to give initial parasite: macrophage ratios within the range of 0.5:1–15:; promastigotes were added to the macrophage cultures. The plates were placed in an incubator maintained at 34°C (temperature relevant for CL [14]) and 5% CO₂ for 24 hours. Subsequently, two thirds of the glass coverslips were transferred to the media perfusion system and maintained under flow conditions at a flow speed of 360 µl/min for 72 hours in a 34°C, 5% CO₂ incubator. The remaining coverslips were used for the static control, with macrophages maintained in the same culture medium without flow. The cells were methanol (Sigma, UK) fixed and stained with Giemsa's stain (Sigma, UK). The infection rate of the macrophages was assessed visually using an oil immersion microscope (100x magnification Zeiss, UK) by counting the number of infected cells per 100 macrophages. Values for percentage infection throughout are shown as mean ± standard deviation.

Incorporation of 5-ethynyl-2'-deoxyuridine (EdU) into dividing amastigotes. Invitrogen Click-iT EdU Imaging Kit (Invitrogen, UK) was used to measure 5-ethynyl-2'-deoxyuridine incorporation as a measure of proliferation. Only the dividing parasites should incorporate the EdU as the macrophage populations used are fully differentiated non dividing cells. The kit comprised of a fluorescently labelled DNA base, which is incorporated into DNA synthesized during amastigote division. Experiments, based on the methodology of Tegazzini et al. [9], were conducted as before except that PEMs were infected with a ratio of 3 *L. major* promastigotes: 1 macrophage and maintained at 34°C, 5% CO₂ in an incubator for 24 hours. Media used contained 50 µM EdU. After 24 hours, cells were placed in a new 24-well plate and were fixed in 4% Paraformaldehyde (PFA) (Sigma, UK) for 15 minutes at room temperature. The samples were treated with 0.2% Triton X-100 (Sigma, UK) in PBS (Sigma, UK) for 20 minutes and then 1% BSA (Sigma, UK) in PBS for 10 minutes. Click-iT reaction cocktail was prepared according to instructions in Invitrogen Click-iT EdU Imaging Kit. Click-iT reaction

cocktail (0.5 mL) was added to each well containing a coverslip, and plates were incubated for 30 minutes at room temperature, protected from light. Cells were then washed with 1 mL of 3% BSA in PBS, then incubated with 300 mM DAPI stain (Sigma, UK) for 10 minutes to stain the nucleus of the cell, coverslips were mounted onto slides and imaged using a confocal microscope (Zeiss LSM510 Axiovert, Germany). The lasers used were Laser Diode: 405 nm for DAPI excitation and Argon laser: 458, 488, 514 nm for EdU excitation. Images were captured at 40x magnification and analysed using Velocity software (PerkinElmer, US) to automatically count the total number of nuclei in each field of view and this is proportional to the total cell number. A minimum of 100 macrophages were counted microscopically from each coverslip. Images were manually viewed to count the number of fluorescent and non-fluorescent parasites within each cell. The results were exported and analysed with Graphpad Prism.

Measurement of macrophage functions. Phagocytosis by macrophages was initially evaluated using 0.5, 1 and 2 μ m diameter fluorescent red labelled latex beads (carboxylate-modified polystyrene) (Sigma-Aldrich, UK) [15,16]; 2 μ m beads were eventually selected as they showed maximal signal. Macrophages were infected with parasites, then transferred to the three flow conditions as described above. To each well, 2 μ m beads (9.12×10^7 latex beads/mL) were added and the cells were incubated for 0.5, 1, 2, 4 and 24 hours at 34 °C under the three different flow conditions. The experiment was terminated by washing the cells 4 times with ice-cold PBS pH 7.4 to remove non-internalized latex beads, followed by the addition of 1 mL of 0.5% Triton X-100 in 0.2 M NaOH to lyse the cells. Phagocytosis was quantified by the analysis of the cell lysate using a fluorescence plate reader (Spectramax M3, at excitation and emission wavelengths set at 575 and 610 nm), calibrated with standard solutions containing different amount of latex beads in a cell lysate mixture. Uptake was expressed as the number of latex beads associated per mg of cellular protein, the protein content of the cell lysate being measured using a Micro BCA protein kit (Thermo Fisher, UK) assay as per supplier's instructions. For control studies, 1 μ g/mL cytochalasin D was used as a phagocytosis inhibitor (Sigma-Aldrich, UK) by incubation with macrophages for 2 hours prior to addition of the latex beads. Phagocytosis was completely inhibited after 0.5, 1, 2 and 4 hours of incubation with cytochalasin D and 90% after 24 hours.

Macropinocytosis. Macropinocytosis was measured using a fluorescence-labeled dextran dye [17] (pHrodo Red dextran, average molecular weight of dextran 10,000 MW, Thermo Fisher, UK). This dye has a pH-sensitive fluorescence emission that increases in intensity with increasing acidity while exhibiting minimal fluorescence at neutral pH. Macrophages were infected with parasites and then transferred to the three flow conditions as described above. Macrophages were washed 3 x by Live Cell Imaging Solution (ThermoFisher, UK) and the cells were returned to RPMI 1640 + 10% hiFCS containing 40 μ g/mL pHrodo Red dextran (1 mL for each well) and incubated at 34 °C / 5% CO₂ for 0.5, 1, 2, 4 and 24 hours under the three different flow conditions. At each time point, the cells were washed with Live Cell Imaging Solution and macropinocytosis was analysed by a Spectramax M3 at excitation and emission wavelengths set at 560 and 585 nm respectively. Chlorpromazine hydrochloride 10 μ g/mL, a known inhibitor (Sigma-Aldrich, UK), was used as a control and was incubated with macrophages for 2 hours prior to addition of fluorescence-labeled dextran dye. Macropinocytosis was completely inhibited after 0.5, 1, 2 and 4 hours of incubation with chlorpromazine hydrochloride and by 90% after 24 hours.

Results

Establishment of infected macrophages in Quasi Vivo systems

Initial experiments using the Quasi Vivo systems involved the adaptation of the QV900 for our experimental purposes and the establishment of media perfusion within the system with a

focus on the optimization of conditions to maintain viable cells within the system. A second objective was to ensure that an infection with *Leishmania* parasites could be sustained, as shown in subsequent experiments.

QV900 media perfusion system modelling

Initially, single chamber simulations were carried out to estimate the height of the insert required to ensure the cell surface flow speed would be within the reported range for interstitial flow in the skin. Table 1 shows the estimated speed of the culture medium on the cell surface for various insert heights. It is clear that a 9mm insert would enable a culture medium flow speed in line with the speed of interstitial fluid flow in the skin, and therefore this height was chosen for subsequent modelling and experiments.

Subsequent mathematical and computational modelling was carried out to match the experimental set up, i.e. we simulated six chambers connected in series, with the first three chambers having cells residing at the base and the next three chambers having cells raised 9mm. Fig 2 illustrates results which are representative of the first three chambers in the series. All plots in Fig 3 show the results for chamber one, with the exception of the lower right plot which shows results for the first three connected chambers. The simulated oxygen concentration decreases from the inlet of the chamber, where oxygen is supplied, to the base of the chamber, where oxygen is consumed by the cells (Fig 2, upper left). At the base of the chamber, the oxygen concentration is highest at the inlet side, reducing towards the centre, before rising again at the outlet side of the chamber (Fig 2, middle left). This gradient, clearly highlighted in the lower left plot of Fig 2, is a combined result of the complex flow field and the fact that oxygen consumption only occurs on the part of the base where the cells reside. Similar results for chambers two and three are shown in the lower right plot of Fig 2. The oxygen concentrations are lower in each consecutive chamber as a result of consumption, but the pattern of oxygen concentrations across the base is consistent between each chamber. The overall gradient of oxygen at the base of the first three connected chambers ranges from a maximum of 0.2059 mol/m³ in chamber one to a minimum of 0.2029 mol/m³ in chamber three.

The upper right plot of Fig 2 illustrates the flow speed and streamlines (the trajectories that particles would follow), demonstrating how the media flows through the chamber. The media flow is fastest at the inlet and outlet, and flow recirculation zones are observed beneath the inlet and at the base of the chamber. In these areas, the media is recirculated which could result in parasites and oxygen/drug molecules being trapped. The flow speed of the media at the base of the first chamber is consistent with the second and third chambers and has a mean value of 1.45×10^{-9} m/s. We note that this is slightly higher than the mean flow speed obtained in a single chamber (Table 1) as a result of the altered fluid dynamics due to connecting the chambers in series. A 2D representation of the magnitude of the shear stress the cells are under at the

Table 1. Simulation results show that a 9mm insert is required to bring the cell surface flow rate in line with the values of 0.1–2 μ m/s reported in [4,6,7].

Insert height (mm)	Mean cell surface flow speed (m/s)
0mm	1.33×10^{-9}
5mm	1.80×10^{-8}
6mm	3.05×10^{-8}
7mm	5.01×10^{-8}
8mm	7.77×10^{-8}
9mm	1.17×10^{-7}

<https://doi.org/10.1371/journal.pone.0219985.t001>

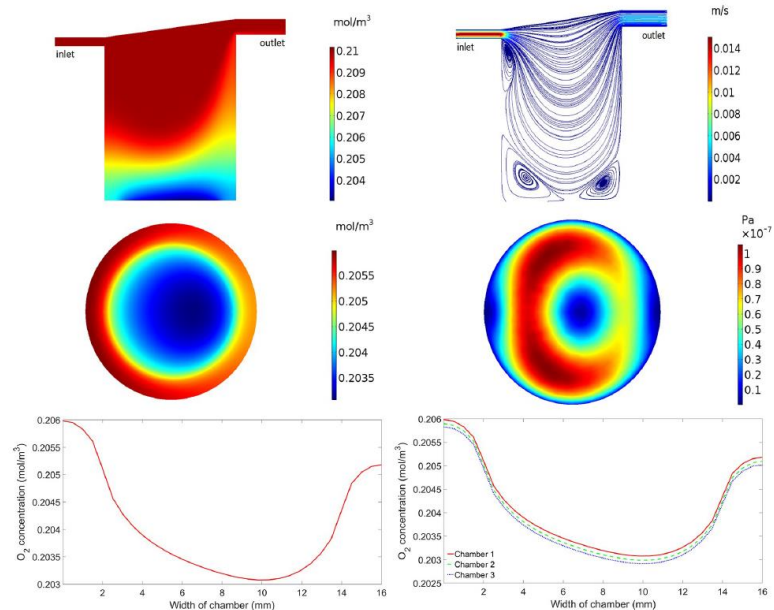


Fig 2. Simulation results for cells at the base of the chamber. Upper left: Oxygen concentration in chamber 1. Upper right: Flow profile in chamber 1. Middle left: Oxygen concentration at the base of chamber 1. Middle right: Magnitude of the shear stress at the base of chamber 1. Lower left: Oxygen concentration across the centre of the base of chamber 1. Lower right: Oxygen concentration across the centre of the base of chambers 1, 2 and 3.

<https://doi.org/10.1371/journal.pone.0219985.g002>

base of the chamber is shown in the middle right plot of Fig 2. The shear stress values range from a minimum of 2.09×10^{-10} Pa to a maximum of 1.06×10^{-7} Pa which is consistent with the second and third chambers.

Fig 3 illustrates results which are representative of the last three chambers in the series i.e. where the cells are placed on a 9mm insert. All plots show the results for chamber four (the first chamber in the series which has the cells raised by 9mm), with the exception of the lower right plot which shows results for the last three connected chambers (chambers 4, 5 and 6). The inclusion of the 9mm insert has an impact on both the pattern and magnitude of the oxygen concentration and fluid flow. Higher oxygen concentrations are observed throughout the whole chamber when compared to the chambers without an insert (Fig 3, upper left), and the minimum oxygen concentration at the base of the chamber occurs closer to the outlet side than when compared to the chambers without an insert (Fig 3, middle left). The oxygen concentration gradient across the base of the chamber is clearly highlighted in the lower left plot of Fig 3. Again, this pattern is a combined result of the complex flow field and the fact that oxygen consumption only occurs on the part of the base where the cells reside. Similar results for chambers 5 and 6 are shown in the lower right plot of Fig 3. As before, the oxygen concentration decreases between consecutive chambers due to consumption but the pattern remains

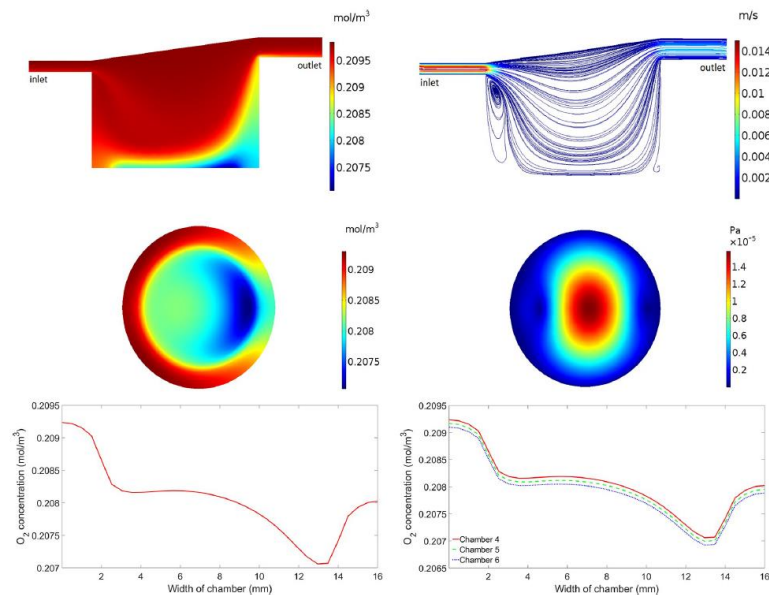


Fig 3. Simulation results for cells on top of the 9mm insert. Upper left: Oxygen concentration in chamber 4. Upper right: Flow profile in chamber 4. Middle left: Oxygen concentration at the base of chamber 4. Middle right: Magnitude of the shear stress at the base of chamber 4. Lower left: Oxygen concentration across the centre of the base of chamber 4. Lower right: Oxygen concentration across the centre of the base of chambers 4, 5 and 6.

<https://doi.org/10.1371/journal.pone.0219985.g003>

the same. The overall gradient of oxygen at the base of the last three connected chambers ranges from a maximum of 0.2093 mol/m^3 in chamber 4 to a minimum of 0.2069 mol/m^3 in chamber 6.

The depth of the last three chambers in the series is dramatically reduced due to the 9mm insert which has a large impact on the pattern of flow (Fig 3, upper right). In this case, the only flow recirculation zone is observed beneath the inlet to the chamber. The mean flow speed of the media at the cells on top of the insert in the fourth chamber is $1.23 \times 10^{-7} \text{ m/s}$ —two orders of magnitude higher than in the chambers without the insert. This is consistent with the fifth and sixth chambers where the mean flow speed is also $1.23 \times 10^{-7} \text{ m/s}$. Due to the difference in the flow profile, the pattern of shear stress at the base of the chamber is also noticeably different when compared to the chambers without an insert (Fig 3, middle right). The shear stress values range from a minimum of $5.75 \times 10^{-9} \text{ Pa}$ at the edges of the base of the chamber to a maximum of $1.58 \times 10^{-5} \text{ Pa}$ at the centre of the base of the chamber. This is again consistent with the fifth and sixth chambers.

Determination of optimal experimental conditions

Initially, we used both THP1 cells and PEMs at different concentrations from 1×10^5 to 4×10^5 cells per chamber, to establish a viable, reproducible and measurable system. After preliminary

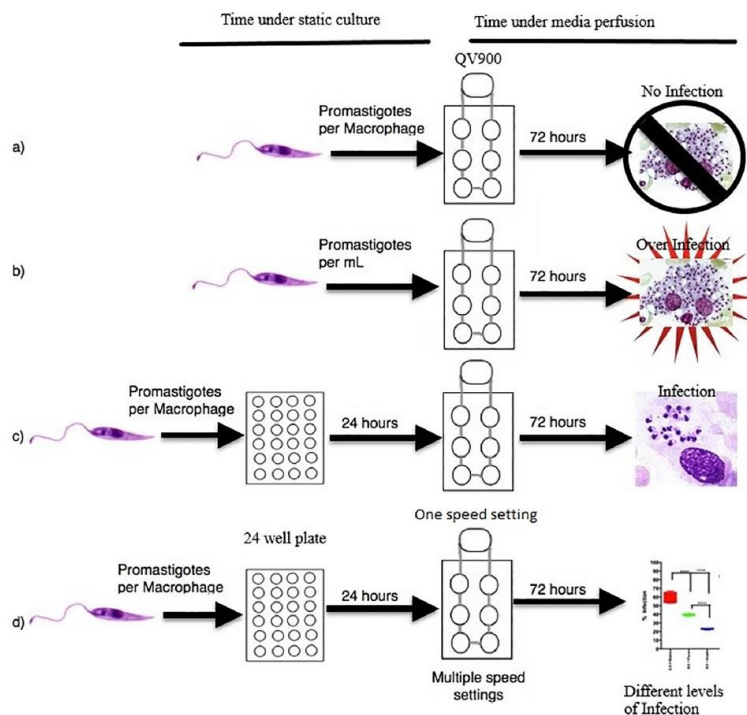


Fig 4. Schematic overview of the initial infection experiments.

<https://doi.org/10.1371/journal.pone.0219985.g004>

work using THP1 cells PEMs were selected for further studies as in this macrophage type infections with *L. major* were easier to establish and to sustain. Peritoneal macrophages at 4×10^5 cells per well were chosen as this concentration gave the most reproducible results following a series of studies at different conditions that were investigated (Fig 4). The initial studies showed that:

1. the addition of parasites in the medium during perfusion, at parasite: macrophage ratios from 0.5:1 to 10:1, resulted in zero macrophage infection after 72 hours and was therefore not pursued.
2. a set number of parasites per ml of circulating media from 4×10^5 to 1.2×10^6 cells per ml caused the parasites to collect within the chambers resulting in over-infection and bursting of the macrophages at the 72 hour time point. This approach was also not pursued.
3. the addition of different numbers of promastigotes before the initiation of media perfusion at parasite:macrophage ratios from 0.5:1 to 25:1 in the medium for a 24 hour pre-infection

before media perfusion resulted in a controllable, reproducible infection after 72 hours. This approach was adopted.

- there were decreased rates of macrophage infection with increasing flow rates from 50 to 360 $\mu\text{l}/\text{min}$ (Fig 5). A flow rate of 360 $\mu\text{l}/\text{min}$ was subsequently selected as it gave an acceptable level of infection.

Infection of mouse peritoneal macrophages (PEMs) in the media perfusion system

The percentage of PEMs infected after 72 hours in each of the three flow conditions i.e. static (0 m/s), base of the chamber (1.45×10^{-9} m/s) and on the insert (1.23×10^{-7} m/s) using different parasite:macrophage ratios are shown in Fig 6. The percentage infection after 24 hours, before the transfer to the media perfusion system, at each of the starting infection ratios were reproducible across all of the infected cultures at that ratio. Mean initial percentage infection

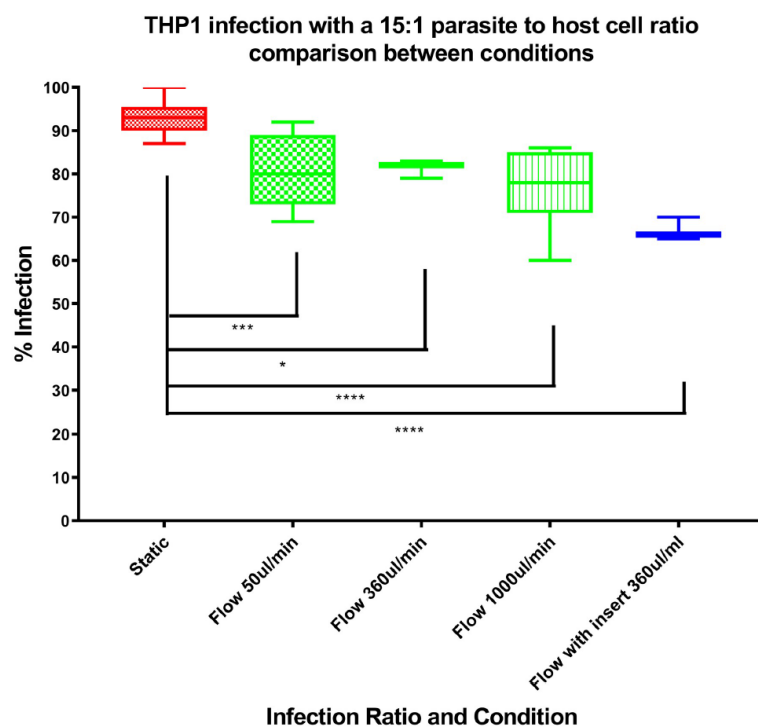


Fig 5. Influence of flow rate on percentage infection at a *L. major* promastigote to macrophage ratio of 15:1.

<https://doi.org/10.1371/journal.pone.0219985.g005>

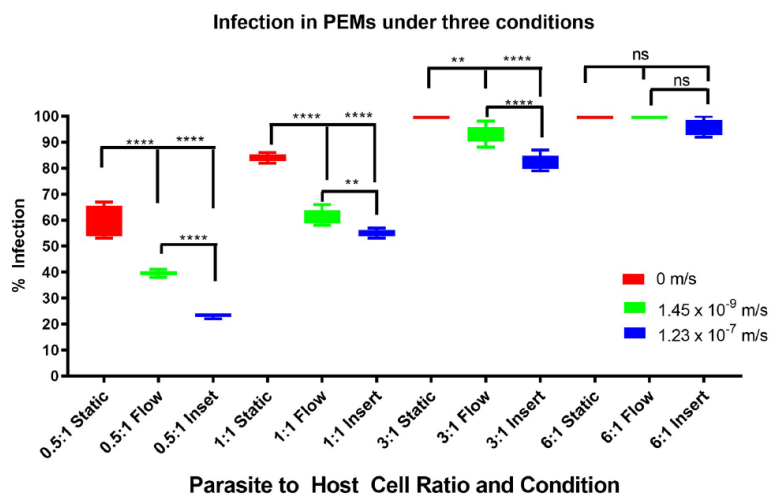


Fig 6. Box and whisker diagram showing the percentage of infected cells over a range of different infection ratios, of parasite: Macrophage number, and different flow conditions. Significance tested using a two tailed t-test $p < 0.01 = **$ $p < 0.0001 = ****$ ns = not significant N = 6.

<https://doi.org/10.1371/journal.pone.0219985.g006>

levels \pm SD after 24 hours were 36 ± 1 , 51 ± 2 , 70 ± 4 and $87 \pm 5\%$ for the four different initial infection ratios of 0.5:1, 1:1, 3:1 and 6:1 parasite concentration to cell concentration. Media perfusion was maintained over the following 72 hours.

As the flow speed of the culture medium was increased from 0 m/s in the static condition to 1.45×10^{-9} m/s to 1.23×10^{-7} m/s (cells on the insert in chambers), the percentage infection of host cells decreased at all parasite to host ratios used (0.5:1, 1:1 and 3:1) (Fig 6). However, the influence of medium flow speed on macrophage infection decreased as the parasite to host ratio increases, until at a parasite to host ratio of 6:1, increasing the flow speed of the culture medium had little effect on the percentage infection levels of the host. As expected increasing the initial parasite to host ratio increases the overall infection levels after 72 hours.

Comparison of data sets showed significant differences (at least $p < 0.01$, by one-way ANOVA) from each other except when comparing the data at the 6:1 ratio (Fig 6).

Incorporation of 5-ethynyl-2'-deoxyuridine (EdU)

The number of amastigotes per macrophage were counted microscopically after 24 hr under the three flow conditions, showing a similar parasite burden with approximately 2 amastigotes per infected cell (Fig 7) across the infected cells that were imaged. Percentage infection rates were identical after the first 24 hr infection (65%) regardless of the speed of media perfusion the cell would be maintained over the following 24 hr. The percentage of amastigotes that incorporated EdU into DNA was significantly lower in cultures maintained under perfusion conditions (Fig 7), with a significant reduction observed (one way ANOVA, $p < 0.05$) in cultures in flow systems compared to static cultures after 24 hr. On average, the mean percentage of amastigotes that incorporated EdU into DNA was $31 \pm 7\%$ in cells maintained in static

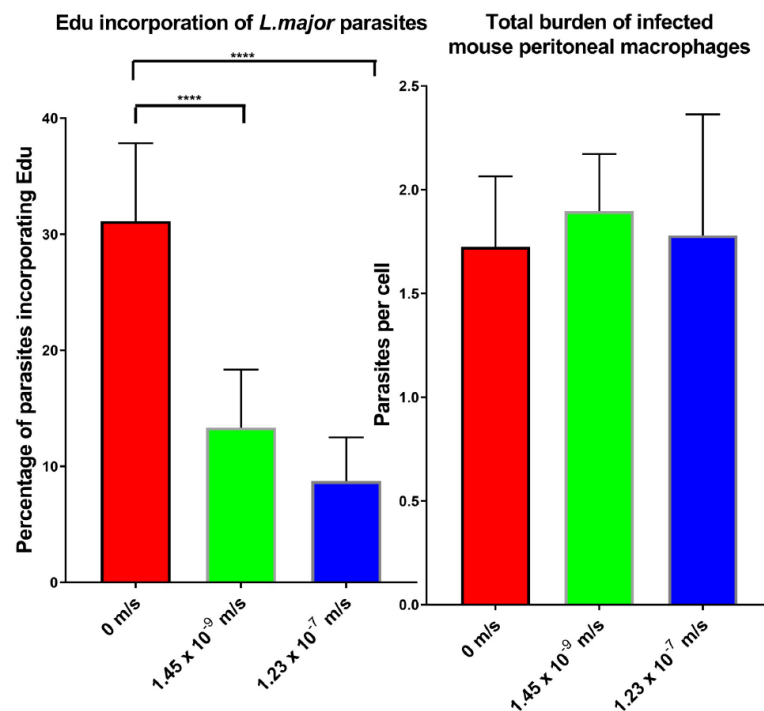


Fig 7. Left: Bar graph showing percentage of *L. major* amastigotes that incorporated the EdU marker into DNA at the three different conditions, static (0m/s), low flow (1.45×10^{-9} m/s) and high flow (1.23×10^{-7} m/s). Right: Bar graph showing parasite burden in mouse peritoneal macrophages, at the three conditions. * = $p < 0.05$ N = 3.

<https://doi.org/10.1371/journal.pone.0219985.g007>

culture, $13 \pm 5\%$ in media flow speed of 1.45×10^{-9} m/s, and $9 \pm 4\%$ when media flow speed was 1.23×10^{-7} m/s.

Macrophage functions

Phagocytosis. Phagocytosis of latex beads by uninfected and infected PEMs showed a clear time dependent response (Fig 8) with phagocytosis increasing with duration of incubation. Phagocytosis was significantly higher ($p < 0.05$ by t-test) in infected macrophages (infection rate of $> 80\%$) compared to uninfected ones ($530 \pm 30 \times 10^5$ versus $421 \pm 30 \times 10^5$) beads/mg protein after 24 hours under static conditions.

Flow conditions caused a significant reduction in phagocytosis by infected macrophages as shown in Fig 9, such that after 24 h of incubation, phagocytosis had significantly decreased from $530 \pm 30 \times 10^5$ beads/mg protein in static cultures to $304 \pm 32 \times 10^5$ beads/mg protein at slow flow speed and $231 \pm 28 \times 10^5$ beads/mg protein at fast flow speed ($p < 0.05$ by one-way ANOVA).

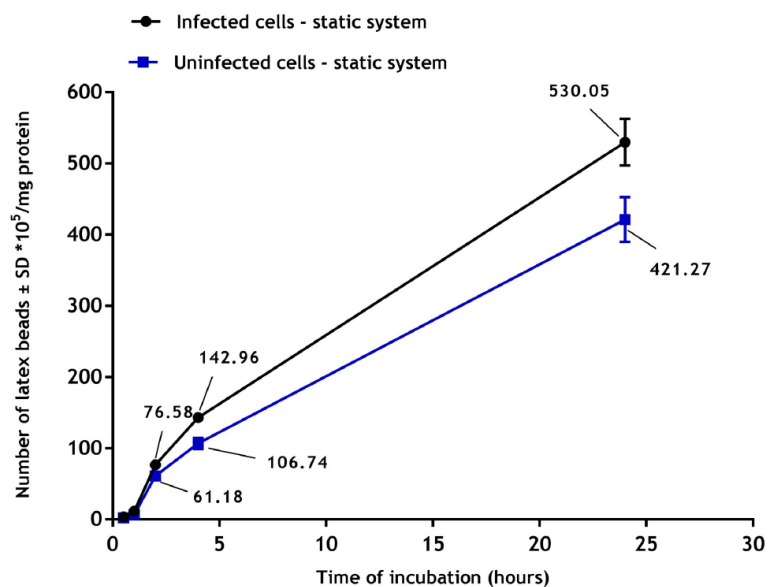


Fig 8. Phagocytosis of fluorescent latex beads (2 μ m) by uninfected and infected PEMs in static culture system. There is a significant increase in phagocytosis by infected PEMs compared to uninfected ones ($p < 0.05$ by t-test). The data show means \pm standard deviations (SD), $N = 3$. Infection rate was $> 80\%$.

<https://doi.org/10.1371/journal.pone.0219985.g008>

Macropinocytosis

Macropinocytosis of pHrodo Red dextran by uninfected and infected PEMs showed a clear time dependent response (Fig 10) with macropinocytosis increasing with duration of incubation. Macropinocytosis was significantly increased in infected PEMs ($p < 0.05$ by t-test) compared to uninfected ones (25 ± 1.1 versus 19 ± 1.0) μ g/mg protein of pHrodo Red dextran after 24 hours of incubation.

Macropinocytosis was significantly reduced under flow conditions (Fig 11), with higher speed of culture medium flow causing greater reduction ($p < 0.05$ by one-way ANOVA) so that after 24 hours of incubation with pHrodo Red dextran, macropinocytosis was 25.3 ± 1.1 , 15.1 ± 0.9 and 9.5 ± 0.9 μ g/mg protein under static, low flow and fast flow respectively.

Discussion

Media perfusion system and modelling

The importance of body fluid flow rates in physiology has been recognized for more than half a century [18]. Understanding the effects of fluid flow on solute transport in biological tissues and on cell-cell signalling and morphogenesis is now substantial. Media perfusion can provide more than just increased cell nourishment, it can also, for example, induce blood and lymphatic capillary morphogenesis *in vitro* [19–21], maintain the functional activity of

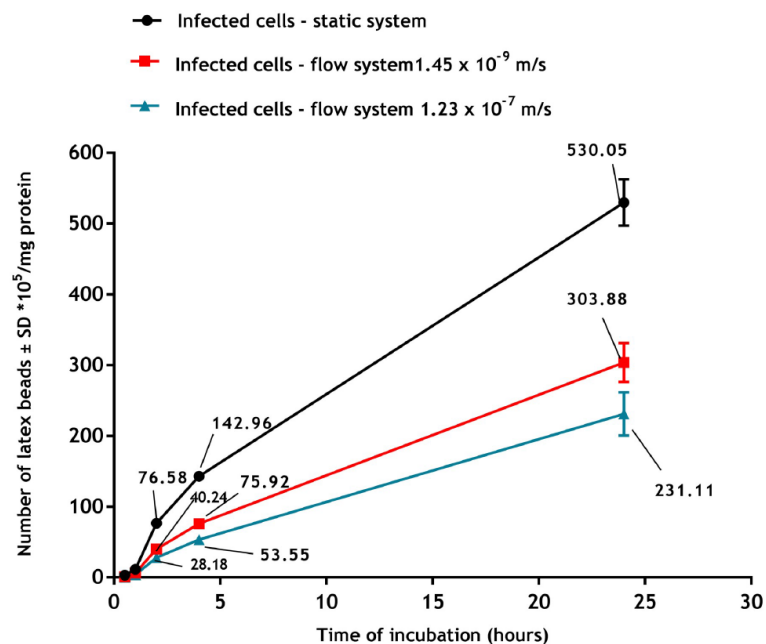


Fig 9. Phagocytosis of fluorescent latex beads (2 μm) by infected PEMs in the three culture systems (static, slow flow rate 1.45 x 10⁻⁹ m/s and fast flow rate 1.23 x 10⁻⁷ m/s). Phagocytosis is significantly higher in static than in flow system ($p < 0.05$ by one-way ANOVA). The data are means ± standard deviations (SD), N = 3. Infection rate > 80%.

<https://doi.org/10.1371/journal.pone.0219985.g009>

chondrocytes and osteocytes [22–25], drive fibroblast differentiation [26] and induce cytokine production by smooth muscle cells [27]. Static systems do not offer any form of dynamic chemical or physical stimulus to cells, such as concentration gradients, flow, pressure, or mechanical stress caused by movement of fluids around them. This is a major limitation in experiments investigating cellular responses *in vitro* since the complex interplay of mechanical and biochemical factors are absent. We used the QV900 system to introduce a fluid flow component to an *in vitro* *L. major* macrophage infection model. In addition, we adapted the QV900 system to enable comparison of the effect of different flow rates to static cultures on infection of macrophages. Experiments were performed with cells cultured at the base of the chamber ('low' flow) and cells cultured on top of a 3D printed insert ('high' flow). The 3D printed insert placed into the chambers enabled us to study media flow speed at the cell surface which is in line with values reported in the literature for interstitial flow in the skin [4,6,7]. Mathematical modelling also showed that cells cultured on the 9mm insert experienced flow speeds and shear stress that were two orders of magnitude higher than those affecting cells cultured at the base of the chamber. Oxygen concentrations at the base of the chambers with the insert were also determined to be higher when compared with the chambers without the insert.

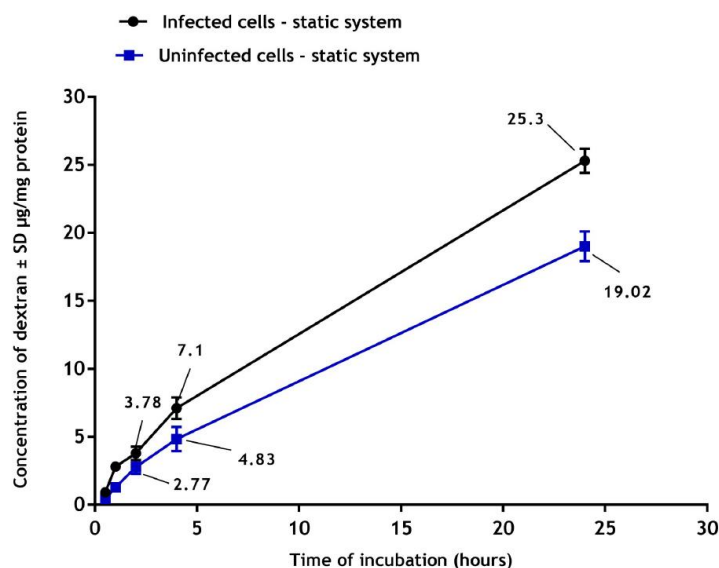


Fig 10. Macropinocytosis of pHrodo Red dextran by uninfected and infected PEMs in static culture system. There is a significant increase in macropinocytosis by infected PEMs compared to uninfected ones ($p < 0.05$ by t-test). The data are means \pm standard deviations (SD), $N = 3$. Infection rate was $> 80\%$.

<https://doi.org/10.1371/journal.pone.0219985.g010>

The significance of our findings is that it is possible to expose cells to vastly different mechanical and chemical environments depending on where they are cultured in the chamber. This is consistent with previous studies where mathematical and computational models showed that changing the geometry of similar perfusion bioreactors has an impact on experimental conditions such as flow speed, shear stress and oxygen concentration [11].

Infection of macrophages in the media perfusion system

The macrophage infection level caused by parasite inocula over the three different conditions varied significantly. Macrophage infection by parasites was reduced by media flow, with significant reductions seen as the media flow speed increased, as shown in Fig 5. This pattern was also seen when using a larger range of initial infection ratios (See S2 File, where we used THP1 cells as the host cells). Possible reasons for the reduction in infection rate with increasing flow rate include: (a) reduced contact time between parasites and cells, (b) increase in the supply of nutrients to the host cells, (c) effect of higher shear stress on receptors, and (d) reduced proliferation of the parasite within the host cell. Promastigotes that are external to the cells but have remained on the glass coverslip may have reduced contact with the cells [28] after transfer to the perfusion system, as they will be pushed away from the cell by the media flow. Without sustained physical contact, the parasites will not be phagocytosed and will not establish an infection within the cell²⁸. A lower probability of parasite invasion into macrophages could lead to

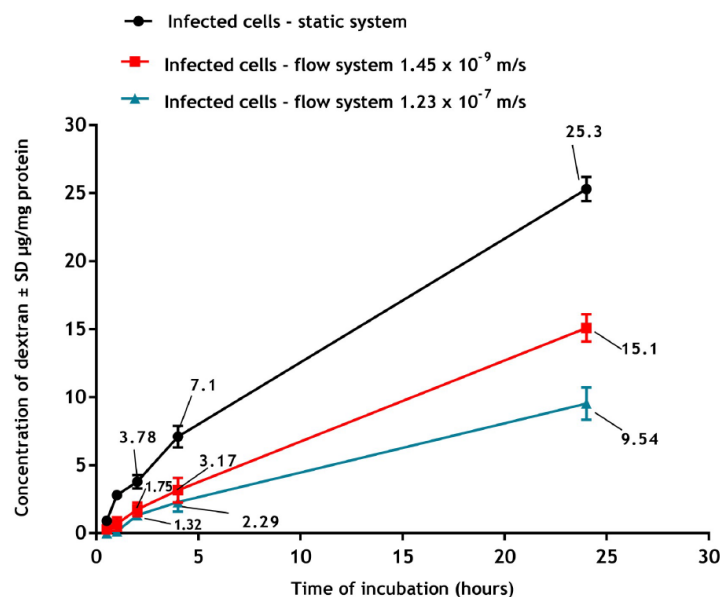


Fig 11. Macropinocytosis of pHrodo Red dextran by infected PEMs at the three culture systems (static, slow flow rate 1.45×10^{-9} m/s and fast flow rate 1.23×10^{-7} m/s). Macropinocytosis is significantly higher in static than in flow systems ($p < 0.05$ by one-way ANOVA). The data are means \pm standard deviations (SD), $N = 3$. Infection rate was > 80 .

<https://doi.org/10.1371/journal.pone.0219985.g011>

a lower infection rate, as fewer parasites would reach the phagolysosome, the site of parasite replication. The first step in the phagocytosis of the *Leishmania* promastigotes is binding to receptors on the cell surface; the Fc receptor (FcR), complement receptor type 3 (CR3), and mannose-fucose receptor have all been shown to be receptors for the parasite [29]. The flow of the media could cause a reduction in binding between the receptor and parasite. Another possible explanation for the effect of media perfusion on the final levels of infection is that the media flow provides more nutrients to the macrophages. Whilst we have considered only oxygen transport in our mathematical modelling, and demonstrated differential concentrations of oxygen at the cell surface with increasing media flow, it follows that the concentration of other important nutrients will be similarly affected. An increased supply of nutrients may provide more starting reagents for the production of anti-parasitic effectors. In addition to this beneficial effect to the host cell, it is possible that the opposite occurs in the parasite, as the parasites could expend more energy [30] resisting the flow of the media reducing successful evasion of the macrophage cellular response and replication once they have been phagocytosed. Cells are sensitive to shear stress and change behaviour depending on physical forces [31,32]. They have been shown to respond to shear stress by changing shape [33], phenotype [34], and release of proteins/chemicals [35]. This stress will undoubtedly have an impact on the phagocytosis process [36].

Another possibility for the lower percentage infection in media perfusion system maintained cultures could be that the rate of parasite proliferation in the host cell is altered. The EdU incorporation assay demonstrated that fewer parasites are actively incorporating the labelled DNA base under media perfusion conditions. Although the average amastigote burden of the PEMs was the same under static, low flow and high flow, the lower EdU incorporation at higher flow speeds shows that parasites were replicating to a lower extent. This is a phenomenon also seen in plankton where increased flow reduces biomass build up [37].

Flow also affected phagocytosis and macropinocytosis of macrophages. Firstly, we established there was a significant increase in both cell functions in PEMs infected with *L. major* compared to uninfected cells. These data are consistent with results described elsewhere, for example macrophages infected with either *L. donovani* or *L. mexicana* increased their pinocytic rates as measured by a fluorescent probe (fluorescein isothiocyanate dextran) [38]. Similar observations have been reported with RAW 264.7 macrophages infected with *L. major* showing increased uptake of fluorescently labelled liposomes [38]. This might be due to morphological changes of the infected cells or the parasitic infection may alter both the metabolic activity of the macrophages and their ability to ingest particulate material [39]. Our results demonstrated that phagocytosis and macropinocytosis were significantly decreased by media flow and that increasing the media flow speed caused a further reduction in the uptake. This is consistent with previous reports of decreased uptake of fluorescein isothiocyanate (FITC)-poly (ethylene glycol) diacrylate particles (200 nm diameter) by human umbilical vein endothelial cells in a dynamic cell culture system exposed to shear stress of 10 dynes/cm² compared to the static culture [40]. Similar findings were also seen with a lower cellular uptake of solid silica particles (350 nm) by RAW 264.7 macrophages under dynamic condition compared with the static culture [41]. One explanation given was that the static system conditions might cause sedimentation of the beads on the cell surface or exposure to higher concentrations of pHrodo Red dextran resulting in a local increase in their concentrations [42]. In contrast, medium flow prevents such localization of materials with subsequently reduced uptake [43].

In conclusion, in the media perfusion *Leishmania*-macrophage model flow speed was shown to affect infection rate even at interstitial fluid rates. This could have an impact on the development of *Leishmania* infection in skin especially when considering the possible higher flow rates in inflammatory sites. The role of mathematical modelling was essential to understanding different chemical and physical conditions resulting from the flow and, highlighting the need for mathematical modelling to be further integrated into this approach. The collateral effects of flow on pathogen replication rate and on host cell metabolism, as indicated by reduction in phagocytosis and macropinocytosis, further indicates research avenues and how these models might be used in studies on immune responses and drug and vaccine discovery. Additionally, our combined experimental and modelling approach has allowed us to generate hypotheses which we will test in future through the development of more advanced mathematical models and experiments.

Supporting information

S1 File. Supplementary material for “Development of a media perfusion model of macrophage infection by *Leishmania major*”.
(DOCX)

S2 File. Supplementary material 2 for “Development of a media perfusion model of macrophage infection by *Leishmania major*”.
(DOCX)

Acknowledgments

AO thanks Dr Vanessa Yardley for mentorship and guidance throughout the project and especially with the animal studies. SM and LH gratefully acknowledge a financial donation from Kirkstall Ltd; this does not alter their adherence to PLOS ONE policies on sharing data and materials.

Author Contributions

Conceptualization: Alec O'Keeffe, Sean McGinty, Simon L. Croft.

Data curation: Lauren Hyndman.

Formal analysis: Alec O'Keeffe, Lauren Hyndman, Sean McGinty.

Funding acquisition: Sean McGinty, Simon L. Croft.

Investigation: Alec O'Keeffe, Lauren Hyndman, Sean McGinty, Alaa Riezk, Simon L. Croft.

Methodology: Alec O'Keeffe, Lauren Hyndman, Sean McGinty, Alaa Riezk.

Project administration: Simon L. Croft.

Software: Sean McGinty.

Supervision: Sean McGinty, Sudaxshina Murdan, Simon L. Croft.

Validation: Alec O'Keeffe.

Visualization: Alec O'Keeffe.

Writing – original draft: Alec O'Keeffe, Lauren Hyndman, Sean McGinty, Alaa Riezk.

Writing – review & editing: Sudaxshina Murdan, Simon L. Croft.

References

1. Horvath P, Aulner N, Bickle M, Davies AM, Del Nery E, Ebner D et al. Screening out irrelevant cell-based models of disease. *Nature Reviews Drug Discovery*. 2016 Nov; 15(11):751. <https://doi.org/10.1038/nrd.2016.175> PMID: 27616293
2. Davies B, Morris T. Physiological parameters in laboratory animals and humans. *Pharmaceutical research*. 1993 Jul 1; 10(7):1093–5. PMID: 8378254
3. Szentistvanyi IS, Patlak CS, Ellis RA, Cserr HF. Drainage of interstitial fluid from different regions of rat brain. *American Journal of Physiology-Renal Physiology*. 1984 Jun 1; 246(6):F835–44.
4. Swartz MA, Fleury ME. Interstitial flow and its effects in soft tissues. *Annu. Rev. Biomed. Eng.* 2007 Aug 15; 9:229–56. <https://doi.org/10.1146/annurev.bioeng.9.060906.151850> PMID: 17459001
5. Reithinger R, Dujardin JC, Louzir H, Pirmez C, Alexander B, Brooker S. Cutaneous leishmaniasis. *The Lancet infectious diseases*. 2007 Sep 1; 7(9):581–96. [https://doi.org/10.1016/S1473-3099\(07\)70209-8](https://doi.org/10.1016/S1473-3099(07)70209-8) PMID: 17714672
6. Dafni H, Israely T, Bhujwalla ZM, Benjamin LE, Neeman M. Overexpression of vascular endothelial growth factor 165 drives peritumor interstitial convection and induces lymphatic drain: magnetic resonance imaging, confocal microscopy, and histological tracking of triple-labeled albumin. *Cancer research*. 2002 Nov 15; 62(22):6731–9. PMID: 12438274
7. Haessler U, Teo JC, Foretay D, Renaud P, Swartz MA. Migration dynamics of breast cancer cells in a tunable 3D interstitial flow chamber. *Integrative Biology*. 2012; 4(4):401–9. <https://doi.org/10.1039/c1ib00128k> PMID: 22143066
8. Kaye P, Scott P. Leishmaniasis: complexity at the host–pathogen interface. *Nature Reviews Microbiology*. 2011 Aug; 9(8):604. <https://doi.org/10.1038/nrmicro2608> PMID: 21747391
9. Tegazzini D, Díaz R, Aguilar F, Peña I, Presa JL, Yardley V et al. A replicative *in vitro* assay for drug discovery against *Leishmania donovani*. *Antimicrobial agents and chemotherapy*. 2016 Jun 1; 60(6):3524–32. <https://doi.org/10.1128/AAC.01781-15> PMID: 27021313

10. Calvo-Álvarez E, Stamatakis K, Punzón C, Álvarez-Velilla R, Tejería A, Escudero-Martínez JM et al. Infrared fluorescent imaging as a potent tool for in vitro, ex vivo and in vivo models of visceral leishmaniasis. *PLoS neglected tropical diseases*. 2015 Mar 31; 9(3):e0003666. <https://doi.org/10.1371/journal.pntd.0003666> PMID: 25826250
11. Mazzei D, Guzzardi MA, Giusti S, Ahluwalia A. A low shear stress modular bioreactor for connected cell culture under high flow rates. *Biotechnology and bioengineering*. 2010 May 1; 106(1):127–37. <https://doi.org/10.1002/bit.22671> PMID: 20091740
12. Ali M, Bahador S. Isolation of infective promastigotes of *Leishmania major* from long-term culture by cocultivation with macrophage cell line. *Biologicals*. 2005 Dec 1; 33(4):257–60. <https://doi.org/10.1016/j.biologicals.2005.06.002> PMID: 16168668
13. Zhang X, Goncalves R, Mosser DM. The isolation and characterization of murine macrophages. *Current protocols in immunology*. 2008 Nov; 83(1):14–1.
14. Callahan HL, Portal IF, Bensinger SJ, Grogl M. *Leishmaniasis*: Temperature Sensitivity of Promastigotes in Vitro as a Model for Tropism in Vivo. *Experimental parasitology*. 1996 Dec 1; 84(3):400–9. <https://doi.org/10.1006/expr.1996.0128> PMID: 8948329
15. Huang M, Khor E, Lim LY. Uptake and cytotoxicity of chitosan molecules and nanoparticles: effects of molecular weight and degree of deacetylation. *Pharmaceutical research*. 2004 Feb 1; 21(2):344–53. PMID: 15032318
16. Lemaire S, Mingot-Leclercq MP, Tulkens PM, Van Bambeke F. Study of macrophage functions in murine J774 cells and human activated THP-1 cells exposed to ornitavancin, a lipoglycopeptide with high cellular accumulation. *Antimicrobial agents and chemotherapy*. 2014 Apr 1; 58(4):2059–66. <https://doi.org/10.1128/AAC.02475-13> PMID: 24449768
17. Xu M, Liu K, Swaroop M, Porter FD, Sidhu R, Finkes S et al. δ -Tocopherol reduces lipid accumulation in Niemann-Pick type C1 and Wolman cholesterol storage disorders. *Journal of Biological Chemistry*. 2012 Nov 16; 287(47):39349–60. <https://doi.org/10.1074/jbc.M112.357707> PMID: 23035117
18. Levick JR. Flow through interstitium and other fibrous matrices. *Experimental Physiology*. 1987 Oct 10; 72(4):409–37.
19. Helm CL, Fleury ME, Zisch AH, Boschetti F, Swartz MA. Synergy between interstitial flow and VEGF directs capillary morphogenesis in vitro through a gradient amplification mechanism. *Proceedings of the National Academy of Sciences of the United States of America*. 2005 Nov 1; 102(44):15779–84. <https://doi.org/10.1073/pnas.0503681102> PMID: 16249343
20. Ng CP, Helm CL, Swartz MA. Interstitial flow differentially stimulates blood and lymphatic endothelial cell morphogenesis in vitro. *Microvascular research*. 2004 Nov 1; 68(3):258–64. <https://doi.org/10.1016/j.mvr.2004.08.002> PMID: 15501245
21. Semino CE, Kamm RD, Lauffenburger DA. Autocrine EGF receptor activation mediates endothelial cell migration and vascular morphogenesis induced by VEGF under interstitial flow. *Experimental cell research*. 2006 Feb 1; 312(3):289–98. <https://doi.org/10.1016/j.yexcr.2005.10.029> PMID: 16337626
22. Buschmann MD, Gluzband YA, Grodzinsky AJ, Hunziker EB. Mechanical compression modulates matrix biosynthesis in chondrocyte/agarose culture. *Journal of cell science*. 1995 Apr 1; 108(4):1497–508. <https://doi.org/10.1038/2191260a0> PMID: 5677422
23. Mow VC, Holmes MH, Lai WM. Fluid transport and mechanical properties of articular cartilage: a review. *Journal of biomechanics*. 1984 Jan 1; 17(5):377–94. PMID: 6376512
24. Grodzinsky AJ, Levenston ME, Jin M, Frank EH. Cartilage tissue remodeling in response to mechanical forces. *Annual review of biomedical engineering*. 2000 Aug; 2(1):691–713.
25. Ng CP, Swartz MA. Mechanisms of interstitial flow-induced remodeling of fibroblast–collagen cultures. *Annals of biomedical engineering*. 2006 Mar 1; 34(3):446–54. <https://doi.org/10.1007/s10439-005-9067-3> PMID: 16482410
26. Wang S, Tarbell JM. Effect of fluid flow on smooth muscle cells in a 3-dimensional collagen gel model. *Arteriosclerosis, thrombosis, and vascular biology*. 2000 Oct 1; 20(10):2220–5. PMID: 11031207
27. Wyler DJ, Sypek JP, McDonald JA. In vitro parasite-monocyte interactions in human leishmaniasis: possible role of fibronectin in parasite attachment. *Infection and immunity*. 1985 Aug 1; 49(2):305–11. PMID: 3160661
28. Guy RA, Belosevic MI. Comparison of receptors required for entry of *Leishmania major* amastigotes into macrophages. *Infection and immunity*. 1993 Apr 1; 61(4):1553–8. PMID: 8454363
29. Martínez-García E, Nikel PI, Chavarría M, Lorenzo V. The metabolic cost of flagellar motion in *Pseudomonas putida* KT2440. *Environmental microbiology*. 2014 Jan 1; 16(1):291–303. <https://doi.org/10.1111/1462-2920.12309> PMID: 24148021

31. Dewey CF, Bussolari SR, Gimbrone MA, Davies PF. The dynamic response of vascular endothelial cells to fluid shear stress. *Journal of biomechanical engineering*. 1981 Aug 1; 103(3):177–85. <https://doi.org/10.1115/1.3138276> PMID: 7278196
32. Kitayama J, Hidemura A, Saito H, Nagawa H. Shear stress affects migration behavior of polymorphonuclear cells arrested on endothelium. *Cellular immunology*. 2000 Jul 10; 203(1):39–46. <https://doi.org/10.1006/cimm.2000.1671> PMID: 10915560
33. Levesque MJ, Nerem RM. The elongation and orientation of cultured endothelial cells in response to shear stress. *Journal of biomechanical engineering*. 1985 Nov 1; 107(4):341–7. <https://doi.org/10.1115/1.3138567> PMID: 4079361
34. Butcher JT, Nerem RM. Valvular endothelial cells regulate the phenotype of interstitial cells in co-culture: effects of steady shear stress. *Tissue engineering*. 2006 Apr 1; 12(4):905–15. <https://doi.org/10.1089/ten.2006.12.905> PMID: 16674302
35. Kuchan MJ, Frangos JA. Shear stress regulates endothelin-1 release via protein kinase C and cGMP in cultured endothelial cells. *American Journal of Physiology-Heart and Circulatory Physiology*. 1993 Jan 1; 264(1):H150–6.
36. Shive MS, Brodbek WG, Colton E, Anderson JM. Shear stress and material surface effects on adherent human monocyte apoptosis. *Journal of biomedical materials research*. 2002 Apr; 60(1):148–58. PMID: 11835170
37. Mampel J, Spirig T, Weber SS, Haagenen JA, Molin S, Hilbi H. Planktonic replication is essential for biofilm formation by *Legionella pneumophila* in a complex medium under static and dynamic flow conditions. *Applied and environmental microbiology*. 2006 Apr 1; 72(4):2885–95. <https://doi.org/10.1128/AEM.72.4.2885-2895.2006> PMID: 16597995
38. Chang KP. Endocytosis of *Leishmania*-infected macrophages. Fluorometry of pinocytic rate, lysosome-phagosome fusion and intralysosomal pH. Elsevier/North-Holland Biomedical Press. 1980; 231–34.
39. Borborema SET, Schwendener RA, O JA Junior, DA HF Junior, and D Nascimento N. Uptake and antileishmanial activity of meglumine antimoniate-containing liposomes in *Leishmania* (*Leishmania*) major-infected macrophages. *International Journal of Antimicrobial Agents*. 2011; 38(4): 341–347. <https://doi.org/10.1016/j.ijantimicag.2011.05.012> PMID: 21783345
40. Jurmey P, Agarwal R, Singh V, Choi D, Roy K, Sreenivasan SV et al. Unique size and shape-dependent uptake behaviors of non-spherical nanoparticles by endothelial cells due to a shearing flow. *J Control Release*. 2017; 245: 170–176. <https://doi.org/10.1016/j.jconrel.2016.11.033> PMID: 27916535
41. Yazdimamaghani M, Barber ZB, Moghaddam SPH, and Ghandehari H. Influence of Silica Nanoparticle Density and Flow Conditions on Sedimentation, Cell Uptake, and Cytotoxicity. *Mol Pharm*. 2018; 15(6): 2372–2383. <https://doi.org/10.1021/acs.molpharmaceut.8b00213> PMID: 29719153
42. Khanbeigi RA, Kumar A, Sadouki F, Lorenz C, Forbes B, Dailey LA et al. The delivered dose: Applying pharmacokinetics to *in vitro* investigations of nanoparticle internalization by macrophages. *J Control Release*. 2012; 162(2): 259–66. <https://doi.org/10.1016/j.jconrel.2012.07.019> PMID: 22824784
43. Mahto SK, Yoon TH, and Rhee SW. A new perspective on *in vitro* assessment method for evaluating quantum dot toxicity by using microfluidics technology. *Biomicrofluidics*. 2010; 4(3).

8.3. Appendix 3: Paper 2

Copyright proof

Reply Reply All Forward
Wed 22/01/2020 13:24

DA Donaldson, Amanda <adonaldson@asmusa.org>
Re: REQUEST TO USE COPYRIGHTED MATERIAL IN THESIS

To Alaa Riezk
Retention Policy Staff mailbox default delete after 7 years (7 years) Expires 20/01/2027

Good morning, Alaa,

Thanks for your message. This paper is being published under an open-access license (<https://creativecommons.org/licenses/by/4.0/>), so permission is not needed. Please see the link for the terms of the license (i.e., attribution).

Best,
Amanda

Amanda Donaldson
Assistant Production Editor
American Society for Microbiology
1752 N Street, NW
Washington, DC 20036
email: adonaldson@asmusa.org

From: Alaa Riezk <alaa.riezk@lshtm.ac.uk>
Sent: Wednesday, January 22, 2020 6:51 AM
To: Donaldson, Amanda
Subject: REQUEST TO USE COPYRIGHTED MATERIAL IN THESIS

Dear Amanda ,

I am currently studying for a PhD at London School of Hygiene and Tropical Medicine.
I am contacting you to seek permission to include the following paper within the electronic version of my PhD thesis:
[Activity of chitosan and its derivatives against *Leishmania* major and *L. mexicana* in vitro].
The thesis will be made available within LSHTM Research Online
<http://researchonline.lshtm.ac.uk/> our institutional repository. The repository is noncommercial and openly available to all.

Yours sincerely,
Alaa

Accepted Manuscript Posted Online

Antimicrob. Agents Chemother. doi:10.1128/AAC.11772-19
Copyright © 2019 Riezk et al.
This is an open-access article distributed under the terms of the Creative Commons Attribution 4.0 International license.

1 Activity of chitosan and its derivatives against *Leishmania* major and *L. mexicana* in
2 vitro.
3 Alaa Riezk ^a, John G Raynes ^a, Vanessa Yardley ^a, Sudarshina Murdan ^a and Simon L.
4 Croft ^a
5
6 ^aDepartment of Infection Biology, London School of Hygiene and Tropical Medicine,
7 London, UK
8 ^bDepartment of Pharmaceutics, UCL School of Pharmacy, University College London,
9 London, UK
10
11
12
13
14
15
16
17 Running Head: Anti-leishmanial activity of chitosan
18 # Corresponding author simon.croft@lshtm.ac.uk
19

1

Accepted Manuscript Posted Online

Antimicrob. Agents Chemother. doi:10.1128/AAC.11772-19
Copyright © 2019 Riezk et al.
This is an open-access article distributed under the terms of the Creative Commons Attribution 4.0 International license.

20 Abstract
21 There is an urgent need for safe, efficacious, affordable and field-adapted drugs for the
22 treatment of cutaneous leishmaniasis which affects around 1.5 million new people
23 worldwide annually. Chitosan, a biodegradable cationic polysaccharide, has previously
24 been reported to have antimicrobial, anti-leishmanial and immunostimulatory activities.
25 We investigated the in vitro activity of chitosan and several of its derivatives and showed
26 that pH of the culture medium plays a critical role on anti-leishmanial activity of chitosan
27 against both extracellular promastigotes and intracellular amastigotes of *Leishmania*
28 major and *Leishmania mexicana*. Chitosan and its derivatives were approximately 7-20
29 times more active at pH 6.5 than at pH 7.5 with high molecular weight chitosan being
30 the most potent. High molecular weight chitosan stimulated the production of nitric oxide
31 and reactive oxygen species by uninfected and *Leishmania* infected macrophages in a
32 time and dose dependent manner at pH 6.5. Despite the in vitro activation of bone
33 marrow macrophages by chitosan to produce nitric oxide and reactive oxygen species,
34 we showed that the anti-leishmanial activity of chitosan was not mediated by these
35 metabolites. Finally, we showed that rhodamine-labelled chitosan is taken up by
36 pinocytosis and accumulates in the parasitophorous vacuole of *Leishmania* infected
37 macrophages.
38 KEYWORDS: Cutaneous leishmaniasis, *Leishmania* major, *Leishmania mexicana*,
39 chitosan, macrophage uptake.
40

2

41 Introduction
42 Leishmaniasis is an infectious disease caused by protozoan parasites belonging to the
43 genus *Leishmania*. The parasite is transmitted between humans and mammalian
44 reservoirs (e.g. dogs and rodents) through the bite of a female phlebotomine sandfly (1).
45 There are two main clinical forms, cutaneous leishmaniasis (CL) and visceral
46 leishmaniasis (VL), with CL being the most common (2). In addition to "simple" CL, there
47 are other complex cutaneous manifestations including mucocutaneous leishmaniasis
48 (MCL), diffuse cutaneous leishmaniasis (DCL), recidivans leishmaniasis (RL) and post-
49 kala-azar dermal leishmaniasis (PKDL) (3, 4).
50 CL is caused mainly by *Leishmania tropica*, *Leishmania major* and *Leishmania*
51 *aethiopica* in the Old World and by *Leishmania braziliensis*, *Leishmania guyanensis*,
52 *Leishmania mexicana* and *Leishmania amazonensis* in the New World(5). Of the 88
53 countries where CL occurs, 90% of the cases are in Afghanistan, Brazil, Iran, Peru,
54 Saudi Arabia and Syria (1). In the mammalian host, the parasite survives and multiplies
55 within macrophages. The cellular immune responses in CL play a critical role in the
56 control and progress of the disease, which include two main mechanisms of
57 macrophage activation: (i) the classical pathway (M1 macrophages) in which Th1 and
58 NK cells produce cytokines (such as IFN- γ) which stimulate the production of nitric oxide
59 (NO) and reactive oxygen species (ROS) and the activation of other lysosomal anti-
60 microbial activities which are responsible for killing the *Leishmania* parasites and (ii) the
61 alternative pathway mediated by Th2 cytokines, such as IL-4 and IL-13 in the early
62 stages of infection forming a favourable environment for *Leishmania* proliferation (6, 7).

3

86 second suggested mechanism is that chitosan binds to microbial DNA and inhibits DNA
87 transcription, assuming that chitosan penetrates the microbial cell membrane and
88 reaches the DNA (19, 20). The third mechanism is via the chitosan chelation of metals
89 and the binding of basic nutrients essential for microbial growth (19). An indirect
90 mechanism of action may be related to the known pro-inflammatory effect of chitosan on
91 macrophages. This involves stimulation of tumour necrosis factor (TNF- α), interleukin 6
92 (IL-6), NO, ROS and interferon gamma (IFN- γ) which play a critical roles in the
93 proinflammatory response against intracellular microbes (by enhancing the production
94 of microbicidal reactive nitrogen species) (21, 22, 23, 24, 25). Chitosan activates
95 polymorphonuclear leukocytes, macrophages and fibroblasts and these properties
96 promote wound healing (18, 26).
97 The poor solubility of chitosan and the loss of the cationic charge at neutral
98 and alkaline environments are two of the major obstacles to the consideration of
99 chitosan as a useful antimicrobial. Recently, the chemical modification of chitosan to
100 produce various derivatives to improve its solubility and widen its application has gained
101 attention (27) (28). Chitosan and its derivatives have been shown to have in vitro anti-
102 leishmanial activity with EC₅₀ values (50% effective concentration) ranging from 70 to
103 240 μ g/ml against *L. infantum*, *L. amazonensis* and *L. chagasi* promastigotes and
104 amastigotes (29, 30, 31, 32, 33, 34). All this makes chitosan an appropriate candidate
105 for further studies to evaluate its suitability for the treatment of CL.
106 The aim of our work was to: (i) determine the in vitro anti-leishmanial activity of chitosan
107 and its derivatives against *L. major* and *L. mexicana* promastigotes and intracellular
108 amastigotes at two different pH values (the culture medium pH of 7.5 and a lower pH of

3

63 Pentavalent antimonial compounds, sodium stibogluconate (Pentostam®) and
64 meglumine antimoniate (Glucantime®), have been the standard treatment for CL for the
65 past 70 years (8). These drugs have several limitations including difficulty of
66 administration, toxicity of the drug and variable sensitivity among *Leishmania* species
67 (9). Second-line treatments include the polyene antifungal amphotericin B which also
68 suffers from toxicity, the oral phospholipid miltefosine, the use of which is limited by
69 teratogenicity, and the aminoglycoside antibiotic paromomycin (PM) which has low cure
70 rates for certain *Leishmania* species (10, 11, 12). Treatment with intravenous
71 AmBisome® (liposomal amphotericin B) is safe and has achieved clinical success at a
72 dose of 3 mg/kg daily for 7 days against CL(13, 14) but the high cost of this formulation
73 limits its use (15). Two Cochrane analyses have clearly shown clinical deficiencies of
74 most drugs. There is an urgent need for new treatments which can eliminate the
75 parasites, improve the healing process, are safe, reliable and also field-adaptable for
76 use in diverse health care systems (16, 17).
77 Chitosan is a biodegradable, biocompatible, positively charged non-toxic muco-
78 adhesive biopolymer produced by the deacetylation of chitin. Chitosan has a pKa of
79 approximately 6.3, is insoluble at alkaline pH but soluble in weak acidic solvents like
80 acetic acid where the amino groups become protonated. Many reports have described
81 the antimicrobial activity of chitosan but the actual mechanism of action has not been
82 fully elucidated (18) although three direct mechanisms have been suggested. The first is
83 the interaction between the protonated NH₃⁺ groups of chitosan and the negative cell
84 membrane of microbes. This interaction changes the permeability of the microbial cell
85 membrane, causing osmotic imbalances, and consequently killing them (18, 19). The

4

109 6.5, which are both suitable for macrophage and parasite growth(35, 36, 37), (ii) to
110 evaluate the in vitro role of chitosan in the activation of macrophage M1 proinflammatory
111 phenotype, via the measurement of NO, ROS and TNF- α production by host cells and
112 by measuring parasite survival, and (iii) investigate chitosan uptake by macrophages to
113 explain its activity against intracellular amastigotes.
114

6

115 **Results**
116
117 *In vitro* activities of chitosan and derivatives against *L. major* and *L. mexicana*.
118 Anti-leishmanial activity (against promastigotes and amastigotes) of high, medium and
119 low molecular weight (HMW, MMW and LMW respectively) chitosan and its derivatives
120 (a total of 11) was tested. Dose dependent activity (Fig S1 and S2) against *Leishmania*
121 promastigotes and amastigotes was observed for chitosan and its derivatives except for
122 carboxymethyl chitosan which showed no activity against either parasite stage within
123 the experimental parameters tested (pH 7.5 or 6.5 and concentrations up to 400 µg/ml).
124 In the 72 h assays, chitosan and its derivatives (except carboxymethyl chitosan) were 7-
125 20 times more active against *L. major* and *L. mexicana* promastigotes and intracellular
126 amastigotes (infecting peritoneal mouse macrophages (PEMs)) in culture medium at
127 pH=6.5 than at pH=7.5 (p<0.05 by t-test) (Tables 1 and 2). HMW, MMW and LMW
128 chitosan, from both crustacean and fungal sources, exhibited significantly higher
129 activities against promastigotes and intracellular amastigotes (EC₅₀ = 6 µg/ml against *L.*
130 *major* promastigotes and 10 µg/ml against *L. mexicana* promastigotes; EC₅₀ = 12 µg/ml
131 against *L. major* amastigotes and 16 µg/ml against *L. mexicana* amastigotes) than the
132 derivatives at pH= 6.5 (Tables 1 and 2) (p<0.05 by an extra sum-of-squares F test).
133 Additionally, *L. major* promastigotes and amastigotes were significantly more sensitive
134 to chitosan and its derivatives than *L. mexicana* promastigotes and amastigotes
135 (approx. 1.5 to 2 times, p<0.05 by an extra sum-of-squares F test).
136 To allow like-for-like comparison, EC₅₀ values were recalculated in terms of molarity
137 using estimated molecular weights (HMW: MW= 342.5 kDa, MMW: MW=250 kDa,

7

138 LMW: MW= 120 kDa and fungal chitosan MW=130 kDa) at pH = 6.5. Based on molarity
139 (Table S4 and S5), HMW chitosan was significantly more active against *L. major* and *L.*
140 *mexicana* promastigotes and amastigotes and hence used in all subsequent studies.
141
142 **Host cell dependence of the anti-leishmanial activity of HMW chitosan at pH 6.5**
143 We aimed to assess the host cell dependence of the anti-leishmanial activity of HMW
144 chitosan and Fungizone by evaluating the *in vitro* activity against *L. major* amastigotes
145 in three different macrophage type; EC₂ and EC₂ values in the three different
146 macrophage populations are summarized in Table 3. There was a significant difference
147 in the activity of HMW chitosan depending on the type of macrophage; PEMs, bone
148 marrow-derived macrophages (BMMs) or human leukaemic monocytes-like derived cell
149 line (THP-1) (p<0.05 by an extra sum-of-squares F test). HMW chitosan was
150 significantly more active against intracellular amastigotes in PEMs and BMMs compared
151 to differentiated THP-1 cells.
152
153 **Effects of HMW chitosan on the production of TNF-α by uninfected or *L. major***
154 **infected BMMs at pH = 6.5**
155 The activation of M1 macrophages by Th1 lymphocyte plays an important role in the
156 control of CL (6, 38, 39). Therefore, we measured TNF-α production by BMMs
157 stimulated by HMW chitosan. Following exposure to HMW chitosan, the TNF-α
158 production by BMMs was found to be dose-dependent, in a bell-shaped manner, in both
159 *Leishmania*-infected and uninfected cells as shown in Fig. 1. After 24 h, the levels of
160 TNF-α in the culture fluid of BMMs exposed to HMW chitosan (at concentrations 14.8,

8

161 44.4 and 133.3 µg/ml) was significantly higher than BMMs (infected and uninfected),
162 that had not been exposed to chitosan with TNF-α being highest at 44.4 µg/ml chitosan.
163 While at other concentrations (1.64, 4.9 and 400 µg/ml), HMW chitosan did not
164 stimulate BMMs to produce TNF-α (p < 0.05 by t-test).
165 HMW chitosan at concentrations 14.8, 44.4 and 133.3 µg/ml stimulated BMMs to
166 produce TNF-α with 87± 4.5 - 71± 9 - 48± 3 pg/ml respectively in uninfected BMMs and
167 56± 3.5 - 46± 10 - 32± 4 pg/ml respectively in *L. major* infected BMMs. Less TNF-α was
168 generated when the chitosan concentration was increased to 133.3 µg/ml and above.
169 Lipopolysaccharides from *Escherichia coli* O26:B6 (LPS; positive control) stimulated
170 TNF-α production in both uninfected and infected BMMs after a 24 h incubation period
171 at a significantly higher level than chitosan (p < 0.05 by t-test). Our results indicated that
172 HMW chitosan activated M1 macrophages.
173
174 **Effects of HMW chitosan on the production of ROS by BMMs at pH = 6.5**
175 ROS plays an important role in the killing of intracellular amastigotes (6, 38, 39)
176 therefore, we measured ROS production by BMMs stimulated by HMW chitosan. HMW
177 chitosan (at concentrations 14.8, 44.4 and 133.3 µg/ml) increased the production of
178 ROS (indicated by H2DCFDA fluorescence) after 4 h of incubation but did not stimulate
179 ROS after 8 h of incubation (Table S1). Other concentrations of HMW chitosan (1.64,
180 4.9 and 400 µg/ml) did not stimulate BMMs to produce ROS after 4 h or 8 h of
181 incubation.

9

182 The ROS dose response in both uninfected and infected BMMs was bell-shaped –
183 similar to that seen with TNF-α. Increasing chitosan concentration from 14.8 to 44.4
184 µg/ml increased ROS production, after which further increase concentration reduced
185 ROS production. In addition, ROS production by BMMs was significantly decreased (p <
186 0.05 by t-test) by infecting the cells with *L. major* as shown in Fig. 2.
187 We found that HMW chitosan had an *in vitro* stimulatory effect on BMMs ROS
188 production after 4h of incubation. We therefore investigated whether this ROS plays any
189 role in the activity of HMW chitosan against intracellular amastigotes. For these
190 experiments, the 4 h post treatment time point was taken because ROS peaked at this
191 point in BMMs in response to chitosan treatment at a time when chitosan does not
192 induce NO in BMMs (*ibid*). Scavenging of ROS by the ROS scavenger, 5mM N-acetyl-
193 L-cysteine (NAC), had no significant impact on the activity of chitosan against
194 intracellular amastigotes (p > 0.05 by t-test) – see Fig. 3. The ROS scavenger caused a
195 complete scavenging of ROS production after 4 h (Table S2) and had no cytotoxicity
196 against KB cells or leishmanicidal activity against *L. major* amastigotes (data not
197 shown). Even though chitosan stimulated ROS production it did not play a role in the
198 anti-leishmanial activity of chitosan.
199
200 **Effects of HMW chitosan on the production of NO by BMMs at pH = 6.5**
201 NO plays an important role in the killing of intracellular amastigotes (6, 38, 39) therefore,
202 we measured NO production by BMMs stimulated by HMW chitosan. We showed that
203 chitosan did not have a stimulatory effect on BMM NO production after 4 h of incubation

10

204 (Table S3). However, after a 24 h incubation, HMW chitosan at pH=6.5 had a
205 stimulatory effect on BMMs NO production in a clear bell-shaped dose dependent
206 manner (Figure 4). HMW chitosan at concentrations of 14.8, 44.4 and 133.3 µg/mL
207 induced both uninfected and infected BMMs to produce NO (at 14.8± 0.3, 34±1.2 and
208 11±1 µM respectively in uninfected BMMs and 11 ±1, 26 ± 2.5 and 8 ± 1.2 µM
209 respectively in infected BMMs), NO being highest at 44.4 µg/mL. While other
210 concentrations of HMW chitosan (1.64, 4.9 and 400 µg/mL) did not stimulate BMMs to
211 produce NO after 24 h of incubation.

212 LPS caused significantly higher NO production compared to HMW chitosan ($p < 0.05$
213 by t-test) in both uninfected and infected BMMs. The levels of NO produced by *L. major*
214 infected BMMs exposed to LPS (positive control) or HMW chitosan were significantly
215 lower than levels produced by uninfected BMMs ($p < 0.05$ by t-test) (Fig 4).

216 As HMW chitosan had an *in vitro* stimulatory effect on BMM NO production after 24h of
217 incubation, we investigated further whether NO has any role in the activity of HMW
218 chitosan against intracellular amastigotes. Inhibition of NO production by the NO
219 inhibitor NG-methyl-L-arginine acetate salt (L-NMMA) at 0.4mM, had no significant
220 influence on the activity of chitosan against intracellular amastigotes ($p > 0.05$ by t-test)
221 (Fig 5), although the NO inhibitor did cause a complete inhibition of NO production
222 (Table S2) after 24 h and had no cytotoxicity effects against KB cells and no
223 leishmanicidal activity against intracellular *L. major* amastigotes (data not shown). Even
224 though chitosan stimulated NO production it did not play a role in the anti-leishmanial
225 activity of chitosan.

226

11

249 in a time-dependent manner. Fig 7 (Panels D and E) shows this uptake after 4 h and 24
250 h respectively, and the accumulation of chitosan in PVs (shown as yellow that indicates
251 co-localization of rhodamine and GFP). Fig 7 (Panel F) also shows that the inhibition of
252 pinocytosis (CME) with dynasore prevented the uptake of chitosan with a negative
253 nMDP colour index that represents no co-localization of chitosan and amastigotes. This
254 is also supporting evidence for the uptake by pinocytosis as seen in Fig 6.

255

256 **Discussion**

257 The literature on the anti-leishmanial activity of chitosan and its derivatives is limited,
258 especially pertaining to its mechanism(s) of action (19, 40, 41). In this study, we
259 assessed the anti-leishmanial activity of various forms of chitosan, including low,
260 medium and high molecular weight chitosan, and chitosan derivatives. Chitosan
261 derivatives are generally produced by chemical modification of the amino or hydroxyl
262 groups of chitosan for the optimization of the physicochemical properties. We found that
263 chitosan and its derivatives had minimal cytotoxicity against KB-cells with LD₅₀ values
264 >750 µg/mL in RPMI 1640 at pH 7.5 or 6.5. This data supports previous reports of
265 chitosan's low cytotoxicity against CCRF-CEM (human lymphoblastic leukaemia) and
266 L132 (human embryonic lung) cells with similar LD₅₀ values (42, 43).

267 We determined that a lower pH 6.5, compared to pH 7.5, enhanced, by 7-20, times the
268 anti-leishmanial activity of chitosan and its derivatives against *L. major* and *L. mexicana*
269 promastigotes and amastigotes. This higher activity of chitosan at the lower pH 6.5
270 could be due to its greater ionisation (protonation of the amino groups; pKa of

13

227 **Cellular uptake of HMW chitosan and inhibition of endocytosis**

228 We found that the activation of M1 macrophages by HMW chitosan did not play a role in
229 its activity against intracellular amastigotes. Therefore, we investigated whether the anti-
230 leishmanial effects of HMW chitosan against intracellular amastigotes after 4 h and 24 h
231 exposure were dependent on the direct activity of chitosan following its entry into the
232 macrophages at pH 6.5. No significant difference was observed in the activity of
233 chitosan against intracellular amastigotes when it was added after prior phagocytosis
234 inhibition with cytochalasin D (Figure 6, $p > 0.05$ by t-test). In contrast, dynasore (an
235 inhibitor of pinocytosis, a clathrin-mediated endocytosis (CME) inhibitor) did significantly
236 affect chitosan mediated parasite killing at pH = 6.5 (Fig. 6, $p < 0.05$ by t-test). The same
237 activity was seen at pH 7.5. – see Fig 6, panel C. The two inhibitors had no cytotoxicity
238 against KB-cells or activity against intracellular *L. major* amastigotes at the
239 concentrations used. Pinocytosis (CME) played a critical role in the efficacy of HMW
240 chitosan against intracellular amastigotes.

241

242 **Fluorescence microscopy of the uptake of chitosan by macrophages**

243 Rhodamine-labelled chitosan was used to track the delivery of chitosan to the
244 parasitophorous vacuole (PV) of *Leishmania* infected macrophages. Fig. 7 illustrates the
245 cellular uptake of chitosan by *L. major*-GFP- or *L. mexicana*-GFP- infected BMMs after
246 4 h and 24 h rhodamine-labelled chitosan exposure. There was co-localization of
247 chitosan and intracellular amastigotes after 4 h and 24 h with nMDP colour index 0.7
248 and 1 respectively (see nMDP material and methods). The uptake of chitosan increased

12

271 chitosan=6.3). The greater positive charge could increase the chitosan antimicrobial
272 activity by interacting with the negatively charged microbial membrane – in accordance
273 with the first postulated mechanism of antimicrobial activity described in the Introduction
274 (18, 19). A higher chitosan activity at lower pH (pH ≈ 5) has previously been reported
275 against *Escherichia coli* and *Salmonella typhimurium* (44, 45).

276 Our study is the first to show the pH dependence of the anti-leishmanial activity of
277 chitosan and its derivatives and could explain why literature reports of the anti-
278 leishmanial activity of chitosan have shown such variability, with EC₅₀ values ranging
279 from 70 to 240 µg/mL against *L. infantum*, *L. amazonensis* and *L. chagasi* promastigotes
280 and amastigotes (29, 30, 31, 32, 33, 34). For example, in one study, the EC₅₀ of
281 chitosan against *L. infantum* amastigotes (in PEMs) in RPMI 1640 medium was 100.81
282 µg/mL, but the pH at which the experiment was conducted was not mentioned (29).
283 Influence of pH was also seen when the anti-leishmanial activity of chitosan (of the
284 different molecular weights) and chitosan derivatives were compared. While the different
285 chitosans and derivatives showed minor differences in their anti-leishmanial activity at
286 pH 7.5, the derivatives were 3 to 5 times less active than the HMW, MMW, LMW and
287 fungal chitosan at lower pH 6.5. This reduced activity could be due to the lower number
288 of amino groups on the chitosan derivatives (see Fig 8). These derivatives are more
289 soluble at a higher pH and have similar activity to chitosan, but at a lower pH the higher
290 protonation of the chitosan improves the anti-leishmanial activity significantly (46, 47).
291 Carboxymethyl chitosan had no anti-leishmanial activity - most of the amino groups on
292 this derivative have been substituted by carboxymethyl moieties making the molecule
293 negatively charged (48).

14

294 The higher anti-leishmanial activity of HMW chitosan compared to MMW and LMW
295 chitosan mirrors its greater antibacterial activity in another study against *Escherichia*
296 *coli*, *Pseudomonas aeruginosa* and *Staphylococcus aureus* (49). HMW has a long
297 chain, and therefore more glucosamine units, and possesses more amino groups (Fig 8)
298 resulting in more protonated groups (-NH³⁺) than MMW and LMW(49) which could
299 explain its greater potency.

300 We also showed that the anti-leishmanial activity of chitosan is significantly greater
301 against *L. major* infected PEMs or BMMs compared to differentiated THP-1 cells in the
302 order PEMs-BMMs-THP-1 cells underlining the need to take the host cell into
303 consideration when conducting similar experiments(50).

304 In order to understand the potential anti-amastigote mechanism(s) of chitosan, we
305 investigated whether the activity of HMW chitosan against the intracellular amastigotes
306 was via direct uptake into the host cell and localisation in the parasitophorous vacuole
307 or indirectly via the activation of M1 macrophages, given that the cellular immune
308 responses in cutaneous leishmaniasis play a critical role in self-cure (51, 52).

309 The activation of M1 macrophages by Th1 lymphocyte subpopulation, which produces
310 different cytokines, primarily IFN- γ and TNF- α , is crucial for the killing of the intracellular
311 *Leishmania* via the triggering of an oxidative burst and therefore, the host cells increase
312 the production of ROS and NO which are responsible for killing of the parasite (38, 39).

313 We found that HMW chitosan stimulated TNF- α production by macrophages and this
314 would be expected to be an indicator of an M1 macrophage that would have greater
315 leishmanicidal activity. Our results show that chitosan stimulated BMMs ROS production
316 with a peak after 4 h and led to a significant increase in the TNF- α and NO production

11

Downloaded from <http://aac.asm.org/> on January 27, 2020 at LONDON SCHOOL OF HYGIENE & TROPICAL MEDICINE

317 after 24 h in a bell-shaped response. Similar findings have been reported showing that
318 HMW chitosan had *in vitro* stimulatory effect on NO production in PEMs (from male rats)
319 (25) and LMW chitosan stimulated RAW264.7 macrophage TNF- α production (24).
320 Another study demonstrated that LMW chitosan induced ROS production in an
321 epithelial, human breast cancer cell line (53). The bell-shaped responses are consistent
322 with a study that showed that chitosan stimulated NO and TNF- α production in
323 peritoneal macrophages in a dose-dependent manner and their levels tended to
324 decrease at higher concentrations of chitosan (320 μ g/ml) (54). This type of response
325 has also been reported previously for tucareosol for both, its immunomodulatory and
326 activity against experimental *L. donovani* infections, albeit at lower doses (55). Despite
327 the observed chitosan-induced ROS and NO production, there was no evidence that
328 this contributed to the anti-leishmanial activity in our study – the inhibitors that we used
329 to suppress their production had no effect on the ability of chitosan to kill intracellular
330 *Leishmania* amastigotes (Figs 3 and 5). This led us to investigate the cellular uptake of
331 HMW chitosan and its relationship to the anti-leishmanial activity.

332 The uptake of the large charged molecule HMW chitosan has not been systematically
333 studied before and there is no clear evidence of its penetration of cell membranes or of
334 its uptake mechanism. Macrophages are known to take up extracellular materials and
335 plasma by endocytosis. Endocytosis mainly occurs via two different cellular uptake
336 mechanisms: pinocytosis or phagocytosis, where pinocytosis is fluid-phase endocytosis
337 and phagocytosis is the process of engulfing large particles (56). Inhibition of
338 pinocytosis (CME) significantly reduced the anti-leishmanial activity of HMW chitosan.
339 Therefore, in our study pinocytosis (CME) was considered to be the main mechanism

16

Downloaded from <http://aac.asm.org/> on January 27, 2020 at LONDON SCHOOL OF HYGIENE & TROPICAL MEDICINE

340 for the uptake of HMW chitosan by BMMs, indicating a direct anti-leishmanial effect of
341 this molecule against amastigotes. Other studies have previously reported pinocytosis
342 as the pathway for the uptake of chitosan of different molecular weights by HEK293
343 epithelial cells (57). The fluorescence imaging in our study showed that in BMMs HMW
344 chitosan is taken up into the parasitophorous vacuole (PV) where the *Leishmania*
345 parasites reside, with the labelled chitosan being internalized within 4 h and increasing
346 up to 24 h later. This is consistent with another study where rhodamine isothiocyanate-
347 chitosan (RITC-chitosan 98-10 K) was found to be directly delivered to the U937
348 macrophage lysosome after 24 h (58). The accumulation of chitosan in the PV might be
349 due to chitosan's relatively high pKa of 6.3, making it more soluble and protonated in the
350 acidic contents of the vacuole. This is consistent with a study using bafilomycin to inhibit
351 acidification and prevent chitosan accumulation within macrophages (58).

352 In summary, our studies indicate that chitosan and its water-soluble derivatives showed
353 anti-leishmanial activity against both *L. major* and *L. mexicana* promastigotes and
354 amastigotes in a pH dependent manner. At pH 6.5 HMW chitosan is more active than
355 MMW and LMW chitosan and chitosan derivatives, in particular those where the amino
356 groups are substituted. In addition, HMW chitosan activated M1 macrophages,
357 stimulating them to produce NO and ROS. However, the anti-leishmanial activity of
358 chitosan was not due to such immune activation, as an NO inhibitor and a ROS
359 scavenger failed to reduce the anti-leishmanial activity. Instead, the anti-leishmanial
360 activity was related to direct uptake of chitosan into the parasitophorous vacuole by
361 pinocytosis (CME). HMW chitosan demonstrated effective *in vitro* anti-leishmanial

17

Downloaded from <http://aac.asm.org/> on January 27, 2020 at LONDON SCHOOL OF HYGIENE & TROPICAL MEDICINE

362 activity with minimal cytotoxicity and future work will focus on *in vivo* studies,
363 formulations and routes of administration.

364

365 **Materials and methods**

366

367 (i) **Drugs and chemicals**

368 Stocks of amphotericin B deoxycholate (5.2 mM [ag]) (Fungizone, Gibco, UK) were
369 prepared, aliquoted, and kept at -20°C until use. Chitosan with three different molecular
370 weights and its derivatives were used and are summarised in Table 1 (28, 59, 60, 61).
371 Solutions of chitosan and derivatives were prepared by dissolving 1 g in 100 ml of 1%
372 (v/v) acetic acid solution at room temperature with continuous stirring for 24 h until a
373 clear solution was obtained. The pH of the solution was adjusted to approximately 6 by
374 adding sodium hydroxide 2N (NaOH, Sigma, UK) solution with a pH meter (Orion Model
375 420A). The chitosan solutions were autoclaved (121 °C, 15 mins). Phosphorylcholine
376 substituted chitosan was kindly provided by Prof F Winnik (Montreal University, Canada)
377 generated through reductive amination of PC-glyceraldehyde with primary amines of
378 deacetylated chitosan (57kD). Percentage of substitution was controlled and determined
379 by NMR (28). Chitosan pKa is approximately 6.3 and therefore, the approximate
380 ionisation degree of chitosan is a 61% and 6% at pH 6.5 and 7.5 respectively.

381

18

Downloaded from <http://aac.asm.org/> on January 27, 2020 at LONDON SCHOOL OF HYGIENE & TROPICAL MEDICINE

(ii) Ethics statement.

All animal work is carried out under a UK Home Office project licence according to the Animal (Scientific Procedures) Act 1986 and the new European Directive 2010/63/EU. The Project Licence (7018427) has been reviewed by LSHTM Animal Welfare & Ethical Review Board prior to submission and consequent approval by the UK Home Office.

(iii) Cell lines

Preparation of macrophages

- Peritoneal mouse macrophages (PEMs) were obtained from 8-12 week old female CD1-mice (Charles River Ltd, UK). Two ml of a 2% (w/v) starch solution in phosphate buffered saline (PBS, Sigma, UK) was injected intraperitoneally (IP). After 24 h, the animal was sacrificed and the PEMs were harvested by peritoneal lavage with cold RPMI 1640 medium (Sigma, UK) containing 200 units penicillin and 0.2 mg streptomycin/mL (PenStrep, Sigma, UK). Subsequently, PEMs were centrifuged at 450 g at 4°C for 15 min and then the pellet was resuspended in RPMI 1640 with 10% (v/v) heat-inactivated fetal calf serum (HFCS; Gibco, UK).
- Bone marrow-derived macrophages (BMMs) were obtained from femurs of 8-12 week old female BALB/c mice (Charles River Ltd). Briefly, the bone marrow cells were carefully flushed from the bone with Dulbecco's Modified Eagle's Medium (DMEM; ThermoFisher, UK) with 10% (v/v) HFCS, 100 U/mL penicillin and 100 mg/mL streptomycin (Sigma, UK). Cells were pelleted by centrifugation (450 g, 10 min) and re-suspended in 10mL DMEM with 10% (v/v) HFCS and human macrophage colony stimulating factor 50ng/mL (hM-CSF; ThermoFisher, UK).

19

After plating out in T175 flasks (Greiner Bio-One, Stonehouse, UK), BMMs were kept at 37°C, 5% CO₂ for 7-10 days after which they were harvested, counted and used.

- THP-1 cell is a human leukemic monocyte-like derived cell line. THP-1 cells were cultured in RPMI 1640 medium supplemented with L-glutamine and 10% HFCS. THP-1 cells were incubated in RPMI 1640 plus 10% (v/v) HFCS and 20 ng/mL phorbol 12-myristate 13-acetate (PMA; Sigma, UK) at 37°C and 5% CO₂ for 72 h to induce maturation transformation of these monocytes into adherent macrophages (50).

Human squamous carcinoma (KB) cells are adherent cells derived from epidermal carcinoma from the mouth. KB cells were cultured in RPMI 1640 medium 10% HFCS.

The number of cells and macrophages was estimated by counting with a Neubauer haemocytometer by light microscopy (x 400 total magnification).

(iv) Parasites

Four *Leishmania* species; two GFP labelled species (*L. major* (MHOM/SU/73/5ASKH) and *L. mexicana* (MNYC/BZ/62/M379), kindly donated by Dr. G Getti (University of Greenwich, UK) were used for the fluorescence microscope study. They were cultured in Schneider's insect medium (Sigma, UK) with 23% (v/v) HFCS, 1× penicillin-streptomycin-glutamine (Gibco-Invitrogen) and supplemented with 700 µg/mL G418 (an aminoglycoside antibiotic, Sigma, UK). *L. major* (MHOM/SA/85/UISH118) and *L. mexicana* (MNYC/BZ/62/M379) were used for other experiments as described, minus the G418. Promastigotes were incubated at 26°C, maximum passage number used = 7.

20

(v) *In vitro* cytotoxicity assays

Re-suspended KB cells (4×10^4 /100µL) were allowed to adhere to the bottom of 96-well plate overnight and then exposed to specific concentrations of the compounds for 72 h at 37°C and 5% CO₂ incubator. Podophyllotoxin (Sigma, UK) was included as a positive control at a starting concentration of 0.05 µM. Cytotoxicity was evaluated by a cell viability assay using the resazurin sodium salt solution (AlamarBlue, Sigma, UK) which was prepared according to the manufacturer's instructions. 20µL of the resazurin solution was added to each well of the plates and fluorescence (cell viability/622) was measured over a period of 1 to 24 h using a Spectramax M3 plate reader (EX/EM 530 / 580 nm and 550 nm cut off). Results were expressed as percentage inhibition = $(100 - \text{x})\%$ viability (means \pm standard deviation σ). Cytotoxicity was evaluated in RPMI 1640 at two pH values (at normal pH of RPMI 7.5 and at a lower pH 6.5). The pH of RPMI 1640 was reduced from 7.5 to 6.5 by adding 0.05M acidic buffer, 2-N-morpholino ethanesulfonic acid (MES, Sigma, UK). RPMI 1640 plus MES (0.05M) at pH=6.5 did not show any cytotoxicity to KB-cells.

(vi) *In vitro* 72 h activity of chitosan and its derivatives against extracellular *L. major* and *L. mexicana* promastigotes

Promastigotes in RPMI 1640 medium were tested while in the exponential growth phase. The promastigotes were diluted to a density of 5×10^6 promastigotes/mL and then exposed to different concentrations of (HMW, MMW, and LMW) chitosan, chitosan derivatives and Fungizone (positive control) in sterile 96-well flat bottom culture plates for 72 h at 26°C. The activity of the compounds against promastigotes was evaluated using the Alamar Blue™ assay as previously described. pH plays a critical role in the

21

solubility and protonation of chitosan, so the activity against promastigotes was evaluated at two different pH values (pH=7.5 and a lower pH of 6.5 by adding MES). Results were expressed as percentage inhibition= $100\% - \text{x}\%$ viability (means \pm SD).

(vii) *In vitro* 72- hour activity of chitosan and its derivatives against intracellular amastigotes of *L. major* and *L. mexicana*

100µL of PEMs culture at 4×10^5 cells/mL, dispensed into each well of a 16-well LabTek tissue culture slide (Thermo Fisher, UK) at pH 7.5 or pH 6.5 and incubated for 24 h at 37 °C in 5 % CO₂. After 24 h, the wells were washed with fresh culture medium to remove non-adherent cells. Stationary phase, low-passage-number *Leishmania* promastigotes were then added at a ratio of 5 :1 PEM. This infection ratio was previously found to give sufficiently high and reproducible infection levels. Slides were incubated for another 24h at 34 °C to mimic dermal temperatures in 5 % CO₂. Any free, extracellular parasites were removed by washing the wells with cold culture medium. One slide was fixed with 100 % methanol for 2 min and stained with 10 % Giemsa for 5 minutes. The number of PEMs infected with *Leishmania* amastigotes per 100 macrophages was microscopically counted. All the experiments were conducted at macrophages infection levels above 80% prior to addition of chitosan. Chitosan, its derivatives and Fungizone® solutions at a range of concentrations (in quadruplicate) were added to the wells (100µL) and the slides were incubated for 72 h at 34 °C in 5 % CO₂. After 72 h, the slides were fixed with 100% methanol for 2 min and stained with 10% Giemsa for 5 min. The slides were examined and the % of macrophages infected was counted. The anti-leishmanial activity of compounds was expressed as percentage

22

471 reduction in infected macrophages compared to untreated control wells (63). RPMI 1640
472 plus MES (0.05M) with pH=6.5 had no activity against *Leishmania* amastigotes.
473 (viii) Influence of the origin of the host cell on the in vitro activity of HMW
474 chitosan against *L. major* amastigotes
475 A further two host cell types, THP-1 and BMMs were infected with *Leishmania* major
476 and the activity of HMW chitosan was assessed. THP-1 cells (cultured in RPMI 1640 +
477 10% HFCS) and BMMs (cultured in DMEM + 10% HFCS) were used to assess the
478 host cell dependence of the anti-leishmanial activity of HMW chitosan(50). The
479 experiment was conducted as described in section (vii) at pH 6.5.
480 (ix) The role of HMW chitosan on BMMs activation
481 We chose BMMs to evaluate the activation effects of HMW chitosan and to study the
482 cell uptake of chitosan as this macrophage population is more homogenous than PEMs
483 and THP-1 cells (64); both PEMs and BMMs have been reported to have a similar acidic
484 pH ~ 5.5 of parasitophorous vacuoles of *L. amazonensis* infected PEMs and BMMs (65,
485 66, 67). 100µL of BMMs (4×10^5 /ml) in DMEM at pH=6.5 were dispensed into each well
486 of 96 well plates (standard clear plates for nitric oxide assay and black wall/clear bottom
487 plates for ROS and TNF- α assay) and incubated for 24 h at 37 °C in 5 % CO₂. Plates
488 were washed with DMEM to remove non-adherent macrophages. *L. major* at 1:5 ratio (5
489 parasites per host cell) was then added to the wells and the plates were incubated for
490 24 h at 34 °C in 5 % CO₂ to allow infection of the adherent macrophages. After 24 h
491 incubation with macrophages, infection rate more than 80%. The effects of HMW

23

492 chitosan on BMMs activation was determined by quantifying the release of TNF- α , ROS
493 and NO, as described below at pH 6.5.
494 A. Measurement of TNF- α
495 HMW chitosan at concentrations of 1.64, 4.9, 14.8, 44.4, 133.3 and 400 µg/ml was
496 added to infected and uninfected macrophages (section x) and the plates were
497 incubated for 4, 24 h at 34°C in 5% CO₂. Lipopolysaccharides from *Escherichia coli*
498 O26:B6 (LPS, 100ng/ml; Sigma, UK) was used as a positive control and inducer. TNF- α
499 release by the BMMs was measured using a mouse TNF- α ELISA kit (ab208348,
500 abcam, UK) according to the manufacturer's instructions using a Spectramax M3
501 microplate reader (wavelength 450 nm).
502 B. Measurement of ROS
503 ROS was measured using a 2',7'-dichlorofluorescein diacetate (DCFDA, cellular
504 reactive oxygen species detection assay kit, abcam, UK). Uninfected and infected
505 macrophages were treated with 25 µM DCFDA in PBS for 45 min at 37°C and then
506 washed once in the buffer. The cells were cultured at 34°C in 5% CO₂ for 0.5, 1, 2, 4, 8
507 and 24 h, with 1.64, 4.9, 14.8, 44.4, 133.3 and 400 µg/ml of HMW chitosan or in the
508 presence of H₂O₂ (25mM) (Thermofisher, UK) as a positive control in DMEM + 10%
509 HFCS (pH=6.5) in quadruplicate wells. In some experiments, cells were pre-treated
510 with a selective inhibitor of ROS, N-acetyl-L-cysteine (NAC, 5mM, Sigma, UK), for 2 h
511 before the addition of the inducer or chitosan. At 0.5, 1, 2, 4, 8 and 24 h the plates were
512 read, using a Spectramax M3 microplate reader (Ex=485nm, Em=535nm).
513 C. Measurement of NO

24

514 NO was measured using Griess reagent (Thermofisher, UK). HMW chitosan at
515 concentrations of 1.64, 4.9, 14.8, 44.4, 133.3 and 400 µg/ml was added to infected and
516 uninfected macrophages and the plates were incubated at 4, 24 h at 34°C in 5% CO₂.
517 LPS (100ng/ml) was used as a positive control. In some experiments, cells were pre-
518 treated with selective inhibitor of nitric oxide with NG-methyl-L-arginine acetate salt (0.4
519 mM, L-NMMA; Sigma, UK) for 2 h before the addition of LPS. NO was quantified
520 according to the kit protocol. Briefly, 150µl of the cell culture supernatants (particulates
521 were removed by centrifugation) was mixed gently with 150µl of the Griess reagent in a
522 96 well plates and the mixture was incubated for 30 minutes at room temperature. The
523 absorbance was measured using a Spectramax M3 plate reader (wavelength 548 nm).
524 Sodium nitrite (Sigma, UK) at different concentrations was used to create a standard
525 curve(68).
526 (x) Uptake of chitosan by macrophages
527 The uptake of HMW chitosan was evaluated using two methods. The first method used
528 two endocytosis inhibitors; cytochalasin D (1µg/ml, Sigma, UK) which is a phagocytosis
529 inhibitor and dynasore (30 µg/ml, Sigma, UK) which inhibits pinocytosis (clathrin-
530 mediated endocytosis (CME) by blocking GTPase activity of dynamin) (69, 70, 71). The
531 second method used dynasore and rhodamine-labelled chitosan (MW 200 kDa,
532 Creative PEGWorks, USA) to track cellular uptake of chitosan over time by fluorescence
533 microscopy.
534
535

25

536 A. Activity of chitosan after inhibition of the endocytic pathway of BMMs
537 100µL of BMMs culture (4×10^5 /ml) in DMEM at pH 6.5 or pH=7.5 were dispensed into
538 each well of 16-well LabTek™ culture slides and were infected with stationary phase *L.*
539 *major* promastigotes. Some of the infected BMMs were pretreated with dynasore (30
540 µg/ml) or cytochalasin D (1µg/ml) for two hours. Subsequently, HMW chitosan was
541 added to each well at concentrations of 1.64, 4.9, 14.8, 44.4, 133.3 and 400 µg/ml and
542 macrophages were incubated for 4 or 24 h at 34 °C in 5 % CO₂. After each point, the
543 slides were examined as described in section (vii).The inhibition activity of the uptake
544 (phagocytosis or pinocytosis) of the two inhibitor was evaluated by using a fluorescence
545 plate reader, by using fluorescent latex beads and pHrodo™ Red dextran (72). We
546 showed that cytochalasin caused 94 and 84% phagocytosis inhibition of fluorescent
547 latex beads (Sigma-Aldrich, UK) after 4 h and 24 h respectively and dynasore caused
548 95 and 90% pinocytosis inhibition of pHrodo™ Red dextran (MW= 10,000 MW, Thermo
549 Fisher, UK) after 4h and 24h respectively (Table S6).
550 B. Microscopic imaging of the cellular uptake of rhodamine-labelled chitosan
551 The qualitative characterisation of chitosan uptake of cells was carried out by wide field
552 microscopy (Nikon Ti-E inverted microscope). Briefly, after deriving BMMs, 500µl of the
553 BMMs (in DMEM plus 10% HFCS at pH 6.5, 4×10^4 macrophages per ml) was seeded
554 on each well of a 4-well LabTek tissue culture slide (Thermo Fisher, UK) and incubated
555 for 24h at 37°C in 5% CO₂. Subsequently, 5 µg/ml Hoechst 33342 stain (EvEm =
556 350/461 nm, Thermofisher, UK) as a nuclear dye was added and the slides were
557 incubated for 30 min at 37°C in 5% CO₂. The macrophages were washed with PBS, *L.*
558 *major*-GFP of *L. mexicana*-GFP was then added, at a ratio of 10:1 and further incubated

26

559 for 24h at 34°C in 5% CO₂ (We used 10:1 ratio not 5:1 as previously as at this
560 experiment different species of *L. major*-GFP and *L. mexicana*-GFP were used and the
561 ratio 10:1 was sufficient to obtain a high infection rate). Macrophages were then washed
562 with PBS and 500 µl of LysoTracker® for Red (50 nM, Ex/Em: 647/668nm; Thermo
563 Fisher, UK) was added to each well. The labelled, infected macrophages were then
564 exposed to 30 µg/ml rhodamine-labelled chitosan (MW 200kDa, Creative PEGWorks,
565 USA) in 500 µl of fresh DMEM plus 10% HFCS pH 6.5 and incubated for 4 h and 24h
566 at 37°C with live imaging at each time point. In some experiments, infected BMMs were
567 pre-incubated with dextranose 30 µg/ml for 2 h before adding rhodamine-labelled
568 chitosan. All the images were collected using a Nikon Ti-E inverted microscope
569 equipped with (63x objective) using Nikon Elements software. Three images for each
570 experiment were then analysed using ImageJ software. The degree of correlation
571 between pixels in the red and green channels was assessed by the Colocalization
572 Colormap plugin in the ImageJ software. This plugin enables quantitative visualisation of
573 colocalization by calculating the normalized mean deviation product (nMDP) in a colour
574 nMDP scale (from -1 to 1); negative refers (cold colours) to no colocalization while
575 indexes more than 0 (hot colours) display colocalization and the higher number refers to
576 more colocalization (73, 74).

577 (xi) Statistical analysis.

578 Dose-response curves and EC₅₀ values were calculated using GraphPad Prism®
579 version 7.02 software and the corresponding sigmoidal dose-response curves were
580 established by using a nonlinear fit with variable slope models. Results represent means
581 ± SD. EC₅₀ values were compared by using extra-sum-of-squares F tests. 1 test was

27

592 References.

- 593
- 594 1. Reithinger R, Dujardin J-C, Louzir H, Pirmes C, Alexander B, Brookler S. 2007.
595 Cutaneous leishmaniasis. The Lancet Infectious Diseases 7:561-566.
- 596 2. Alvar J, Velez ID, Bern C, Herrero M, Desjeux P, Cano J, Jannin J, den Boer M.
597 2012. Leishmaniasis worldwide and global estimates of its incidence. PLoS One
598 7:e35671.
- 599 3. Croft SL, Sundar S, Faircliff AH. 2006. Drug Resistance in Leishmaniasis.
600 Clinical Microbiology Reviews 19:1111.
- 601 4. Stenvik D. 2017. The history of leishmaniasis. Parasit Vectors 10:82.
- 602 5. De Luca PM, Macedo ABB. 2016. Cutaneous Leishmaniasis Vaccination: A
603 Matter of Quality. Frontiers in Immunology 7:151-151.
- 604 6. da Silva Santos C, Brodsky CI. 2014. The Role of CD4 and CD8 T Cells in
605 Human Cutaneous Leishmaniasis. Front Public Health 2:165.
- 606 7. Liu D, Uzonon JE. 2012. The early interaction of Leishmania with macrophages
607 and dendritic cells and its influence on the host immune response. Frontiers in
608 cellular and infection microbiology 2:83-83.
- 609 8. Garner T, Croft SL. 2002. Topical treatment for cutaneous leishmaniasis. Curr
610 Opin Investig Drugs 3:538-44.
- 611 9. Blum J, Desjeux P, Schwartz E, Beck B, Hatz C. 2004. Treatment of cutaneous
612 leishmaniasis among travellers. J Antimicrob Chemother 53:158-65.
- 613 10. Winant CJ, Van Bocklaere K, Yandley V, Harris A, Morden S, Croft SL. 2018.
614 Relation between Skin Pharmacokinetics and Efficacy in Ambisome Treatment of
615 Murine Cutaneous Leishmaniasis. Antimicrob Agents Chemother 62.
- 616 11. Yandley V, Croft SL. 1997. Activity of liposomal amphotericin B against
617 experimental cutaneous leishmaniasis. Antimicrobial agents and chemotherapy
618 41:752-756.
- 619 12. Organizaçao WH. 2010. Control of the leishmaniasis: report of a meeting of the WHO
620 Expert Committee on the Control of Leishmaniasis, on World Health Organization.
621 <http://apps.who.int/media/doc/default.aspx/10665/44412>. Accessed 22-29 March.
- 622 13. Wortmann G, Zapor M, Rössner R, Fraser S, Hartzell J, Pierson J, Weintrob A,
623 Magill A. 2010. Liposomal amphotericin B for treatment of cutaneous
624 leishmaniasis. Am J Trop Med Hyg 83:1026-33.
- 625 14. Aronson N, Herwaldt BL, Libman M, Pearson R, Lopez-Velez R, Weina P,
626 Carvalho E, Ephros M, Jeronimo S, Magill A. 2017. Diagnosis and Treatment of
627 Leishmaniasis: Clinical Practice Guidelines by the Infectious Diseases Society of
628 America (IDSA) and the American Society of Tropical Medicine and Hygiene
629 (ASTMH). The American journal of tropical medicine and hygiene 96:24-45.
- 630 15. Tuman TS, Santos AO, Ueda-Nakamura T, Filho BP, Nakamura CV. 2011.
631 Recent advances in leishmaniasis treatment. Int J Infect Dis 15:625-32.
- 632 16. Gonzalez U, Pinart M, Rieck L, Alvar J. 2008. Interventions for Old World
633 cutaneous leishmaniasis. Cochrane Database Syst Rev
634 doi:10.1002/14651858.CD005067.pub3.CD005067.

29

582 used to compare differences between means of two or more groups respectively and p
583 values of 0.05 were considered statistically significant.

584 Acknowledgements

585 Alaa Rieck's doctoral project received funding from the London School of Hygiene and
586 Tropical Medicine (LSHTM) and the Council for At-Risk Academics (CARA, UK).

587 We are grateful to Dr S. Somavaram (UCL School of Pharmacy) and Dr K. Van
588 Bocklaere (University of York) for supply of chemicals and helpful discussions. The
589 authors acknowledge the facilities and the scientific and technical assistance of the
590 LSHTM Wolfson Cell Biology Facility, with specific thanks to Dr. E. McCarthy.

591

35

- 615 17. Gonzalez U, Pinart M, Rieck L, Pardo M, Macaya A, Alvar J, Tweed JA. 2009.
616 Interventions for American cutaneous and mucocutaneous leishmaniasis.
617 Cochrane Database Syst Rev
618 doi:10.1002/14651858.CD004434.pub2.CD004434.
- 619 18. Cheung RC, Ng TS, Wong JH, Chan WY. 2015. Chitosan: An Update on
620 Potential Biomedical and Pharmaceutical Applications. Mar Drugs 13:5156-86.
- 621 19. Goy RC, Brito DD, Assis CBG. 2009. A review of the antimicrobial activity of
622 chitosan. Polimeros 19:241-247.
- 623 20. Hadwiger LA, Kendra DF, Frittersky BW, Wagoner W. 1986. Chitosan Both
624 Activates Genes in Plants and Inhibits RNA Synthesis in Fungi. p 239-214. In
625 Muzzarelli R, Jeuniaux C, Gooday GW (ed). Chitin in Nature and Technology
626 doi:10.1007/978-1-4613-2167-5_28. Springer US, Boston, MA.
- 627 21. Sarkar K, Xue Y, Sant S. 2017. Host Response to Synthetic Versus Natural
628 Biomaterials, p 81-105. In Corradetti B (ed). The Immune Response to Implanted
629 Materials and Devices: The Impact of the Immune System on the Success of an
630 Implant doi:10.1007/978-3-319-45433-7_5. Springer International Publishing,
631 Cham.
- 632 22. Porporato C, Bianco ID, Riera CM, Correa SC. 2003. Chitosan induces different
633 L-arginine metabolic pathways in resting and inflammatory macrophages.
634 Biochem Biophys Res Commun 304:266-72.
- 635 23. Ravindranathan S, Koppolu BP, Smith SG, Zakhoff DA. 2016. Effect of Chitosan
636 Properties on Immunoreactivity. Marine drugs 14:91.
- 637 24. Wu N, Wen ZS, Xiang XW, Huang YN, Gao Y, Qu YL. 2015. Immunostimulative
638 Activity of Low Molecular Weight Chitosans in RAW264.7 Macrophages. Mar
639 Drugs 13:6210-25.
- 640 25. Peluso G, Petillo C, Ranieri M, Santini M, Ambrosio L, Calabrò D, Avalone B,
641 Balsano G. 1994. Chitosan-mediated stimulation of macrophage function.
642 Biomaterials 15:1215-1220.
- 643 26. Dai T, Tanaka M, Huang Y-Y, Hamblin MR. 2011. Chitosan preparations for
644 wounds and burns: antimicrobial and wound-healing effects. Expert review of
645 anti-infective therapy 9:857-879.
- 646 27. Fu X, Shen Y, Jiang X, Huang D, Yan Y. 2011. Chitosan derivatives with dual-
647 antibacterial functional groups for antimicrobial finishing of cotton fabrics.
648 Carbohydrate Polymers 85:221-227.
- 649 28. Tiera MJ, Guo XP, Bedhaouch S, Shi Q, Fernandes JC, Winik FM. 2006.
650 Synthesis and characterization of phosphorylcholine-substituted chitosans
651 soluble in physiological pH conditions. Biomacromolecules 7:3151-6.
- 652 29. Pujals G, Bure-Negre JM, Perez P, Garcia E, Portu M, Tico JR, Minarro M,
653 Carrio J. 2008. In vitro evaluation of the effectiveness and cytotoxicity of
654 meglumine antimonate microspheres produced by spray drying against
655 Leishmania infantum. Parasitol Res 102:1243-7.
- 656 30. Ribeiro TG, Chaves-Fumagalli MA, Valadares DG, Franca JR, Rodrigues LB,
657 Duarte MC, Lage PS, Andrade PFR, Lage DP, Amada LV, Abades DR, Costa
658 LE, Martins VT, Tavares CAP, Castanho RO, Coelho EAF, Faraco AAO. 2014.
659 Novel targeting using nanoparticles: an approach to the development of an
660 effective anti-leishmanial drug-delivery system. International journal of
661 nanomedicine 9:877-890.

35

- 682 31. Salari-Tazdabi R, Tazdabi D, Hamzai Z, Eddakka N, Momeni N. 2015. Antiparasitic Activity of Chitosan doi:10.17758/UR.U0615223.
- 683
- 684 Bahrami S, Esmailzadeh S, Zarei M, Ahmad F. 2015. Potential application of
- 685 nanochitosan film as a therapeutic agent against cutaneous leishmaniasis
- 686 caused by L. major. *Parasitol Res* 114:4617-24.
- 687 33. Hosseini MH, Moradi M, Alimohammadian MH, Shahgoli VK, Dorati H, Rostami A.
- 688 2016. Immunotherapeutic effects of chitin in comparison with chitosan against
- 689 *Leishmania* major infection. *Parasitol Int* 65:96-104.
- 690 34. Ashana S, Jaiswal AK, Gupta PK, Pawar VK, Dube A, Chourasia MK. 2013.
- 691 Immunomodulant chemotherapy of visceral leishmaniasis in hamsters using
- 692 amphotericin B-encapsulated nanoemulsion template-based chitosan
- 693 nanocapsules. *Antimicrob Agents Chemother* 57:1714-22.
- 694 35. McKidams TA, Miller WM, Papadoulakis ET. 1997. Variations in culture pH affect
- 695 the cloning efficiency and differentiation of progenitor cells in *ex vivo*
- 696 haemopoiesis. *Br J Haematol* 97:889-95.
- 697 36. Fernandes AC, Soares DC, Saraiva EM, Meyer-Fernandes JR, Souto-Padron T.
- 698 2013. Different secreted phosphatase activities in *Leishmania* amazonensis.
- 699 *FEMS Microbiol Lett* 340:117-28.
- 700 37. Xu W, Xin L, Soong L, Zhang K. 2011. Sphingolipid degradation by *Leishmania*
- 701 major is required for its resistance to acidic pH in the mammalian host. *Infection*
- 702 and *Immunity* 179:3377-3387.
- 703 38. Gupta G, Oghumu S, Satskar AR. 2013. Mechanisms of immune evasion in
- 704 leishmaniasis. *Adv Appl Microbiol* 82:155-84.
- 705 39. Scott P, Novais FO. 2016. Cutaneous leishmaniasis: immune responses in
- 706 protection and pathogenesis. *Nat Rev Immunol* 16:581-92.
- 707 40. Ballica-Ramirez A, Wojtas-Pajak A, Piarczyk B, Ramirez A, Laurans L. 2005.
- 708 Antibacterial and antifungal activity of chitosan, vol 2.
- 709 Sharmagum A, Kathiresan K, Nayak L. 2015. Preparation, characterization and
- 710 antibacterial activity of chitosan and phosphorylated chitosan from cuttlebone of
- 711 *Sepia kobeensis* (Hoyle, 1885). *Biotechnology reports* (Amsterdam, Netherlands)
- 712 9:25-30.
- 713 42. Kean T, Thanou M. 2010. Biodegradation, biodistribution and toxicity of chitosan.
- 714 *Adv Drug Deliv Rev* 62:3-11.
- 715 Richardson SC, Kolbe HV, Duncan R. 1999. Potential of low molecular mass
- 716 chitosan as a DNA-delivery system: biocompatibility, body distribution and ability
- 717 to complex and protect DNA. *Int J Pharm* 178:231-43.
- 718 43. Andia N, Daglie F, Heuzey MC, Ag A. 2017. Effect of Chitosan Physical Form on
- 719 Its Antibacterial Activity Against Pathogenic Bacteria. *J Food Sci* 82:3779-868.
- 720 44. Tsai GJ, Su WH. 1999. Antibacterial activity of shrimp chitosan against
- 721 *Escherichia coli*. *J Food Prot* 62:239-43.
- 722 45. Saharun P, Masson M. 2017. Antimicrobial Chitosan and Chitosan Derivatives: A
- 723 Review of the Structure-Activity Relationship. *Biomacromolecules* 18:3646-3668.
- 724 47. Seyfarth F, Schliemann S, Eiserich P, Hiper UC. 2008. Antifungal effect of high-
- 725 and low-molecular-weight chitosan hydrochloride, carboxymethyl chitosan,
- 726 chitosan oligosaccharide and N-acetyl-D-glucosamine against *Candida albicans*,
- 727 *Candida krusei* and *Candida glabrata*. *International Journal of Pharmaceutics*
- 728 353:139-148.

31

- 729 48. Qiu M, Wu C, Ren G, Liang X, Wang X, Huang J. 2014. Effect of chitosan and its
- 730 derivatives as antifungal and preservative agents on postharvest green
- 731 asparagus. *Food Chem* 155:105-11.
- 732 49. Jeon Y-J, Park P-J, Kim S-K. 2001. Antimicrobial effect of chitooligosaccharides
- 733 produced by bioreactor. *Carbohydrate Polymers* 44:71-76.
- 734 50. Seifert K, Escobar P, Croft SL. 2010. In vitro activity of anti-leishmanial drugs
- 735 against *Leishmania donovani* is host cell dependent. *J Antimicrob Chemother*
- 736 65:508-11.
- 737 51. Green SJ, Scheller LF, Marietta MA, Seguin MC, Klotz FW, Slayter M, Nelson
- 738 BJ, Nacy CA. 1994. Nitric oxide: cytokine-regulation of nitric oxide in host
- 739 resistance to intracellular pathogens. *Immunol Lett* 43:87-94.
- 740 52. Tokura S, Tamura H, Azuma I. 1999. Immunological aspects of chitin and chitin
- 741 derivatives administered to animals. *Evs* 87:278-92.
- 742 53. Salehi F, Behboudi H, Kavousi G, Ardeshani SK. 2017. Chitosan promotes ROS-
- 743 mediated apoptosis and S phase cell cycle arrest in triple-negative breast cancer
- 744 cells: evidence for intercalative interaction with genomic DNA. *RSC Advances*
- 745 7:43141-43150.
- 746 54. Li H, Shi B, Yan S, Zhao T, Li J, Guo X. 2014. Effects of Chitosan on the
- 747 Secretion of Cytokines and Expression of Inducible Nitric Oxide Synthase mRNA
- 748 in Peritoneal Macrophages of Broiler Chicken. *Brazilian Archives of Biology and*
- 749 *Technology* 57:466-471.
- 750 55. Smith AC, Yardley V, Rhodes J, Croft SL. 2000. Activity of the Novel
- 751 Immunomodulatory Compound Tucareosol against Experimental Visceral
- 752 Leishmaniasis. *Antimicrob Agents and Chemotherapy* 44:1464-1468.
- 753 56. Soltani T, Schliwa M. 2006. Powering membrane traffic in endocytosis and
- 754 recycling. *Nat Rev Mol Cell Biol* 7:897-908.
- 755 57. Hoemann CD, Guzman-Morales J, Tran-Khanh N, Lavallee G, Jolicoeur M,
- 756 Lavertu M. 2013. Chitosan rate of uptake in HEK293 cells is influenced by
- 757 soluble versus microparticle state and enhanced by serum-induced cell
- 758 metabolism and lactate-based media acidification. *Molecules* 18:1015-35.
- 759 58. Fong D, Gregoire-Gelinas P, Cheng AP, Mecherilsky T, Lavertu M, Sato S,
- 760 Hoemann CD. 2017. Lysosomal rupture induced by structurally distinct chitosans
- 761 either promotes a type 1 IFN response or activates the inflammasome in
- 762 macrophages. *Biomaterials* 129:127-138.
- 763 59. Szczepanska J, Pawlowska E, Synowiec E, Czarny P, Rekas M, Blasiaz J,
- 764 Szaflik JP. 2011. Protective effect of chitosan oligosaccharide lactate against
- 765 DNA double-strand breaks induced by a model methacrylate dental adhesive.
- 766 Medical science monitor : international medical journal of experimental and
- 767 clinical research 17:BR201-BR208.
- 768 60. Abrica-Gonzalez P, Zamora-Justo JA, Sotelo-Lopez A, Vazquez-Martinez GR,
- 769 Balderas-Lopez JA, Mullick-Diosdado A, Ibanez-Hernandez M. 2019. Gold
- 770 nanoparticles with chitosan, N-acetylated chitosan, and chitosan oligosaccharide
- 771 as DNA carriers. *Nanoscale Research Letters* 14:258.
- 772 61. Tzanava D, Simitchiev A, Pelkova N, Nenov V, Stoyanova D, Denev P. 2017.
- 773 Synthesis of Carboxymethyl Chitosan and its Rheological Behaviour in
- 774 Pharmaceutical and Cosmetic Emulsions, vol 7.

32

819 Tables:

- 775 62. Barros LM, Duarte AE, Moraes-Braga MF, Waczuk EP, Vega C, Leite NF, de
- 776 Menezes IR, Coutinho HD, Rocha JB, Kamdem JP. 2016. Chemical
- 777 Characterization and Trypanocidal, Leishmanicidal and Cytotoxicity Potential of
- 778 *Lantana camara* L. (Verbenaceae) Essential Oil. *Molecules* 21.
- 779 63. Wijntant GJ, Van Boocklaer K, Yardley V, Murdan S, Croft SL. 2017. Efficacy of
- 780 Panomycin-Chloroquine Combination Therapy in Experimental Cutaneous
- 781 Leishmaniasis. *Antimicrob Agents Chemother* 61.
- 782 64. Zhao Y-L, Tian P-X, Han F, Zheng J, Xia X-X, Xue W-J, Ding X-M, Ding C-G.
- 783 2017. Comparison of the characteristics of macrophages derived from murine
- 784 spleen, peritoneal cavity, and bone marrow. *Journal of Zhejiang University*
- 785 *Science B* 18:1025-1033.
- 786 65. Chang KP. 1980. Endocytosis of *Leishmania*-infected macrophages. Fluorometry
- 787 of pinocytic rate, lysosome-phagosome fusion and intralysosomal pH. p 231-234.
- 788 Elsevier/North-Holland Biomedical Press. Amsterdam, The
- 789 Antoine JC, Prina E, Jouanne C, Bongrand P. 1990. Parasitophorous vacuoles of
- 790 *Leishmania* amazonensis-infected macrophages maintain an acidic pH. *Infect*
- 791 *Immun* 58:770-777.
- 792 67. Miguel DC, Yokoyama-Yasunaka JK, Andreoli WK, Mortara RA, Uliana SR.
- 793 2007. Tamoxifen is effective against *Leishmania* and induces a rapid
- 794 alkalization of parasitophorous vacuoles harbouring *Leishmania* (*Leishmania*)
- 795 *amazonensis* amastigotes. *J Antimicrob Chemother* 60:526-34.
- 796 68. Flores N, Correa-Azogue N, Amenta M, Ambrunnen A, Creus C, Lamattina L.
- 797 2016. Detection of Nitric Oxide and Determination of Nitrite Concentrations in
- 798 *Arabidopsis thaliana* and *Azospirillum brasilense*. *Bio-protocol* 6:e1765.
- 799 69. Dulla D, Donaldson JS. 2012. Search for inhibitors of endocytosis. Intended
- 800 specificity and unintended consequences. *Cell Logist* 2:203-208.
- 801 70. Kruth HS, Jones NL, Huang W, Zhao B, Ishii I, Chang J, Combs CA, Malide D,
- 802 Zhang WY. 2005. Macropinocytosis is the endocytic pathway that mediates
- 803 macrophage foam cell formation with native low density lipoprotein. *J Biol Chem*
- 804 280:2352-60.
- 805 71. Michael DR, Ashlin TG, Davies CS, Gallagher H, Stoneman TW, Buckley ML,
- 806 Rami DP. 2013. Differential regulation of macropinocytosis in macrophages by
- 807 cytokines: Implications for foam cell formation and atherosclerosis. *Cytokine*
- 808 64:357-61.
- 809 72. O'Keefe A, Hyndman L, McGinty S, Rieck A, Murdan S, Croft SL. 2019.
- 810 Development of an in vitro media perfusion model of *Leishmania* major
- 811 macrophage infection. *PLoS one* 14:e0219685-e0219685.
- 812 73. Jaskolski F, Mule C, Manzoni OJ. 2005. An automated method to quantify and
- 813 visualize colocalized fluorescent signals. *J Neurosci Methods* 146:42-9.
- 814 74. Valiante S, Falanga A, Cigliano L, Iachetta G, Busiello RA, La Merca V, Galdiero
- 815 M, Lombardi A, Galdiero S. 2015. Peptide gH625 enters into neuron and
- 816 astrocyte cell lines and crosses the blood-brain barrier in rats. *Int J*
- 817 *Nanomedicine* 10:1885-98.
- 818

33

TABLE 1 In vitro activity of chitosan and its derivatives against promastigotes at two pH values

Compound	pH 5.5				pH 6.5			
	L. major		L. mexicana		L. major		L. mexicana	
	EC ₅₀ µg/ml	EC ₅₀ µg/ml	EC ₅₀ µg/ml	EC ₅₀ µg/ml	EC ₅₀ µg/ml	EC ₅₀ µg/ml	EC ₅₀ µg/ml	EC ₅₀ µg/ml
Funigzone	0.05 ± 0.01	0.3 ± 0.02	0.14 ± 0.01	0.3 ± 0.02	0.07 ± 0.02	0.3 ± 0.1	0.15 ± 0.07	0.3 ± 0.02
HMW chitosan	105 ± 12	165 ± 52	165 ± 12	210 ± 108	6.5 ± 0.5	37 ± 9	10.5 ± 1.4	59 ± 33
LMW chitosan	117 ± 4	207 ± 80	150 ± 10	222 ± 401	6.2 ± 0.3	43 ± 9	10.5 ± 1.4	84 ± 27
FWW chitosan	118 ± 11	123 ± 58	187 ± 13	222 ± 703	6.7 ± 0.3	40 ± 9	10.5 ± 1.4	84 ± 26
Fungal chitosan	118 ± 11	122 ± 58	187 ± 13	187 ± 580	6.2 ± 0.3	43 ± 9	10.5 ± 1.4	67 ± 17
Chitosan oligosaccharide	133 ± 13	185 ± 30	190 ± 20	255 ± 481	8.5 ± 0.4	44 ± 32	75 ± 3.7	432 ± 38
Chitosan oligosaccharide lactate	88 ± 9	122 ± 10	124 ± 14	78 ± 63	14 ± 0.1	13 ± 2	23 ± 1.4	11 ± 2
Chitosan HCl	86 ± 9	118 ± 21	110 ± 24	142 ± 18	13 ± 0.1	11 ± 3	20 ± 2.4	20 ± 1
PC1-CHPheopropionate substituted chitosan	117 ± 20	187 ± 20	174 ± 4	283 ± 432	15.9 ± 2.0	30 ± 2.2	33 ± 4.0	33 ± 4.0
PC2-CH	154 ± 8	148 ± 29	170 ± 8	244 ± 371	18.6 ± 2.7	33 ± 4.0	30 ± 2.4	28 ± 0.3
PC3-CH	117 ± 19	185 ± 36	187 ± 16	177 ± 580	23.3 ± 2.5	27 ± 4.4	37 ± 2.5	44 ± 0.5
Carboxymethyl chitosan	No activity up to 400 µg/ml							

Experiments were conducted in triplicate cultures, data expressed as mean ± SD (experiment was reproduced further two times with confirmed similar data not shown). Statistically significant differences were found for the EC₅₀ values of chitosan and its derivatives at pH 5.5 and pH 6.5 by using t-test. L. major promastigotes were significantly more susceptible to chitosan and derivatives than L. mexicana (p<0.05 by an extra sum-of-squares F test). Penicillamine & dimethylsulfoxide (DMSO) were used as a positive control. Both when alone pH 5.5 and chitosan solvent did not show any activity against promastigotes.

20

TABLE 2 In vitro activity of chitosan and its derivatives against amastigotes infecting PEMs and their cytotoxicity

Compound	pH 5.5				pH 6.5			
	L. major		L. mexicana		L. major		L. mexicana	
	EC ₅₀ µg/ml	EC ₅₀ µg/ml	EC ₅₀ µg/ml	EC ₅₀ µg/ml	EC ₅₀ µg/ml	EC ₅₀ µg/ml	EC ₅₀ µg/ml	EC ₅₀ µg/ml
Funigzone	0.07 ± 0.01	0.15 ± 0.05	0.15 ± 0.05	0.15 ± 0.05	0.09 ± 0.01	0.15 ± 0.05	0.15 ± 0.05	0.15 ± 0.05
HMW chitosan	105 ± 12	165 ± 52	165 ± 12	210 ± 108	6.5 ± 0.5	37 ± 9	10.5 ± 1.4	59 ± 33
LMW chitosan	117 ± 4	207 ± 80	150 ± 10	222 ± 401	6.2 ± 0.3	43 ± 9	10.5 ± 1.4	84 ± 27
FWW chitosan	118 ± 11	123 ± 58	187 ± 13	222 ± 703	6.7 ± 0.3	40 ± 9	10.5 ± 1.4	84 ± 26
Fungal chitosan	118 ± 11	122 ± 58	187 ± 13	187 ± 580	6.2 ± 0.3	43 ± 9	10.5 ± 1.4	67 ± 17
Chitosan oligosaccharide	133 ± 13	185 ± 30	190 ± 20	255 ± 481	8.5 ± 0.4	44 ± 32	75 ± 3.7	432 ± 38
Chitosan oligosaccharide lactate	88 ± 9	122 ± 10	124 ± 14	78 ± 63	14 ± 0.1	13 ± 2	23 ± 1.4	11 ± 2
Chitosan HCl	86 ± 9	118 ± 21	110 ± 24	142 ± 18	13 ± 0.1	11 ± 3	20 ± 2.4	20 ± 1
PC1-CH	144 ± 10	120 ± 2	169 ± 12	202 ± 2	88 ± 3	34 ± 28	81.7 ± 8	27 ± 38
PC2-CH	133 ± 8	185 ± 36	187 ± 16	177 ± 580	23.3 ± 2.5	27 ± 4.4	37 ± 2.5	44 ± 0.5
PC3-CH	153 ± 11	148 ± 29	170 ± 8	244 ± 371	18.6 ± 2.7	33 ± 4.0	30 ± 2.4	28 ± 0.3
Carboxymethyl chitosan	No activity up to 400 µg/ml							

Experiments were conducted in quadruplicate cultures, data expressed as mean ± SD (experiment was reproduced further two times with confirmed similar data not shown). Statistically significant differences were found between the EC₅₀ values of chitosan and its derivatives at pH 5.5 and pH 6.5 by using t-test. Chitosan and its derivatives did not show cytotoxicity at both pH values 5.5 and 6.5 against the cells. There was no significant difference in the cytotoxicity of three test pH values (p<0.05 by t-test). No statistically significant difference was found in EC₅₀ values when alone versus between three types of chitosan and other derivatives against the cells. Penicillamine & dimethylsulfoxide (DMSO) were used as a positive control. Both when alone pH 5.5 and chitosan solvent did not show any activity against amastigotes.

21

TABLE 3 HMW chitosan activity against L. major amastigotes in three different macrophage cultures after 72 h at pH 6.5

Host cell / infection rate % at 24 h	HMW chitosan		Funigzone	
	EC ₅₀ µg/ml	EC ₅₀ µg/ml	EC ₅₀ µM	EC ₅₀ µM
PEMs / > 80%	10.31 ± 1.22*	89.07 ± 20.46	0.02 ± 0.004**	0.27 ± 0.07
BMMs / > 80%	14.80 ± 1.79*	145.7 ± 36.2	0.04 ± 0.005**	0.43 ± 0.1
THP-1 / > 80%	24.28 ± 2.87*	200.1 ± 46.8	0.08 ± 0.009**	1.15 ± 0.37

Experiments were conducted in quadruplicate cultures, data expressed as mean ± SD (experiment was reproduced further two times with confirmed similar data and data not shown). ** statistically significant difference in EC₅₀ values between the three types of cells (chitosan and Funigzone were significantly more active in PEMs and BMMs compared with THP-1 cells) (p<0.05 by an extra sum-of-squares F test). % infection rate gives the percentage of infected macrophages. Both RPMI and DMEM alone pH 6.5 and chitosan solvent did not show any activity against amastigotes.

821

TABLE 4 Details of chitosan and its derivatives used in the study

Compounds	Properties	Supplier
HMW (source: crustacean shells)	MW=310-375 KDa	Sigma, UK
MMW (source: crustacean shells)	MW=190-310 KDa	Sigma, UK
LMW (source: crustacean shells)	MW=50-190 KDa	Sigma, UK
Fungal chitosan (white mushroom)	MW=110-150 KDa	Dr. S Somavarapu
Chitosan oligosaccharide	MW=5 KDa	Dr. S Somavarapu
Chitosan oligosaccharide lactate	MW=average Mn 5, oligosaccharide 55%	Dr. S Somavarapu
Chitosan- HCl	MW= 47 - 65 KDa	Dr. S Somavarapu

35

822
823

Carboxymethyl chitosan	MW=543,519 Da, level of substitution is 95%	Dr. S Somavarapu
PC1-CH (Phosphorylcholine substituted chitosan)	MW=33 KDa, PC(mol%)= 30	Prof F Winnik
PC2-CH	MW=108 KDa, PC(mol%)= 20	Prof F Winnik
PC3-CH	MW=108 KDa, PC(mol%)= 30	Prof F Winnik

39

824 Figures

825

Fig 1 TNF- α production in uninfected and *L. major* infected BMMs after 24 h of exposure to 1.64, 4.9, 14.8, 44.4, 133.3 and 400 μ g/ml of chitosan at pH 6.5. The dose response in both uninfected and *L. major* infected BMMs was bell-shaped. TNF- α production was significantly decreased ($p < 0.05$ by t-test) by infecting the cells with *L. major*. Experiments were conducted in quadruplicate, data is expressed as mean \pm SD (experiment was reproduced further two times with confirmed similar data and data not shown). Positive control= BMMs treated with LPS 10 μ g/ml. Negative control = BMMs not exposed to chitosan. *Initial macrophage infection rate was ~80% after 24 h. Chitosan solvent did not cause any TNF- α production.

Fig 2 ROS production in uninfected and *L. major* infected BMMs after 4 h of exposure to 1.64, 4.9, 14.8, 44.4, 133.3 and 400 μ g/ml of HMW chitosan at pH=6.5. High levels of ROS were induced by both uninfected and *L. major* infected BMMs exposed to HMW chitosan compared to those that were not ($P < 0.05$ by t-test). Maximum production of ROS occurred at 44.4 μ g/ml of chitosan. ROS production by *L. major* infected BMMs was significantly lower compared to uninfected cells ($p < 0.05$ by t-test). Experiments were conducted in quadruplicate, data is expressed as mean \pm SD (experiment was reproduced a further two times with confirmed similar data (not shown). Positive control = BMMs treated with H_2O_2 25 mM (a known ROS inducer). Negative control = BMMs not exposed to chitosan. *Initial macrophage infection rate was ~80% after 24 h. Chitosan solvent alone did not cause any ROS production.

Fig 3 Activity of HMW chitosan against *L. major* amastigotes in BMMs* after 4 h, with and without ROS scavengers at pH = 6.5. Infected macrophages were pre-incubated with 5 mM NAC for 2 h, after which HMW chitosan at concentrations 1.64, 4.9, 14.8, 44.4, 133.3 and 400 μ g/ml was added and the cells were incubated for a further 4 h. Chitosan activity against intracellular amastigotes was evaluated as described in section (vi). Values are expressed as % inhibition of infection relative to untreated controls. After 4 h, there was no significant difference in the anti-leishmanial activity of chitosan after scavenging of ROS ($p > 0.05$ by t-test). Experiments were conducted in quadruplicate, data is expressed as mean \pm SD. Experiment was reproduced further two times with confirmed similar data (not shown). *Initial macrophage infection rate was ~80% after 24 h.

827

40

828

Fig 4 NO production in uninfected and *L. major* infected BMMs after 24 h of exposure to 1.64, 4.9, 14.8, 44.4, 133.3 and 400 μ g/ml of chitosan at pH = 6.5. The response in both uninfected and infected BMMs was bell-shaped in relation to chitosan concentration. Maximal production of NO was stimulated by 44.4 μ g/ml of chitosan. NO production was significantly decreased ($p < 0.05$ by t-test) when the cells had been infected with *L. major*. Experiment was conducted in quadruplicate cultures, data expressed as mean \pm SD (experiment was reproduced a further two times with confirmed similar data and data not shown). Positive control = BMMs treated with LPS 10 μ g/ml. Negative control = BMMs not exposed to chitosan. *Initial macrophage infection rate was ~80% after 24 h. Chitosan solvent alone did not cause any NO production.

829

Fig 5 Activity of HMW chitosan against *L. major* infected BMMs* after 24 h in the presence or absence of an NO inhibitor at pH = 6.5. Infected macrophages were pre-incubated with the NO inhibitor L-NAME (0.4 mM) for 2 h, following which HMW chitosan at concentrations 1.64, 4.9, 14.8, 44.4, 133.3 and 400 μ g/ml was added and the cells were incubated for a further 24 h. Chitosan activity against intracellular amastigotes was evaluated as described in section (vi). Values are expressed as % inhibition of infection relative to untreated controls. After 24 h, there was no significant difference in the activity of chitosan after inhibition of NO ($p > 0.05$ by t-test). Experiment was conducted in quadruplicate cultures, data expressed as mean \pm SD. Experiment was reproduced a further two times and confirmed the results (data not shown). *Initial macrophage infection rate was ~80% after 24 h.

Fig 6 Activity of HMW chitosan against *L. major* infected BMMs* after 4 h, pH=6.5 (A), 24 h, pH=6.5 (B) and at 24h, pH=7.5 with or without phagocytosis inhibitor or pinocytosis (CME) inhibitor. We found that chitosan requires pinocytosis (CME) not phagocytosis by BMMs for killing of *L. major* amastigotes at pH = 6.5 and 7.5. BMMs were infected with stationary-phase promastigotes. Some of the infected macrophages were pre-incubated with cytochalasin D (phagocytosis inhibitor) or dynasore (pinocytosis (CME) inhibitor) and exposed to various concentrations (1.64, 4.9, 14.8, 44.4, 133.3 and 400 μ g/ml) of chitosan for 4 h and 24 h, followed by microscopic counting of the number of infected macrophages. There was no

41

significant difference in the activity of HMW chitosan after inhibition of phagocytosis ($p > 0.05$ by t-test). In contrast, a significant inhibition of chitosan-mediated parasite killing occurred in the presence of dynasore at two pH values ($p < 0.05$ by t-test). Values are expressed as % inhibition of infection relative to untreated controls. Experiment was conducted in quadruplicate cultures, data expressed as mean \pm SD. Experiment was reproduced a further two times and confirmed the results (data not shown). *Initial macrophage infection rate was ~80% after 24 h.

830

Fig 7 Fluorescence microscopy images of the cellular uptake of rhodamine-labelled chitosan at 4h and 24 h at pH=6.5 by BMMs infected with *L. major*-GFP (XA) or with *L. mexicana*-GFP (XB). Blue represents the nuclei of BMMs. Green represents intracellular amastigotes, red represents labelled chitosan and yellow represents merged red chitosan and green Leishmania. Panels A-F represent the following: Infected BMMs unexposed to chitosan after 4 h (panel A) or 24 h (panel B); Infected BMMs exposed to chitosan after 4h (panel D) or 24 h (panel E); Infected BMMs unexposed to chitosan after 24 h (panel C) and Infected BMMs exposed to chitosan and pinocytosis inhibitor (dynasore) after 24 h (panel F)

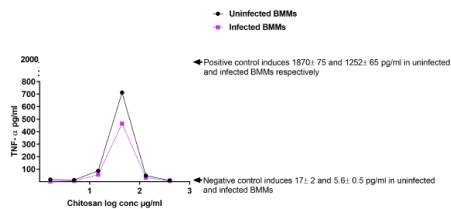
831

Fig 8 The structure of chitosan (60) and its derivatives, (chitosan HCl, carboxymethyl chitosan (61), chitosan oligosaccharide (60), PC-CH (reprinted with permission from reference 28) and chitosan oligosaccharide lactate (59))

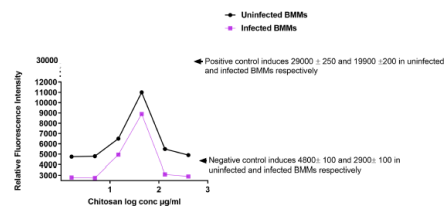
832

833

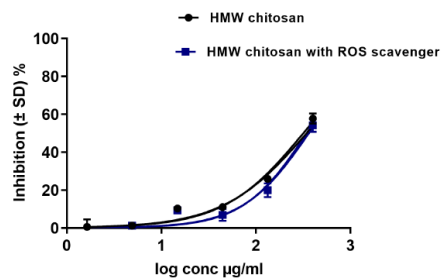
7



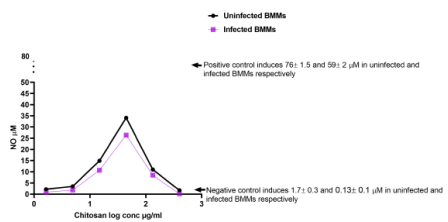
Downloaded from <http://aac.asm.org/> on January 27, 2020 at LONDON SCHOOL OF HYGIENE & TROPICAL MEDICINE



Downloaded from <http://aac.asm.org/> on January 27, 2020 at LONDON SCHOOL OF HYGIENE & TROPICAL MEDICINE



Downloaded from <http://aac.asm.org/> on January 27, 2020 at LONDON SCHOOL OF HYGIENE & TROPICAL MEDICINE



Downloaded from <http://aac.asm.org/> on January 27, 2020 at LONDON SCHOOL OF HYGIENE & TROPICAL MEDICINE

